The Ecology and Evolution of the Extracellular Vesicles of Halophilic Archaea

Dissertation zu Erlangung des Grades eines

Doktors der Naturwissenschaften

- Dr. rer. nat. –

dem Fachbereich Biologie/Chemie

der Universität Bremen

vorgelegt von

Joshua Mathew Mills

Bremen, November 2023

Gutachten/Reviewers:

Gutachterin: Dr. Susanne Erdmann

Gutachterin: Prof. Dr. Sonja-Verena Albers

Gutachter: Prof. Dr. Andreas Dotzauer

Prüfer: Prof. Dr. Michael Friedrich

Prüfer: Prof. Dr. Andreas Dotzauer

Prüferin: Prof. Dr. Sonja-Verena Albers

Prüferin: Dr. Susanne Erdmann

Datum des Promotionskolloquiums: 26.01.2024

"Our task now is to resynthesize biology; put the organism back into its environment; connect it again to its evolutionary past; and let us feel that complex flow that is organism, evolution, and environment united. The time has come for biology to enter the nonlinear world" – Carl Woese, *A New Biology for a New Century*, 2004

Die vorliegene Arbeit wurde in der Zeit von Mai 2020 bis November 2023 in der Arbeitsgruppe Archaea Virologie am Max-Planck-Institüt für Marine Mikrobiologie unter der Leitung von Dr. Susanne Erdmann durchgeführt. Sie wurde weiterhin im Rahmen der International Max Planck Research School of Marine Microbiology (MarMic) angefertigt.

The research that forms the basis for this thesis was conducted from May 2020 to November 2023 in the Archaeal Virology Group at the Max Planck Institute for Marine Microbiology under the supervision of Dr. Susanne Erdmann. The thesis was prepared under the framework of the International Max Planck Research School of Marine Microbiology (MarMic).

ACKNOWLEDGEMENTS

I would like to thank the Max Planck Society and the International Max Planck Research School of Marine Microbiology for providing the funding and resources that allowed me to carry out this work.

I would like to thank Dr. Susanne Erdmann for believing in me and guiding me through this very transformative experience. I am immensely grateful for your feedback throughout this project and allowing me the appropriate level of independence to pursue ideas. I am truly honored to have been a part of the first batch of the Erdmann group. I would also like to thank the Erdmann group for the amazing support. I honestly cannot imagine how this would have turned out if I was with anyone else. Thank you for listening to me lament about lab failures and celebrate lab victories.

I would like to thank my amazing MarMic cohort for the endless brainstorming sessions and fun times to give my brain a break from thinking about vesicles. My experience with you all have been very formative and I will always treasure my memories with my Bremen family.

I would like to thank the co-authors and collaborators of this project for your guidance, as well as your patience through the struggles of trying to publish this work. I would also like to thank Dr. Anita Marchfelder and the Marchfelder group at the University of Ulm for supporting and hosting me during the first year of my PhD.

Finally, I would like to thank my friends and family for their unwavering support of my journey. Thank you to my brother, Eddie, for always being there for me when I need you most. Thank you to Van and Deka, without you I would not be where I am today. Thank you, Giovanni, for being the beacon of light during this process. And thank you to Mom and Grandmom, wish you both could be here for this.

SUMMARY

Extracellular vesicles (EV) are small, spherical structures that bud from the cell envelope. These particles are produced by cells across all three domains of life, marking them as a ubiquitous feature of cell biology. EVs transport proteins, lipids, nucleic acids, and other bioactive compounds in membrane-enclosed packages, which allows them to mediate a multitude of different functions. While much has been uncovered for bacterial and eukaryotic EVs, little is known about the functions and production of EVs from the archaeal domain.

The work presented in this dissertation aims to explore the mechanisms of production, biochemical composition, and function of EVs produced by halophilic Archaea. In **Chapter II**, I present a standardized method for the isolation and purification of EVs from archaeal cultures. This method details the isolation of EVs from liquid cultures, the purification from other extracellular contaminants, and protocols related to the subsequent downstream analysis. By providing a standardized protocol, I aim to promote additional research into archaeal EV production that is comparable to each other. Using these methods in **Chapter III**, I characterize the biochemical composition of EVs from *Haloferax volcanii* and other halophilic Archaea. I uncover that halophilic Archaea produce EVs enriched with small-sized RNA with regulatory potential, which has not been demonstrated for archaeal EVs previously. Proteomic analysis reveals a conserved small GTPase that is crucial to EV production, which we have named archaeal vesiculating GTPase (ArcV). Structurally and functionally, ArcV bears similarities to the Arf-family of GTPases, which are responsible for regulating vesicle formation in the eukaryotic endomembrane system. We propose that this provides evidence for previously established hypotheses regarding the archaeal origins for the eukaryotic endomembrane system, and that small GTPase-dependent vesicle formation could have emerged earlier than previously considered. In **Chapter IV**, I further characterize EV-associated RNA from *Halorubrum lacusprofundi*, with and without virus infection. I observe that the RNA population exported in EVs changes upon viral stress, leading to the enrichment of specific RNAs. I also explore the effects on the cell transcriptome after incubation with EVs, suggesting that EVs are able to affect gene expression in the receiving cell.

The characterization of archaeal EVs has implications on both microbial community dynamics and prokaryotic evolutionary history. The ability for EVs to induce changes in gene expression in the receiving cell suggests a regulatory mechanism that acts on a population-wide scale. Additionally, the presence of a small GTPase-dependent mechanism for EV production in Archaea requires us to reevaluate our current understanding of prokaryotic membrane remodeling mechanisms and the evolutionary history of eukaryotic-like features.

ZUSAMMENFASSUNG

Extrazelluläre Vesikel (EV) sind kleine, kugelförmige Strukturen, die sich aus der Zellhülle lösen. Diese Partikel werden von Zellen in allen drei Lebensbereichen produziert, was sie zu einem allgegenwärtigen Merkmal der Zellbiologie macht. EVs transportieren Proteine, Lipide, Nukleinsäuren und andere bioaktive Verbindungen in membranumschlossenen Paketen, was es ihnen ermöglicht, eine Vielzahl unterschiedlicher Funktionen zu vermitteln. Während über bakterielle und eukaryotische EVs viel bekannt ist, ist über die Funktionen und die Produktion von EVs aus dem archaeellen Bereich wenig bekannt.

Die in dieser Dissertation vorgestellten Arbeiten zielen darauf ab, die Produktionsmechanismen, die biochemische Zusammensetzung und die Funktion von EVs zu untersuchen, die von halophilen Archaeen produziert werden. In **Kapitel II** stelle ich eine standardisierte Methode für die Isolierung und Reinigung von EVs aus Archaeen-Kulturen vor. Diese Methode beschreibt detailliert die Isolierung von EVs aus Flüssigkulturen, die Reinigung von anderen extrazellulären Verunreinigungen und Protokolle für die anschließende Analyse. Durch die Bereitstellung eines standardisierten Protokolls möchte ich die weitere Forschung im Bereich der archäologischen EV-Produktion verbessern. Mithilfe dieser Methoden charakterisiere ich in **Kapitel III** die biochemische Zusammensetzung von EVs aus *Haloferax volcanii* und anderen halophilen Archaea. Ich decke auf, dass halophile Archaeen EVs produzieren, die mit kleiner RNA mit regulatorischem Potenzial angereichert sind, was für archaeelle EVs bisher nicht nachgewiesen wurde. Die Proteomanalyse zeigt eine konservierte kleine GTPase, die für die EV-Produktion entscheidend ist und die wir archaeal vesiculating GTPase (ArcV) genannt haben. Strukturell und funktionell weist ArcV Ähnlichkeiten mit der Arf-Familie von GTPasen auf, die für die Regulierung der Vesikelbildung im eukaryontischen Endomembransystem verantwortlich sind. Wir schlagen vor, dass dies Beweise für zuvor aufgestellte Hypothesen bezüglich der archaeischen Ursprünge des eukaryotischen Endomembransystems liefert, und dass die von kleinen GTPasen abhängige Vesikelbildung früher als bisher angenommen entstanden sein könnte. In **Kapitel IV** charakterisiere ich die EV-assoziierte RNA aus Halorubrum lacusprofundi mit und ohne Virusinfektion weiter. Ich beobachte, dass sich die RNA-Population, die in EVs exportiert wird, bei viraler Belastung verändert, was zu einer Anreicherung spezifischer RNAs führt. Ich untersuche auch die Auswirkungen auf das Zelltranskriptom nach der Inkubation mit EVs, was darauf hindeutet, dass EVs die Genexpression in der aufnehmenden Zelle beeinflussen können.

Die Charakterisierung archäischer EVs hat Auswirkungen sowohl auf die Dynamik mikrobieller Gemeinschaften als auch auf die Evolutionsgeschichte von Prokaryonten. Die Fähigkeit von EVs, Veränderungen in der Genexpression in der aufnehmenden Zelle zu bewirken, lässt auf einen Regulationsmechanismus schließen, der auf einer populationsweiten Ebene wirkt. Darüber hinaus erfordert das Vorhandensein eines von kleinen GTPasen abhängigen Mechanismuses für die EV-Produktion in Archaea eine Neubewertung unseres derzeitigen Verständnisses von prokaryotischen Membranumbau-Mechanismen und der Evolutionsgeschichte eukaryotischer Merkmale.

LIST OF ORIGINAL PUBLICATIONS

This thesis is based on the following scientific articles. Each manuscript corresponds to an individual chapter as indicated:

Mills, Joshua; Erdmann, Susanne. "Isolation, Purification, and Characterization of Membrane Vesicles from Haloarchaea". *Archaea. Methods in Molecular Biology*, vol 2522, pages 435 – 448, (2022). https://doi.org/10.1007/978-1-0716-2445-6_30.

Mills, Joshua; Gebhard, L. Johanna; Schubotz, Florence; Shevchenko, Anna; Speth, Daan R.; Liao, Yan; Duggin, Iain G.; Marchfelder, Anita; Erdmann, Susanne. "Extracellular vesicle formation in Euryarchaeota is driven by a small GTPase". *Proceedings of the National Academy of Sciences*, under review.

Mills, Joshua; Erdmann, Susanne. "The regulatory impact of archaeal extracellular vesicles on microbe-microbe interactions". In preparation.

CONTENTS

CHAPTER I. INTRODUCTION

The cellular envelope represents an intricate tapestry of complex compounds, activity, and biochemical functions. This encapsulating structure acts not only as a boundary used to separate the cell from the extracellular world, but also as a controlled, dynamic interface for the cell to interact with the vast abyss that surrounds it. Through this thin divider, cells can acquire nutrients, generate energy, navigate their surroundings, and alter their localized environment. Each cell acts as a microscopic factory with infinitesimal contributions to the chemical composition of their immediate surroundings, collectively contributing to the geochemical cycling of elements on a global scale. This ability for single cells to manipulate their surroundings further adds to the complexity of microbial ecosystems. Each organism rewires their activity in response to the cells that cohabitate their environment and the ever-changing abiotic factors, generating an interconnected network of feedback loops.

Typically, when we consider the process of intercellular communications, we think of the communication between the different cell types that make up a multicellular organism. However, in the context of microbial ecosystems, compounds are continuously passed from organism to organism to be either reduced, oxidized, assimilated into biomass, or trigger a cascade of reactions within the cell. This can represent a form of communication between cells, a cross-talk mediated through metabolism with each cell influencing the actions (or gene expression) of other cells. Though the mechanisms utilized in prokaryotic intercellular communication are many, one mechanism has gained interest in recent years: the microbial production of extracellular vesicles (EV) and how they potentially drive microbial community dynamics. In this dissertation, I will focus primarily on EV production in the archaeal domain and explore the ecological and evolutionary implications of this system.

1.1 THE THIRD DOMAIN

Before the advent of genetic sequencing, the taxonomic organization of life and their evolutionary relationships were dictated by morphological and physiological differences. Cells were divided into prokaryote (simple and un-compartmentalized) and eukaryote (complex and compartmentalized). Prokaryotes were considered a monophyletic group, containing both Archaea and Bacteria due to their similarities of their respective cell structures. Building off of the idea that genomic mutations can trace back the phylogenetic record of genes [1], pioneering work from Carl Woese and George Fox established phylogenetic patterns based on ribosomal RNA sequences to construct a quantitatively generated tree of life [2]. Constructing the tree of life based on phylogeny rather than morphology introduced an additional prokaryotic group as its own domain separate from the Eukaryota and Bacteria, thus concluding that prokaryotes were not monophyletic. Though Archaea and Bacteria appear similar at the surface, Woese and Fox note that there are differences in the biochemistry and structure of Archaea in comparison to Bacteria that would support their distinction from each other [2]. Further observations distinguished the archaeal domain from the rest of the tree of life, such as differences in lipid composition [3], cell envelope structures [4], translation mechanisms [5], DNA replication [6].

Though often overlooked, Archaea represent a substantial diversity of organisms that span a wide range of environments and metabolic capabilities [7, 8]. Archaea tend to dominate in extreme environments, such as those with high temperatures or high acidity [7, 9]. Since most identification strategies at the time relied on cultivation rather than sequencing, Archaea were first considered to be a domain of extremophiles [10]. However, advances in metagenomic sampling suggested that they are more ubiquitous than previously considered [11]. Archaeal organisms have been discovered in more moderate environments such as freshwater [12] and human skin [13], even making up to 20% of prokaryotic organisms in marine environments [14, 15]. Due to their ubiquity and diversity in metabolic potentials, Archaea have proven to be key components to global geochemical cycling [16].

Initially, the archaeal domain was divided into two distinct lineages, Crenarchaeota and Euryarchaeota [17], but the increase in genome-resolved metagenomic sampling from a wider range of environmental sites further expanded our understanding of the diversity and metabolic potentials hidden in the archaeal domain. While the organization of the archaeal tree has undergone various major changes over the past decade, the current archaeal taxonomy by the Genome Taxonomy Database (GTDB) in 2023 (release 214) has now organized the domain into 20 separate phyla [18]. Generally, these mostly consist of *Thermoproteota*, *Asgardarchaeota*, DPANN Archaea, and the different phyla that fall under the superphylum of Euryarchaeota (Figure 1).

The superphylum of Euryarchaeota stands out as the most diverse of the archaeal branches, comprising itself with five distinct phyla. Notably, the first isolated Archaeon, *Methanobrevibacter ruminantium* (formerly *Methanobacterium ruminantium*), was a methanogenic Euryarchaeon of the phylum *Methanobacteriota* sampled from bovine rumen in 1958 [19]. Since then, the diversity of Euryarchaeota has largely expanded to include organisms other than methanogens (phylum *Methanobacteriota* and some classes within phylum *Halobacteriota*). Euryarchaeota also encompasses halophilic Archaea (phylum *Halobacteriota*, see section "1.2.1 Halophilic Archaea"), acidophilic Archaea (phylum *Thermoplasmata*), and thermophilic Archaea (class *Archaeoglobi* and *Thermococci*) [7, 18, 20]. Along with their wide distribution of habitats, Euryarchaeota also mediate a diverse range of ecological roles, such as methanogenesis, sulfur cycling, nitrogen cycling and iron cycling [7, 20], and in some cases the metabolism of short-chain hydrocarbons [21].

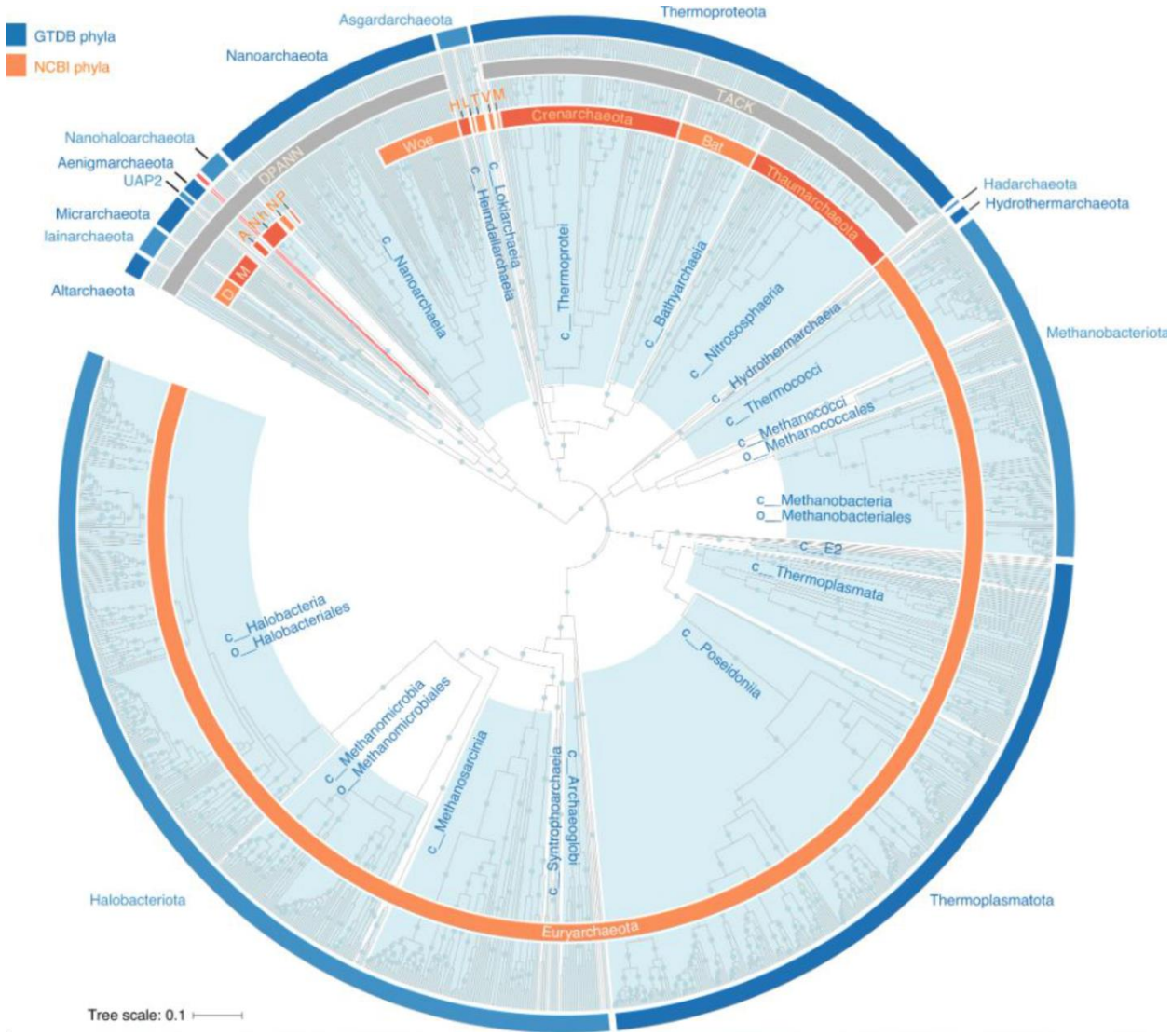

Figure 1. Rank-normalized archaeal GTDB taxonomy. Figure adapted from [18]. Outer blue ring denotes GTDB rank-normalized archaeal phyla. Inner orange ring denotes NCBI archaeal phyla.

In 2002, Huber and colleagues reported one of the smallest archaeal genomes belonging to the newly discovered *Nanoarchaeum equitans*, and what was to be uncovered later as a new superphylum of Archaea [22]. *N. equitans* was characterized as an ultra-small obligate symbiont to the thermoproteotal species, *Ignococcus hospitalis*, with a unique 16S rRNA sequence that was not amplified by universal and Archaea-specific primer sets [22]. The discovery of other similarly reduced genomes from sister phyla from a wider range of environments and other symbiotic partners suggested that the discovery of *N. equitans* was not an outlier, but rather the norm for this new branch of archaeal life [23–26]. This new branch was named DPANN after the major phyla *Diapherotrites*, *Parvarchaeota*, *Aenigmarchaeota*, *Nanoarchaeota* and *Nanohaloarchaeota*, though other phyla have since been uncovered belonging to DPANN. The genomes belonging to many DPANN organisms were found to lack many essential pathways, such as genes in the electron transport pathway, amino acid synthesis, lipid synthesis, and nucleotide synthesis to name a few [26], suggesting that they mostly rely on the metabolism of their symbiotic partner. From the few cultivatable examples of DPANN organisms, the interaction with their respective host organisms has proven to be quite diverse and unique. For

example, interaction between *N. equitans* and *I. hospitalis* has been shown to involve the fusion of the two membranes to create a cytoplasmic bridge [27], while the interaction between *Nanohaloarchaeum antarcticus* and *Halorubrum lacusprofundi* involves the complete internalization of *Nha. antarcticus* [28]. This demonstrates a common thread of membrane remodeling among DPANN-host interactions, though many DPANN and their cognate partner organisms remain uncharacterized. In relation to other Archaea, the placement of DPANN into the archaeal tree has been tumultuous [26]. According to GTDB and other recent studies, DPANN has been classified as its own phylum that place basally in the archaeal tree [18, 29, 30], implying an early emerging lineage of Archaea. However, some argue that the placement could be a result of long branch attraction, the erroneous grouping and long branching of genomes as a result of biased evolutionary pressures and reduced genomes [31, 32], and still remains debated to date.

In 2015, another archaeal organism from a novel phylum was discovered that required us to rethink the tree of life and the relationship between Archaea and Eukarya. *Lokiarchaeota* were discovered from metagenomic assemblies of Archaea belonging to the Deep-Sea Archaeal Group/Marine Benthic Group B from samples isolated from deep marine sediments near the hydrothermal vent site, Loki's Castle, near the Arctic Mid-Ocean Ridge [33]. Phylogenetic analysis of the resulting genomes placed Eukarya as a monophyletic group with *Lokiarchaeota*. They were also observed to encode a wider collection of eukaryotic signature proteins than other archaeal groups [33]. Additional sister clades to *Lokiarchaeota*, such as *Thorarchaeota*, *Odinarchaeota* and *Heimdallarchaeota*, were discovered from other sediment samples from aquatic systems, which altogether were given the name *Asgardarchaeota* [34, 35]. Characterization of multiple asgardarchaeotal genomes revealed that the presence of eukaryotic signature proteins was wide-spread within the phylum [36–38], implicating the phylum as the closest prokaryotic relative to Eukaryotes. A few *Asgardarchaeota* have recently been isolated or enriched in culture [39, 40], which has allowed for microscopy and qualitative characterization. While microscopy of these organisms did not exhibit eukaryotic-like intracellular compartmentalization the individual lokiarchaeotal cells exhibited long membranous protrusions from the main cell body [39, 40]. This suggested a higher capacity for membrane remodeling and complexity in comparison to other archaeal organisms. The discovery of Archaea with genomes containing Eukaryote-like complexity and the functional capacity for complex membrane remodeling strikingly matched previous models of the origins of Eukaryotes (see section "1.2.2 Origins of the eukaryotic cell") [41–43], further implying the close relationship between Archaea and Eukaryota.

1.1.1 Halophilic archaea

Halophilic Archaea (haloarchaea) are Euryarchaeota belonging to the phylum *Halobacteriota* that are characterized by their proclivity towards extreme salt environments, some even up to the saturation point of NaCl [44]. These types of environments are typically characterized as highly evaporative and tend to experience steep and sudden local fluxes to salinity and high amounts of UV radiation. While the ability to thrive in hypersaline environments exists in all three domains of life [45, 46], high concentrations of salt in the environment exerts tremendous osmotic pressure on the organism. In order to thrive in these pressures, halophilic cells maintain intracellular ionic concentrations similar to extracellular concentrations. There are generally two mechanisms that microorganisms utilize. The first, and most prevalent in haloarchaea, is the "salt in" method that imports K^+ and Cl^- into the cell to maintain osmotic equilibrium

[47]. The second method is the "salt out" method that actively pumps out ions while importing charged organic compounds to maintain osmotic equilibrium [48]. Energetically, the "salt in" method is not as expensive as the "salt out" method, but requires that protein sequences have been optimized to retain function under high salt conditions. Further, to overcome the mutagenic pressures of UV radiation and high oxidative stress, most haloarchaea express carotenoids in their membranes [49], giving them their signature pink color. Haloarchaea are also predominantly aerobic heterotrophs, but there are exceptions, such as fermenters, haloarcheaea that can use nitrate or sulfate as electron receivers, and even halophilic methanogens [46].

Haloferax volcanii, the main organism of study in this thesis, was first isolated from the Dead Sea in 1975 [50] and continues to be the standard model organism for microbiological research on haloarchaea. As one of the first haloarchaeal organisms to have its genome mapped [51], it is a useful model organism due to its ability to grow on simple media [52], take up foreign DNA including shuttle vectors [53, 54], and the presence of selection markers for the generation of knock out strains through homologous recombination [55, 56]. More recently, a functional CRISPR-Cas system was identified in *H. volcanii* that was developed into a genetic manipulation tool for the organism [57]. Additionally, the first virus has been isolated for *H. volcanii* [58], opening the doors to studying halophilic viruses in a well-established model system.

1.1.2 The origins of the eukaryotic cell

From the conception of Darwin's tree of life, a major implication was that each taxonomic branch at one point in evolutionary history was connected to another. Therefore, at some point in Earth's timeline, a eukaryotic cell emerged from prokaryotic life. This transition from "simple" to "complex" life remains one of the biggest questions in evolutionary biology to date. This process, known as eukaryogenesis, describes the origins of eukaryotic signature features, such as internal cell compartmentalization, the presence of the nucleus, their cell division machinery, and the order in which they emerged during the proto-eukaryotic stage of evolutionary history.

At first glance of the structure of the tree of life proposed by Woese, one would notice that it is surprisingly asymmetrical, with the original tree showing that Archaea and Eukaryota share a common ancestor [17]. This was based on the higher degree of specific protein similarities that were found between Archaea and Eukaryota, compared to between Archaea and Bacteria [59, 60]. This led to the conclusion that Archaea and Eukaryota were sister groups. Analysis of other components, such as elongation factors and ribosomal structure [61, 62], showed that Eukaryota shared closer similarities to *Thermoproteota* than *Euryarchaeota*, planting the seed for the idea that Eukaryotes may have branched from an archaeal organism. In fact, much of the informational processing core of Eukaryotes, such as transcription [63], translation [64], and DNA replication [65] appeared to have archaeal roots. The discovery of additional archaeal lineages and increasing resolution for genomic sequencing further supported this theory that Archaea was not a monophyletic group, implying that what was once a three domain tree of life was in fact two [42, 33, 66]. This further implied that both prokaryotic groups, Archaea and Bacteria, existed long before the emergence of Eukaryota, and that Eukaryota emerged from a single archaeal organism [67].

Piecing together the events that transpired to form the last eukaryotic common ancestor (LECA) poses quite the daunting task, as this would be speculating on events estimated to have occurred anywhere from 1.0 – 1.9 billion years ago [68]. It is thought that the acquisition of the alphaproteobacterial endosymbiont was the defining event of eukaryogenesis [69, 70]; however, it is still uncertain whether this acquisition was performed by an archaeal host or an already diverged "proto-eukaryotic" host. The "mito-late" hypothesis suggests that the mitochondrial endosymbiont was taken up by a "proto-eukaryotic" host that had already diverged from Archaea [67]. This host would have then already contained signature eukaryotic features such as a nucleus, an endomembrane system, and a functional cytoskeletal system. The alternative hypothesis suggests that the mitochondrial endosymbiont was acquired early by an archaeal organism, which then provided the fuel for further complexification [67]. Whether the organism that begat the entirety of the eukaryotic domain was "archaeal" or "eukaryotic" seems more so a question of semantics; rather, the question requires a functional understanding of the complex cell biology already extant within the archaeal domain.

To understand the complexity of the first eukaryotic common ancestor (FECA), we can look at the homologues to essential eukaryotic genes that are present in extant archaeal species and infer the functional potentials for FECA [67, 41]. Based on sequence alignment, we can already identify distantly related homologues of eukaryote-specific functions across the archaeal domain. For example, distant homologues of eukaryotic actin [71, 72], ubiquitin protein modifier system [73] and an ESCRT-like system [74] have been identified in the phylum *Thermoproteota*. Further eukaryotic signature genes are also encoded on genomes across the *Asgardarchaeota* phylum [35, 38]. However, phylogenetic analyses of highly diverged sequences deep in evolutionary history can lead to the amplification of systemic artifacts that can cloud our understanding of the evolution of the genes in question [75]. With the development of structure-based searches for protein homologs [76] and structure-based phylogeny [77, 78], perhaps the higher resolution provided by these methods can bring us closer to resolving the clouded interface that lies between prokaryotes and Eukaryota.

1.2 From cell trash to cell treasure

Extracellular vesicles (EV) were first observed and reported in electron micrographs in the 1960s for both Eukaryotes and Prokaryotes. Initially, they were described as "dust" [79] or "circular structures" [80] associated with the extracellular space. This dismissive phrasing clearly conveyed the lack of significance attributed to EVs at the time. It was still not understood whether these structures conveyed biological activity or biological waste products or artifacts of sample preparation. As more observations of EVs from other organisms began to accumulate, their presence and the potential to mediate significant biological functions became harder to ignore. In the following years, EVs from bats [81], algae [82], and *Staphylococcus aureus* [83] were observed, some appearing to contain electron dense material suggesting that they encapsulate specific compounds.

The first images of EV production from mammalian cells demonstrated a connection between EV release and intracellular multivesicular bodies (MVB) [84]. At the same time in another mammalian system, EVs were observed for the first time to enrich for specific compounds distinct from the plasma membrane [85]. Both studies suggested that an active and coordinated mechanism was behind the release of EVs from eukaryotic cells. Considering that MVBs are specific to eukaryotic cells, it also appeared that there was a stark divide in EV-producing mechanisms between

eukaryotes and prokaryotes. Whereas eukaryotic EVs derived from budding into MVBs and their subsequent release into the extracellular space, no such mechanism was observed in Bacteria, suggesting that multiple mechanisms exist for EV formation. In electron micrographs from 1966, small "blebs" could be observed budding off of the outer membrane of *Escherichia coli* under lysine-limiting conditions, attributing to the extracellular enrichment of lipopolysaccharides [86]. Further studies showed similar, conditionally-dependent production of EVs in other bacterial organisms, a compilation of which can be found in the 1989 review of bacterial outer membrane vesicles (OMV) by Mayrand and Grenier [87]. However, the exact mechanism of EV formation remained (and continues to remain) enigmatic. One hypothesis that arose from suggested that OMV production arose from the disproportional growth of the outer membrane in comparison to the peptidoglycan layer [88]. Another hypothesis suggested that areas of the outer membrane with low lipoprotein linkages are linked to OMV production, predicting that the lack of tethering of the outer membrane to the peptidoglycan layer results in the outward blebbing [89]. However, the absence of a bacterial strain that did not produce EVs weakened the claim that bacterial EVs were a coordinated and active process. The search for a bacterial mechanism of EV production remains unresolved to this day.

The significance of bacterial EVs started becoming apparent from observations in the 1960s, where the antigenic compound, lipopolysaccharide, was observed to be enriched in bacterial EVs [86]. Further examples of the potential for function were published in the following decades [87], all suggesting that bacterial EVs play a role in pathogenicity. A clear example of the early establishment of the relationship between bacterial EVs and human immune responses can be found from the EVs of *Bacteroides gingivalis* W50 (currently known as *Porphyromonas gingivalis*). Purified EVs alone were demonstrated to suppress chemotaxis and exhibit cytotoxic activity in human white blood cells, which are essential immune responses [90]. While these studies point to the idea that bacteria utilize EVs to facilitate colonization of host organisms, they also bring up the potential for EVs to mediate communication between different organisms and domains of life. However, as the studies primarily focused on pathogenesis, evidence for EVs in Archaea did not appear until 2000 in the thermophilic *Sulfolobus* genus (phylum *Thermoproteota*) [91].

These early studies and characterizations of EVs from Bacteria and Eukaryotes helped establish the foundations of this budding field of cell biology, driving forth further investigations into the various cargo and functions that these enigmatic extracellular structures harbor. As more names joined the hunt for EVs and evidence accumulated of the importance of EVs, the International Society for Extracellular Vesicles was established in 2011 [92], providing structure and standards to EV research and cementing it as a significant subfield of cellular biology.

1.3 EUKARYOTIC MEMBRANE REMODELING SYSTEMS

A general theme arises in the various eukaryogenesis models, that the proto-eukaryotic cell should harbor some sort of capacity to manipulate their cell membrane, a trait that is present in all eukaryotic cells as we know them today. Eukaryotic cells distinguish themselves from bacterial and archaeal cells not only for their internal membrane-bound compartmentalization, but also for the complex network of intracellular membrane trafficking between these organelles. This process, known as the endomembrane system, consists of the formation and designated trafficking of intracellular membrane vesicles. Further, systems for cytosolic membrane remodeling are used for endocytosis, crawling motility

and the production of eukaryotic EVs (referred to as exosomes), making membrane remodeling mechanisms quite essential to the eukaryotic cell.

1.3.1 The endomembrane system

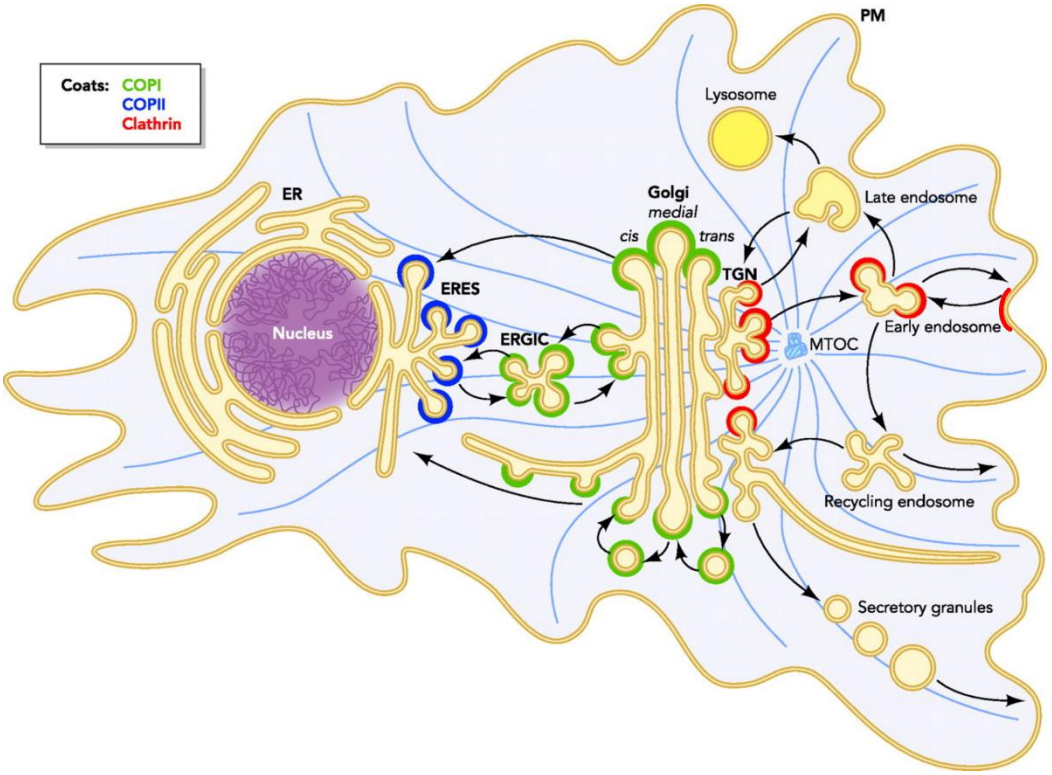

Figure 2. Coat complex localization in the eukaryotic endomembrane system. Intracellular membrane trafficking in eukaryotes uses three distinct coat complexes for the formation of vesicles. COPII coat complexes form vesicles budding from the endoplasmic reticulum to the golgi (blue), COPI coat complexes form vesicles that bud from the Golgi (green) and Clathrin coat complexes form vesicles that exit the Golgi and also mediate endocytosis (red). Figure modified from [93].

For specialized proteins and lipids to be transported to their intended destination within the eukaryotic cell, a complex network of intracellular vesicle trafficking communicates various cargo between multiple membrane-bound organelles (Figure 2). These vesicles are categorized by the protein coat complexes that encapsulate them, either clathrin-coated, COPI-coated or COPII-coated, which is dependent on their point of origin and target destination within the cell [94, 95]. Intracellular vesicles have the potential to carry out a wide range of functions based on the cargo they carry, the proteins involved in their biogenesis and the organelles that they interact with, allowing for a multitude of permutations that the cell can adapt to its needs. In general, the process of intracellular vesicle formation follows the same procedure of initiation, recruitment of the coat complex and cargo, vesicle budding and scission, vesicle uncoating, and fusion to the target membrane. However, each mechanism for vesicle formation as well as the proteins involved remain distinct from one another (Figure 3).

Starting from the initial step of the secretory pathway, COPII-coated vesicles describe the transport of newly synthesized and folded proteins from the endoplasmic reticulum (ER) to the Golgi [93, 96, 97]. The process is initiated by the interaction between small GTPase, Sar1, and its corresponding membrane associated GEF, Sec12 [98, 99]. Sec12

contains a transmembrane domain that anchors the protein to the ER, and a cytosolic β-propeller domain with seven WD-40 repeats (blades) and a potassium loop extension at the first blade [100]. The Sar1-Sec12 interaction allows for the insertion of the N-terminal α-helix into the ER membrane and the subsequent transition from Sar1-GDP to Sar1-GTP (REF), thus activating the GTPase. The recruitment of the rest of the complex occurs as a cascade of interactions, starting with the recruitment of the Sec23-Sec24 heterodimer to the membrane-bound Sar1, forming the pre-budding complex [101]. Sec23 directly interacts with Sar1, and all three components of the pre-budding complex form an elongated structure that lies parallel to the ER membrane resembling a bowtie, each interfacing with the membrane forming the inner coat of the COPII coat complex [102]. The concave structure of the pre-budding complex also suggests that this interaction further stimulates membrane deformation [102]. Protein sorting to the pre-budding complex is mediated mostly by interactions between protein cargo and Sec24 [97]. After the inner coat is formed, the outer coat composed of Sec13-Sec31 heterotetramer is recruited through interaction between Sec23 and a proline rich region of Sec31 [103]. These three main protein components of the COPII coat complex (Sar1, Sec23-Sec24 and Sec13-Sec31) are the minimal required components for vesicle formation [104]. Sec31 is comprised of a seven-bladed N-terminal ß-propeller domain followed by two α-solenoid domains, while Sec13 is comprised of a single ß-propeller domain with six blades [105]. Structural analysis of this outer cage-like structure shows that it is rather flexible and able to conform to different membrane curvatures [106, 107], suggesting that the outer cage is not the main contributor to membrane deformation. It is predicted that function of the outer coat is to link multiple pre-budding complexes together, thus accumulating the membrane deformation sites [96]. As coat assembly is stimulated by the GDP-GTP exchange, coat disassembly is stimulated by GTP hydrolysis. While Sec23 from the inner coat acts as the cognate GAP, this catalytic activity is increased up to ten-fold with the presence of Sec31 from the outer coat [104]. It remains unclear how the balance between nucleotide exchange and GTP hydrolysis plays a role in the timing of vesicle formation, vesicle scission, and coat disassembly [108]. A mutant Sec23 that was constructed to prevent interaction with Sec31 was shown to be unable to complete fission [109], implying that the outer coat is required for the release of the vesicle from the donor membrane. However, whether the increase in GTP hydrolysis is relevant for vesicle fission is undetermined.

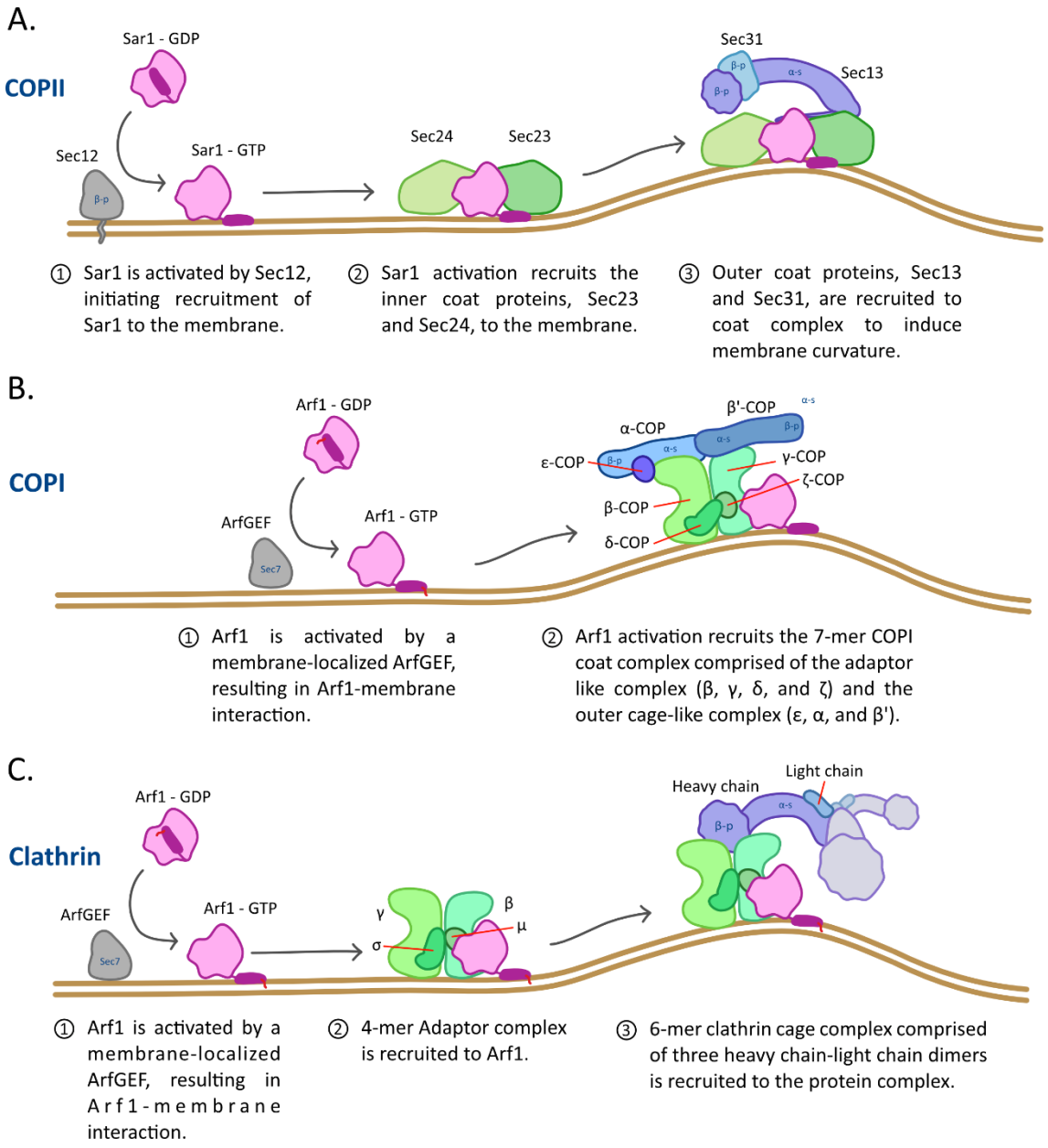

Figure 3. COPII (A), COPI (B), and Clathrin (C) coat complex assembly. Schematic representation of the assembly of intracellular vesicles of eukaryotic cells. Each mechanism starts with the activation of a small Arf-family GTPase (pink), which promotes recruitment to the membrane. Activation and membrane interaction of the GTPase initiates the recruitment of a coat complex. Each coat complex is comprised of an inner/adaptor complex (green) and an outer cage-like complex (blue). Relevant protein structures are also shown (β-p: beta-propeller, α-s: alpha-solenoid).

Continuing on the path of the secretory pathway, COPI-coated vesicles mediate transport between cisternae of the Golgi as well as from the Golgi to the ER [110, 111]. Recruitment of the COPI coat complex (coatomer) begins with the activation of the small GTPase Arf1 (ADP-ribosylation factor 1) [112]. Unlike the singular GEF, Sec12, that activates Sar1, Arf1 has multiple GEFs depending on the position in the Golgi, each conferring different functions to the COP1 vesicle [110, 113]. The family of Arf-GEFs represent a diverse family of proteins with multiple functional domains, such as pleckstrin homology domains and Ankyrin repeats, though they all share a core Sec7 domain that interacts with the Arf GTPase [114, 115]. Sec7 domains are around 200 amino acids in length that folds into a flared cylinder comprised of ten α-helices [116], strikingly unrelated to the β-propeller Sec12. Activation of Arf1 also exposes its N-

terminal amphipathic α-helix, but differs with a post-translational modification at the N-terminal glycine residue with a lipid myrisoyl group to stabilize membrane interaction [117, 118]. Unlike the sequential recruitment of the COPII coatomer, the COPI coatomer is recruited as a single large complex with 7 subunits: α-COP, β'-COP, ε-COP, β-COP, δ-COP, γ-COP and ζ-COP [119]. The coatomer can be organizationally broken down into two components, a coat or cage-like subcomplex (ε, α and β') and an adaptor-like subcomplex (γ, ζ, β and δ) [110, 120]. The cage-like subcomplex somewhat resembles Sec31 of the COPII outer coat, in that α and β' both contain N-terminal β-propellers followed by α-solenoids [121]. The adaptor-like subcomplex is comprised of longin domains, HEAT repeats, and β-sandwiches that interface with Arf1 [110, 122–124]. Both the cage-like and adaptor-like subcomplexes are involved in cargo sorting into the budding vesicle [125]. Fission of the budding vesicle is uniquely mediated by Brefeldin-A ADP-Ribosylated Substrate (BARS) [126], a protein that is able to interact and deform the Golgi membrane [127]. Unlike COPII coat complexes, the cognate ArfGAP is not a structural component of the COPI coatomer, but rather acts on the already assembled vesicle to initiate GAP activity and subsequent uncoating [128].

Traffic of compounds from among the *trans*-Golgi network (TGN) as well as the endocytic pathway is mediated by clathrin-coated vesicles (CCV) by the activation and membrane association of a small Arf family GTPase (Arf1-6), depending on the subcellular point of origin [113, 129]. In the same mechanism as COPI vesicle formation, the Arf GTPase is activated by a Sec7 domain-containing, membrane-associated protein, resulting in the recruitment of the GTPase to the membrane [113]. Membrane association of the activated GTPase results in the recruitment of adaptor protein (AP) complexes, such as AP-1 for trafficking among the TGN. However, the mechanism for endocytosis via AP-2 seems to be regulated differently, as AP-2 does not require a GTPase to initiate membrane interaction [130], but the activation of plasma membrane-associated Arf6 does stimulate AP-2 recruitment [131]. Structurally, adaptors consist of two large subunits, one medium subunit, and one small subunit that are able to bind to the membrane and GTPase, recognize specific cargo motifs, and facilitate binding to the clathrin complex [132–134]. The outer, cage-like clathrin coat is a triskelia with three heavy chain-light chain dimers [135]. The N-terminal of the heavy chain is a seven-bladed β-propeller that mediates interaction between clathrin and the AP complex, followed by a long α-solenoid that forms the majority of the cage-like structure [134, 135]. Unlike COPI and COPII vesicles, CCV expend energy for vesicle scission as well as uncoating through GTP and ATP hydrolysis respectively [136, 137].

Specific aspects of each intracellular vesicle production share certain similar features with one another that some have hypothesized reflects a common ancestry among eukaryotes [95, 138, 139]. Each process mostly begins with the activation of an small single domain Arf-family GTPase (either Arf or Sar) by a GEF to induce positive membrane curvature and recruit the complexes required for vesicle formation and cargo sorting [140]. While structurally Arf and Sar are quite similar in their nucleotide-bound state, their cognate GEFs (the Sec7 domain and cytosolic domain of Sec12 respectively) share no structural similarities themselves or in the interface with their respective GTPases [141]. Sec12 also differentiates itself from other Arf-GEFs as an integral membrane protein, whereas the GEFs of Arf rely on protein interactions to dictate subcellular localization. However, GEFs of the various small single-domain GTPases of the eukaryotic cell are a diverse class of typically unrelated proteins [142], so it is unsurprising that the GEFs acting on Arf and Sar do not resemble each other. Once activated, the now membrane-bound GTPase is able to recruit its

respective coat complex, which also intriguingly shares certain homologies. The coat complexes of COPI, COPII, and clathrin vesicles share subunits composed of either one or two β-propeller folds followed by α-solenoid domains [139]. Similar architecture is also found in the proteins that compose other membrane deforming complexes such as the nuclear pore complex [143], the cilium [144], the late endocytic pathway [145], and the vacuole [146]. The identification of commonalities between multiple membrane-deforming protein complexes lead to the proposition that a "protocoatomer" had existed during the early stages of the eukaryotic domain that diversified via paralogous expansion to mediate different functions in the cell [139, 147, 148]. Certain features of the protocoatomer have been bioinformatically predicted in the genomes of *Asgardarchaeota*, mainly the presence of small GTPases [33, 138, 149]. However, functional characterization of a protocoatomer-like system for membrane deformation among prokaryotic organisms is still missing. Thus, membrane remodeling through coat complexes remains a eukaryote-exclusive mechanism.

1.3.2 Exosome production

Besides the protocoatomer-based mechanism for producing vesicles, eukaryotic cells utilize an unrelated mechanism for the formation of a specialized class of EVs, known as exosomes. The endosomal sorting complex required for transport (ESCRT) mechanism describes the different protein complexes that coordinate the budding of vesicles into endosomes and their subsequent release into the extracellular space [150–152]. The ESCRT machinery can be divided into five functional complexes: ESCRT-0, ESCRT-I/II/III, and Vps4. Initiation of the ESCRT pathway is driven by the binding of the heterodimeric ESCRT-0 complex to ubiquitinated cargo-enriched endosomes [153], and allows for the subsequent binding of the ESCRT-I complex [154]. The ESCRT-I complex binds to the ESCRT-II subcomplex, which recruits ESCRT-III subcomplex to the membrane [150, 155]. ESCRT-III subunit, snf7, homo-oligomerizes to form flexible filaments that interface with the membrane [156, 157], which acts as the driving force for membrane remodeling [158], though the exact mechanism is still uncertain. Finally, AAA ATPase, Vps4, is recruited to the membrane and mediates vesicle scission through ATP hydrolysis [159]. This process also allows for the unfolding and recycling of the ESCRT complexes. Mechanistically and evolutionarily, protocoatomer- and ESCRT-based vesicle formation are not related [139]. While protocoatomer-based vesicle production relies on coat assembly to confer negative curvature on the target membrane, ESCRT-based vesicles are formed by the generation of positive curvature through constriction.

Exosome production in eukaryotic organisms is mainly a mechanism for intercellular and inter-organismal communication [160]. Proteomic analyses of exosomes revealed that they contain cytosolic and membrane-bound proteins, including antigen-presenting proteins, signaling receptors, tetraspanins and heat shock proteins, as well as donor cell-specific proteins [161], demonstrating their versatility in signal communication. They have also been observed to contain nucleic acids such as DNA [162] and RNA (including regulatory RNA) [163], though how these components are incorporated into budding exosomes is still being investigated. Since exosome-mediated interactions are still a relatively new field of research, there is very little known about how eukaryote-derived EVs operate in microbial communities. Most studies on the topic come from a medical perspective, but with their results we can still hypothesize about the role of exosomes in microbial communities. For example, the single-celled fungus, *Cryptococcus neoformans*, has been shown to secrete exosomes enriched with a polysaccharide that acts as a virulence factor in the host organism [164]. EVs can also be used as a nutrient source for marine heterotrophic organisms [165]. Therefore, a

more mutualistic function could be conveyed from other polysaccharide-associated exosomes (this idea of "public goods" is expanded on further in "1.3.2 Cargo and function of bacterial EVs"). From investigations with *Saccharomyces cerevisiae*, it was also shown that exosome production is linked to cell wall remodeling [166], implicating exosome production as a defense mechanism for cell wall stress.

Eukaryotic cells also produce EVs through outward budding directly from the plasma membrane, forming what are known as ectosomes (also sometimes called microvesicles) [167, 168]. Similar to exosome production, ectosome production starts with the clustering of cargo proteins, followed by the recruitment of proteins and other factors to stimulate membrane curvature and the final fission of the vesicle. However, the exact mechanism and factors of ectosome production is still being uncovered as ectosomes are still a relatively recent field of research. Ectosomes have been observed to be enriched in cholesterol, and depletion of cholesterol leads to reduced ectosome production [169], suggesting that lipid composition plays an important role in ectosome biogenesis. Several ESCRT complexes have also been implicated in ectosome release, such as ESCRT-I and Vps4 [170], though the mechanism remains to be elucidated. It has also been shown that Rho GTPase, RhoA, is involved in ectosome production as overexpression leads to a hypervesiculation phenotype and gene repression leads to a hypovesiculation phenotype [171]. This effect is caused by interactions with downstream effectors in the regulon that influence actin and cytoskeletal remodeling, rather than a direct effect of the GTPase as observed with Arf-family GTPases. However, Arf6 has also been implicated in the production of ectosomes. EV particles sedimented at lower speeds were observed to contain Arf6 and inhibition of Arf6 GTPase similarly leads to a hypovesiculation phenotype [172]. Rather than the recruitment of a coatomer complex to facilitate membrane budding, Arf6 mediates ectosome production through myosin activity at the plasma membrane [172]. Intriguingly, Arf6 activation was also observed to be involved with the packaging of microRNA into ectosomes [173]. This not only implies the direct involvement of an Arf-family GTPase in eukaryotic EV production, but also that EVs from eukaryotic cells have multiple mechanisms for their production. However, the majority of studies on ectosome release are conducted in human tumor cells, so whether these observations are universal across the eukaryotic domain still needs to be uncovered.

1.4 Bacterial extracellular vesicles: biogenesis, composition, and function

Bacteria, much like the other domains, also produce EVs into the surrounding milieu, allowing them to transfer different organic (and sometimes inorganic) compounds into their environment and to other cells. In recent years, bacterial secretion of EVs has been considered a type of secretion system for the cell (secretion system type zero) [174], its advantages being the protection given to the cargo as well as the unique ability to transfer lipids and hydrophobic compounds. However, unlike the well characterized orchestration of multiple protein complexes that coordinate the various membrane trafficking events in Eukaryotes, the machinery behind bacterial EV production remains elusive. They are known to produce vesicles that can take on a wide range of morphologies and cargo, but unravelling the mechanisms behind their production has not been as straight forward and appears to rely on many different factors [175–177]. Further, due to the different cell envelope conformations that bacteria take on (gram-negative versus gram-positive), there are multiple permutations of bacterial EV membrane and cargo. While a vast amount of new information has accumulated in the past decades, there is still no clear universal answer to how Bacteria produce EVs. Further, in

comparison to the vast amount of research on bacterial EVs in pathogenesis and medical applications, there have been few investigations focused on how these extracellular entities influence microbial communities or interactions between bacterial cells. Though EV production in the bacterial domain is known to be ubiquitous, there are still many open questions regarding their roles in environmental microbial systems.

1.4.1 Bacterial EV production and morphology

There remains no universal explanation regarding the production of EVs in the bacterial domain (also referred to as membrane vesicles). However, multiple studies have shown that specific factors are involved in the rate of EV production, suggesting that a combination of these factors likely produce EVs. Unlike eukaryotic vesicle production though, the factors that have been investigated do not require the expense of energy. This suggests a more passive method of EV production and perhaps that EV production is an innate feature of bacterial growth. While exceptions do exist among species, certain trends are apparent in EV production in the bacterial domain.

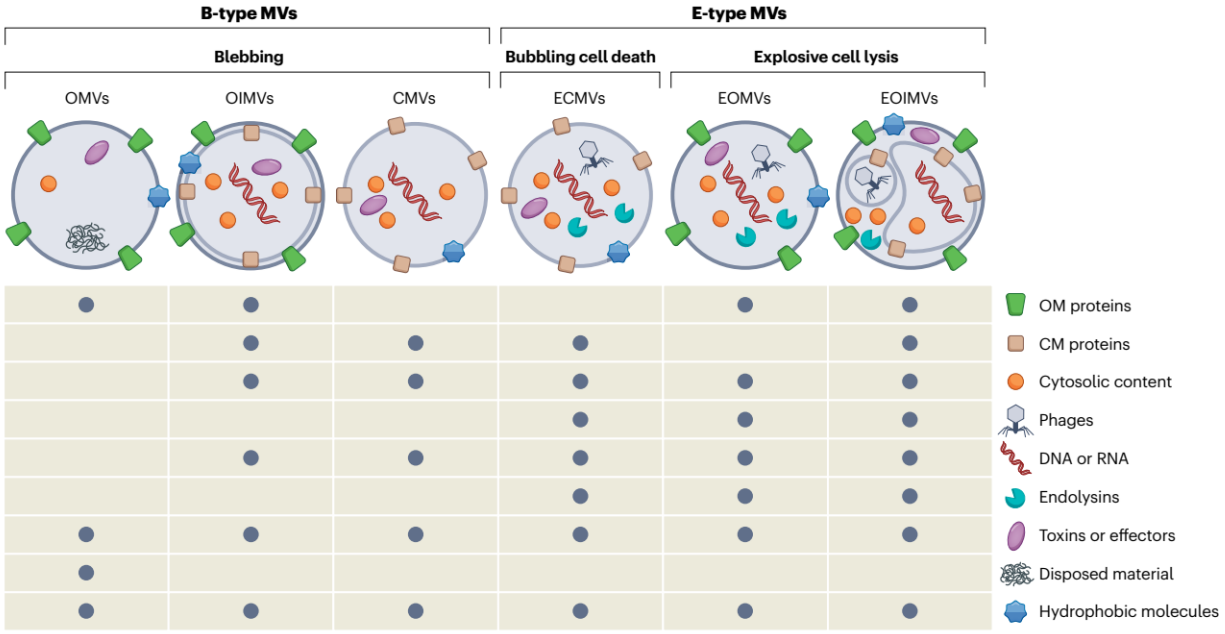

Figure 4. Morphologies and associated cargo of bacterial EVs (denoted as MVs in this figure). Bacteria have two distinct routes of EV production: blebbing type (B-type) and explosive type (E-type). B-type EVs derive from budding events on the cell membrane, while E-type EVs are linked to cell lysis, either triggered by autogenous endolysin expression or phage-induced. Each results in their own subclass of morphologies and the typical cargo that are associated with them. Outer membrane vesicles (OMVs) and outer-inner membrane vesicles (OIMVs) are produced by gram-negative bacteria, while cytosolic membrane vesicles (CMVs) are mostly produced by gram-positive bacteria. CMVs and OIMVs contain both cytosolic and periplasmic content, including nucleic acids. OMVs are typically devoid of cytosolic content. E-type EVs are produced by both gram-negative and gram-positive bacteria. Explosive cytosolic membrane vesicles (ECMVs) in gram-positive bacteria result from bubbling cell death, where the cell membrane forms vesicles contained within the rigid cell wall prior to complete lysis. Explosive outer membrane vesicles (EOMVs) and explosive outer-inner membrane vesicles (EOIMVs) are produced by gram-negative bacteria following explosive cell lysis. Figure adapted from [178].

In general, bacterial EVs can be divided into their different morphologies based on the mechanism of production and biochemical composition (Figure 4). EVs can be generated by either "blebbing" outer membranes of active cells (B-type EVs) or through phage or self-induced explosive cell lysis (E-type EVs) [178]. This difference is more apparent in

EVs of gram-negative bacteria, since the biochemical composition of E-type EVs in gram-positive bacteria are indistinguishable from B-type EVs. Gram-positive bacteria only have one membrane encapsulating their cytoplasm, so regardless of how EVs are produced, they will always contain cytoplasmic material, whereas gram-negative bacteria have multiple membranes with specialized spaces that they enclose. Therefore, we can also subdivide bacterial EVs into those produced by gram-negative and gram-positive bacteria.

Starting with gram-negative bacteria, the most studied type of bacterial EVs are outer membrane vesicles (OMV) that derive from the blebbing of the outer membrane [174, 176, 179]. OMVs typically contain compounds associated with the outer membrane and periplasm, and rarely contain cytoplasmic contents such as DNA, RNA, or ATP [178]. Several factors are involved in the production of OMVs. For example, disrupting specific protein complexes that anchor the outer membrane to the peptidoglycan layer leads to a hypervesiculation phenotype [180, 181], suggesting that OMV production is dependent on local regions of low outer membrane-peptidoglycan interaction [182]. In comparison to the outer membrane, OMVs from *E. coli* were observed to contain fewer lipoproteins, such as Lpp that is known to anchor the outer membrane to the peptidoglycan layer, further suggesting that outer membrane-peptidoglycan interactions influence OMV production [88, 183]. Another study showed that the accumulation of misfolded proteins in the periplasm by the deletion of a periplasmic chaperone/protease also leads to a hypervesiculation phenotype [184], suggesting that OMV production could be an alternative means of periplasmic turnover to alleviate the accumulation of potentially toxic compounds and periplasmic turgor. This is further supported by the observation of low molecular weight peptidoglycan fragments typically found inside OMVs from several different species [185, 186]. Another factor contributing to the production of OMVs is the presence of charged lipopolysaccharides (LPS) on the surface of gram-negative bacteria. OMVs from *Pseudomonas aeruginosa* were observed to only contain the negatively-charged B-band LPS [187], leading to the hypothesis that membrane curvature and subsequent EV production is a means to alleviate the electrostatic repulsion generated by the accumulation of charged LPS. A hypervesiculation phenotype was observed in *P. aeruginosa* cells producing only B-band LPS, and a hypovesiculation phenotype was observed when only producing the neutral A-band LPS [188], affirming this hypothesis in *P. aeruginosa*. It was also shown upon invasion, *Salmonella enterica* deacylates LPS, which increases vesicle production of OMVs lacking LPS with acyl groups [189]. The proposed reason was the change in geometry of the outer leaflet of the lipid bilayer, with deacylation forcing the outer leaflet to take on an inverted-cone shape that would be more conducive to higher membrane curvature [190]. While each factor has some exceptions among gram-negative bacteria, it is likely bacteria utilize a combination of the above-mentioned factors to produce OMVs.

Though the experiments outlining OMV production seemed to generate a fitting model for gram-negative bacterial EV biogenesis, they did not account for the gram-negative bacterial EVs that contain cytoplasmic molecules. For example, EVs from *P. aeruginosa* were observed to contain DNA, and it is proposed that breaks in the peptidoglycan layer allow for the outward protrusion of the inner membrane into the periplasm as well as cytoplasmic contents in the formation of EVs [187]. EVs purified from other gram-negative bacteria also carry DNA and RNA [191], suggesting that cytosolic-containing EVs from gram-negative bacteria are a typical occurrence. However, the model presented required that both membranes were present inside the EVs, which was first observed through transmission electron cryomicroscopy of

EVs from *Shewanella vesiculosa* [192]. These EVs showed the morphology of typical OMVs as well as double-membraned EVs with an electron-dense core. These were aptly named outer-inner membrane vesicles (OIMV) and have since been observed in other gram-negative bacteria [193]. More recently, however, the production of OIMVs from *S. vesiculosa* were observed to be dependent on prophage-mediated cell lysis [194], unveiling yet another type of bacterial EVs (EOIMVs) and route of production. It remains unclear if they carry out different functions than OIMVs, how different their biochemical composition is, and whether the other observed producers of OIMVs are prophage-dependent.

While it is under debate whether E-type EV production is a valid mechanism for EV production, they still represent a substantial biological entity in the extracellular space regardless of their production. Vesicle formation as the result of phage-induced lysis could potentially result in the majority of extracellular particles in a microbial system, considering that bacteriophages are biological entities with the highest abundance [195]. Like *S. vesiculosa*, other lytic activity has been shown to enhance the production of EVs in other Bacteria. Endolysins, which are typically bacteriophage-encoded hydrolases that cleave the cell wall to promote cell lysis, were first shown to be involved in the production of E-type EVs from *P. aeruginosa* [196]. Here, DNA stress induces the expression of a prophage-associated endolysin, triggering cell lysis and releasing cytosolic compounds into the extracellular milieu. The resulting membrane fragments re-form into vesicles, encapsulating the released compounds and presenting an alternative model to blebbing EVs in gram-negative bacteria. Further complicating the matter, deletion of the endolysin was only shown to elicit an EV production defect under the same DNA stress conditions, whereas under normal conditions, EV production from the endolysin knockout strain was comparable to the control. This suggests that multiple condition-dependent mechanisms exist for EV production in *P. aeruginosa*, and likely in other gram-negative bacteria as well [178, 194, 197]. Rather, lytic origins of EV production in *P. aeruginosa* is a stress response [198], likely conveying different functions than EVs produced under normal conditions. Surprisingly, this type of EV production was also observed in the gram-positive bacteria, *Bacillus subtilis*, where expression of prophage-encoded endolysins similarly induced EV production and cell lysis under stress conditions [199]. However, rather than EV production resulting from re-circularizing membrane fragments, EV production occurrs prior to lysis as membrane blebbing through holes generated in the external peptidoglycan layer. This effect is also condition-dependent, as no endolysin-dependent EV production was measured under non-stress conditions. Prophage-induced EV production was also observed in other gram-positive bacteria [200, 201], altogether implying that explosive EV production accounts for a significant percentage of bacterial EVs present in microbial systems.

Besides prophage-induced EV production, little is known about the production of EVs in gram-positive bacteria [202], though they are also known producers of EVs [203, 204]. Efforts to identify genes responsible for EV production have shown that deletion of specific global regulators has a negative effect on EV production [205–207], though the precise gene within the respective regulons has not been determined. There is also the observation of species-specific mechanisms of EV production, with the example of a modulin specific to *Staphylococcus aureus*, whose deletion resulted in an EV production defect [208]. Certain proteomic analysis of EVs from gram-positive bacteria show the enrichment of autolysins and other peptidoglycan-degrading proteins [203, 209, 210], suggesting that peptidoglycan

degradation may play a role in EV production. Alternatively, production of specific hydrophobic quinolones in *P. aeruginosa* are crucial for EV production [211], though the exact mechanism is unknown.

1.4.2 Cargo and functions of bacterial EVs

Considering that multiple factors and many different mechanisms have been implicated in the production of bacterial EVs, they have been also been shown to transport a diverse assortment of cargo and in turn mediate a diverse range of functions. While many studies have investigated the function of bacterial EVs in regards to their pathogenic effects on the host organism, I will not focus on the pathogenesis aspects of bacterial EVs, but rather focus on implications about cell biology and microbial ecology. For the most part, functionality can be analyzed based on the various cargo that are transported in EVs, such as DNA, RNA, proteins, and signaling molecules.

Multiple examples exist of DNA-harboring EVs from both gram-positive and gram-negative Bacteria [187, 194, 192, 165, 212], and even those transporting plasmids [213, 214]. However, with the recent discovery of E-type EVs in Bacteria [196, 194, 199], it remains unclear whether the presence of MV-associated DNA is generated through explosive cell lysis or actively packaged into budding vesicles [178]. In *S. aureus*, EVs that derive from prophage-induced lysis contain more DNA than wild type EVs [215], suggesting that prophage activity regulates the presence of MV-associated DNA, though it is uncertain if this trend exists in other Bacteria. Regardless of the nature of the production of DNA-containing EVs, they are a significant contributor to the amount of extracellular genetic material in environmental systems [165, 216], and have therefore been theorized to play roles in horizontal gene transfer and nutrient cycling. For example, EVs from the dominant marine cyanobacterium, *Prochlorococcus*, were found to contain fragmented DNA representing the majority of the genome [165]. It was estimated that around 10^{27} to 10^{28} vesicles could be produced daily by *Prochlorococcus* alone, each representing a potential vector for horizontal gene transfer. The transfer of DNA between cells was shown in *Acinetobacter baylyi* [217], confirming that EVs can indeed be sources for genetic exchange. Further, DNA (as well as the EV-associated RNA) is a valuable source of carbon, nitrogen and phosphorous. Growth of marine heterotrophic Bacteria was able to be sustained with *Prochlorococcus* EVs as the sole carbon source [165], suggesting a role for EVs in nutrient cycling.

The presence of RNA in bacterial EVs has been observed across the bacterial domain [191], and has unique implications since RNA can be used as food source, genetic material, and signaling compound. It was shown that *Prochlorococcus* EVs that contain RNA can be used as a carbon source by heterotrophs [165], though whether this is a result of the presence of RNA, DNA, or both is undetermined. EVs from multiple strains of *E. coli* were also identified to contain large abundancies of RNA [218, 219]. When compared to intracellular levels, both studies found an enrichment of tRNA fragments, RNA species that have been known to convey regulatory functions [220]. *P. aeruginosa* EVs were also observed to contain tRNA fragments as well as small RNAs (sRNA) [221], an RNA species capable of post-transcriptional regulation of specific genes through perfect or imperfect base-pairing [222]. The identification of these regulatory RNA species paints an alluring picture that RNA-associated EVs can be used as a means to influence the gene expression of the surrounding organisms, specifically in regards to pathogenesis. RNA is a highly unstable molecule, prone to degradation by abundant RNases. Packaging of RNA into EVs would provide them protection from

the environment and ensure their delivery to the target organism [191]. While small regulatory RNAs have been observed in some examples of pathogenic Bacteria EVs [223, 224, 221], few studies have demonstrated that EVs themselves elicit a specific sRNA-dependent regulation on another organism. In the thorough characterization of RNA-associated EVs from *Vibrio fischerii*, it was found that the packaging of a specific sRNA in EVs functioned to suppress the immune responses of its eukaryotic symbiotic partner and allow for the colonization of the host organism [225]. This not only confirmed that EV-associated sRNA are regulatory in the recipient organism, but also demonstrates the ability for EVs to mediate cross-talk across domains. Since most investigations into EV-dependent trafficking of RNA focus solely on pathogenesis, inter-bacterial cross talk of the same kind has not been investigated thus far. It therefore remains unknown whether this type of gene regulation is prominent in microbial ecosystems.

Bacterial EVs have also been observed to play directly antagonistic roles for cell-cell interactions via the enrichment of proteinacious toxins. Stress-induced EVs from *P. aeruginosa* were observed to be enriched with endolysins, which has been proven to be crucial for EV production [198, 196]. EV-associated endolysins remain active upon secretion with EVs and are able to lyse other bacterial cells [226]. The secretion of EVs with lethal effects has also been reported in other gram-negative bacteria [227], as well as within the context of pathogenic interactions between Bacteria and eukaryotic host [228]. More recently, the predatory Bacteria, *Lysobacter enzymogenes*, has been observed to express antifungal proteins that localize to EVs, suggesting the use of bacterial EVs to interact and kill prey [229]. However, the exact role of EV-associated toxin release in the context of microbial ecology is still unclear, since many studies focus on Bacteria as antagonists to eukaryotic organisms. Since there is a link between stress conditions and EV-associated endolysins, lytic EVs could provide a means for population control during times of stress, or facilitate the release of nutrients from other organisms.

Bacterial EVs also play a role in the secretion and dispersal of hydrophobic compounds in aqueous environments. For example, pseudomonas quinolone signal (PQS) is a severely hydrophobic signaling molecule involved in quorum sensing in *P. aeruginosa* [230] that was found to be enriched in *P. aeruginosa* EVs and able to convey a quorum sensing signal [211]. Other bacterial EVs have also been observed to package quorum sensing-related signaling molecules [231, 232], suggesting that EV-mediated quorum sensing may be a typical mechanism in the bacterial domain.

Proteomic analyses of EVs from different bacterial organisms have similarly demonstrated an enrichment of outer membrane-associated proteins such as transporters, solute-binding proteins, and metabolic degrading proteins [193, 233–237], suggesting that EVs can perhaps be a tool for nutrient sequestration. For example, comparisons between outer membrane proteins and EV-associated proteins in *Bacterioides fragilis* and *Bacterioides thetaiotaomicron* revealed an enrichment of glycosidases and proteases [237]. It was later confirmed that these polysaccharide degrading enzymes associated with EVs of *Bacterioides* were active [238], confirming a role for EVs in nutrient acquisition. Similar results were observed in *Prochlorococcus*, where enzymatic activity could be measured in EVs [233]. These have led to the hypothesis that EV production in a microbial community and their subsequent nutrient acquisition properties can be used as “public goods” that benefit the whole community [239]. However, this was slightly challenged by the finding that EV uptake can be organism specific depending on the producing organism [233], suggesting that not all EV-sequestered nutrients are publicly available but rather available to a specific subpopulation. Further, since each EV-

producing organism in a microbial community encodes for unique polysaccharide utilization loci, meaning each organism specializes in the degradation of specific carbon sources, each EV in turn would allow for the degradation and uptake of nutrients that an organism may not normally have access to.

EV-virus interactions have been observed in multiple bacterial organisms [165, 240, 241], suggesting that EVs can play a role in phage defense. Phages initiate interaction with their bacterial host through the outer membrane, which EVs are encapsulated by. It has therefore been suggested that EVs act as decoys for phages to inject their genome into, thereby deactivating the phage and preventing infection of the target host organism. In testing the effect of *E. coli* EVs on T4 phage, incubation of EVs and phage significantly reduced the number of plaque forming units [240], suggesting that EV release is an efficient method of viral defense. Similar inhibitory effects of phages by bacterial EVs were observed in *P. aeruginosa* [241]. However, studies that explore this interaction further are limited, leaving many questions unanswered for EV-virus interactions.

1.5 Archaeal membrane trafficking: a key question in eukaryogenesis

As we have seen thus far, research into eukaryotic and bacterial vesicle production is rather extensive; comparatively, studies that have looked into archaeal vesicle production are represented by a handful of papers and by only a few model organisms [242]. Archaea make up significant proportions of populations in microbial ecosystems, and just how bacterial EVs have been shown to potentially influence these environments [165], the same can likely be said about archaeal EVs. As was described earlier, membrane trafficking intracellularly and extracellularly is a crucial element to eukaryotic cell biology. The capacity for which Archaea are able to similarly coordinate the trafficking of membranes can shed light onto the origins of this seemingly eukaryote-exclusive feature and expand upon what we consider the functional potential of the archaeal domain. The question of the relative complexity of FECA requires a more comprehensive understanding of archaeal cell biology to draw conclusions about how these respective features arose in eukaryotes. So for the case of vesicle trafficking (intracellular and extracellularly), perhaps observing the mechanisms that Archaea utilize to produce vesicles can grant us a better foundation for constructing the model of eukaryogenesis.

1.5.1 Archaeal EVs

EVs from the archaeal domain were first observed from the thermophilic *Sulfolobus* (phylum *Thermoprotea*) in the year 2000, which were associated with proteinaceous toxins [91]. The small particles observed from culture supernatants were 90 – 180 nm in diameter and associated with S-layer protein, suggesting that they derived from the respective cell envelopes. Around a decade later, the first proteomic analysis of archaeal EVs was published, focusing on three *Solfolobus* species, *S. solfataricus*, *S. acidocaldarius* and *S. tokodaii* [243]. Cell-free supernatants from all three species were observed to contain similar S-layer- and membrane-bound spherical particles that ranged from 90 – 230 nm in diameter, similar to what was observed in the initial study. They reported that the amount of EVs in preparations was low in early exponential, but increased with growth phase. Biochemical characterization demonstrated an enrichment of specific lipid types and proteins in comparison to the cytoplasmic membrane. Surprisingly, ESCRT-III-like proteins and a Vps4 ortholog were identified to be abundant in EV preparations from all three *Sulfolobus* species [243], providing the first hints that Archaea could be using ESCRT-like mechanisms for membrane remodeling similar to Eukaryota.

The ESCRT-like machinery (ESCRT-III-like proteins and Vps4 homolog) encoded by *Sulfolobus* had previously been characterized to play a crucial role in cell division [244], so it was curious that these components were identified in EV preparations. In fact, the link between the ESCRT-like machinery and EV production was not uncovered until 2021 with the investigation of EVs from *S. islandicus* and *Saccharolobus solfataricus* [74]. Proteomic analysis of EVs identified all components of the respective ESCRT-like machinery, and silencing of the majority of these genes leads to a hypovesiculation phenotype. Further, overexpression of specific components of the ESCRT-like machinery leads to hypervesiculation phenotypes. It was concluded that cell division and EV production are temporally linked and both utilize the ESCRT-like system. Much like *Prochlorococcus* EVs, EVs from *Sulfolobus* were also observed for the first time to contain genomic and plasmid DNA and was able to act as a nutrient source, suggesting that *Sulfolobus* could use EVs as a means for horizontal gene transfer or "public goods".

EVs from *Euryarchaeota* were first described in the hyperthermophilic and anaerobic order of *Thermococcales* in 2008, as genomic DNA-containing contaminants of viral preparations [245], and in 2011 as plasmid DNA-associated virus-like particles [246]. In a follow up study focusing on the EVs of *T. kodakaraensis* and *T. gammatolerans*, electron microscopy revealed the presence of spherical objects around 100 nm in diameter similarly associated with S-layer [247]. Lipid and protein analysis also showed that EVs had a different biochemical composition compared to the cell envelope. Between the two organisms tested, the only EV-associated protein found in common belonged to a substrate-binding protein family associated with ABC transporters, which curiously was also identified in *Sulfolobus* EVs [243]. The 2013 study was also able to demonstrate the ability for EVs in *T. kodakarensis* to not only protect DNA from DNase digestion, but also to transport plasmid DNA between cells [246], the first time that EV-mediated DNA transfer was shown in Archaea. It was also later shown that *Thermococcales* EVs had the potential to transport viral genomes between cells [248], suggesting a role for archaeal EVs in viral life cycles. Similar DNA-containing EVs were also observed with *T. onnurineus*, but RNA was also reported be associated and protected by EVs [249], though no further characterization of the RNA content was conducted. Other *Thermococcales* organisms were shown to produce specialized EVs that adhere to the cell surface containing elemental sulfur [250], and are predicted to be a detoxification system. ESCRT-like homologs are not encoded by *Euryarchaeota* [251] and no hints for EV-forming proteins were identified in proteomic analysis of EV preparations from *Thermococcales*, leaving the mechanisms for EV production in *Thermococcales* undetermined.

EVs in haloarchaea (*Euryarchaeota*) were first hinted at in 2013, where UV stress induced a distinct population of small particles to appear during flow cytometry analysis in *Haloferax volcanii* [253]. In 2017, a unique type of plasmid-containing EVs, plasmid vesicles (PV), were identified in *Halorubrum lacusprofundi* that was able to transfer plasmid DNA between cells [252]. Unlike the plasmid-associated EVs of *Thermococcales* [246, 248], *Hrr. lacusprofundi* PVs also contained plasmid-encoded genes, similar to membrane-bound viruses. *Hrr. lacusprofundi* cells that did not contain the specialized plasmid, pR1SE, were also shown to produce EVs that had a distinct protein composition compared to the cell envelope. Among the EV-associated protein subpopulation was a small single-domain GTPase as well as a β-propeller domain-containing protein, and so a protocoatomer-like mechanism was suggested for haloarchaeal EV

production [252]. However, further evidence for an archaeal protocoatomer-like mechanism for EV production has not been observed thus far.

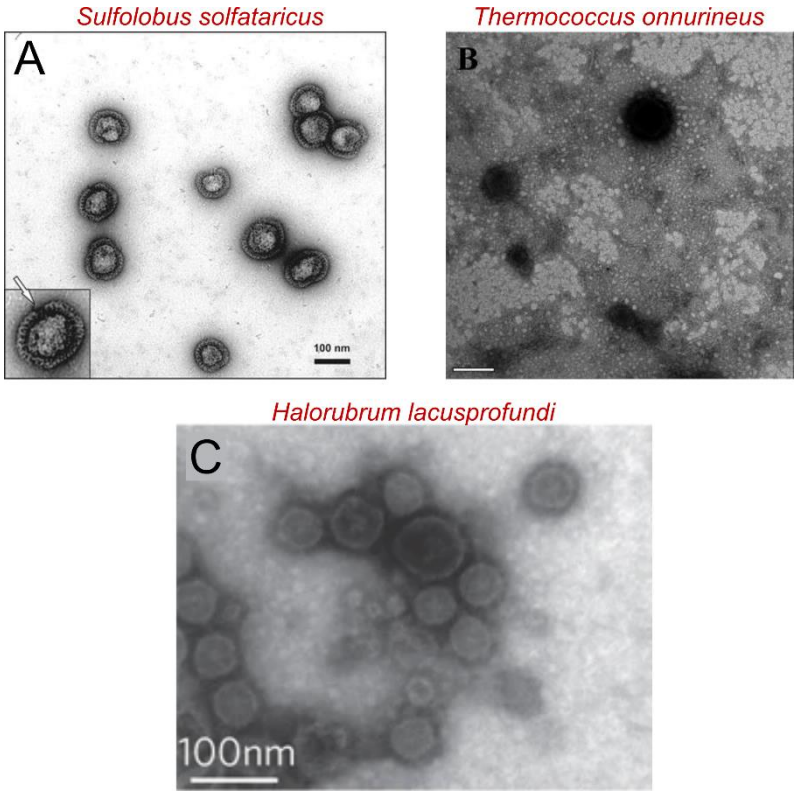

Figure 5. Transmission electron micrographs of archaeal EVs. (A) EVs from *Sulfolobus solfataricus* (phylum *Thermoprotea*). Scale bar indicates 100 nm. Figure adapted from [243]. **(B)** EVs from *Thermococcus onnurineus* (phylum *Euryarchaeota*). Scale bar indicates 100 nm. Figure adapted from [249]. **(C)** Evs from *Halorubrum lacusprofundi* (phylum *Euryarchaeota*). Scale bar indicates 100 nm. Figure adapted from [252].

1.5.2 Traces of Eukaryotes' past

From the studies of EV-producing archaeal organisms so far, we can already see a trend of eukaryotic-like mechanisms being deployed for membrane remodeling, which has not been observed for bacterial EV production. While it has been observed that ESCRT-like homologs are encoded in archaeal genomes [251], it is still uncertain whether these distantly related proteins function in the same way as their eukaryotic counterparts. EV production in *S. islandicus* was shown to be dependent on its ESCRT-like cell division mechanism [74], demonstrating that archaeal ESCRT-like proteins similarly mediate membrane remodeling mechanisms. While this provided evidence that the eukaryotic ESCRT machinery derives its roots from archaeal ancestors, it did not provide any conclusions for other membrane remodeling systems like the endomembrane system.

Currently, the evolutionary origins for flexibility and sophistication of the eukaryotic endomembrane system are unknown and remain a missing puzzle piece in the question of eukaryogenesis [254]. The endomembrane system describes the intracellular trafficking of membranes and cargo between the endoplasmic reticulum, Golgi, trans-Golgi network, and endosomes [94, 93], organelles that were likely autogenous in origin [255]. Each node of the endomembrane system utilizes a similar mechanism of coat recruitment by an Arf-family GTPase, with paralogous

protein families and protein structures involved [139]. The organelle paralogy hypothesis describes the emergence of these autogenous organelles through the duplication and neofunctionalization of a previous membrane remodeling system [256, 255]. Tracing this back, one could theoretically back-calculate the emergence of autogenous organelles based on the timing of gene duplication events. In fact, this predicts that the last eukaryotic common ancestor already contained several forms of the prototypical membrane trafficking machinery [254]. Other hypotheses for the emergence of the eukaryotic endomembrane system exist that use the EV production processes of Bacteria to explain the presence of the endomembrane system [257]. This hypothesis suggests that vesiculation of the bacterial endosymbiont acted as the first endomembrane system, which eventually diversified into the modern eukaryotic system observed today. While this does provide an explanation of intracellular vesiculation, it does not take into account the proteins involved in the highly coordinated endomembrane system, homologs of which are not identified in bacterial genomes.

The current evidence points more towards an archaeal ancestry of the endomembrane system [138], with the most compelling evidence arising from the abundance of eukaryotic signature proteins encoded in the genomes of *Asgardarchaeota* [33, 38]. The presence of small single-domain GTPases with similar motif sequences to Arf-family GTPases in *Lokiarchaeota* [138] as well as putative COP-I homologues in *Heimdallarchaeota* [38] strongly suggests that eukaryotic membrane trafficking derives from Archaea. However, as was the problem originally with the identification of ESCRT-like homologues in the archaeal domain, it remains uncertain if the protocoatomer-like homologues conveyed similar functionality or whether the functions were acquired during the emergence of the eukaryotic domain. Further, the question of the original function of these systems in the archaeal domain remains uncertain, and exploring this facet of archaeal cell biology could help us paint a more comprehensive picture of the enigmatic process of eukaryogenesis.

1.6 Aim of this dissertation

Though EVs are produced by all domains of life, the impact of EVs on microbial communities is not entirely understood. Their ability to selectively transport cargo between cells implies that EVs play significant roles in microbial ecology. While EV-mediated communication is well established in the interactions between pathogenic Bacteria and eukaryotic host organisms, little is known about EV-mediated communication in microbe-microbe interactions. Additionally, the mechanisms behind archaeal EV production in organisms without an ESCRT-like system remain unresolved. Uncovering such mechanisms can broaden our understanding of the functional potential of archaeal cell biology and potentially trace back the evolutionary history of eukaryotic-like features, specifically the complexification of membrane trafficking mechanisms.

In this dissertation, I provide the first characterization of EVs enriched with RNA in the archaeal domain, and explore their role in microbe-microbe interactions. I also uncover elements of the mechanism driving EV production in haloarchaea and investigate its conservation within the archaeal domain. The specific aims of the dissertation are:

1. To establish a standardized method for isolating and purifying EVs from archaeal cultures.
2. To characterize the biochemical composition EV from haloarchaea in order to explore their potential function and mechanism of production.

3. To investigate how the production and composition of EVs change depending on growth conditions, and how this may impact intercellular interactions within a microbial community.

REFERENCES

1. Fitch WM, Margoliash E (1967) Construction of phylogenetic trees. Science 155:279–284. https://doi.org/10.1126/science.155.3760.279
2. Woese CR, Fox GE (1977) Phylogenetic structure of the prokaryotic domain: the primary kingdoms. Proc Natl Acad Sci U S A 74:5088–5090. https://doi.org/10.1073/pnas.74.11.5088
3. Koga Y, Morii H (2007) Biosynthesis of ether-type polar lipids in archaea and evolutionary considerations. Microbiol Mol Biol Rev 71:97–120. https://doi.org/10.1128/MMBR.00033-06
4. Albers S-V, Meyer BH (2011) The archaeal cell envelope. Nat Rev Microbiol 9:414–426. https://doi.org/10.1038/nrmicro2576
5. Schmitt E, Coureux P-D, Kazan R et al. (2020) Recent Advances in Archaeal Translation Initiation. Front Microbiol 11:584152. https://doi.org/10.3389/fmicb.2020.584152
6. Robinson NP, Bell SD (2005) Origins of DNA replication in the three domains of life. FEBS J 272:3757–3766. https://doi.org/10.1111/j.1742-4658.2005.04768.x
7. Baker BJ, Anda V de, Seitz KW et al. (2020) Diversity, ecology and evolution of Archaea. Nat Microbiol 5:887–900. https://doi.org/10.1038/s41564-020-0715-z
8. Spang A, Caceres EF, Ettema TJG (2017) Genomic exploration of the diversity, ecology, and evolution of the archaeal domain of life. Science 357. https://doi.org/10.1126/science.aaf3883
9. Kan J, Clingenpeel S, Macur RE et al. (2011) Archaea in Yellowstone Lake. ISME J 5:1784–1795. https://doi.org/10.1038/ismej.2011.56
10. Chaban B, Ng SYM, Jarrell KF (2006) Archaeal habitats--from the extreme to the ordinary. Can J Microbiol 52:73–116. https://doi.org/10.1139/w05-147
11. Robertson CE, Harris JK, Spear JR et al. (2005) Phylogenetic diversity and ecology of environmental Archaea. Curr Opin Microbiol 8:638–642. https://doi.org/10.1016/j.mib.2005.10.003
12. Wang H, Bier R, Zgleszewski L et al. (2020) Distinct Distribution of Archaea From Soil to Freshwater to Estuary: Implications of Archaeal Composition and Function in Different Environments. Front Microbiol 11:576661. https://doi.org/10.3389/fmicb.2020.576661
13. Probst AJ, Auerbach AK, Moissl-Eichinger C (2013) Archaea on human skin. PLoS One 8:e65388. https://doi.org/10.1371/journal.pone.0065388
14. Karner MB, DeLong EF, Karl DM (2001) Archaeal dominance in the mesopelagic zone of the Pacific Ocean. Nature 409:507–510. https://doi.org/10.1038/35054051
15. Santoro AE, Richter RA, Dupont CL (2019) Planktonic Marine Archaea. Ann Rev Mar Sci 11:131–158. https://doi.org/10.1146/annurev-marine-121916-063141
16. Offre P, Spang A, Schleper C (2013) Archaea in biogeochemical cycles. Annu Rev Microbiol 67:437–457. https://doi.org/10.1146/annurev-micro-092412-155614
17. Woese CR, Kandler O, Wheelis ML (1990) Towards a natural system of organisms: proposal for the domains Archaea, Bacteria, and Eucarya. Proc Natl Acad Sci U S A 87:4576–4579. https://doi.org/10.1073/pnas.87.12.4576
18. Rinke C, Chuvochina M, Mussig AJ et al. (2021) A standardized archaeal taxonomy for the Genome Taxonomy Database. Nat Microbiol 6:946–959. https://doi.org/10.1038/s41564-021-00918-8

19. SMITH PH, HUNGATE RE (1958) Isolation and characterization of Methanobacterium ruminantium n. sp. Journal of Bacteriology 75:713–718. https://doi.org/10.1128/jb.75.6.713-718.1958

20. Oren A (2005-2010) E uryarchaeota. In: John Wiley & Sons L (ed) Encyclopedia of life sciences. John Wiley & Sons, London, New York, pp 1–17

21. Laso-Pérez R, Wegener G, Knittel K et al. (2016) Thermophilic archaea activate butane via alkyl-coenzyme M formation. Nature 539:396–401. https://doi.org/10.1038/nature20152

22. Huber H, Hohn MJ, Rachel R et al. (2002) A new phylum of Archaea represented by a nanosized hyperthermophilic symbiont. Nature 417:63–67. https://doi.org/10.1038/417063a

23. Krause S, Bremges A, Münch PC et al. (2017) Characterisation of a stable laboratory co-culture of acidophilic nanoorganisms. Sci Rep 7:3289. https://doi.org/10.1038/s41598-017-03315-6

24. La Cono V, Messina E, Rohde M et al. (2020) Symbiosis between nanohaloarchaeon and haloarchaeon is based on utilization of different polysaccharides. Proc Natl Acad Sci U S A 117:20223–20234. https://doi.org/10.1073/pnas.2007232117

25. Hamm JN, Erdmann S, Eloe-Fadrosh EA et al. (2019) Unexpected host dependency of Antarctic Nanohaloarchaeota. Proc Natl Acad Sci U S A 116:14661–14670. https://doi.org/10.1073/pnas.1905179116

26. Dombrowski N, Lee J-H, Williams TA et al. (2019) Genomic diversity, lifestyles and evolutionary origins of DPANN archaea. FEMS Microbiol Lett 366. https://doi.org/10.1093/femsle/fnz008

27. Heimerl T, Flechsler J, Pickl C et al. (2017) A Complex Endomembrane System in the Archaeon Ignicoccus hospitalis Tapped by Nanoarchaeum equitans. Front Microbiol 8:1072. https://doi.org/10.3389/fmicb.2017.01072

28. Hamm JN, Liao Y, Kügelgen A von et al. (2023) The parasitic lifestyle of an archaeal symbiont

29. Moody ERR, Mahendrarajah TA, Dombrowski N et al. (2022) An estimate of the deepest branches of the tree of life from ancient vertically evolving genes. Elife 11. https://doi.org/10.7554/eLife.66695

30. Aouad M, Flandrois J-P, Jauffrit F et al. (2022) A divide-and-conquer phylogenomic approach based on character supermatrices resolves early steps in the evolution of the Archaea. BMC Ecol Evol 22:1. https://doi.org/10.1186/s12862-021-01952-0

31. Bergsten J (2005) A review of long-branch attraction. Cladistics 21:163–193. https://doi.org/10.1111/j.1096-0031.2005.00059.x

32. Aouad M, Taib N, Oudart A et al. (2018) Extreme halophilic archaea derive from two distinct methanogen Class II lineages. Mol Phylogenet Evol 127:46–54. https://doi.org/10.1016/j.ympev.2018.04.011

33. Spang A, Saw JH, Jørgensen SL et al. (2015) Complex archaea that bridge the gap between prokaryotes and eukaryotes. Nature 521:173–179. https://doi.org/10.1038/nature14447

34. Seitz KW, Lazar CS, Hinrichs K-U et al. (2016) Genomic reconstruction of a novel, deeply branched sediment archaeal phylum with pathways for acetogenesis and sulfur reduction. ISME J 10:1696–1705. https://doi.org/10.1038/ismej.2015.233

35. Zaremba-Niedzwiedzka K, Caceres EF, Saw JH et al. (2017) Asgard archaea illuminate the origin of eukaryotic cellular complexity. Nature 541:353–358. https://doi.org/10.1038/nature21031

36. MacLeod F, Kindler GS, Wong HL et al. (2019) Asgard archaea: Diversity, function, and evolutionary implications in a range of microbiomes. AIMS Microbiol 5:48–61. https://doi.org/10.3934/microbiol.2019.1.48

37. Liu Y, Makarova KS, Huang W-C et al. (2021) Expanded diversity of Asgard archaea and their relationships with eukaryotes. Nature 593:553–557. https://doi.org/10.1038/s41586-021-03494-3

38. Eme L, Tamarit D, Caceres EF et al. (2023) Inference and reconstruction of the heimdallarchaeial ancestry of eukaryotes. Nature. https://doi.org/10.1038/s41586-023-06186-2

39. Imachi H, Nobu MK, Nakahara N et al. (2020) Isolation of an archaeon at the prokaryote-eukaryote interface. Nature 577:519–525. https://doi.org/10.1038/s41586-019-1916-6

40. Rodrigues-Oliveira T, Wollweber F, Ponce-Toledo RI et al. (2023) Actin cytoskeleton and complex cell architecture in an Asgard archaeon. Nature 613:332–339. https://doi.org/10.1038/s41586-022-05550-y

41. Koonin EV, Yutin N (2014) The dispersed archaeal eukaryome and the complex archaeal ancestor of eukaryotes. Cold Spring Harb Perspect Biol 6:a016188. https://doi.org/10.1101/cshperspect.a016188

42. Guy L, Ettema TJG (2011) The archaeal 'TACK' superphylum and the origin of eukaryotes. Trends Microbiol 19:580–587. https://doi.org/10.1016/j.tim.2011.09.002

43. Baum DA, Baum B (2014) An inside-out origin for the eukaryotic cell. BMC Biol 12:76. https://doi.org/10.1186/s12915-014-0076-2

44. Eichler J (2023) Halobacterium salinarum: Life with more than a grain of salt. Microbiology (Reading) 169. https://doi.org/10.1099/mic.0.001327

45. Oren A (2002) Diversity of halophilic microorganisms: environments, phylogeny, physiology, and applications. J Ind Microbiol Biotechnol 28:56–63. https://doi.org/10.1038/sj/jim/7000176

46. Andrei A-Ş, Banciu HL, Oren A (2012) Living with salt: metabolic and phylogenetic diversity of archaea inhabiting saline ecosystems. FEMS Microbiol Lett 330:1–9. https://doi.org/10.1111/j.1574-6968.2012.02526.x

47. Lanyi JK (1974) Salt-dependent properties of proteins from extremely halophilic bacteria. Bacteriol Rev 38:272–290. https://doi.org/10.1128/br.38.3.272-290.1974

48. Roberts MF (2005) Organic compatible solutes of halotolerant and halophilic microorganisms. Saline Syst 1:5. https://doi.org/10.1186/1746-1448-1-5

49. Shahmohammadi HR, Asgarani E, Terato H et al. (1998) Protective roles of bacterioruberin and intracellular KCl in the resistance of Halobacterium salinarium against DNA-damaging agents. J Radiat Res 39:251–262. https://doi.org/10.1269/jrr.39.251

50. Mullakhanbhai MF, Larsen H (1975) Halobacterium volcanii spec. nov., a Dead Sea halobacterium with a moderate salt requirement. Arch Microbiol 104:207–214. https://doi.org/10.1007/BF00447326

51. Charlebois RL, Hofman JD, Schalkwyk LC et al. (1989) Genome mapping in halobacteria. Can J Microbiol 35:21–29. https://doi.org/10.1139/m89-004

52. Dyall-Smith, Michael (2009) The Halohandbook: Protocols for haloarchaeal genetics

53. Lam WL, Doolitle WF (1989) Shuttle vectors for the archaebacterium halobacterium volcanii. Proc. Natl. Acad. Sci. USA 86:5478–5482

54. Cline SW, Schalkwyk LC, Doolittle WF (1989) Transformation of the archaebacterium Halobacterium volcanii with genomic DNA. Journal of Bacteriology 171:4987–4991. https://doi.org/10.1128/jb.171.9.4987-4991.1989

55. Bitan-Banin G, Ortenberg R, Mevarech M (2003) Development of a gene knockout system for the halophilic archaeon Haloferax volcanii by use of the pyrE gene. Journal of Bacteriology 185:772–778. https://doi.org/10.1128/JB.185.3.772-778.2003

56. Allers T, Ngo H-P, Mevarech M et al. (2004) Development of additional selectable markers for the halophilic archaeon Haloferax volcanii based on the leuB and trpA genes. Appl Environ Microbiol 70:943–953. https://doi.org/10.1128/AEM.70.2.943-953.2004

57. Maier L-K, Stachler A-E, Brendel J et al. (2019) The nuts and bolts of the Haloferax CRISPR-Cas system I-B. RNA Biol 16:469–480. https://doi.org/10.1080/15476286.2018.1460994

58. Alarcón-Schumacher T, Naor A, Gophna U et al. (2022) Isolation of a virus causing a chronic infection in the archaeal model organism Haloferax volcanii reveals antiviral activities of a provirus. Proc Natl Acad Sci U S A 119:e2205037119. https://doi.org/10.1073/pnas.2205037119

59. Pühler G, Leffers H, Gropp F et al. (1989) Archaebacterial DNA-dependent RNA polymerases testify to the evolution of the eukaryotic nuclear genome. Proc Natl Acad Sci U S A 86:4569–4573. https://doi.org/10.1073/pnas.86.12.4569

60. Kimura M, Arndt E, Hatakeyama T et al. (1989) Ribosomal proteins in halobacteria. Can J Microbiol 35:195–199. https://doi.org/10.1139/m89-030

61. Rivera MC, Lake JA (1992) Evidence that eukaryotes and eocyte prokaryotes are immediate relatives. Science 257:74–76. https://doi.org/10.1126/science.1621096

62. Lake JA, Henderson E, Oakes M et al. (1984) Eocytes: a new ribosome structure indicates a kingdom with a close relationship to eukaryotes. Proc Natl Acad Sci U S A 81:3786–3790. https://doi.org/10.1073/pnas.81.12.3786

63. Langer D, Hain J, Thuriaux P et al. (1995) Transcription in archaea: similarity to that in eucarya. Proc Natl Acad Sci U S A 92:5768–5772. https://doi.org/10.1073/pnas.92.13.5768

64. Yutin N, Puigbò P, Koonin EV et al. (2012) Phylogenomics of prokaryotic ribosomal proteins. PLoS One 7:e36972. https://doi.org/10.1371/journal.pone.0036972

65. Barry ER, Bell SD (2006) DNA replication in the archaea. Microbiol Mol Biol Rev 70:876–887. https://doi.org/10.1128/MMBR.00029-06

66. Williams TA, Cox CJ, Foster PG et al. (2020) Phylogenomics provides robust support for a two-domains tree of life. Nat Ecol Evol 4:138–147. https://doi.org/10.1038/s41559-019-1040-x

67. Eme L, Spang A, Lombard J et al. (2017) Archaea and the origin of eukaryotes. Nat Rev Microbiol 15:711–723. https://doi.org/10.1038/nrmicro.2017.133

68. Javaux EJ (2016) Eukaryotes, Appearance and Early Evolution of. In: Gargaud M, Irvine WM, Amils R et al. (eds) Encyclopedia of astrobiology, Living Reference Work. Springer Berlin Heidelberg, Berlin, Heidelberg, pp 1–5

69. Martin WF, Garg S, Zimorski V (2015) Endosymbiotic theories for eukaryote origin. Philos Trans R Soc Lond B Biol Sci 370:20140330. https://doi.org/10.1098/rstb.2014.0330

70. Baum B, Baum DA (2020) The merger that made us. BMC Biol 18:72. https://doi.org/10.1186/s12915-020-00806-3

71. Ettema TJG, Lindås A-C, Bernander R (2011) An actin-based cytoskeleton in archaea. Mol Microbiol 80:1052–1061. https://doi.org/10.1111/j.1365-2958.2011.07635.x

72. Bernander R, Lind AE, Ettema TJG (2011) An archaeal origin for the actin cytoskeleton: Implications for eukaryogenesis. Commun Integr Biol 4:664–667. https://doi.org/10.4161/cib.16974

73. Nunoura T, Takaki Y, Kakuta J et al. (2011) Insights into the evolution of Archaea and eukaryotic protein modifier systems revealed by the genome of a novel archaeal group. Nucleic Acids Res 39:3204–3223. https://doi.org/10.1093/nar/gkq1228

74. Liu J, Cvirkaite-Krupovic V, Commere P-H et al. (2021) Archaeal extracellular vesicles are produced in an ESCRT-dependent manner and promote gene transfer and nutrient cycling in extreme environments. ISME J 15:2892–2905. https://doi.org/10.1038/s41396-021-00984-0

75. Philippe H, Vienne DM de, Ranwez V et al. (2017) Pitfalls in supermatrix phylogenomics. EJT. https://doi.org/10.5852/ejt.2017.283

76. Holm L, Laiho A, Törönen P et al. (2023) DALI shines a light on remote homologs: One hundred discoveries. Protein Sci 32:e4519. https://doi.org/10.1002/pro.4519

77. Carpentier M, Chomilier J (2019) Protein multiple alignments: sequence-based versus structure-based programs. Bioinformatics 35:3970–3980. https://doi.org/10.1093/bioinformatics/btz236

78. Moi D, Bernard C, Steinegger M et al. (2023) Structural phylogenetics unravels the evolutionary diversification of communication systems in gram-positive bacteria and their viruses

79. Wolf P (1967) The nature and significance of platelet products in human plasma. Br J Haematol 13:269–288. https://doi.org/10.1111/j.1365-2141.1967.tb08741.x

80. Mergenhagen SE, Bladen HA, Hsu KC (1966) Electron microscopic localization of endotoxic lipopolysaccharide in gram-negative organisms. Ann N Y Acad Sci 133:279–291. https://doi.org/10.1111/j.1749-6632.1966.tb52371.x

81. Grillo MA (1970) Extracellular synaptic vesicles in the mouse heart. J Cell Biol 47:547–553

82. Aaronson S, Behrens U, Orner R et al. (1971) Ultrastructure of intracellular and extracellular vesicles, membranes, and myelin figures produced by Ochromonas danica. Journal of Ultrastructure Research 35:418–430. https://doi.org/10.1016/S0022-5320(71)80003-5

83. Eda T, Kanda Y, Mori C et al. (1977) Extracellular membranous structures in a stable L-form of Staphylococcus aureus. Journal of General Microbiology 103:189–191. https://doi.org/10.1099/00221287-103-1-189

84. Harding C, Heuser J, Stahl P (1983) Receptor-mediated endocytosis of transferrin and recycling of the transferrin receptor in rat reticulocytes. J Cell Biol 97:329–339. https://doi.org/10.1083/jcb.97.2.329

85. Pan BT, Johnstone RM (1983) Fate of the transferrin receptor during maturation of sheep reticulocytes in vitro: selective externalization of the receptor. Cell 33:967–978. https://doi.org/10.1016/0092-8674(83)90040-5

86. Knox KW, Vesk M, Work E (1966) Relation between excreted lipopolysaccharide complexes and surface structures of a lysine-limited culture of Escherichia coli. Journal of Bacteriology 92:1206–1217. https://doi.org/10.1128/jb.92.4.1206-1217.1966

87. Mayrand D, Grenier D (1989) Biological activities of outer membrane vesicles. Can J Microbiol 35:607–613. https://doi.org/10.1139/m89-097

88. Wensink J, Witholt B (1981) Outer-membrane vesicles released by normally growing Escherichia coli contain very little lipoprotein. Eur J Biochem 116:331–335. https://doi.org/10.1111/j.1432-1033.1981.tb05338.x

89. Hoekstra D, van der Laan JW, Leij L de et al. (1976) Release of outer membrane fragments from normally growing Escherichia coli. Biochim Biophys Acta 455:889–899. https://doi.org/10.1016/0005-2736(76)90058-4

90. Kay HM, Birss AJ, Smalley JW (1990) Interaction of extracellular vesicles of Bacteroides gingivalis W50 with human polymorphonuclear leucocytes. FEMS Microbiol Lett 60:69–73. https://doi.org/10.1016/0378-1097(90)90347-s

91. Prangishvili D, Holz I, Stieger E et al. (2000) Sulfolobicins specific proteinaceous toxins produced by strains of the extremely thermophilic archaeal genus Sulfolobus. Journal of Bacteriology 182:2985–2988

92. Couch Y, Buzàs EI, Di Vizio D et al. (2021) A brief history of nearly EV-erything - The rise and rise of extracellular vesicles. J Extracell Vesicles 10:e12144. https://doi.org/10.1002/jev2.12144

93. Szul T, Sztul E (2011) COPII and COPI traffic at the ER-Golgi interface. Physiology (Bethesda) 26:348–364. https://doi.org/10.1152/physiol.00017.2011

94. Kirchhausen T (2000) Three Ways to Make a Vesicle. Nature 1:187–198

95. Faini M, Beck R, Wieland FT et al. (2013) Vesicle coats: structure, function, and general principles of assembly. Trends Cell Biol 23:279–288. https://doi.org/10.1016/j.tcb.2013.01.005

96. Sato K, Nakano A (2007) Mechanisms of COPII vesicle formation and protein sorting. FEBS Letters 581:2076–2082. https://doi.org/10.1016/j.febslet.2007.01.091

97. D'Arcangelo JG, Stahmer KR, Miller EA (2013) Vesicle-mediated export from the ER: COPII coat function and regulation. Biochim Biophys Acta 1833:2464–2472. https://doi.org/10.1016/j.bbamcr.2013.02.003

98. Nakańo A, Muramatsu M (1989) A novel GTP-binding protein, Sar1p, is involved in transport from the endoplasmic reticulum to the Golgi apparatus. J Cell Biol 109:2677–2691. https://doi.org/10.1083/jcb.109.6.2677

99. Barlowe C, Schekman R (1993) SEC12 encodes a guanine-nucleotide-exchange factor essential for transport vesicle budding from the ER. Nature 365:347–349. https://doi.org/10.1038/365347a0

100. McMahon C, Studer SM, Clendinen C et al. (2012) The structure of Sec12 implicates potassium ion coordination in Sar1 activation. J Biol Chem 287:43599–43606. https://doi.org/10.1074/jbc.M112.420141

101. Kuehn MJ, Herrmann JM, Schekman R (1998) COPII-cargo interactions direct protein sorting into ER-derived transport vesicles. Nature 391:187–190. https://doi.org/10.1038/34438

102. Bi X, Corpina RA, Goldberg J (2002) Structure of the Sec23/24-Sar1 pre-budding complex of the COPII vesicle coat. Nature 419:271–277. https://doi.org/10.1038/nature01040

103. Bi X, Mancias JD, Goldberg J (2007) Insights into COPII coat nucleation from the structure of Sec23.Sar1 complexed with the active fragment of Sec31. Dev Cell 13:635–645. https://doi.org/10.1016/j.devcel.2007.10.006

104. Antonny B, Madden D, Hamamoto S et al. (2001) Dynamics of the COPII coat with GTP and stable analogues. Nat Cell Biol 3:531–537. https://doi.org/10.1038/35078500

105. Fath S, Mancias JD, Bi X et al. (2007) Structure and organization of coat proteins in the COPII cage. Cell 129:1325–1336. https://doi.org/10.1016/j.cell.2007.05.036

106. Zanetti G, Prinz S, Daum S et al. (2013) The structure of the COPII transport-vesicle coat assembled on membranes. Elife 2:e00951. https://doi.org/10.7554/eLife.00951

107. Hutchings J, Stancheva VG, Brown NR et al. (2021) Structure of the complete, membrane-assembled COPII coat reveals a complex interaction network. Nat Commun 12:2034. https://doi.org/10.1038/s41467-021-22110-6

108. van der Verren SE, Zanetti G (2023) The small GTPase Sar1, control centre of COPII trafficking. FEBS Letters 597:865–882. https://doi.org/10.1002/1873-3468.14595

109. Fromme JC, Ravazzola M, Hamamoto S et al. (2007) The genetic basis of a craniofacial disease provides insight into COPII coat assembly. Dev Cell 13:623–634. https://doi.org/10.1016/j.devcel.2007.10.005

110. Arakel EC, Schwappach B (2018) Formation of COPI-coated vesicles at a glance. J Cell Sci 131. https://doi.org/10.1242/jcs.209890

111. Hsu VW, Yang J-S (2009) Mechanisms of COPI vesicle formation. FEBS Letters 583:3758–3763. https://doi.org/10.1016/j.febslet.2009.10.056

112. Donaldson JG, Cassel D, Kahn RA et al. (1992) ADP-ribosylation factor, a small GTP-binding protein, is required for binding of the coatomer protein beta-COP to Golgi membranes. Proc Natl Acad Sci U S A 89:6408–6412. https://doi.org/10.1073/pnas.89.14.6408

113. Sztul E, Chen P-W, Casanova JE et al. (2019) ARF GTPases and their GEFs and GAPs: concepts and challenges. Mol Biol Cell 30:1249–1271. https://doi.org/10.1091/mbc.E18-12-0820

114. Chardin P, Paris S, Antonny B et al. (1996) A human exchange factor for ARF contains Sec7- and pleckstrin-homology domains. Nature 384:481–484. https://doi.org/10.1038/384481a0

115. Pipaliya SV, Schlacht A, Klinger CM et al. (2019) Ancient complement and lineage-specific evolution of the Sec7 ARF GEF proteins in eukaryotes. Mol Biol Cell 30:1846–1863. https://doi.org/10.1091/mbc.E19-01-0073

116. Cherfils J, Ménétrey J, Mathieu M et al. (1998) Structure of the Sec7 domain of the Arf exchange factor ARNO. Nature 392:101–105. https://doi.org/10.1038/32210

117. Helms JB, Palmer DJ, Rothman JE (1993) Two distinct populations of ARF bound to Golgi membranes. J Cell Biol 121:751–760. https://doi.org/10.1083/jcb.121.4.751

118. Liu Y, Kahn RA, Prestegard JH (2009) Structure and membrane interaction of myristoylated ARF1. Structure 17:79–87. https://doi.org/10.1016/j.str.2008.10.020

119. Hara-Kuge S, Kuge O, Orci L et al. (1994) En bloc incorporation of coatomer subunits during the assembly of COP-coated vesicles. J Cell Biol 124:883–892. https://doi.org/10.1083/jcb.124.6.883

120. Bykov YS, Schaffer M, Dodonova SO et al. (2017) The structure of the COPI coat determined within the cell. Elife 6. https://doi.org/10.7554/eLife.32493

121. Lee C, Goldberg J (2010) Structure of coatomer cage proteins and the relationship among COPI, COPII, and clathrin vesicle coats. Cell 142:123–132. https://doi.org/10.1016/j.cell.2010.05.030

122. Franceschi N de, Wild K, Schlacht A et al. (2014) Longin and GAF domains: structural evolution and adaptation to the subcellular trafficking machinery. Traffic 15:104–121. https://doi.org/10.1111/tra.12124

123. Neuwald AF, Hirano T (2000) HEAT repeats associated with condensins, cohesins, and other complexes involved in chromosome-related functions. Genome Res 10:1445–1452. https://doi.org/10.1101/gr.147400

124. Watson PJ, Frigerio G, Collins BM et al. (2004) Gamma-COP appendage domain - structure and function. Traffic 5:79–88. https://doi.org/10.1111/j.1600-0854.2004.00158.x

125. Cosson P, Letourneur F (1994) Coatomer interaction with di-lysine endoplasmic reticulum retention motifs. Science 263:1629–1631. https://doi.org/10.1126/science.8128252

126. Yang J-S, Lee SY, Spanò S et al. (2005) A role for BARS at the fission step of COPI vesicle formation from Golgi membrane. EMBO J 24:4133–4143. https://doi.org/10.1038/sj.emboj.7600873

127. Yang J-S, Gad H, Lee SY et al. (2008) A role for phosphatidic acid in COPI vesicle fission yields insights into Golgi maintenance. Nat Cell Biol 10:1146–1153. https://doi.org/10.1038/ncb1774

128. Beck R, Adolf F, Weimer C et al. (2009) ArfGAP1 activity and COPI vesicle biogenesis. Traffic 10:307–315. https://doi.org/10.1111/j.1600-0854.2008.00865.x

129. Adarska P, Wong-Dilworth L, Bottanelli F (2021) ARF GTPases and Their Ubiquitous Role in Intracellular Trafficking Beyond the Golgi. Front Cell Dev Biol 9:679046. https://doi.org/10.3389/fcell.2021.679046

130. Takei K, Mundigl O, Daniell L et al. (1996) The synaptic vesicle cycle: a single vesicle budding step involving clathrin and dynamin. J Cell Biol 133:1237–1250. https://doi.org/10.1083/jcb.133.6.1237

131. Krauss M, Kinuta M, Wenk MR et al. (2003) ARF6 stimulates clathrin/AP-2 recruitment to synaptic membranes by activating phosphatidylinositol phosphate kinase type Igamma. J Cell Biol 162:113–124. https://doi.org/10.1083/jcb.200301006

132. Owen DJ, Collins BM, Evans PR (2004) Adaptors for clathrin coats: structure and function. Annu Rev Cell Dev Biol 20:153–191. https://doi.org/10.1146/annurev.cellbio.20.010403.104543

133. Park SY, Guo X (2014) Adaptor protein complexes and intracellular transport. Biosci Rep 34. https://doi.org/10.1042/BSR20140069

134. Kovtun O, Dickson VK, Kelly BT et al. (2020) Architecture of the AP2/clathrin coat on the membranes of clathrin-coated vesicles. Sci Adv 6:eaba8381. https://doi.org/10.1126/sciadv.aba8381

135. Kirchhausen T, Owen D, Harrison SC (2014) Molecular structure, function, and dynamics of clathrin-mediated membrane traffic. Cold Spring Harb Perspect Biol 6:a016725. https://doi.org/10.1101/cshperspect.a016725

136. Ungewickell E, Ungewickell H, Holstein SE et al. (1995) Role of auxilin in uncoating clathrin-coated vesicles. Nature 378:632–635. https://doi.org/10.1038/378632a0

137. Cheng X, Chen K, Dong B et al. (2021) Dynamin-dependent vesicle twist at the final stage of clathrin-mediated endocytosis. Nat Cell Biol 23:859–869. https://doi.org/10.1038/s41556-021-00713-x

138. Klinger CM, Spang A, Dacks JB et al. (2016) Tracing the Archaeal Origins of Eukaryotic Membrane-Trafficking System Building Blocks. Mol Biol Evol 33:1528–1541. https://doi.org/10.1093/molbev/msw034

139. Field MC, Sali A, Rout MP (2011) Evolution: On a bender--BARs, ESCRTs, COPs, and finally getting your coat. J Cell Biol 193:963–972. https://doi.org/10.1083/jcb.201102042

140. Lundmark R, Doherty GJ, Vallis Y et al. (2008) Arf family GTP loading is activated by, and generates, positive membrane curvature. Biochem J 414:189–194. https://doi.org/10.1042/BJ20081237

141. Joiner AMN, Fromme JC (2021) Structural basis for the initiation of COPII vesicle biogenesis. Structure 29:859-872.e6. https://doi.org/10.1016/j.str.2021.03.013

142. Cherfils J, Zeghouf M (2013) Regulation of small GTPases by GEFs, GAPs, and GDIs. Physiol Rev 93:269–309. https://doi.org/10.1152/physrev.00003.2012

143. Devos D, Dokudovskaya S, Alber F et al. (2004) Components of coated vesicles and nuclear pore complexes share a common molecular architecture. PLoS Biol 2:e380. https://doi.org/10.1371/journal.pbio.0020380

144. Jékely G, Arendt D (2006) Evolution of intraflagellar transport from coated vesicles and autogenous origin of the eukaryotic cilium. Bioessays 28:191–198. https://doi.org/10.1002/bies.20369

145. Nickerson DP, Brett CL, Merz AJ (2009) Vps-C complexes: gatekeepers of endolysosomal traffic. Curr Opin Cell Biol 21:543–551. https://doi.org/10.1016/j.ceb.2009.05.007

146. Dokudovskaya S, Waharte F, Schlessinger A et al. (2011) A conserved coatomer-related complex containing Sec13 and Seh1 dynamically associates with the vacuole in Saccharomyces cerevisiae. Mol Cell Proteomics 10:M110.006478. https://doi.org/10.1074/mcp.M110.006478

147. Field MC, Dacks JB (2009) First and last ancestors: reconstructing evolution of the endomembrane system with ESCRTs, vesicle coat proteins, and nuclear pore complexes. Curr Opin Cell Biol 21:4–13. https://doi.org/10.1016/j.ceb.2008.12.004

148. Field MC, Rout MP (2022) Coatomer in the universe of cellular complexity. Mol Biol Cell 33. https://doi.org/10.1091/mbc.E19-01-0012

149. Neveu E, Khalifeh D, Salamin N et al. (2020) Prototypic SNARE Proteins Are Encoded in the Genomes of Heimdallarchaeota, Potentially Bridging the Gap between the Prokaryotes and Eukaryotes. Curr Biol 30:2468-2480.e5. https://doi.org/10.1016/j.cub.2020.04.060

150. Henne WM, Buchkovich NJ, Emr SD (2011) The ESCRT pathway. Dev Cell 21:77–91. https://doi.org/10.1016/j.devcel.2011.05.015

151. Juan T, Fürthauer M (2018) Biogenesis and function of ESCRT-dependent extracellular vesicles. Semin Cell Dev Biol 74:66–77. https://doi.org/10.1016/j.semcdb.2017.08.022

152. Olmos Y (2022) The ESCRT Machinery: Remodeling, Repairing, and Sealing Membranes. Membranes (Basel) 12. https://doi.org/10.3390/membranes12060633

153. Raiborg C, Bremnes B, Mehlum A et al. (2001) FYVE and coiled-coil domains determine the specific localisation of Hrs to early endosomes. J Cell Sci 114:2255–2263. https://doi.org/10.1242/jcs.114.12.2255

154. Lu Q, Hope LW, Brasch M et al. (2003) TSG101 interaction with HRS mediates endosomal trafficking and receptor down-regulation. Proc Natl Acad Sci U S A 100:7626–7631. https://doi.org/10.1073/pnas.0932599100

155. Babst M, Katzmann DJ, Estepa-Sabal EJ et al. (2002) Escrt-III: an endosome-associated heterooligomeric protein complex required for mvb sorting. Dev Cell 3:271–282. https://doi.org/10.1016/s1534-5807(02)00220-4

156. Tang S, Henne WM, Borbat PP et al. (2015) Structural basis for activation, assembly and membrane binding of ESCRT-III Snf7 filaments. Elife 4. https://doi.org/10.7554/eLife.12548

157. Pfitzner A-K, Moser von Filseck J, Roux A (2021) Principles of membrane remodeling by dynamic ESCRT-III polymers. Trends Cell Biol 31:856–868. https://doi.org/10.1016/j.tcb.2021.04.005

158. Pfitzner A-K, Mercier V, Jiang X et al. (2020) An ESCRT-III Polymerization Sequence Drives Membrane Deformation and Fission. Cell 182:1140-1155.e18. https://doi.org/10.1016/j.cell.2020.07.021

159. Alonso Y Adell M, Migliano SM, Teis D (2016) ESCRT-III and Vps4: a dynamic multipurpose tool for membrane budding and scission. FEBS J 283:3288–3302. https://doi.org/10.1111/febs.13688

160. Gurung S, Perocheau D, Touramanidou L et al. (2021) The exosome journey: from biogenesis to uptake and intracellular signalling. Cell Commun Signal 19:47. https://doi.org/10.1186/s12964-021-00730-1

161. Li X-X, Yang L-X, Wang C et al. (2023) The Roles of Exosomal Proteins: Classification, Function, and Applications. Int J Mol Sci 24. https://doi.org/10.3390/ijms24043061

162. Ghanam J, Chetty VK, Barthel L et al. (2022) DNA in extracellular vesicles: from evolution to its current application in health and disease. Cell Biosci 12:37. https://doi.org/10.1186/s13578-022-00771-0

163. Bhome R, Del Vecchio F, Lee G-H et al. (2018) Exosomal microRNAs (exomiRs): Small molecules with a big role in cancer. Cancer Lett 420:228–235. https://doi.org/10.1016/j.canlet.2018.02.002

164. Rodrigues ML, Nimrichter L, Oliveira DL et al. (2007) Vesicular polysaccharide export in Cryptococcus neoformans is a eukaryotic solution to the problem of fungal trans-cell wall transport. Eukaryot Cell 6:48–59. https://doi.org/10.1128/EC.00318-06

165. Biller SJ, Schubotz F, Roggensack SE et al. (2013) Bacterial Vesicles in Marine Ecosystems. Science 343:183–186

166. Zhao K, Bleackley M, Chisanga D et al. (2019) Extracellular vesicles secreted by Saccharomyces cerevisiae are involved in cell wall remodelling. Commun Biol 2:305. https://doi.org/10.1038/s42003-019-0538-8

167. Meldolesi J (2022) Unconventional Protein Secretion Dependent on Two Extracellular Vesicles: Exosomes and Ectosomes. Front Cell Dev Biol 10:877344. https://doi.org/10.3389/fcell.2022.877344

168. van Niel G, D'Angelo G, Raposo G (2018) Shedding light on the cell biology of extracellular vesicles. Nat Rev Mol Cell Biol 19:213–228. https://doi.org/10.1038/nrm.2017.125

169. Del Conde I, Shrimpton CN, Thiagarajan P et al. (2005) Tissue-factor-bearing microvesicles arise from lipid rafts and fuse with activated platelets to initiate coagulation. Blood 106:1604–1611. https://doi.org/10.1182/blood-2004-03-1095

170. Nabhan JF, Hu R, Oh RS et al. (2012) Formation and release of arrestin domain-containing protein 1-mediated microvesicles (ARMMs) at plasma membrane by recruitment of TSG101 protein. Proc Natl Acad Sci U S A 109:4146–4151. https://doi.org/10.1073/pnas.1200448109

171. Li B, Antonyak MA, Zhang J et al. (2012) RhoA triggers a specific signaling pathway that generates transforming microvesicles in cancer cells. Oncogene 31:4740–4749. https://doi.org/10.1038/onc.2011.636

172. Muralidharan-Chari V, Clancy J, Plou C et al. (2009) ARF6-regulated shedding of tumor cell-derived plasma membrane microvesicles. Curr Biol 19:1875–1885. https://doi.org/10.1016/j.cub.2009.09.059

173. Clancy JW, Zhang Y, Sheehan C et al. (2019) An ARF6-Exportin-5 axis delivers pre-miRNA cargo to tumour microvesicles. Nat Cell Biol 21:856–866. https://doi.org/10.1038/s41556-019-0345-y

174. Guerrero-Mandujano A, Hernández-Cortez C, Ibarra JA et al. (2017) The outer membrane vesicles: Secretion system type zero. Traffic 18:425–432. https://doi.org/10.1111/tra.12488

175. Toyofuku M, Tashiro Y, Hasegawa Y et al. (2015) Bacterial membrane vesicles, an overlooked environmental colloid: Biology, environmental perspectives and applications. Adv Colloid Interface Sci 226:65–77. https://doi.org/10.1016/j.cis.2015.08.013

176. Sartorio MG, Pardue EJ, Feldman MF et al. (2021) Bacterial Outer Membrane Vesicles: From Discovery to Applications. Annu Rev Microbiol 75:609–630. https://doi.org/10.1146/annurev-micro-052821-031444

177. Toyofuku M, Nomura N, Eberl L (2019) Types and origins of bacterial membrane vesicles. Nat Rev Microbiol 17:13–24. https://doi.org/10.1038/s41579-018-0112-2

178. Toyofuku M, Schild S, Kaparakis-Liaskos M et al. (2023) Composition and functions of bacterial membrane vesicles. Nat Rev Microbiol. https://doi.org/10.1038/s41579-023-00875-5

179. Mozaheb N, Mingeot-Leclercq M-P (2020) Membrane Vesicle Production as a Bacterial Defense Against Stress. Front Microbiol 11:600221. https://doi.org/10.3389/fmicb.2020.600221

180. Bernadac A, Gavioli M, Lazzaroni J-C et al. (1998) Escherichia coli tol-pal Mutants Form Outer Membrane Vesicles. Journal of Bacteriology 180:4872–4878

181. Moon DC, Choi CH, Lee JH et al. (2012) Acinetobacter baumannii outer membrane protein A modulates the biogenesis of outer membrane vesicles. J Microbiol 50:155–160. https://doi.org/10.1007/s12275-012-1589-4

182. Deatherage BL, Lara JC, Bergsbaken T et al. (2009) Biogenesis of bacterial membrane vesicles. Mol Microbiol 72:1395–1407. https://doi.org/10.1111/j.1365-2958.2009.06731.x

183. Schwechheimer C, Sullivan CJ, Kuehn MJ (2013) Envelope control of outer membrane vesicle production in Gram-negative bacteria. Biochemistry 52:3031–3040. https://doi.org/10.1021/bi400164t

184. Schwechheimer C, Kuehn MJ (2013) Synthetic effect between envelope stress and lack of outer membrane vesicle production in Escherichia coli. Journal of Bacteriology 195:4161–4173. https://doi.org/10.1128/JB.02192-12

185. Bielig H, Rompikuntal PK, Dongre M et al. (2011) NOD-like receptor activation by outer membrane vesicles from Vibrio cholerae non-O1 non-O139 strains is modulated by the quorum-sensing regulator HapR. Infect Immun 79:1418–1427. https://doi.org/10.1128/IAI.00754-10

186. Kaparakis M, Turnbull L, Carneiro L et al. (2010) Bacterial membrane vesicles deliver peptidoglycan to NOD1 in epithelial cells. Cell Microbiol 12:372–385. https://doi.org/10.1111/j.1462-5822.2009.01404.x

187. Kadurugamuwa JL, Beveridge TJ (1995) Virulence factors are released from Pseudomonas aeruginosa in association with membrane vesicles during normal growth and exposure to gentamicin: a novel mechanism of enzyme secretion. Journal of Bacteriology 177:3998–4008. https://doi.org/10.1128/jb.177.14.3998-4008.1995

188. Nguyen TT, Saxena A, Beveridge TJ (2003) Effect of surface lipopolysaccharide on the nature of membrane vesicles liberated from the Gram-negative bacterium Pseudomonas aeruginosa. J Electron Microsc (Tokyo) 52:465–469. https://doi.org/10.1093/jmicro/52.5.465

189. Elhenawy W, Bording-Jorgensen M, Valguarnera E et al. (2016) LPS Remodeling Triggers Formation of Outer Membrane Vesicles in Salmonella. mBio 7. https://doi.org/10.1128/mBio.00940-16

190. Zimmerberg J, Kozlov MM (2006) How proteins produce cellular membrane curvature. Nat Rev Mol Cell Biol 7:9–19. https://doi.org/10.1038/nrm1784

191. Dauros-Singorenko P, Blenkiron C, Phillips A et al. (2018) The functional RNA cargo of bacterial membrane vesicles. FEMS Microbiol Lett 365. https://doi.org/10.1093/femsle/fny023

192. Pérez-Cruz C, Carrión O, Delgado L et al. (2013) New type of outer membrane vesicle produced by the Gram-negative bacterium Shewanella vesiculosa M7T: implications for DNA content. Appl Environ Microbiol 79:1874–1881. https://doi.org/10.1128/AEM.03657-12

193. Pérez-Cruz C, Delgado L, López-Iglesias C et al. (2015) Outer-inner membrane vesicles naturally secreted by gram-negative pathogenic bacteria. PLoS One 10:e0116896. https://doi.org/10.1371/journal.pone.0116896

194. Baeza N, Delgado L, Comas J et al. (2021) Phage-Mediated Explosive Cell Lysis Induces the Formation of a Different Type of O-IMV in Shewanella vesiculosa M7T. Front Microbiol 12:713669. https://doi.org/10.3389/fmicb.2021.713669

195. Breitbart M, Rohwer F (2005) Here a virus, there a virus, everywhere the same virus? Trends Microbiol 13:278–284. https://doi.org/10.1016/j.tim.2005.04.003

196. Turnbull L, Toyofuku M, Hynen AL et al. (2016) Explosive cell lysis as a mechanism for the biogenesis of bacterial membrane vesicles and biofilms. Nat Commun 7:11220. https://doi.org/10.1038/ncomms11220

197. Jiang M, Wang Z, Xia F et al. (2022) Reductions in bacterial viability stimulate the production of Extra-intestinal Pathogenic Escherichia coli (ExPEC) cytoplasm-carrying Extracellular Vesicles (EVs). PLoS Pathog 18:e1010908. https://doi.org/10.1371/journal.ppat.1010908

198. Toyofuku M, Zhou S, Sawada I et al. (2014) Membrane vesicle formation is associated with pyocin production under denitrifying conditions in Pseudomonas aeruginosa PAO1. Environ Microbiol 16:2927–2938. https://doi.org/10.1111/1462-2920.12260

199. Toyofuku M, Cárcamo-Oyarce G, Yamamoto T et al. (2017) Prophage-triggered membrane vesicle formation through peptidoglycan damage in Bacillus subtilis. Nat Commun 8:481. https://doi.org/10.1038/s41467-017-00492-w

200. Nagakubo T, Tahara YO, Miyata M et al. (2021) Mycolic acid-containing bacteria trigger distinct types of membrane vesicles through different routes. iScience 24:102015. https://doi.org/10.1016/j.isci.2020.102015

201. Liu Y, Tempelaars MH, Boeren S et al. (2022) Extracellular vesicle formation in Lactococcus lactis is stimulated by prophage-encoded holin-lysin system. Microb Biotechnol 15:1281–1295. https://doi.org/10.1111/1751-7915.13972

202. Briaud P, Carroll RK (2020) Extracellular Vesicle Biogenesis and Functions in Gram-Positive Bacteria. Infect Immun 88. https://doi.org/10.1128/IAI.00433-20

203. Lee E-Y, Choi D-Y, Kim D-K et al. (2009) Gram-positive bacteria produce membrane vesicles: proteomics-based characterization of Staphylococcus aureus-derived membrane vesicles. Proteomics 9:5425–5436. https://doi.org/10.1002/pmic.200900338

204. Rivera J, Cordero RJB, Nakouzi AS et al. (2010) Bacillus anthracis produces membrane-derived vesicles containing biologically active toxins. Proc Natl Acad Sci U S A 107:19002–19007. https://doi.org/10.1073/pnas.1008843107

205. Lee JH, Choi C-W, Lee T et al. (2013) Transcription factor σB plays an important role in the production of extracellular membrane-derived vesicles in Listeria monocytogenes. PLoS One 8:e73196. https://doi.org/10.1371/journal.pone.0073196

206. Resch U, Tsatsaronis JA, Le Rhun A et al. (2016) A Two-Component Regulatory System Impacts Extracellular Membrane-Derived Vesicle Production in Group A Streptococcus. mBio 7. https://doi.org/10.1128/mbio.00207-16

207. White DW, Elliott SR, Odean E et al. (2018) Mycobacterium tuberculosis Pst/SenX3-RegX3 Regulates Membrane Vesicle Production Independently of ESX-5 Activity. mBio 9. https://doi.org/10.1128/mbio.00778-18

208. Wang X, Thompson CD, Weidenmaier C et al. (2018) Release of Staphylococcus aureus extracellular vesicles and their application as a vaccine platform. Nat Commun 9:1379. https://doi.org/10.1038/s41467-018-03847-z

209. Jeon J, Mok HJ, Choi Y et al. (2017) Proteomic analysis of extracellular vesicles derived from Propionibacterium acnes. Proteomics Clin Appl 11. https://doi.org/10.1002/prca.201600040

210. Kim HY, Lim Y, An S-J et al. (2020) Characterization and immunostimulatory activity of extracellular vesicles from Filifactor alocis. Mol Oral Microbiol 35:1–9. https://doi.org/10.1111/omi.12272

211. Mashburn LM, Whiteley M (2005) Membrane vesicles traffic signals and facilitate group activities in a prokaryote. Nature 437:422–425. https://doi.org/10.1038/nature03925

212. Bitto NJ, Chapman R, Pidot S et al. (2017) Bacterial membrane vesicles transport their DNA cargo into host cells. Sci Rep 7:7072. https://doi.org/10.1038/s41598-017-07288-4

213. Tashiro Y, Hasegawa Y, Shintani M et al. (2017) Interaction of Bacterial Membrane Vesicles with Specific Species and Their Potential for Delivery to Target Cells. Front Microbiol 8:571. https://doi.org/10.3389/fmicb.2017.00571

214. Aktar S, Okamoto Y, Ueno S et al. (2021) Incorporation of Plasmid DNA Into Bacterial Membrane Vesicles by Peptidoglycan Defects in Escherichia coli. Front Microbiol 12:747606. https://doi.org/10.3389/fmicb.2021.747606

215. Andreoni F, Toyofuku M, Menzi C et al. (2019) Antibiotics Stimulate Formation of Vesicles in Staphylococcus aureus in both Phage-Dependent and -Independent Fashions and via Different Routes. Antimicrob Agents Chemother 63. https://doi.org/10.1128/AAC.01439-18

216. Lücking D, Mercier C, Alarcón-Schumacher T et al. (2023) Extracellular vesicles are the main contributor to the non-viral protected extracellular sequence space

217. Fulsundar S, Harms K, Flaten GE et al. (2014) Gene transfer potential of outer membrane vesicles of Acinetobacter baylyi and effects of stress on vesiculation. Appl Environ Microbiol 80:3469–3483. https://doi.org/10.1128/AEM.04248-13

218. Ghosal A, Upadhyaya BB, Fritz JV et al. (2015) The extracellular RNA complement of Escherichia coli. Microbiologyopen 4:252–266. https://doi.org/10.1002/mbo3.235

219. Blenkiron C, Simonov D, Muthukaruppan A et al. (2016) Uropathogenic Escherichia coli Releases Extracellular Vesicles That Are Associated with RNA. PLoS One 11:e0160440. https://doi.org/10.1371/journal.pone.0160440

220. Li Z, Stanton BA (2021) Transfer RNA-Derived Fragments, the Underappreciated Regulatory Small RNAs in Microbial Pathogenesis. Front Microbiol 12:687632. https://doi.org/10.3389/fmicb.2021.687632

221. Koeppen K, Hampton TH, Jarek M et al. (2016) A Novel Mechanism of Host-Pathogen Interaction through sRNA in Bacterial Outer Membrane Vesicles. PLoS Pathog 12:e1005672. https://doi.org/10.1371/journal.ppat.1005672

222. Storz G, Vogel J, Wassarman KM (2011) Regulation by small RNAs in bacteria: expanding frontiers. Mol Cell 43:880–891. https://doi.org/10.1016/j.molcel.2011.08.022

223. Choi J-W, Kwon T-Y, Hong S-H et al. (2018) Isolation and Characterization of a microRNA-size Secretable Small RNA in Streptococcus sanguinis. Cell Biochem Biophys 76:293–301. https://doi.org/10.1007/s12013-016-0770-5

224. Choi J-W, Kim S-C, Hong S-H et al. (2017) Secretable Small RNAs via Outer Membrane Vesicles in Periodontal Pathogens. J Dent Res 96:458–466. https://doi.org/10.1177/0022034516685071

225. Moriano-Gutierrez S, Bongrand C, Essock-Burns T et al. (2020) The noncoding small RNA SsrA is released by Vibrio fischeri and modulates critical host responses. PLoS Biol 18:e3000934. https://doi.org/10.1371/journal.pbio.3000934

226. Kadurugamuwa JL, Beveridge TJ (1996) Bacteriolytic effect of membrane vesicles from Pseudomonas aeruginosa on other bacteria including pathogens: conceptually new antibiotics. Journal of Bacteriology 178:2767–2774. https://doi.org/10.1128/jb.178.10.2767-2774.1996

227. Li Z, Clarke AJ, Beveridge TJ (1998) Gram-negative bacteria produce membrane vesicles which are capable of killing other bacteria. Journal of Bacteriology 180:5478–5483. https://doi.org/10.1128/JB.180.20.5478-5483.1998

228. Macion A, Wyszyńska A, Godlewska R (2021) Delivery of Toxins and Effectors by Bacterial Membrane Vesicles. Toxins (Basel) 13. https://doi.org/10.3390/toxins13120845

229. Yue H, Jiang J, Taylor AJ et al. (2021) Outer Membrane Vesicle-Mediated Codelivery of the Antifungal HSAF Metabolites and Lytic Polysaccharide Monooxygenase in the Predatory Lysobacter enzymogenes. ACS Chem Biol 16:1079–1089. https://doi.org/10.1021/acschembio.1c00260

230. Pesci EC, Milbank JB, Pearson JP et al. (1999) Quinolone signaling in the cell-to-cell communication system of Pseudomonas aeruginosa. Proc Natl Acad Sci U S A 96:11229–11234. https://doi.org/10.1073/pnas.96.20.11229

231. Toyofuku M, Morinaga K, Hashimoto Y et al. (2017) Membrane vesicle-mediated bacterial communication. ISME J 11:1504–1509. https://doi.org/10.1038/ismej.2017.13

232. Brameyer S, Plener L, Müller A et al. (2018) Outer Membrane Vesicles Facilitate Trafficking of the Hydrophobic Signaling Molecule CAI-1 between Vibrio harveyi Cells. Journal of Bacteriology 200. https://doi.org/10.1128/JB.00740-17

233. Biller SJ, Lundeen RA, Hmelo LR et al. (2022) Prochlorococcus extracellular vesicles: molecular composition and adsorption to diverse microbes. Environ Microbiol 24:420–435. https://doi.org/10.1111/1462-2920.15834

234. Zakharzhevskaya NB, Vanyushkina AA, Altukhov IA et al. (2017) Outer membrane vesicles secreted by pathogenic and nonpathogenic Bacteroides fragilis represent different metabolic activities. Sci Rep 7:5008. https://doi.org/10.1038/s41598-017-05264-6

235. Yun SH, Lee S-Y, Choi C-W et al. (2017) Proteomic characterization of the outer membrane vesicle of the halophilic marine bacterium Novosphingobium pentaromativorans US6-1. J Microbiol 55:56–62. https://doi.org/10.1007/s12275-017-6581-6

236. Lappann M, Otto A, Becher D et al. (2013) Comparative proteome analysis of spontaneous outer membrane vesicles and purified outer membranes of Neisseria meningitidis. Journal of Bacteriology 195:4425–4435. https://doi.org/10.1128/JB.00625-13

237. Elhenawy W, Debelyy MO, Feldman MF (2014) Preferential packing of acidic glycosidases and proteases into Bacteroides outer membrane vesicles. mBio 5:e00909-14. https://doi.org/10.1128/mbio.00909-14

238. Valguarnera E, Scott NE, Azimzadeh P et al. (2018) Surface Exposure and Packing of Lipoproteins into Outer Membrane Vesicles Are Coupled Processes in Bacteroides. mSphere 3. https://doi.org/10.1128/mSphere.00559-18

239. Caruana JC, Walper SA (2020) Bacterial Membrane Vesicles as Mediators of Microbe - Microbe and Microbe - Host Community Interactions. Front Microbiol 11:432. https://doi.org/10.3389/fmicb.2020.00432

240. Manning AJ, Kuehn MJ (2011) Contribution of bacterial outer membrane vesicles to innate bacterial defense. BMC Microbiol 11:258. https://doi.org/10.1186/1471-2180-11-258

241. Augustyniak D, Olszak T, Drulis-Kawa Z (2022) Outer Membrane Vesicles (OMVs) of Pseudomonas aeruginosa Provide Passive Resistance but Not Sensitization to LPS-Specific Phages. Viruses 14. https://doi.org/10.3390/v14010121

242. Liu J, Soler N, Gorlas A et al. (2021) Extracellular membrane vesicles and nanotubes in Archaea. Microlife 2:uqab007. https://doi.org/10.1093/femsml/uqab007

243. Ellen AF, Albers S-V, Huibers W et al. (2009) Proteomic analysis of secreted membrane vesicles of archaeal Sulfolobus species reveals the presence of endosome sorting complex components. Extremophiles 13:67–79. https://doi.org/10.1007/s00792-008-0199-x

244. Samson RY, Obita T, Freund SM et al. (2008) A role for the ESCRT system in cell division in archaea. Science 322:1710–1713. https://doi.org/10.1126/science.1165322

245. Soler N, Marguet E, Verbavatz J-M et al. (2008) Virus-like vesicles and extracellular DNA produced by hyperthermophilic archaea of the order Thermococcales. Res Microbiol 159:390–399. https://doi.org/10.1016/j.resmic.2008.04.015

246. Soler N, Gaudin M, Marguet E et al. (2011) Plasmids, viruses and virus-like membrane vesicles from Thermococcales. Biochem Soc Trans 39:36–44. https://doi.org/10.1042/BST0390036

247. Gaudin M, Gauliard E, Schouten S et al. (2013) Hyperthermophilic archaea produce membrane vesicles that can transfer DNA. Environ Microbiol Rep 5:109–116. https://doi.org/10.1111/j.1758-2229.2012.00348.x

248. Gaudin M, Krupovic M, Marguet E et al. (2014) Extracellular membrane vesicles harbouring viral genomes. Environ Microbiol 16:1167–1175. https://doi.org/10.1111/1462-2920.12235

249. Choi DH, Kwon YM, Chiura HX et al. (2015) Extracellular Vesicles of the Hyperthermophilic Archaeon "Thermococcus onnurineus" NA1T. Appl Environ Microbiol 81:4591–4599. https://doi.org/10.1128/AEM.00428-15

250. Gorlas A, Marguet E, Gill S et al. (2015) Sulfur vesicles from Thermococcales: A possible role in sulfur detoxifying mechanisms. Biochimie 118:356–364. https://doi.org/10.1016/j.biochi.2015.07.026

251. Makarova KS, Yutin N, Bell SD et al. (2010) Evolution of diverse cell division and vesicle formation systems in Archaea. Nat Rev Microbiol 8:731–741. https://doi.org/10.1038/nrmicro2406

252. Erdmann S, Tschitschko B, Zhong L et al. (2017) A plasmid from an Antarctic haloarchaeon uses specialized membrane vesicles to disseminate and infect plasmid-free cells. Nat Microbiol 2:1446–1455. https://doi.org/10.1038/s41564-017-0009-2

253. Delmas S, Duggin IG, Allers T (2013) DNA damage induces nucleoid compaction via the Mre11-Rad50 complex in the archaeon Haloferax volcanii. Mol Microbiol 87:168–179. https://doi.org/10.1111/mmi.12091

254. Schlacht A, Herman EK, Klute MJ et al. (2014) Missing pieces of an ancient puzzle: evolution of the eukaryotic membrane-trafficking system. Cold Spring Harb Perspect Biol 6:a016048. https://doi.org/10.1101/cshperspect.a016048

255. Dacks JB, Poon PP, Field MC (2008) Phylogeny of endocytic components yields insight into the process of nonendosymbiotic organelle evolution. Proc Natl Acad Sci U S A 105:588–593. https://doi.org/10.1073/pnas.0707318105

256. Dacks JB, Field MC (2007) Evolution of the eukaryotic membrane-trafficking system: origin, tempo and mode. J Cell Sci 120:2977–2985. https://doi.org/10.1242/jcs.013250

257. Gould SB, Garg SG, Martin WF (2016) Bacterial Vesicle Secretion and the Evolutionary Origin of the Eukaryotic Endomembrane System. Trends Microbiol 24:525–534. https://doi.org/10.1016/j.tim.2016.03.005

CHAPTER II.

Isolation, Purification, and Characterization of Membrane Vesicles from Haloarchaea

Joshua Mills and Susanne Erdmann

The manuscript is published in *Archaea: Methods and Protocols. Methods in Molecular Biology* vol. 2522 (2022)

Chapter 30

Isolation, Purification, and Characterization of Membrane Vesicles from Haloarchaea

Joshua Mills and Susanne Erdmann

Abstract

Membrane vesicles (MVs), also described as extracellular vesicles (EVs), exosomes, or outer membrane vesicles (OMVs), are nano-sized (10–300 nm) spherical, membrane-bound structures deriving from the cell envelope. MVs have been studied extensively in both eukaryotic and prokaryotic systems, revealing a plethora of unique functions including cell-to-cell communication and protection of the cell. They are able to encapsulate specific cargos from nucleic acids to proteins, thereby concentrating cargo and providing protection from the extracellular environment. While MV production has been identified for all domains of life, with extensive investigation particularly for Bacteria and Eukaryota, it has only been studied in a few members of the archaeal domain, leaving a void of information concerning the role of MVs for the majority of Archaea. In addition, several discrepancies exist in the process of MV preparation and analysis between studies of MV production in different archaeal organisms. To further encourage the investigation of MVs in Archaea among the scientific community, we present a standardized method for the isolation, purification, and characterization of MVs based on the archaeal model organism, *Haloferax volcanii*. However, the described protocol can be applied to other Archaea with the appropriate modifications that are highlighted in Subheading 4.

Key words Membrane vesicles, Extracellular vesicles, Archaea, Haloarchaea, Cellular communication, Density gradient purification

1 Introduction

Membrane vesicles (MVs) are spherical, membrane-bound structures that bud off from the cellular envelope (also sometimes denoted as extracellular vesicles, exosomes, or outer membrane vesicles). With more research accumulating on the ubiquity and diversity of MV formation among all domains of life, it is clear that vesicle production plays significant roles in both cellular function and inter- and intracellular communication [1, 2]. These structures are able to harbor a wide range of cargo, subsequently allowing for MVs to carry out a variety of functions.

Sébastien Ferreira-Cerca (ed.), *Archaea: Methods and Protocols*, Methods in Molecular Biology, vol. 2522,
https://doi.org/10.1007/978-1-0716-2445-6_30,

Vesicles of specific organisms such as *Pseudomonas aeruginosa*, *Halorubrum lacusprofundi* and humans have been shown to contain DNA in the form of either linear fragments or plasmids [3–5], and have also been shown in some cases to act as a vehicle for horizontal gene transfer [6]. RNA in the form of mRNA, sRNA, and miRNA have also been observed in a multitude of bacterial and eukaryotic organisms as well as the archaeal organism *Thermococcus onnurineus* [7–10]. Furthermore, functions such as quorum sensing, viral defense, and the secretion of toxins have been associated with MV release [11–13].

While research into this mechanism has revealed many insights for MV trafficking pertaining to bacterial and eukaryotic organisms, the field of archaeal MV formation is still relatively unexplored, with several variations in methodology for MV isolation. Isolation of extracellular vesicles typically utilizes one or a combination of several strategies including: ultracentrifugation, size-exclusion-based methods, immunoaffinity-based methods, microfluidic-based methods, and polymer-based vesicle precipitation [14, 15]. Each method provides their own respective advantages and disadvantages, and therefore selection of the proper MV isolation strategy depends on both the organism being studied and the intended downstream analysis.

Ultracentrifugation is the most common approach in MV isolation processes and is often referred to as the "gold standard" for MV isolation. Ultracentrifugation is used for the separation of particles in suspension according to their molecular weight or density. Isolation of MVs through differential centrifugation typically pellets cells, dead cells and cell debris through low-speed centrifugation (300–10,000 $\times g$), followed by high-speed ultracentrifugation to pellet MVs as well as free proteins and other extracellular structures (100,000–200,000 $\times g$). Ultracentrifugation is typically favored as it has a high yield of product. However, the downside of this strategy is that the g-force generated through ultracentrifugation may damage MV structure, leading to misshapen or broken MVs [16, 17]. While this may not be relevant to downstream protein analysis, other purposes that require intact vesicles such as nucleic acid analysis or fusion experiments would not favor the loss of sample through ultracentrifugation.

In order to bypass the high speed required for ultracentrifugation, precipitation of MVs through the addition of a polymer, typically polyethylene glycol (PEG), allows for the gentle sedimentation of MVs at much lower g-force. PEG is able to tie up water molecules more effectively than MVs, pushing the MVs and other small contaminants like proteins and extracellular substances out of solution [14]. PEG precipitation typically follows a pre-isolation step of low-speed centrifugation in order to remove cells and cell debris from the media that would also sediment with the MVs. This has been shown to be quite effective in both yield and for

downstream analysis of cargo [18, 19]. However, PEG precipitation does have its limitations, including the proclivity for the precipitation of other contaminants including protein aggregates, extracellular nucleic acids, and extracellularly secreted polymers [14, 15]. A post-isolation purification step is typically required to remove small, non-MV contaminates, as well as any residual PEG that may interfere with downstream analysis.

Filtration is also a common strategy for MV isolation, where isolation is based on separation according to the relative size of the particles. Typically, a series of filters with pore sizes ranging from 0.8, 0.45, and 0.22 μm are employed. These naturally would retain any MVs with diameters close to the pore size, so the selection of pore size should be dependent on the range of diameters observed of the MVs. There are several caveats to this method though, as MVs can adhere to filter membranes and clogging can occur from excess large contaminants [15]. And while filtration may provide a means of concentrating samples, there is still the possibility of small contaminants being retained, so a post-isolation purification step would be needed.

To further separate the MVs from the other contaminants, MV isolation is typically supplemented by purification through density gradient. Density gradient purification of MVs, usually with iodixanol (Optiprep™) or sucrose, is able to separate a heterogeneous solution by the densities of the particles. Due to the low density of MVs in comparison to typical contaminants such as proteins and other polymeric substances, density gradient ultracentrifugation is able to effectively separate MVs into a discrete band that can be easily isolated [20, 21].

In previous studies on archaeal MV production, combinations of the methods mentioned above have been implemented. In a study of the proteomic contents of MVs deriving from *Sulfolobus* species, differential ultracentrifugation, low pH density gradient purification, and ultrafiltration were all used to isolate and purify MVs [22]. The study of MVs from *Thermococcales* species similarly used a combination of ultracentrifugation and filtration to isolate and purify MVs [8]. Plasmid vesicles from the halophile *Halorubrum lacusprofundi* were isolated through low-speed centrifugation, filtration, and PEG precipitation [3]. While each of the methods had been successful in isolation of MVs, in order for cross-species comparison of MV characterization, it is imperative that a standard be established for MV isolation and purification in Archaea.

The following protocols and experimental workflow (*see* Fig. 1) detail the process of cell cultivation, MV isolation, and MV purification, including suggestions for some downstream analyses customized for the haloarchaeal model organism *Haloferax volcanii*. With an established framework for MV isolation and purification in place, hopefully this can instigate further investigation into the fascinating field of MV production in Archaea.

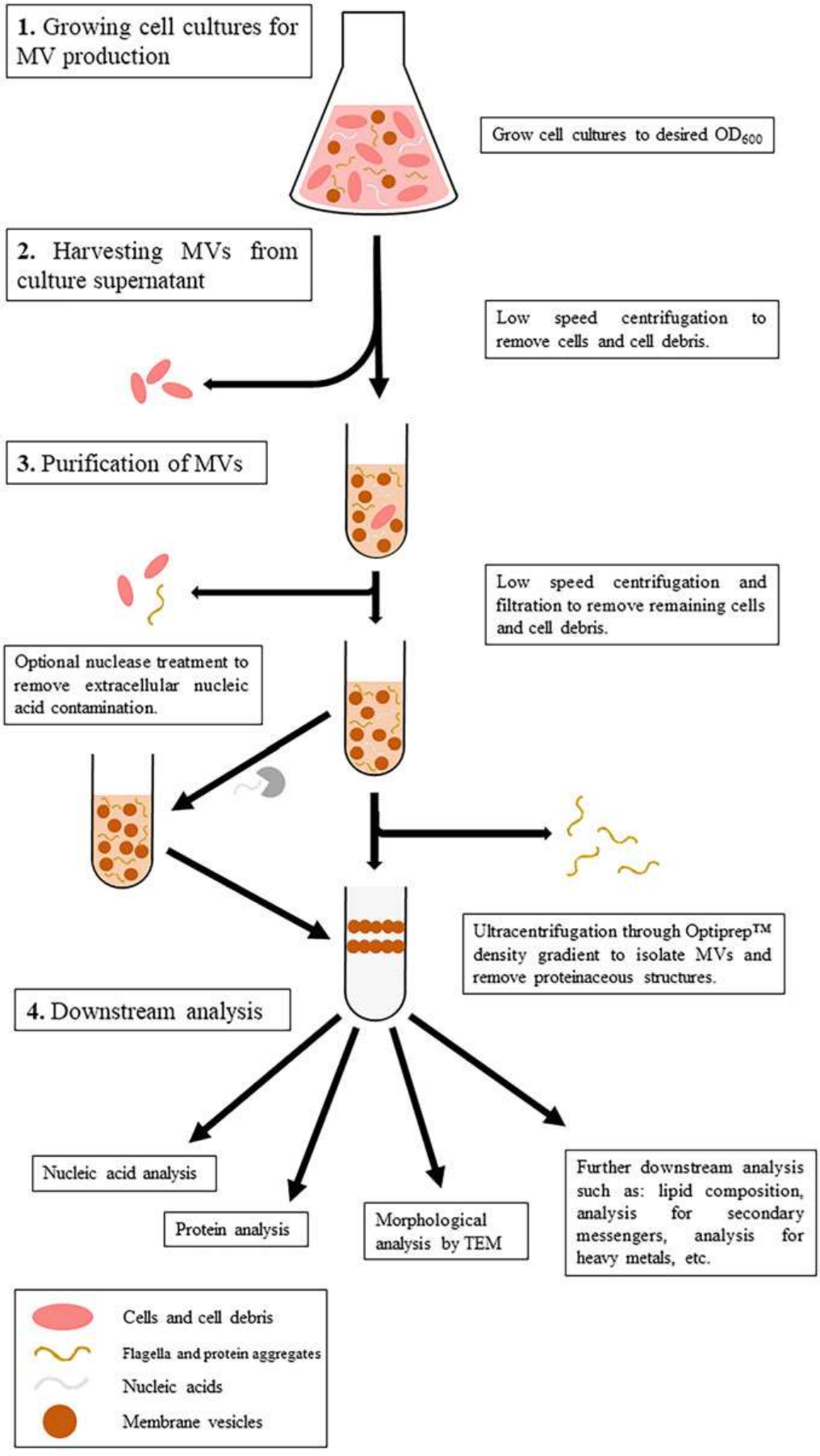

Fig. 1 Flowchart illustrating the workflow for MV isolation, purification, and characterization

2 Materials

All solutions are prepared with ultrapure water and autoclaved at 121 °C for 25 min, unless specified otherwise. All solutions are stored at room temperature unless stated otherwise. If the brand of a chemical was shown to be influential, it is stated.

2.1 Microbiological Cultures

1. Strain: *Haloferax volcanii* DS2 [23].
2. 1 M Tris-HCl pH 7.4.
3. 1 M $CaCl_2$.
4. 30% BSW: 240 g/L NaCl, 30 g/L $MgCl_2.6H_2O$, 35 g/L $MgSO_4.7H_2O$, 14 g/L KCl, 40 mL/L 1 M Tris-HCl pH 7.4, 10 mL 1 M $CaCl_2$.
5. 10× casamino acid solution: 50 g/L casamino acids (Oxoid: LP0041), pH adjusted to 7.4 with KOH. Autoclave for 10 min. Store at 4 °C.
6. Trace elements solution: 10 mL/L 25% HCl, 1.5 g/L $FeCl_2.4H_2O$, 190 mg/L $CoCl_2.6H_2O$, 100 mg/L $MnCl_2.4H_2O$, 70 mg/L $ZnCl_2$, 6 mg/L H_3BO_3, 36 mg/L $NaMoO_4.2H_2O$, 24 mg/L $NiCl_2.6H_2O$, 2 mg/L $CuCl_2$. Sterilize through a cellulose acetate syringe filter (0.22 μm) and store at 4 °C.
7. Vitamin solution: 130 mg/L 4-aminobenzoate; 30 mg/L D-(+)-biotin; 330 mg/L nicotinic acid; 170 mg/L D-(+)-panthothenate; 500 mg/L pyridoxamine hydrochloride; 330 mg/L thiamine chloride hydrochloride; 170 mg/L cyanocobalamin; 100 mg/L lipoic acid; 100 mg/L riboflavin; 40 mg/L folic acid. Sterilize through a cellulose acetate syringe filter (0.22 μm) and store at 4 °C.
8. HV-cab media: 600 mL/L 30% BSW, 300 mL/L sterile H_2O, 100 mL/L 10× casamino acid solution, 100 μL/L trace elements solution, 100 μL/L vitamin solution. Media is prepared by mixing the sterile media components in a sterile graduated cylinder without additional autoclaving.
9. 10× YPC solution: 50 g/L yeast extract (Oxoid: LP0021), 10 g/L peptone (Oxoid: LP0037), 10 g/L casamino acids (Oxoid: LP0041), with pH adjusted to 7.4 with KOH. Autoclave for 10 min. Store at 4 °C.
10. HV-YPC media: 600 mL/L 30% BSW, 300 mL/L sterile H_2O, 100 mL/L 10× YPC solution, 100 μL/L trace elements solution, 100 μL/L vitamin solution. Media is prepared by mixing the sterile media components in a sterile graduated cylinder without additional autoclaving.

11. HV-YPC 1% Agar plates: Mix 600 mL/L 30% BSW, 300 mL/L sterile H_2O, 100 mL/L 10× YPC solution, and 10 g/L agar (Oxoid: LP0011B) in a Schott bottle. Autoclave the solution to sterilize. Once the solution has cooled to 50 °C, add 100 μL/L trace elements solution and 100 μL/L vitamin solution. Mix thoroughly before pouring into plates. Allow for the plates to cool at RT before storing at 4 °C.
12. 50 mL tubes.
13. Sterile, autoclaved Erlenmeyer flasks: This protocol describes a 1 L final culture, but volumes can be scaled up or down. For the 100 mL culture, a 250 mL flask is used. For the 1 L culture, a 2 L flask is used (*see* **Note 1**).

2.2 Harvesting MVs from Culture Supernatant

1. Sterile centrifugation bottles (250 mL to 1 L) and large capacity high-speed centrifuge, including rotor.
2. Sterile Schott bottles: For a 1 L culture, a 2 L Schott bottle is used for PEG precipitation.
3. 40% PEG 6000 solution: Add 400 g PEG 6000 to 600 mL H_2O, and bring the volume to 1 L. Make sure solution is completely dissolved before autoclaving.
4. 22% BSW: Dilute 30% BSW to 22% with sterile water.

2.3 Purification of MVs

1. Small capacity high-speed centrifuge.
2. Ultracentrifuge.
3. Cellulose acetate syringe filters (0.45 and 0.22 μm) and syringes.
4. Optiprep™ gradient solutions: From a 60% stock of Optiprep™ Density Gradient Medium, make aliquots of 35%, 30%, 25%, 20%, and 15% Optiprep™ solutions in 22% BSW (*see* **Note 2**).
5. 12 mL ultraclear tubes for ultracentrifuge.
6. RNase A (10 mg/mL).
7. DNase I (2000 U/mL).

2.4 Downstream Analysis of MVs

1. Parafilm and filter paper.
2. 2% uranyl acetate solution: Dissolve 0.2 g of uranyl acetate dihydrate (*see* **Note 3**) in 10 mL of ddH_2O and sterilize through a cellulose acetate syringe filter (0.22 μm).
3. Transmission electron microscopy (TEM) grids: Formvar/carbon supported copper grids.
4. Lysis Buffer: 50 mM Tris–HCl pH 7.5, protease inhibitor, 5 mM DTT. Sterilize through a cellulose acetate syringe filter (0.22 μm) and use timely.

5. Sonicator (Sonoplus, Bandelin electronic, tip: MS72/MS73) (*see* **Note 4**).
6. DNase I (2000 U/mL).
7. Ultracentrifuge and corresponding rotor and tubes.
8. RNase A (10 mg/mL).
9. 1.5 and 2 mL tubes.
10. Water bath sonicator (Bandelin Sonorex TK52) (*see* **Note 4**).
11. 25% SDS in water. Sterilize through a cellulose acetate syringe filter (0.22 μm).
12. 30% CHAPS in water. Sterilize through a cellulose acetate syringe filter (0.22 μm).
13. Trichloroacetic acid (4 °C).
14. Acetone (4 °C).

3 Methods

At each step of the protocol, aliquots can be taken and abundance and purity of MVs inspected by transmission electron microscopy (TEM). The experimental workflow is summarized in Fig. 1.

3.1 Growing Cell Cultures for MV Production

To obtain sufficient amounts for downstream analysis, we recommend at least a 500 mL culture per downstream analysis for *Haloferax volcanii* DS2 (*see* **Note 5**). All solutions used are at room temperature unless stated otherwise.

1. From a frozen glycerol stock, streak out *H. volcanii* DS2 for single colonies on a HV-YPC agar plate. Incubate at 45 °C until colonies form.
2. Inoculate 10 mL HV-cab media in a sterile 50 mL Falcon culture tube with one colony. Grow at 45 °C for approximately 2 days (OD_{600nm} ~ 1.0, in exponential growth) (*see* **Note 6**).
3. Add the 10 mL culture to 90 mL HV-cab media (final volume 100 mL) in an Erlenmeyer flask. Grow at 45 °C for approximately 2 days (OD_{600nm} ~ 1.0, in exponential growth).
4. From the 100 mL culture, inoculate 1 L of HV-YPC in a flat-bottomed Erlenmeyer flask with a starting OD_{600nm} of 0.05. Grow at 28 °C at low shaking speed (100–120 rpm) until stationary phase is reached (6–10 days) (*see* **Note 7**).

3.2 Harvesting MVs from Culture Supernatant

1. Once cells have reached stationary phase, centrifuge the culture at 11,295.1 × *g* (e.g., 8000 rpm on JA-10 rotor, Beckman) for 40 min at RT (*see* **Note 8**). Cells and cell debris will be pelleted while other smaller structures, such as the MVs, will remain in suspension in the supernatant (*see* **Note 9**).

2. Transfer the supernatant into a sterile Schott bottle (*see* **Note 10**).
3. Add 40% PEG 6000 to the supernatant to a final concentration of 10% PEG 6000. Invert the bottle to mix thoroughly and incubate at 4 °C overnight (*see* **Note 11**).
4. Invert the bottle to mix. Centrifuge the solution to pellet the MVs at 29,993.7 × *g* (minimum 10,000 × *g* at the top of the tube, e.g., 14,000 rpm on JA-14 rotor, Beckman) for 50 min at 4 °C.
5. Discard the supernatant (*see* **Note 12**) and resuspend the pellet in the least possible amount of 22% BSW (1 mL of 22% BSW is usually enough per rotor tube). Transfer the resuspended MV pellet to 2 mL tubes. To recover remaining MVs and MV containing solution from the centrifuge bottles, you may add another 1 mL 22% BSW, resuspend remaining traces of the pellet and transfer the solution into the same 2 mL tube. This maximizes the amount of MVs recovered during this process (*see* **Note 13**). Store preparation at 4 °C or continue with MV purification.

3.3 Purification of MVs

1. To remove the remaining larger contaminants such as cells or cell debris, spin down the samples in a benchtop centrifuge at max speed (~20,000 × *g*) for 10 min at RT. Transfer the supernatant to a new 2 mL tube and repeat this centrifugation step. Transfer the supernatant to a new 2 mL tube.
2. Pool samples and filter through a 0.45 μm syringe filter (*see* **Note 14**). Use 1–2 mL 22% BSW to wash the filter (so that the total amount of flow through corresponds at least to the amount of MV solution you added to the filter), and save all the flow through (*see* Fig. 2a). For additional purity, samples can then be filtered again through a 0.22 μm syringe filter (*see* **Notes 15** and **16**).
3. If the sample will be used for downstream nucleic acid analysis, add 10 μL RNase A and 10 μL DNase I per 1 mL sample. Mix carefully and incubate for at least 2 h at 37 °C (or overnight). If not proceed directly to **step 4**.
4. Add 40% PEG 6000 to the sample for a final concentration of 10% PEG 6000. Incubate sample at 4 °C for 4 h or overnight.
5. Precipitate MVs in a tabletop centrifuge at max speed (minimum 10,000 × *g*) for 40 min at 4 °C. Remove the supernatant and all remaining liquid with a pipette, making sure not to disturb the MV pellet. Wash the MV pellet by adding 500 μL 22% BSW without dissolving the pellet, centrifuge for 5 min (same settings as previous centrifugation), and discard the supernatant.

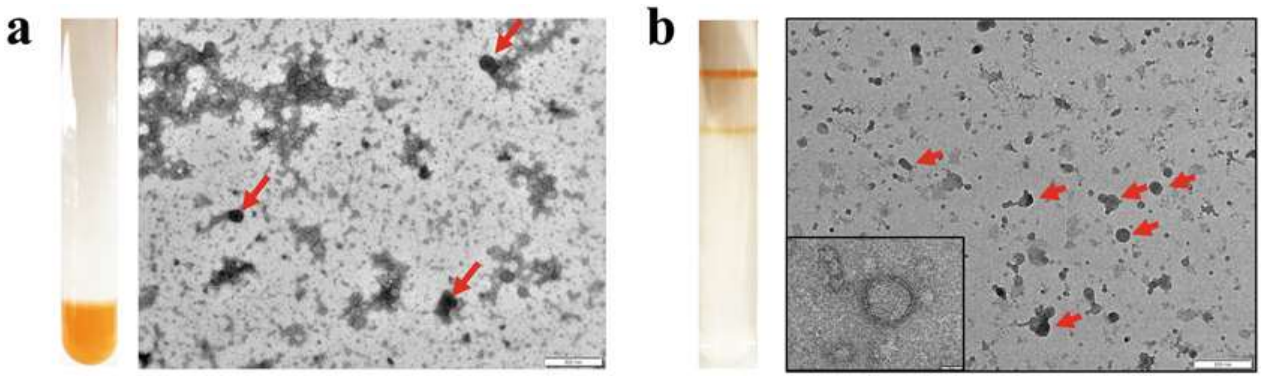

Fig. 2 Purification of MVs. (**a**) *Left*: Optiprep™ density gradient with MV solution prepared as described in **step 7** before ultracentrifugation. *Right*: TEM image of MVs before purification by Optiprep™ density gradient. MVs are marked with red arrows and contaminating debris are visible. (**b**) *Left*: Optiprep™ density gradient after ultracentrifugation with purified and concentrated MVs visible as red bands. *Right*: TEM image of MVs after purification by Optiprep™ density gradient. MVs are more concentrated (marked with red arrows) and most of the contaminating debris have been removed

6. Resuspend pellet in 650 µL 22% BSW (*see* **Note 17**). Then add 1350 µL 60% Optiprep solution and mix carefully so the solution is uniform.
7. Add the 2 mL sample to the bottom of a 12 mL ultracentrifuge tube. Carefully layer on top of the sample 2 mL of the 35% Optiprep gradient solution, then 2 mL of the 30%, and so forth until the final 15% Optiprep gradient solution is placed on top. Mixing of layers can be avoided by slowly pipetting the solutions against the wall of the tube. You should be able to see the individual layers and interfaces.
8. Ultracentrifuge the samples for at least 4 h at 151,263 × *g* in a swing-out rotor (e.g., 35,000 rpm on a SW40Ti rotor) at 4 °C. For more dense samples, 12 h centrifugation was observed to be more effective.
9. Carefully remove the tubes from the rotor. The MVs should be visible as a band at the interface(s) of two layers (*see* Fig. 2b). Carefully remove the MV band(s) with a syringe and needle and deposit into 2 mL tube. Add 40% PEG 6000 to the sample for a final concentration of 10% PEG 6000. Incubate sample at 4 °C for 4 h or overnight.
10. Spin down the sample in a tabletop centrifuge at max speed (minimum 10,000 × *g*) for 40 min at 4 °C. Remove the supernatant and all remaining liquid with a pipette, making sure not to disturb the MV pellet. This pellet should now contain purified MVs that can be used for downstream analyses, and can be frozen in nitrogen and stored at −80 °C. MVs can also be resuspended in 22% BSW and stored at 4 °C, e.g., for TEM.

3.4 Downstream Analyses of MVs

A variety of cargos have been detected in MVs such as nucleic acids or proteins. Here we describe three possible downstream analyses for elucidating the biochemical composition and morphology of MVs.

3.4.1 Preparation of MVs for Transmission Electron Microscopy (TEM)

MV morphology and purity can be analyzed by TEM at each step of the purification process (*see* **Note 18**).

1. Fix a piece of Parafilm on the lab bench. Place a TEM-grid (coated side up) on the Parafilm and apply a 10 μL drop of the sample. Allow the MVs to adsorb to the TEM-grid for about 5 min. Remove the residual sample with a filter paper.
2. Transfer the grid with the sample side down onto a 20 μL drop of 2% uranyl acetate for 2 s. Remove residual liquid with a filter paper.
3. Stain the sample by transferring the grid with the sample side down on a second 20 μL drop of 2% uranyl acetate. Incubate for 2 min and remove residual uranyl acetate by absorption with a filter paper.
4. Analyze the grids for MVs using a transmission electron microscope (*see* **Note 18**).

3.4.2 Nucleic Acid Extraction

1. MV pellets that have been previously nuclease treated (*see* **step 3**, Subheading 3.3) can be used for nucleic acid extraction using a kit or conventional phenol chloroform extractions. Higher yields of RNA have been observed when using TRIzol protocols.
2. MV RNA sequencing and transcript abundance should be compared to intracellular transcript levels, and therefore RNA extraction should be paired with a preserved cellular sample from the time of MV harvesting (*see* **Note 4**).

3.4.3 Proteomic Analysis

To allow a statistical significant analysis of the protein content of MVs, at least three replicate samples are required. We recommend 500 mL of culture supernatant per replicate. The protein content of MVs should be compared with the protein content of cell membranes of the MV-producing cells in order to identify proteins enriched in MVs (*see* **Note 4**). Isolation of cellular membranes is described first. All steps are performed on ice unless stated otherwise.

1. Dissolve cell pellet in cold 20 mL Lysis buffer.
2. Sonicate the sample three times for 30 s (35% output) with 1 min breaks and mixing in between.
3. Add 10 μL DNase I.
4. Centrifuge sample at 8000 × *g* for 30 min at 4 °C to remove remaining intact cells.

5. Transfer the supernatant into an ultracentrifugation tube and centrifuge at 256,136 × *g* (e.g., 38,000 rpm in a SW40Ti rotor) for 15 min at 4 °C to pellet the cell membranes (*see* **Note 19**).
6. Dissolve MV pellet or cell membrane pellet in cold 2 mL Lysis Buffer and add 2 μL RNase A.
7. Transfer the sample into two 1.5 mL tubes (1 mL in each tube), and sonicate for 15 min in a water bath at 4 °C.
8. Add 40 μL 25% SDS and 60 μL 30% CHAPS per 1 mL and mix rigorously by vortexing.
9. Sonicate the sample for 30 min in a water bath at 4 °C.
10. Centrifuge at 12,000 × *g* at 4 °C for 12 min to remove debris and transfer the supernatant of each sample into a fresh 2 mL tube (*see* **Note 20**).
11. Add 250 μL cold (4 °C) trichloroacetic acid to 1 mL sample.
12. Incubate for 10 min at 4 °C.
13. Spin tube on a tabletop centrifuge at 15,800 × *g* for 8 min.
14. Remove supernatant, leaving protein pellet intact.
15. Wash pellet with 200 μL cold (4 °C) acetone.
16. Spin tube in a microfuge at 15,800 × *g* for 5 min.
17. Repeat **steps 14–16** for a total of two acetone washes.
18. Dry the pellet by placing tube at 95 °C in a heat block for 5–10 min to remove acetone.
19. Store at RT until further analysis (*see* **Note 21**).
20. Proteins can be identified by LC-MS/MS after trypsin digest.

4 Notes

1. For *H. volcanii*, we have found it best to use flat-bottomed flasks for the final culture, but other flasks have worked for other haloarchaeal organisms.
2. Optiprep™ density solutions were diluted in 22% BSW as high salt concentrations must be maintained for haloarchaeal MVs. The diluting buffer can be adapted to the organism being used (i.e., low pH buffer for acidophiles).
3. Uranyl acetate is a hazardous substance. Please refer to the safety data sheet for handling and disposal.
4. Protocol is optimized for the instruments stated. Other instruments are suitable, but might require minor adjustments and optimization.

5. The amount of MVs in culture supernatants can vary significantly depending on the organism and growth conditions. MV production can be linked to stress conditions and optimal growth conditions may not induce MV production for specific organisms. Therefore, the amount grown and conditions of growth should be adjusted appropriately to yield a sufficient amount of sample for downstream analysis.
6. Cells can be activated on rich media plates. However, synchronizing the cells in lower nutrient media prior to transferring the cells into rich media for MV production has worked for other haloarchaea [3]. Nevertheless, it is difficult to judge whether it would enhance MV production in other archaea.
7. The same organism grown in different laboratories can reach stationary phase at different times and with different terminal maximum OD_{600nm}. Therefore, the point of harvesting a culture should be adjusted based on the growth of the organism in your laboratory.
8. If the MVs are intended for nucleic acid or protein analysis downstream, spin down 15–20 mL of cell culture separately 10,000 × *g*, 10 min at RT. The supernatant from this centrifugation can be pooled with the rest of the supernatant from the MV harvest. Wash the cell pellet once with 1 mL 22% BSW and centrifuge in a benchtop centrifuge. Cell pellet should be frozen and stored at −80 °C until nucleic acid or protein extraction.
9. For efficient pelleting of cells, 10,000 × *g* should be maintained across the entire height of the centrifuge bottle.
10. For further purification from cells and cell debris, supernatant can be filtered prior to PEG precipitation. Consider the size of the MVs when deciding on filter cut-off.

    For organisms growing in media with less than 1 M NaCl, the salt concentration in the culture supernatant has to be adjusted to a final of 1 M NaCl for PEG precipitation.
11. Samples incubating with PEG should be kept at 4 °C for a week maximally.
12. For larger quantities of supernatant, multiple rounds of centrifugation may be required. After the final round of centrifugation, place the centrifuge bottles upside-down onto a paper towel for 10 min to ensure that all solution is removed before resuspension.
13. Depending on the organism, conditions of growth, and time of harvest, resuspension of the MV pellet can be difficult. Note that heavily vortexing samples could result in damaged MVs.

14. Sometimes a sample may be too viscous to pass through a 0.45 μm filter. Filtering the sample with a 0.8 μm filter before the 0.45 μm filter may help making the process smoother.
15. If the MVs being isolated have an upper diameter range of >200 nm, then the 0.22 μm filter may retain some of your sample, leading to a downstream bias in particle size. This filtration step in this case may then be omitted.
16. At this step, the protocol may be paused and stored at 4 °C. Long-term stability of MV samples depends on the organism (i.e., for *H. volcanii* we typically keep samples in 4 °C for no longer than a week if proceeding with further purification, but samples for pre-purification TEM imaging have lasted up to a month at 4 °C).
17. If only running one sample through an Optiprep™ density gradient, it is recommended that the sample not be split into two separate samples for a balancing tube, but rather use 22% BSW in place of a sample in another tube. Loss of sample is typical during this step and splitting the sample may result in further loss of sample.
18. For high-resolution TEM images, we recommend using MVs purified as described (*see* Fig. 2b inlet).
19. After this step, the host membrane pellet can be stored at −80 °C or continue with protein isolation as described below. The protocol for protein isolation is the same for MVs and host membranes.
20. After this step, the protein solution can be stored at −80 °C.
21. We recommend running the protein samples on a SDS-PAGE to visualize proteins. Extract the whole lane from the gel for an in-gel trypsin digest and LC-MS/MS identification of proteins.

References

1. Deatherage BL, Cookson BT (2012) Membrane vesicle release in bacteria, eukaryotes, and archaea: a conserved yet underappreciated aspect of microbial life. Infect Immun 80: 1948–1957. https://doi.org/10.1128/IAI.06014-11
2. Gill S, Catchpole R, Forterre P (2019) Extracellular membrane vesicles in the three domains of life and beyond. FEMS Microbiol Rev 43:273–303. https://doi.org/10.1093/femsre/fuy042
3. Erdmann S, Tschitschko B, Zhong L et al (2017) A plasmid from an Antarctic haloarchaeon uses specialized membrane vesicles to disseminate and infect plasmid-free cells. Nat Microbiol 2:1446–1455. https://doi.org/10.1038/s41564-017-0009-2
4. Cai J, Wu G, Jose PA et al (2016) Functional transferred DNA within extracellular vesicles. Exp Cell Res 349:179–183. https://doi.org/10.1016/j.yexcr.2016.10.012
5. Renelli M, Matias V, Lo RY et al (2004) DNA-containing membrane vesicles of Pseudomonas aeruginosa PAO1 and their genetic transformation potential. Microbiology 150:

2161–2169. https://doi.org/10.1099/mic.0.26841-0

6. Soler N, Forterre P (2020) Vesiduction: the fourth way of HGT. Environ Microbiol 22: 2457–2460. https://doi.org/10.1111/1462-2920.15056
7. Ahmadi Badi S, Bruno SP, Moshiri A et al (2020) Small RNAs in outer membrane vesicles and their function in host-microbe interactions. Front Microbiol 11:1209. https://doi.org/10.3389/fmicb.2020.01209
8. Choi DH, Kwon YM, Chiura HX et al (2015) Extracellular vesicles of the hyperthermophilic archaeon "Thermococcus onnurineus" NA1T. Appl Environ Microbiol 81:4591–4599. https://doi.org/10.1128/AEM.00428-15
9. Dauros-Singorenko P, Blenkiron C, Phillips A et al (2018) The functional RNA cargo of bacterial membrane vesicles. FEMS Microbiol Lett 365. https://doi.org/10.1093/femsle/fny023
10. Valadi H, Ekström K, Bossios A et al (2007) Exosome-mediated transfer of mRNAs and microRNAs is a novel mechanism of genetic exchange between cells. Nat Cell Biol 9: 654–659. https://doi.org/10.1038/ncb1596
11. Prangishvili D, Holz I, Stieger E et al (2000) Sulfolobicins specific proteinaceous toxins produced by strains of the extremely thermophilic. J Bacteriol 182:2985–2988
12. Li J, Azam F, Zhang S (2016) Outer membrane vesicles containing signalling molecules and active hydrolytic enzymes released by a coral pathogen Vibrio shilonii AK1. Environ Microbiol 18:3850–3866. https://doi.org/10.1111/1462-2920.13344
13. Manning AJ, Kuehn MJ (2011) Contribution of bacterial outer membrane vesicles to innate bacterial defense. BMC Microbiol 11:258. https://doi.org/10.1186/1471-2180-11-258
14. Li P, Kaslan M, Lee SH et al (2017) Progress in exosome isolation techniques. Theranostics 7: 789–804. https://doi.org/10.7150/thno.18133
15. Taylor DD, Shah S (2015) Methods of isolating extracellular vesicles impact down-stream analyses of their cargoes. Methods 87:3–10. https://doi.org/10.1016/j.ymeth.2015.02.019
16. Brown PN, Yin H (2017) Polymer-based purification of extracellular vesicles. Methods Mol Biol 1660:91–103. https://doi.org/10.1007/978-1-4939-7253-1_8
17. Jeppesen DK, Hvam ML, Primdahl-Bengtson B et al (2014) Comparative analysis of discrete exosome fractions obtained by differential centrifugation. J Extracell Vesicles 3:25011. https://doi.org/10.3402/jev.v3.25011
18. Rider MA, Hurwitz SN, Meckes DG (2016) ExtraPEG: a polyethylene glycol-based method for enrichment of extracellular vesicles. Sci Rep 6:23978. https://doi.org/10.1038/srep23978
19. García-Romero N, Madurga R, Rackov G et al (2019) Polyethylene glycol improves current methods for circulating extracellular vesicle-derived DNA isolation. J Transl Med 17:75. https://doi.org/10.1186/s12967-019-1825-3
20. Klimentová J, Stulík J (2015) Methods of isolation and purification of outer membrane vesicles from gram-negative bacteria. Microbiol Res 170:1–9. https://doi.org/10.1016/j.micres.2014.09.006
21. Horstman AL, Kuehn MJ (2000) Enterotoxigenic e coli secretes active heat labile enterotoxin via OMV. J Biol Chem 275: 12489–12496
22. Ellen AF, Albers S-V, Huibers W et al (2009) Proteomic analysis of secreted membrane vesicles of archaeal Sulfolobus species reveals the presence of endosome sorting complex components. Extremophiles 13:67–79. https://doi.org/10.1007/s00792-008-0199-x
23. Mullakhanbhai MF, Larsen H (1975) Halobacterium volcanii spec. nov., a Dead Sea Halobacterium with a moderate salt requirement. Arch Microbiol 104:207–214

CHAPTER III.

Extracellular Vesicle Formation in *Euryarchaeota* is Driven by a Small GTPase

Joshua Mills[1], L. Johanna Gebhard[1], Florence Schubotz[2], Anna Shevchenko[3], Daan R. Speth[4], Yan Liao[5], Iain G. Duggin[5], Anita Marchfelder[6], Susanne Erdmann[1*]

[1] Archaeal Virology, Max Planck Institute for Marine Microbiology, Celsiusstrasse 1, 28359, Bremen, Germany

[2]MARUM Center for Marine Environmental Sciences, University of Bremen, Bremen 28359, Germany

[3]Max Planck Institute of Molecular Cell Biology and Genetics, Pfotenhauerstrasse 108, 01307, Dresden, Germany

[4]Department of Biogeochemistry, Max Planck Institute for Marine Microbiology, Celsiusstrasse 1, 28359, Bremen, Germany

[5]The Australian Institute for Microbiology and Infection, University of Technology Sydney, Sydney, New South Wales, Australia

[6]Biology II, Ulm University, Ulm, Germany

* To whom correspondence should be addressed: Susanne Erdmann; Tel: +49 421 2028-7340; Email: serdmann@mpi-bremen.de

Author Contributions: J.M. performed the majority of the experimental work. L.J.G. and F.S. performed the lipid analysis. A.S. performed proteomics. Y.L. generated the AglB mutant. D.R.S. performed ArcV phylogeny analysis. S.E. discovered the presence of RNA in EVs, conceived and led the study. I.G.D. and A.M. led the initial phase of the study. Some of the experiments were performed in A.M. laboratory. J.M. and S.E. performed the primary writing of the manuscript. All authors participated in the analysis and interpretation of the data and contributed to the writing of the manuscript.

Competing Interest Statement: The authors declare no competing interests.

Classification: Biological Sciences/Microbiology

Keywords: Extracellular vesicles; Archaea; small RNAs; *Haloferax volcanii;* small GTPase

Proceedings of the National Academy of Sciences, under review.

ABSTRACT

Since their discovery, extracellular vesicles (EVs) have changed our view on how organisms interact with their extracellular world. EVs are able to traffic a diverse array of molecules across different species and even domains, facilitating numerous functions. In this study, we investigate EV production in *Haloferax volcanii*, as representative for *Euryarchaeota*. We uncover that EVs enclose RNA, with specific transcripts preferentially enriched, including those with regulatory potential, and conclude that EVs can act as an RNA communication system between haloarchaea. We demonstrate the key role of an EV-associated small GTPase for EV formation in *H. volcanii* that is also present across other diverse evolutionary branches of Archaea. We propose the name, ArcV, for the newly identified archaeal vesiculating GTPase. Membrane deforming processes that are driven by small GTPases are universal amongst eukaryotes but not bacteria, further supporting the hypothesis that eukaryotes emerged from an archaeal ancestor. Therefore, we propose that archaeal EV formation could reveal insights into the origin of eukaryotic vesiculating GTPases.

SIGNIFICANCE STATEMENT

Extracellular vesicles (EV) play important roles in intercellular communication by transferring various molecules, including proteins, nucleic acids, lipids, and metabolites, between cells. Few studies have investigated their role in the archaeal domain. Here we show that EVs of halophilic Archaea (Haloarchaea), members of the *Euryarchaeota*, transfer an RNA cargo enriched in ncRNAs, and likely contribute to intercellular communication. Additionally, we show that EV formation in Haloarchaea is driven by a small GTPase, that is also conserved across other archaeal lineages, and is both functionally and structurally similar to small GTPases driving intracellular vesicle formation in Eukaryotes. Our work will help in resolving the origin of vesiculating GTPases and thereby shed light on the origin of the eukaryotic endomembrane system.

INTRODUCTION

Extracellular vesicles (EVs) are small membrane bound structures that bud off from the cellular envelope, and are produced by living cells across all domains of life [1–3]. They are able to enclose a wide range of cargo, including proteins, nucleic acids, and signaling molecules, facilitating a mechanism of interaction with the extracellular world. Communication mediated through EVs provides specific advantages for the cell, such as protection of the cargo from environmental stressors and degradation, the concentration of specific molecules into a self-contained structure, and the potential for selective delivery to designated targets [4, 5]. With the diversity of EV composition and the advantages of EV-based communication, prokaryotic EV trafficking has been connected to a wide range of cellular functions. EVs have been discovered to act as defense against viral infection and antibiotic stress [6], mediating Bacteria-host interactions through the trafficking of regulatory RNA [7, 8], and facilitating the transfer of genetic material between cells [9, 10]. Both their ubiquity amongst organisms and cellular functions make EVs an exciting new field for exploring intercellular communication and expand our view of the dynamics driving microbial environments.

EVs are known to be present in marine and aquatic samples [11, 12], and they likely play important roles in regulating environmental microbial populations. However, while there is a growing amount of research focusing on EVs deriving from pathogenic Bacteria and their role in Bacteria-host interactions, fewer studies have investigated the role that EVs play in microbial ecology, and even less investigate EVs in Archaea. Within the archaeal domain, EVs from only a few organisms have been studied [13]. For the *Thermoproteota* (formerly *Crenarchaeota*) genus, *Sulfolobus*, vesicles were found to enclose proteinaceous toxins [14] as well as fragmented genomic DNA [15]. Members of the *Euryarchaeota* have also been found to produce EVs enriched with DNA such as *Thermococcus* [16]. *Halorubrum lacusprofundi* [17] was found to produce specialized EVs including plasmid-encoded proteins and plasmid DNA (named plasmid vesicles, PVs), and plasmid DNA was also found in EVs of *Thermococcus* species [18]. These studies demonstrate the ability of archaeal EVs to transport DNA between cells, which suggests that EV production may play an important role in horizontal gene transfer in Archaea.

EV production in *Sulfolobus* has been linked to its cell division machinery that is driven by ESCRT (endosomal sorting complex required for transport)-like proteins (Cdv proteins) [15]. The ESCRT system is well studied in Eukaryotes, and is responsible for the sorting and production of exosomes and the budding of various viruses [19]. However, ESCRT-like proteins are not present in most currently annotated *Euryarchaeota* genomes [20], suggesting that a different mechanism is responsible for EV production. Instead, proteins with homology to proteins of the eukaryotic intracellular vesicle trafficking system, such as a small GTPase [21] and potential components of a vesicle coat [22] were identified in both EVs and PVs from *Hrr. lacusprofundi*, a member of the *Euryarchaeota*, implying that multiple mechanisms of vesicle production exist within the archaeal domain [17]. Intracellular vesicle trafficking in Eukaryotes is coordinated by different vesicle coat complexes, such as COPI, COPII and clathrin coat complexes, each mediating the trafficking of cargo between different membrane-bound organelles [23]. Vesicle formation is initiated by the activation of a small GTPase, allowing for the recruitment of the respective coat complex [22, 24]. GTPase-mediated intracellular vesicle formation and ESCRT-mediated vesicle formation evolved from different pathways [25]. Additionally, small GTPases and other proteins predicted to be related to components of the eukaryotic endomembrane system were found in the genomes of *Lokiarchaeota* and other Asgardarchaea [26–28], suggesting that the root of eukaryotic, small GTPase-dependent, intracellular vesicle formation lies within Archaea. Intracellular vesicle formation and membrane trafficking mechanisms are essential components of the eukaryotic endomembrane system, and have been hypothesized to be crucial for the emergence of Eukaryotes [29]. While there are hypotheses that argue for either bacterial or archaeal roots of the endomembrane system [30, 31, 27], the experimental evidence to support either hypotheses remains absent.

In order to understand EV production in *Euryarchaeota,* and in particular halophilic Archaea (haloarchaea), we used the model organism *Haloferax volcanii*, to investigate the composition of EVs as well as their capacity to transfer their cargo to other organisms. We observe particular RNAs being enriched in EVs of various haloarchaea, and demonstrate that the RNA cargo can be transferred between cells of the same species. We also investigated the roles of various genes in EV production, including an EV-associated small GTPase, that suggests a mechanism for EV generation in halophilic Archaea that is related to intracellular vesicle trafficking in Eukaryotes. From our findings, we hypothesize that

halophilic Archaea utilize EVs to communicate and potentially regulate the microbial community in hypersaline environments.

RESULTS

Extracellular vesicle production in H. volcanii is dependent on growth conditions

The production of EVs and a set of specific EV-associated proteins has been reported previously for the Haloarchaeon, *Halorubrum lacusprofundi* [17]. To investigate the generation and potential function of EVs in haloarchaea, we chose *H. volcanii*, because it is a well-established model organism for haloarchaeal cell biology with a number of genetic tools available [32, 33]. The capability of *H. volcanii* to produce EVs was also previously reported under UV irradiation [34].

EVs were isolated from culture supernatants of *H. volcanii* and were observed to be spherical with a diameter ranging from 50 to 150 nm (Figure 1A). Purification of EVs by iodixanol (OptiPrep™) density-based gradient purification resulted in EVs concentrating into two distinct bands in the gradient (Supplementary Figure 1A and B). No obvious differences distinguishing the two bands could be observed by TEM (Supplementary Figure 1C and D).

Initial efforts to isolate EVs close to the documented optimal temperature of *H. volcanii* at 45 °C yielded low amounts of EVs while lowering the temperature of growth to 28 °C increased EV yields, suggesting that EV production is temperature dependent. Therefore, we tested different growth temperatures using a fluorescence-based method for EV quantification. We observed a 2.7-fold decrease in EV production between 28 °C and 45 °C during the same stage of growth ($p = 0.014$) (Figure 1B). EV production was determined to peak during the early stationary phase of growth (Figure 1C, Supplementary Figure 2C).

Since stress has also been reported to induce EV production, we tested environmental stress conditions such as UV exposure and virus infection using immunodetection-based EV quantification. UV stress induced a slight increase in EV production (1.3-fold increase, $p = 0.025$), while infection with the chronic infecting virus, HFPV-1 [35], slightly decreased EV production (1.27-fold decrease, $p = 0.043$) (Supplementary Figure 2D and E).

H. volcanii extracellular vesicles are associated with RNA

EVs of both *Sulfolobus* (*Thermoproteota*) and *Thermococcus* (*Euryarchaeota*) were previously shown to enclose DNA [16, 15]. To determine the nucleic acid contents of *H. volcanii* EVs, we attempted to isolate both DNA and RNA from a purified EV preparation. While DNA extraction yielded negligible amounts of DNA, RNA extraction revealed high yields of EV-associated RNA. Nuclease (DNase and RNase) treatment of the EVs prior to RNA extraction did not eliminate the presence of RNA, confirming that the transcripts are protected and likely enclosed within the vesicles. Analysis of the size distribution of the enclosed RNA revealed differences between EV-associated RNA and intracellular RNA (Figure 2A). While ribosomal 16S and 23S rRNA subunits were prominent in both EV and cellular preparations, we observed populations of RNAs that are significantly enriched in EVs with a tendency towards smaller transcripts (Supplementary Figure 3).

Extracellular vesicle-associated RNA is enriched in tRNAs, rRNAs and ncRNAs

Preliminary sequencing approaches of EV-associated RNA revealed that using small RNA libraries (enriching for transcripts below 150 nt in length) best reflects the RNA content of EVs (refer to Supplementary Results for details). Additionally, we compared the RNA content of upper and lower EV bands in density gradients (Supplementary Table 4 and Supplementary Results), revealing that the RNA content alone is unlikely the major factor leading to two subpopulations of EVs. To determine RNA enriched in EVs we normalized EV-associated with intracellular RNA levels at the time point of EV isolation (refer to Supplementary Results for details).

We identified around 4,400 genes represented by EV-associated transcripts, comprising the majority of the *H. volcanii* genome with around 79.5% ± 10.5% of genome covered by at least one read (85.2% ± 0.8% for intracellular reads). Though this encompasses nearly all genes in the *H. volcanii* genome, only 474 of the transcripts identified had a TPM (transcript per million) greater than 10, suggesting the majority of identified EV-associated RNA can be considered transcriptional noise. The most abundant of the identified transcripts were tRNAs (68.9 ± 2.1%), followed by non-coding RNAs (ncRNA, transcripts that do not encode a protein, excluding rRNA and tRNA) and rRNAs (16S, 23S, and 5S) (16.1 ± 0.9% and 10.4 ± 1.2% respectively) (Figure 2B). The identified ncRNA include intergenic sRNAs [36, 37] and antisense RNAs (asRNA). While we also detected mRNAs in the EV fraction, they only constitute about 4.6 ± 0.1% of the RNA population. Notably, when normalized to the intracellular RNA, the EV-associated RNA represented a unique subset of transcripts with little variation among replicates (Figure 3A, Supplementary Table 6). We identified 230 transcripts as highly abundant (TPM > 10) and highly enriched (log2 > 1) in EVs. This population comprised of tRNAs, rRNAs, ncRNAs and mRNAs, with tRNAs being the most dominant group. Surprisingly, while the mRNA fraction was the least represented among EV-associated RNA, the most enriched (242-fold) among all transcripts was the mRNA for the S-layer glycoprotein (HVO_2072). A Northern blot analysis probing for the full-length mRNA (gene length 2484 bp) in intracellular and EV-associated RNA revealed only small fragments of the transcript to be associated with EVs (Supplementary Figure 4). While this could indicate that mRNAs are in general transferred as fragments in EVs, this has not been confirmed for each transcript. Besides HVO_2072, the remainder of highly enriched mRNAs were relatively low in abundance (TPM < 10).

Within the population of ncRNAs associated with EVs, we identified 74 ncRNAs that are both highly abundant and enriched in EVs (Supplementary Table 6). This population consists of intergenic RNAs as well as asRNAs. However, no function has been predicted for any of the intergenic ncRNAs so far. We also screened the ncRNAs for consensus sequences or a common secondary structure as specific selection markers for EV packaging; however, no common motif could be identified. Nevertheless, the identified asRNAs (21 asRNAs) appeared to exhibit sequence and structural similarities (Supplementary Figure 5). The average length of these asRNAs was 45.5 nt (± 5.8 nt), and all are associated with the 5' end of ISH3-, ISH5-, ISH8-, ISH9- and ISH11-type transposases from across the genome, overlapping with the predicted start codons of the respective transposase.

While direct interactions between EVs and viruses have been documented [38, 6], we did not detect any changes to the transcriptional landscape of EVs derived from cultures infected with a chronic virus (see Supplementary Results,

Supplementary Figure 6). However, we identified viral transcripts associated with EVs from infected cultures (Supplementary Figure 7), suggesting that infected cells transport both host and virus-derived transcripts in EVs. However, it remains to be determined whether these transcripts are transferred as a whole or as fragments.

Generation of RNA-enriched extracellular vesicles is also found amongst other haloarchaea

EV production and presence of EV-associated RNA were tested in two other haloarchaeal organisms, *Halobacterium salinarum* and *Halorubrum lacusprofundi*. EVs could be isolated from both organisms (Supplementary Figure 8A and B), and they were likewise found to be enriched in RNA. The size distribution of EV-associated RNA indicates an enrichment for a specific RNA population (Figure 2A and Supplementary Figure 8C).

RNA sequencing of *Hbt. salinarum* EVs revealed 85.4% of the *Hbt. salinarum* genome to be covered by at least one read from EV-associated RNA (94.5% from intracellular RNA library). The distribution of RNA populations were very similar between *H. volcanii* and *Hbt. salinarum* EVs (Figure 2B), with the majority of EV-associated transcripts being tRNAs.

We identified 228 transcripts as highly abundant and highly enriched in *Hbt. salinarum* EVs (Supplementary Table 7). The transcript for the S-layer glycoprotein was also one of the most enriched EV-associated transcripts in *Hbt. salinarum*. The most enriched transcript was a 29 nt asRNA mapping to the coding region of VNG_RS00640, a predicted helix-turn-helix domain protein of unknown function. We also identified 16 highly enriched transposase-associated asRNA that associate with a larger range of transposase families than those from *H. volcanii*, some of which overlap with the respective predicted start codon. In total, 35 ncRNAs were identified as highly enriched and highly abundant in EVs of *Hbt. salinarum*. Of the ncRNA enriched in *Hbt. salinarum* EVs, 6 are sense-overlapping transposase-associated RNA (sotRNA) [39], and 2 are intergenic sRNAs with high sequence identities to the predicted sRNAs from *H. volcanii*, HVO_2908s and H3.2 [36], that were also found in *H. volcanii* EVs.

Extracellular vesicles are enriched with specific proteins

The protein compositions of *H. volcanii* EVs and their respective cellular membranes were identified by mass spectrometry (LC-MS). Comparison of upper and lower EV bands in gradients revealed no significant differences in protein content (Supplementary Figure 9). Therefore, we concluded that protein content alone is most likely not the major factor causing the separation into two bands and pooled the results from both bands for further analysis.

In total, we identified 328 proteins associated with EVs and 668 proteins in the cellular membrane preparations. We compared the abundancies of proteins in EVs with those in cell membranes and obtained 11 proteins significantly enriched in EVs ($\log2 > 1$, adjusted p-value < 0.05) (Supplementary Table 8, Figure 3B), including one protein exclusively detected in EVs (hypothetical protein, HVO_2519, with unknown function and no detectable conserved domains). Several CetZ proteins, including CetZ5 (HVO_2013), CetZ1 (HVO_2204), and CetZ2 (HVO_0745), were identified to be enriched in EVs. CetZ1 and CetZ2 have been shown to be involved in controlling cell shape and motility

in *H. volcanii*, and the CetZ protein family has been predicted to be involved in other cell surface-related functions in Archaea [40, 41].

Other highly enriched proteins include FtsZ2 (cell division protein) [42], HVO_1134 (hypothetical protein), HVO_1987 (Signal peptide peptidase SppA), HVO_2985 (hypothetical protein, no conserved domains), HVO_1964 (PRC-barrel domain), and HVO_B0079 (ABC transporter protein).

Most interesting was the enrichment of a small, single domain GTPase, HVO_3014 (OapA) (Figure 3B), a homolog of the GTPase, Hlac_2746, which was also found to be enriched in *Hrr. lacusprofundi* EVs [17]. OapA was initially thought to have an influence on genome replication due to its association with the origin of replication. However, despite a study characterizing a mutant strain, no distinct function could be assigned to OapA so far [43]. Hidden Markov Model (HMM) based searches [44] identified similarities between the haloarchaeal, vesicle-associated GTPase and other eukaryotic small GTPases involved in vesicle formation.

Differential expression analysis only identifies proteins that are present in higher abundancies in EVs than in cell membranes, leaving out other proteins that could be functionally relevant but are present in equal or lower abundancies when normalized to the cell membrane. For instance, the small GTPase, HVO_3014, was not identified to be enriched in EVs from UV-treated cells using a standard threshold (see Supplementary Results), yet we observe its integral relationship to EV production in *H. volcanii* (see below). Therefore, we also identified the proteins that were found to be present amongst all 12 EV samples analyzed (Supplementary Table 10) and identified 285 proteins present across all samples. All proteins identified as enriched by differential expression analysis were also present in this list, except HVO_2399 identified as enriched only in EVs from UV-treated cells, suggesting that the protein composition slightly changes upon UV exposure. The most abundant protein was cytoskeletal protein, CetZ1 (HVO_2204), followed by the S-layer glycoprotein, HVO_2072. Other notable proteins within this list were ribonuclease J (HVO_2724), diadenylate cyclase (HVO_1660), and a hypothetical protein (HVO_1020). RNase J is an exonuclease, and could be relevant to the enrichment of RNAs found associated in the EVs. Diadenylate cyclases are responsible for the production of cyclic-di-AMP, a common secondary messenger among Bacteria and Archaea, including *H. volcanii* [45]. HVO_1020 is a homolog (55% sequence identity) to *H. lacusprofundi* Hlac_2402, which was also identified in *H. lacusprofundi* EVs. HVO_1020 is predicted to contain an α-solenoid domain, which is found in adaptor proteins of eukaryotic intracellular vesicles coat complexes [25, 46]. A candidate protein possibly representing part of the vesicle coat, exhibiting WD40 repeats conserved in coat complex proteins, was identified in *Hrr. lacusprofundi* EVs (Hlac_0271) [17]. A WD40 repeat-containing protein was also detected as slightly enriched in *Hfx. volcanii* EVs (HVO_2606), though it did not pass the threshold (p-value <0.05).

Knockout of the small GTPase, OapA, abolishes formation of RNA associated EVs

To investigate the proposed involvement of OapA in EV production in *H. volcanii*, we compared the phenotypes of an OapA knockout strain [43] to the respective parental strain (H26). The OapA knockout strain yielded a dramatically

reduced amount of EVs in comparison to the parental strain (about 2.94-fold reduction, p-value = 0.0086) (Figure 4A, Supplementary Figure 11A).

Gradient purification of concentrated OapA mutant supernatant resulted in either no distinct band or only one band with reduced intensity in density gradients of the parental strain (Supplementary Figure 12A and B). RNA extracted from this single band yielded very low RNA concentrations and was not detectable on a fragment analyzer. Therefore, we propose that the remaining particles isolated from supernatants of OapA knockout strain cultures (Supplementary Figure 12C) are vesicles deriving from lysed cells. Additionally, they could represent virus particles from a provirus region that was described to produce virus particles previously [47], which was confirmed to be active in the OapA mutant by genome sequencing (PRJEB58368). We conclude that the strain is unable to produce EVs associated with RNA. Phenotypic changes of the cell morphology were also observed for the knockout strain (Supplementary Figure 13A and B). The formation of rod-shaped cells appears to be less frequent when *oapA* is deleted. Interestingly, the OapA mutant also showed a slightly increased growth rate when compared to the parental strain under the conditions tested (Supplementary Figure 13C).

Further, overexpression of OapA in a wild-type background strain (H26) resulted in increased vesicle production (3.5-fold increase, p-value = 0.0051) (Figure 4B, Supplementary Figure 11B). The hypervesiculation phenotype could also be observed by TEM (Supplementary Figure 11D), further implicating the crucial role of OapA for EV production in haloarchaea. Therefore, we propose the name, ArcV, for the newly identified archaeal vesiculating GTPase.

Two genes (HVO_3013, *oapB*, and HVO_3012, *oapC*) are located in the same operon with *oapA* (Figure 4C), and we identified these genes to be associated with *oapA* homologs in other archaeal lineages (Supplementary Figure 14A and see paragraph '*Archaeal vesiculating GTPase, ArcV, is conserved amongst various archaeal clades*'). Therefore, we will refer to them as ArcV associated proteins, ArcVapA (OapB) and ArcVapB (OapC). Analysis of the predicted tertiary structure (Alphafold2 [48]) of ArcVapA/B did not allow solid conclusions about their function. However, we also investigated their role for EV production in *H. volcanii*, despite the fact that none of the two proteins were identified as EV-associated proteins by mass spectrometry. The proteins are single domain proteins, ArcVapA with a DUF2073 domain and (domain of unknown function) and ArcVapB with a DUF2072 domain (Zn-Ribbon domain of unknown function) (Figure 4C). The knockout strain for ArcVapA resulted in a 3.13-fold reduction in EV production (p = 0.001), while the knockout strain for the Zn-ribbon protein ArcVapB, resulted in a 1.65-fold increase in EV production (p = 0.02) (Supplementary Figure 14B and C).

Extracellular vesicle-associated RNA is taken up by H. volcanii cells

In order to test the ability for EVs to deliver the RNA cargo to a target organism, we used ^{14}C-labelled uracil as a reporter to track the movement of RNA. EV preparations from the EV-defective ArcV knockout strain served as a control.

About 98% of the introduced radioactivity was taken up by both the parental strain and the ArcV knockout strain over 6 days of growth. Subsequently, 1.90% of the radioactivity was detected in EV preparations of the parental strain, whereas only 0.11% was detected in EV preparations of the ArcV knockout strain. After 20 min of incubation of the

labelled EV preparations with fresh cells, we could detect a transfer of radioactivity into the unlabeled cells, with parental strain EVs transferring significantly more radioactivity than the ArcV knockout strain EV preparation ($p = 0.04$) (Figure 5). Measurements after 90 min of incubation did not show a change of radioactive uptake from EVs of both strains ($p = 0.025$ between uptake from parental strain and ArcV knockout strain-prepared EVs), indicating that the transfer was already complete after 20 min. Thereby we confirm that the RNA enclosed in *H. volcanii* EVs can be taken up by *H. volcanii* cells in a short time frame. While we strongly assume that the EV-RNA is internalized by the receiving cells, we cannot exclude that we detect RNA containing EVs that are strongly bound to the cells and were not removed by washing.

Archaeal vesiculating GTPase, ArcV, is conserved amongst various archaeal clades

To get an overview of whether the archaeal vesiculating GTPase, ArcV, is present in other Archaea, we searched for proteins with high similarity to HVO_3014 against archaeal and bacterial GTDB species representatives using an alignment score ratio approach (see methods) [49]. 1666 archaeal proteins were identified across 14 phyla of Archaea, with an uneven distribution of ArcV across these phyla (Supplementary Figure 17, Supplementary Table 12). The majority of ArcV homologs were identified among the *Euryarchaeota* (*Halobacteriota* and *Methanobacteriota*), as well as in 7 DPANN phyla, including *Nanoarchaeota*, *Nanohaloarchaeota*, and *Altiarchaeota*. Interestingly, only 8 *Korarchaeota* out of 970 *Thermoproteota* genomes analyzed contained a homologous small GTPase. Further, only 8 out of 183 *Asgardarchaeota* genomes were identified to contain an ArcV homolog. Notably, we were also unable to identify any homologs in two well-studied EV-producing organisms: *Sulfolobus* (*Thermoproteota*), which is known to generate EVs using ESCRT-like proteins, and *Thermococcus* (*Methanobacteriota_B*), for which the mechanisms of EV formation has not been determined [50, 15].

A phylogenetic tree was constructed from the alignment of ArcV homologs (Figure 6A). Both DPANN and *Euryarchaeota* form well supported (≥ 99 % bootstrap) distinct clades. *Asgardarchaeota*, *Thermoproteota*, and *Hydrothermarchaeota* form a third clade, however, not as well supported (bootstrap value of 56). Overall, the ArcV phylogeny agrees well with the taxonomy of the respective organisms. While we cannot rule out horizontal transfer events during the emergence of ArcV, evidence suggests that ArcV diverged separately within Euryarchaota and DPANN, and might have been inherited vertically. Since Era GTPases represent the closest hit to ArcV in PDB, we included Era representatives into the analysis. Era GTPases clearly build a separate lineage (Supplementary Figure 18) strongly suggesting that ArcV GTPases represent a family distinct from Era GTPases.

Alphafold2 [48, 51] models of *H. volcanii* ArcV were computed as a homodimer (Supplementary Figure 19), because this conformation is known to be required for the activity of eukaryotic vesiculating small GTPases such as Arf1, as well as Era GTPases [52, 53]. Two different structural conformations were predicted that resemble the conformational changes occurring in the activation of eukaryotic Arf1 [54]. ArcV and Arf1 are structurally similar and differ in their dimerization interface (PDB 2F7S, not superimposable with a root mean square deviation of 5.94-Å out of 100 C-alphas). Both proteins contain an N-terminal amphipathic α-helix with hydrophobic residues that are either tucked with the main body of the protein (Figure 6B) or released away from the main body of the protein (Figure 6C). Further, the

release of the α-helix and the alignment of the hydrophobic residues suggest that this protein might interact with the cell membrane in this conformation.

The downstream genes of ArcV (Figure 4C) were analyzed in all 1,666 organisms in which we identified ArcV (Supplementary Table 13). For about 95% of genomes containing ArcV we could identify an ArcVapA homolog with 93% located directly downstream of ArcV, while ArcVapB was identified in 91% with 78% located up to 2 genes downstream.

DISCUSSION

While more evidence arises that extracellular vesicles play important roles in mediating important cellular functions in Bacteria and Eukaryota, there is still a disproportionate lack of information about the function and cargo of EVs in Archaea [13]. EV production has been previously reported in haloarchaea [17, 34], and here we used the haloarchaeal model organism, *H. volcanii*, to investigate the nature of these EVs and the mechanisms of EV production.

EV production by *H. volcanii* appeared to be influenced by temperature and growth phase, with highest yields below reported optimal growth temperatures and during exponential and early stationary growth phases. Interestingly, we detected a drop in EV production as the cultures entered late stationary phase. We suggest this to be due to the cells increasing the rate of uptake or preserving energy for other processes during this stage of growth. Infection with the membrane-surrounded virus, HFPV-1, yielded slightly lower EV production, which we attribute to the increased resources required for virus particle production. While a previous study showed increased EV production under UV exposure at 45 °C [34], we observed a negligible influence of UV exposure under the conditions tested (28 °C), which might be due to the fact that EV production is already increased at 28°C when compared to 45 °C. Analysis of the nucleic acid content of EVs produced by *H. volcanii*, as well as other haloarchaea, revealed that EVs are associated with RNA, as it has been described for some bacterial and eukaryotic EVs [55, 56], indicating that RNA associated EVs are conserved among all three domains of life. *Thermococcus onnurineus* (*Euryarchaeota*) has previously been reported to produce EVs containing RNA [50]; however, no characterization of EV-associated RNA was carried out for this organism. Treatment of EVs with nucleases did not eliminate the presence of EV-associated RNA, therefore, we infer that the RNA is internalized within EVs.

The RNA composition of *H. volcanii* EVs appears to reflect intracellular levels to a certain extent when tested under normal growth conditions and under infection with a virus. However, there is a distinct population of transcripts associated with EVs that does not correlate with the relative intracellular abundance, but is instead more enriched within EVs. The majority of highly enriched transcripts encode for tRNAs and rRNA, and we suggest that they are enriched due to both their structural stability and their high intracellular abundance. Both tRNAs and rRNAs have been observed at high abundancies in vesicle-associated transcriptomics in bacterial EVs [57, 8], and could therefore be a commonality among EVs from prokaryotic organisms. Interestingly, the most enriched mRNA (coding for the S-layer glycoprotein) that we detected was shown to be non-specifically fragmented in the EV-associated RNA fraction, however, the processing of other mRNA transcripts will need to be determined individually. Since we could not identify a common sequence or structural motif that would allow for a specific selection of particular RNAs to be enclosed into EVs, we

suggest that the size, stability or both are a defining factor for packaging. Additionally, the positioning of an mRNA close to the cell envelope, such as the mRNA of the S-layer glycoprotein, could play a role in determining the RNA population of EVs. Results we obtained from EVs of viral infected cultures (see Supplementary results) showed that the RNA composition did not change significantly upon infection in both cells and EVs; however, we detected viral RNAs in the cells and subsequently also in EVs, clearly demonstrating that the RNA content of EVs represents the current transcriptional state of the EV-producing cell. When exposing cells to UV radiation, we subsequently observed changes to the RNA composition in EVs of UV-treated cells when compared to those of untreated cells (see Supplementary Results). Considering that UV-exposure is known to influence the transcriptional landscape in *H. volcanii* cells [34], we assume that the changes observed in EVs are reflecting changes in the cell. In conclusion, we propose that RNA is taken up randomly into EVs, with transcripts that are highly enriched in the cell as well as transcripts that are translated at the cell envelope being preferably packaged. The respective cargo could be processed within EVs by RNases present in the vesicles, such as an RNase J that was detected by mass spectrometry in EVs, leading to the degradation of mRNAs and a selection towards more stable RNAs (ncRNAs, tRNAs, rRNAs). Alternatively, there could also be a preselection for small-sized RNAs for packaging into EVs. Both scenarios lead to an RNA cargo representing a transcriptomic snapshot of the cell with a particular enrichment in RNAs with a regulatory potential (ncRNAs, tRNAs), as we observe in *H. volcanii* EVs.

The expression of ncRNAs in *H. volcanii* has been observed to shift dramatically under different conditions [58], and we predict that the population of packaged ncRNAs also reflects this shift. There are some notable, studied examples showing EV-packaged ncRNAs regulating gene expression in a receiving organism, such as EV-associated ncRNAs of *Vibrio fischeri* [8] and *Pseudomonas aeruginosa* [7]. We identify ncRNAs with regulatory potential associated with *H. volcanii* and *Hbt. salinarium* EVs. For example, we find a number of asRNAs overlapping with the start codon of various transposases that could potentially modulate transposase activity in a receiving organism. Unfortunately, the other identified ncRNAs are currently uncharacterized or do not have predicted functions. We have demonstrated that EVs of *H. volcanii* are able to transfer RNA between cells, and that RNA associated EVs are also produced by other haloarchaea. Therefore, we propose that halophilic archaea produce EVs as an intercellular communication mechanism to reflect the current intracellular state of the organism, and possibly influence gene expression in the receiving cell, allowing a timely response to environmental stimuli.

Proteomic analysis of EVs allowed us to draw conclusions about the mechanisms of the formation of EVs in haloarchaea. We identified an EV-associated small GTPase (OapA), a protein exhibiting an α-solenoid domain (HVO_1020) and a protein containing WD40 repeats (HVO_2606) with homologs also identified in EVs from *Hrr. lacusprofundi* [17]. Small GTPases and proteins containing WD40-repeats and α-solenoids represent major components of vesicle coats in the eukaryotic endomembrane system [22, 25, 46, 59]. Manipulation of OapA expression had strong effects on EV production. While the knockout of OapA resulted in an EV-defective strain, overexpression of OapA lead to hypervesiculation, demonstrating the key role of this protein in EV formation in *H. volcanii*. The only other known system where small GTPases are crucial for the production and trafficking of various vesicles, is the eukaryotic endomembrane system [60]. The production of these vesicles requires the activation of the small Arf-family GTPase in

order to recruit the coat complex, resulting in deformation of the membrane and subsequent budding of the vesicle [61, 62]. Deletion of this protein in Eukaryotes results in the elimination in the production of these intracellular vesicles [63], and we have observed a similar suppression when knocking out the small GTPase in *H. volcanii*, proving the existence of an archaeal vesiculating (ArcV) GTPase that regulates vesicle production in Archaea. Structural prediction of ArcV as a homodimer reveals similarities to eukaryotic Arf-family GTPases. Two different structures were predicted for ArcV with the N-terminal α-helix either tucked into the protein or released away from the main body of the protein, opening extra room in the GDP binding site. This suggests that upon activation and incorporation of GTP, a amphiphilic α-helix is able to protrude and likely interacts with the cell membrane, similar to what has been observed for Arf1 [64, 52]. Therefore, we predict that vesicle generation in haloarchaea follows a mechanism similar to eukaryotic endomembrane vesicle formation, in that activated ArcV uses the N-terminal α-helix to interact with the cell membrane. Activation would then promote membrane deformation either from ArcV itself or through recruitment of other coat components, such as HVO_1020 or HVO_1134.

We identified other proteins that could also play a role in EV function, such as those with enzymatic functions or transport related proteins. Enzymatic activity was detected for EVs from the abundant marine cyanobacterium, *Prochlorococcus* [65], suggesting that EV-associated proteins can facilitate specific reactions extracellularly. CetZ proteins were found particularly prominent in EVs of *H. volcanii* and *Hrr. lacusprofundi* [17]. However, EV production was not altered in knockout strains of the respective CetZ proteins (Supplementary Results), suggesting that they do not play a significant role in EV formation in *H. volcanii*. CetZ proteins are known to be associated with the cell envelope [40], and we assume that this loose association could lead to enclosing of CetZ proteins during EV formation. Components of ABC transport systems, in particular also solute-binding proteins of ABC transporters, make up the overall majority of proteins associated with EVs of *H. volcanii*, and were also detected in high abundancies in EVs and PVs of *Hrr. lacusprofundi* [17] as well as other characterized EVs [15]. While this enrichment could be due to their high abundance in the cell envelope, the binding capacity of the EV-associated solute-binding proteins could also allow sequestration of rare nutrients that could be incorporated by the receiving cell [66]. Alternatively, EVs could play a role in the removal of obsolete proteins from the cell envelope, such as components of ABC transporters, allowing the cell to refresh the composition of the envelope to better adapt to their environment. Furthermore, we identified a highly enriched diadenylate-cyclase, an enzyme involved in the formation of cyclic di-AMP. These molecules are known secondary messengers in *H. volcanii* [45] and could be enriched with EVs, providing an additional mechanism of communication.

Analysis of the lipid composition of EVs in comparison to the lipid composition of whole cells and cell membranes revealed some unexpected differences (see Supplementary Results and Supplementary Discussion). We were able to detect the major bilayer forming lipids PG-AR, Me-PGP-AR, S-2G-AR, C-AR, 2G-AR and cardiolipins, that were previously described for *H. volcanii* [67, 68] in all samples. However, the lipid composition of EVs differed significantly to that of cells and cell membranes when comparing the relative abundance patterns of different lipid groups. EVs were observed to be enriched with saturated lipids as has been observed in other bacterial EVs [12, 69], suggesting that membrane rigidity may play a role in EV production [11]. EVs of the hyperthermophilic *Sulfolobus solfataricus* were

also shown to contain the same lipid species as their respective producing cells with significant shifts in the ratio of particular lipid compounds [70], similar to what we observe in *H. volcanii*. Differences between the lipid composition of cells and EVs suggests a specific enrichment of particular lipid compounds in the EVs. This evidence, along with the enrichment of specific proteins and RNA in EVs and temperature-dependency point towards an active mechanism for EV production.

Since the GTPase ArcV appears to be central to EV formation in *H. volcanii*, we searched for homologous proteins in public databases. While ArcV is absent from organisms that have been shown to exhibit an alternative mechanisms for EV formation [16], we identified ArcV GTPases across not only haloarchaea and *Euryarchaeota*, but also within other major branches in the archaeal domain, such as the deep-branching lineage of DPANN Archaea. This suggests that the ArcV-driven mechanism of EV production is widespread among specific clades of Archaea, and we propose to classify these GTPases as ArcV-family GTPases. Phylogenetic analyzes of the ArcV GTPases show that they group in accordance to their taxonomy, suggesting that they could have been inherited vertically. However, without experimental investigation, we do not know whether all ArcV-family GTPases are involved in EV production; though the presence of ArcV in DPANN and *Euryarchaeota* shows that vesiculating GTPases evolved much earlier in evolution than previously thought [27, 28]. Small eukaryote-like GTPases have been identified previously in Archaea and Bacteria, some of which clustering closely with known eukaryotic Ras-like or Arf-like GTPases [27, 71]. While it has been speculated that the origins of intracellular vesicle trafficking could stem from a bacterial endosymbiont [30], there is no evidence for any similar mechanism to the eukaryotic endomembrane system existing in the bacterial domain. Rather, the evidence presented in this paper suggest that the mechanisms for GTPase-dependent membrane deformation and vesicle production already existed in Archaea as is suggested by other hypotheses [72, 27]. Additionally, while we only provide one example of an archaeal GTPase that functions in EV production, this does not exclude the possibility for other homologs to facilitate invagination processes. Further investigation into the function of archaeal GTPases in other lineages (such as in DPANN) as well as mechanistic studies are required in order to draw conclusions on the nature of this novel family of GTPases.

We identified two genes downstream of ArcV (*arcvapA* and *arcvapB*) that are also present in the majority of other organisms encoding for ArcV. While ArcVapA is most often located directly downstream of ArcV, the position of ArcVapB is slightly less conserved. Both genes are also observed to be involved in vesicle formation. While the function of the DUF2073 domain in ArcVapA is unknown, Zn-finger domains (present in ArcVapB) are known to be crucial components of GTPase activating proteins (GAP) for Arf [73, 74]. GAPs are negative regulators of GTPases required for transitioning the GTPase from the active form (membrane-bound) to the inactive form (membrane-free). Since knockout of ArcVapB leads to overvesiculation, possibly due to disregulation of ArcV, we suggest that this conserved Zn-ribbon protein could represent a GAP. Knockout of ArcVapA, the DUF2073 protein, leads to an EV-defective strain, suggesting that ArcVapA could be the corresponding guanine nucleotide exchange factor (GEF). GEFs are required for inducing the release of GDP from the GTPase, allowing for the association of GTP and subsequent activation of the GTPase [75]. For Arf and Sar, activation of the GTPase results in membrane binding and the recruitment of the coat complex [23]. However, neither ArcVapA nor ArcVapB show any homology to the functional domains in the eukaryotic

GAPs and GEFs, and the predicted structure does not allow reasonable conclusion about their function. Therefore, further experimental evidence is required to confirm the relationship between these proteins and EV production in Archaea.

In summary, we show that EV production and the enclosing of RNA into EVs is common for multiple haloarchaeal species. We propose that the formation of EVs in haloarchaea is an active and conserved process, considering the conditionality of EV production along with their molecular composition that differs significantly from the originating cell, as well as the crucial involvement of a GTPase that is conserved among haloarchaea and other archaeal lineages. The enrichment of RNA with regulatory potential in EVs and the conservation of this process among different species lets us propose that halophilic Archaea utilize EVs as a communication mechanism, influencing gene expression at a population-wide scale, as it has been proposed for some Bacteria [7, 8]. Our work suggests that vesiculating GTPases driving intracellular vesicle trafficking in Eukaryotes could have emerged from an archaeal ancestor, as it has been proposed earlier [17], and evolved earlier in evolution than previously thought. While both, an archaeal and a bacterial origin has been proposed [17, 27, 30], the experimental evidence presented in this work supports the hypothesis of an archaeal origin of the eukaryotic endomembrane system.

METHODS

Strains and media

Haloferax volcanii strains and other haloarchaea used in this study are summarized in Supplementary Table 1. *H. volcanii* was either grown in Hv-Ca supplemented with the SL10 trace elements and vitamins as described for DBCM2 [76] (Hv-Cab), or Hv-YPC supplemented with the same trace elements and vitamins [76]. For auxotrophic strains, media was supplemented with uracil (50 µg/mL) and tryptophan (50 µg/mL), as required (Supplementary Table 1). *Halobacterium salinarum* was grown as described in [77]. *Halorubrum lacusprofundi* was grown in DBCM2 media [76]. UV treatment (0.05 J) was performed in a petri dish using a UV crosslinker (Biometra™). Infection of *H. volcanii* cultures with the virus HFPV-1 was performed as described in [35]. Cultures were grown in glass flasks aerobically at 120 rpm at the temperatures indicated.

Generation of knock out strains

To construct plasmids for the deletion of *aglB* gene, PCR fragments of the upstream and downstream flanking sequences (~ 530 bp) (primers listed in Supplementary Table 2) were joined by Gibson assembly and ligated into pTA131 [78] using *Bam*HI and *Hind*III restriction sites. The resulting plasmid was demethylated and transformed into *H. volcanii* H26 using the two-step procedure (pop-in and pop-out) [78]. The oapA deletion strain [43] was obtained from Jörg Soppa and confirmed by genome sequencing. Library preparation (FS DNA Library, NEBNext® Ultra™) and sequencing (Illumina HiSeq3000, 2 x 150 bp, 1 Gigabase per sample) was performed at the Max Planck-Genome-Centre Cologne (Cologne, Germany).

Isolation and purification of EVs

EVs from *H. volcanii* were isolated and purified as described in [79] (for details see supplementary methods). Purification using an OptiPrep™ density gradient yielded two bands containing EVs.

EVs from *Hrr. lacusprofundi* were isolated and purified following methods in [17]. EVs from *Hbt. salinarum* were isolated as described for *H. volcanii*, with growth temperature of 45 °C.

Transmission electron microscopy

Samples were adsorbed onto a carbon coated copper grid (FCF200-Cu) for 3 min and negatively stained with 2% uranyl acetate for 45 s. Grids were imaged at 200 kV with JEOL JEM-2100 Plus transmission electron microscope.

EV quantification

Two different quantification methods were used, because each of them proved unsuitable for some conditions tested (see Supplementary Methods for details).

EVs were quantified from 2 mL of culture supernatant after removal of cells through centrifugation at room temperature (~20,000 x *g*, 10 min twice, followed by 30 min) and filtration through a 0.22 µm pore filter.

For quantification using fluorescence labeling, MitoTracker® Green (Invitrogen) (final concentration 500 nM) was added to the EV solution containing 10% PEG6000, inverted to mix, and incubated at room temperature for 30 min. EVs were pelleted by centrifugation (~20,000 x *g*, 40 min, 4 °C). The EV pellet was then resuspended in 200 µL 22% buffered sea water (BSW) [76]. Fluorescence was measured on a Spectrophotometer (DeNovix, DS-11 FX+) with blue excitation (470 nm) and emission between 514-567 nm. Background fluorescence was determined by performing the same procedure on sterile media. Normalized relative fluorescence units (RFU) were determined by subtracting background fluorescence from each measurement, and dividing by the OD_{600} of the respective culture at the time of harvesting.

For quantification using immunodetection, EVs were pelleted by centrifugation (20,000 x *g*, 4 °C, 40 min) after PEG precipitation (10% final concentration). The pellet was resuspended in 100 µL of 50 mM Tris-HCl to lyse EVs. 10 µL of the EV preparation was spotted onto a nitrocellulose membrane (BioRad), and dried for 1.5 hours. Blocking was performed with blocking solution (60 g skimmed milk powder in 20 mL 1X TBS buffer [10X TBS buffer: 24 g/L Tris-HCl, 5.6 g/L Tris, and 88 g/L NaCl, with pH adjusted to pH 7.6 with HCl]) for 30 min, followed by incubation with the primary antibody (against HVO_2204, CetZ1 [40], that was found to be highly enriched in EVs [17]) 1:1,000 diluted in blocking solution for 1 hr. The membrane was washed twice with 1X TBS-TT (10X TBS-TT is 10X TBS buffer with 5 mL/L Tween 20 and 5 mL/L Triton X) and once with 1X TBS before incubation with the secondary antibody (IgG anti-rabbit HRP conjugate, Promega) 1:1,000 diluted in blocking solution for 1 hr. Washing steps were repeated and chemiluminescence was visualized using Clarity Western ECL Substrate (Bio Rad). Chemiluminescence intensity was calculated using ImageJ [80].

RNA extraction and transcriptomic analysis

RNA was extracted from cell pellets or EV pellets using TRIzol™ (Thermo Fischer Scientific) [81] (see Supplementary Methods for details). Total RNA libraries (NEBNext® Ultra™ II RNA Library Prep Kit for Illumina) and small RNA libraries (RealSeq®-AC miRNA Library Kit) were prepared and sequenced (1x 150bp, 1 Gb per sample) at the Max Planck-Genome-Center (Cologne, Germany). Preliminary RNA sequencing experiments (see Supplementary Results) were conducted with one replicate, while the final RNA sequencing for both untreated and HFPV-1 infected *H. volcanii* were performed in triplicates. RNA sequencing for *H. salinarum* was conducted with one replicate of cellular RNA, and two replicates of EV-associated RNA pooled together. Read mapping and calculations of gene expression and differential expression was performed using Geneious Prime® (2021.0.1). Reads were mapped to a compiled version of all genomic elements using the Geneious mapper (including a standard read trimming step) with 99% minimum overlap identity (90% minimum overlap identity for preliminary *H. volcanii* read mapping and *Hbt. salinarum* RNAseq). For samples with 3 or more replicates, differential expression was calculated with DESeq2, thereby normalizing EV-associated RNA to intracellular RNA. For samples with only one replicate, the default Geneious differential expression calculator was used. Transcripts were considered significant if transcripts per million (TPM) was greater than 10, log2 fold change was greater than 1, and p-value was lower than 0.05. Consensus sequences were predicted using MEME [82] with default settings. Sequence alignment and structural alignment among asRNA was predicted using locaRNA [83–85], with the temperature setting set to 28 °C.

Northern blot

The Northern blotting protocol was adapted from [86] (see Supplementary Methods for details).

Plasmid construction and expression of OapA

The coding region for *oapA* was amplified by PCR (primers listed in Supplementary Table 2), and ligated into pTA1852 (see supplementary methods for details) using *Pci*I and *Eco*RI restriction sites. The resulting plasmid was demethylated [87] and transformed into *H. volcanii* strain H26 [88].

Expression of tagged OapA ($OapA_t$) was adapted from [89]. Transformed strains were grown in Hv-YPC supplemented with 200 µg/mL tryptophan at 28 °C until OD_{600} of approximately 1. Cultures were then supplemented with 18% BSW containing 5 mg/mL tryptophan (final concentration of 450 µg/mL tryptophan). Cultures were grown for 2 hrs at 28 °C before EVs were quantified as described. Affinity purification of $OapA_t$ was modified from [90] (see supplementary methods for details).

Protein extraction and analysis

Protein content of EVs was compared with protein content of cell membranes as described previously [17]. Proteins were isolated from purified EVs (triplicates of each upper band and lower band in density gradients) and host membranes (in triplicates) from untreated and UV-treated samples as described in [79]. TCA precipitated proteins were dissolved in 30 µL 1 x Laemmli sample buffer and separated (3 cm) on Any kD™ Mini-PROTEAN® TGX™ Precast Protein

Gels (Bio-Rad Laboratories, Germany). The gels were visualized with Coomassie staining and each gel lanes cut into two slabs, which were processed individually. Proteins were in-gel reduced with dithiothreitol, alkylated with iodoacetamide and digested overnight with trypsin (Promega Mannheim, Germany). Resulting peptide mixtures were extracted twice by exchange of 5% of formic acid (FA) and acetonitrile, extracts pooled together and dried down in a vacuum centrifuge. Peptides were then re-suspended in 25 µL of 5% formic acid and a 5 µL aliquot was analyzed by LC-MS/MS on a nano-UPLC system Ultimate3000 series interfaced to a LTQ Orbitrap-Velos mass spectrometer (both Thermo Fisher Scientific, Bremen, Germany). The nano-UPLC was equipped with an Acclaim PepMap100 C18 75 µm i.d. x 20 mm trap column and a 75 µm x 15 cm analytical column (3 µm/100 Å, Thermo Fisher Scientific, Bremen, Germany). Peptides were separated using 80 min linear gradient; solvent A was 0.1% aqueous formic acid and solvent B was 0.1% formic acid in neat acetonitrile. Spectra were acquired using Data Dependent Acquisition (DDA) method and Top 20 approach; lock mass was set on m/z = 445.1200 (polydimethylcyclosiloxane). Three blank runs were performed after each sample analysis to avoid carryover. Acquired spectra were searched against *H. volcanii* proteins in NCBI database (June 2020, 12045 entries) by MaxQuant software (v. 1.6.10.43) using default settings and MBR (Matched Between Runs) option. False Discovery Rate (FDR) was 1%, variable modifications – methionine oxidized, cysteine carbamidomethylated and propionamide; two miscleavages allowed; minimal number of matched peptides – two. Relative quantification was performed using LFQ intensity values calculated by MaxQuant. Proteins were only considered present in EVs if matched with two or more peptides in all EV samples for that condition, and a respective LFQ value was identified in all EV samples for that condition.

Differential expression of proteins was calculated using R package, DEP (differential enrichment analysis of proteomics data) (v. 1.21.0) [91], based on the LFQ intensity values generated by MaxQuant. We analyzed biological triplicates of upper and lower EV bands in OptiPrep™ gradients separately for protein content. However, only 1 protein was found to be more abundant in the upper band and 2 more abundant in the lower band, while the majority of proteins appeared to be consistent between upper and lower bands (Supplementary Figure 9). Therefore, results from upper and lower bands were pooled for a total of 6 biological replicates of EV samples and compared to 3 biological replicates of cell membrane samples. The threshold for significant enrichment in EVs was a log2 fold change greater than 1 and adjusted p-value lower than 0.05.

Identification and phylogenetic analysis of small GTPases and associated proteins across the archaeal domain

Tertiary structure of the OapA dimer was predicted with AlphaFold v2 [48, 51]. Homologs of small GTPase, HVO_3014, were identified in major archaeal clades using DELTA-BLAST (default settings), and only hits that contained a complete GTPase binding domain and had a similar length (< 250 aa) were included. This resulted in 21 sequences from different organisms, including *H. volcanii* and *Hrr. lacusprofundi*. These 21 sequences were used as a reference database in a DIAMOND [92] search (score cutoff = 50) using as query the entire protein content of a non-redundant set of 78,768 archaeal and bacterial genomes comprised of the genome taxonomy database (GTDB) species representatives (r207) [93] and the global catalog of earth's microbiomes (GEM) OTU dataset [94] dereplicated at 95%

average nucleotide identity using fastANI [95]. This search resulted in 96,121 hits, and 1,686 true positive hits were subsequently selected using an alignment score ratio approach, allowing us to identify sequences with both high identity to the proteins of interest as well as a similar length [96, 49]. This set was further manually curated, removing the only 5 bacterial GTPases based on protein phylogeny using FastTree 2 [97] and MUSCLE [98], as well as removing 15 sequences longer than 250 amino acids. This resulted in a final protein set of 1,666 archaeal GTPase sequences. The final dataset was aligned with MUSCLE and a phylogenetic tree was constructed using IQ-Tree [99] with ultrafast bootstrap analysis [100] using 1000 bootstrap replicates and default settings, auto-selecting the substitution model [101]. The phylogenetic tree was visualized on iTOL (v 6.6) [102] as unrooted, and taxonomy was mapped onto the resulting tree. The same approach was used to identify ArcVapA and ArcVapB homologs (for details refer to Supplementary Methods).

Tracking of EV uptake using 2-14C Uracil

To generate EVs containing radiolabeled RNA, uracil auxotrophic parental strain, H26 [78], and uracil auxotrophic deletion mutant H26Δ*oapA* were inoculated into 50 mL of Hv-Cab supplemented with a mix of unlabeled uracil and 14C labeled uracil (8.621 µg/mL final concentration, 25 µCi per culture) with an optical density (600 nm) of 0.05, each in triplicates. Cultures were grown at 28 °C for seven days before EVs were harvested. To harvest the EVs, cells were pelleted by centrifugation (4000 x *g*, 1 hr). The supernatant was filtered through a 0.22 µm pore filter to remove the remainder of larger contaminants. EVs in the flow through were then concentrated with Vivaspin® 20 (10,000 MWCO, Sartorius). The filters were washed three times with 22% BSW to remove residual unincorporated 14C uracil and subsequently concentrated to 500 µL of radiolabeled EVs per replicate. *H. volcanii DS2* was grown in HV-YPC media at 45 °C until OD (600 nm) of 1. 60 mL of culture were harvested by centrifugation (4000 x *g*, 20 min), washed with 6 mL HV-YPC and subsequently resuspended in 6 mL HV-YPC. For each replicate, 500 µL of cell concentrate were incubated with the 500 µL of EV concentrate in a heat block at 28 °C, 300 rpm. After 20 and 90 minutes post incubation, 300 µL were removed for measurement. The cells were pelleted (5 min, 10000 x *g*) and washed 3 times with 22% BSW to remove any residual EVs present. The resulting cell pellet was resuspended in 500 µL 22% BSW, added to 4 mL scintillation fluid (Ultima Gold™ XR, Perkin Elmer) and measured in a scintillation counter (Tri-Carb 4910 TR, Perkin Elmer). Significance was calculated using one-tailed t-test.

DATA AVAILABILITY

Raw data for resequencing of H26 Δ*oapA* mutant are available at ENA under project number PRJEB58368. Raw data for all RNA sequencing experiments for *H. volcanii* and *Hbt. salinarum* are available at ENA under project numbers PRJEB58342 and PRJEB58367 respectively. The mass spectrometry proteomics data have been deposited to the ProteomeXchange Consortium via the PRIDE [103] partner repository with the dataset identifier PXD038319 and 10.6019/PXD038319.

ACKNOWLEDGMENTS

We thank the Max Planck-Genome-Centre Cologne (Cologne, Germany) for assistance with DNA and RNA sequencing. We thank Ingrid Kunze (MPI for Marine Microbiology, Bremen, Germany) for assistance with the experiments. We thank Thandi Schwarz (Ulm University) for help with the Northern Blots. We thank Jörg Soppa (Goethe-University Frankfurt) for providing the OapA knockout strain. We thank Thorsten Allers for providing the vector used in this study. We thank José Vicente Gomes-Filho (MPI for Terrestrial Microbiology, Marburg) for assistance with transcriptomic analysis. Finally, we want to thank the Max-Planck-Institute for Marine Microbiology and the Max-Planck-Society for continuous support.

REFERENCES

1. Deatherage BL, Cookson BT (2012) Membrane vesicle release in bacteria, eukaryotes, and archaea: a conserved yet underappreciated aspect of microbial life. Infect Immun 80:1948–1957. https://doi.org/10.1128/IAI.06014-11
2. Gill S, Catchpole R, Forterre P (2019) Extracellular membrane vesicles in the three domains of life and beyond. FEMS Microbiol Rev 43:273–303. https://doi.org/10.1093/femsre/fuy042
3. Schatz D, Vardi A (2018) Extracellular vesicles - new players in cell-cell communication in aquatic environments. Curr Opin Microbiol 43:148–154. https://doi.org/10.1016/j.mib.2018.01.014
4. Hasegawa Y, Futamata H, Tashiro Y (2015) Complexities of cell-to-cell communication through membrane vesicles: implications for selective interaction of membrane vesicles with microbial cells. Front Microbiol 6:633. https://doi.org/10.3389/fmicb.2015.00633
5. Tashiro Y, Hasegawa Y, Shintani M et al. (2017) Interaction of Bacterial Membrane Vesicles with Specific Species and Their Potential for Delivery to Target Cells. Front Microbiol 8:571. https://doi.org/10.3389/fmicb.2017.00571
6. Manning AJ, Kuehn MJ (2011) Contribution of bacterial outer membrane vesicles to innate bacterial defense. BMC Microbiol 11:258. https://doi.org/10.1186/1471-2180-11-258
7. Koeppen K, Hampton TH, Jarek M et al. (2016) A Novel Mechanism of Host-Pathogen Interaction through sRNA in Bacterial Outer Membrane Vesicles. PLoS Pathog 12:e1005672. https://doi.org/10.1371/journal.ppat.1005672
8. Moriano-Gutierrez S, Bongrand C, Essock-Burns T et al. (2020) The noncoding small RNA SsrA is released by Vibrio fischeri and modulates critical host responses. PLoS Biol 18:e3000934. https://doi.org/10.1371/journal.pbio.3000934
9. Cai J, Wu G, Jose PA et al. (2016) Functional transferred DNA within extracellular vesicles. Exp Cell Res 349:179–183. https://doi.org/10.1016/j.yexcr.2016.10.012
10. Soler N, Forterre P (2020) Vesiduction: the fourth way of HGT. Environ Microbiol 22:2457–2460. https://doi.org/10.1111/1462-2920.15056
11. Toyofuku M, Tashiro Y, Hasegawa Y et al. (2015) Bacterial membrane vesicles, an overlooked environmental colloid: Biology, environmental perspectives and applications. Adv Colloid Interface Sci 226:65–77. https://doi.org/10.1016/j.cis.2015.08.013
12. Biller SJ, Schubotz F, Roggensack SE et al. (2013) Bacterial Vesicles in Marine Ecosystems. Science 343:183–186
13. Liu J, Soler N, Gorlas A et al. (2021) Extracellular membrane vesicles and nanotubes in Archaea. Microlife 2:uqab007. https://doi.org/10.1093/femsml/uqab007

14. Prangishvili D, Holz I, Stieger E et al. (2000) Sulfolobicins specific proteinaceous toxins produced by strains of the extremely thermophilic archaeal genus Sulfolobus. Journal of Bacteriology 182:2985–2988

15. Liu J, Cvirkaite-Krupovic V, Commere P-H et al. (2021) Archaeal extracellular vesicles are produced in an ESCRT-dependent manner and promote gene transfer and nutrient cycling in extreme environments. ISME J 15:2892–2905. https://doi.org/10.1038/s41396-021-00984-0

16. Gaudin M, Gauliard E, Schouten S et al. (2013) Hyperthermophilic archaea produce membrane vesicles that can transfer DNA. Environ Microbiol Rep 5:109–116. https://doi.org/10.1111/j.1758-2229.2012.00348.x

17. Erdmann S, Tschitschko B, Zhong L et al. (2017) A plasmid from an Antarctic haloarchaeon uses specialized membrane vesicles to disseminate and infect plasmid-free cells. Nat Microbiol 2:1446–1455. https://doi.org/10.1038/s41564-017-0009-2

18. Gaudin M, Krupovic M, Marguet E et al. (2014) Extracellular membrane vesicles harbouring viral genomes. Environ Microbiol 16:1167–1175. https://doi.org/10.1111/1462-2920.12235

19. Henne WM, Buchkovich NJ, Emr SD (2011) The ESCRT pathway. Dev Cell 21:77–91. https://doi.org/10.1016/j.devcel.2011.05.015

20. Makarova KS, Yutin N, Bell SD et al. (2010) Evolution of diverse cell division and vesicle formation systems in Archaea. Nat Rev Microbiol 8:731–741. https://doi.org/10.1038/nrmicro2406

21. Segev N (2011) GTPases in intracellular trafficking: an overview. Semin Cell Dev Biol 22:1–2. https://doi.org/10.1016/j.semcdb.2010.12.004

22. Faini M, Beck R, Wieland FT et al. (2013) Vesicle coats: structure, function, and general principles of assembly. Trends Cell Biol 23:279–288. https://doi.org/10.1016/j.tcb.2013.01.005

23. Kirchhausen T (2000) Three Ways to Make a Vesicle. Nature 1:187–198

24. Devos D, Dokudovskaya S, Alber F et al. (2004) Components of coated vesicles and nuclear pore complexes share a common molecular architecture. PLoS Biol 2:e380. https://doi.org/10.1371/journal.pbio.0020380

25. Field MC, Sali A, Rout MP (2011) Evolution: On a bender--BARs, ESCRTs, COPs, and finally getting your coat. J Cell Biol 193:963–972. https://doi.org/10.1083/jcb.201102042

26. Spang A, Saw JH, Jørgensen SL et al. (2015) Complex archaea that bridge the gap between prokaryotes and eukaryotes. Nature 521:173–179. https://doi.org/10.1038/nature14447

27. Klinger CM, Spang A, Dacks JB et al. (2016) Tracing the Archaeal Origins of Eukaryotic Membrane-Trafficking System Building Blocks. Mol Biol Evol 33:1528–1541. https://doi.org/10.1093/molbev/msw034

28. Eme L, Tamarit D, Caceres EF et al. (2023) Inference and reconstruction of the heimdallarchaeial ancestry of eukaryotes. Nature. https://doi.org/10.1038/s41586-023-06186-2

29. Schlacht A, Herman EK, Klute MJ et al. (2014) Missing pieces of an ancient puzzle: evolution of the eukaryotic membrane-trafficking system. Cold Spring Harb Perspect Biol 6:a016048. https://doi.org/10.1101/cshperspect.a016048

30. Gould SB, Garg SG, Martin WF (2016) Bacterial Vesicle Secretion and the Evolutionary Origin of the Eukaryotic Endomembrane System. Trends Microbiol 24:525–534. https://doi.org/10.1016/j.tim.2016.03.005

31. Dacks JB, Field MC (2007) Evolution of the eukaryotic membrane-trafficking system: origin, tempo and mode. J Cell Sci 120:2977–2985. https://doi.org/10.1242/jcs.013250

32. Lam WL, Doolitle WF (1989) Shuttle vectors for the archaebacterium halobacterium volcanii. Proc. Natl. Acad. Sci. USA 86:5478–5482

33. Bitan-Banin G, Ortenberg R, Mevarech M (2003) Development of a gene knockout system for the halophilic archaeon Haloferax volcanii by use of the pyrE gene. Journal of Bacteriology 185:772–778. https://doi.org/10.1128/JB.185.3.772-778.2003

34. Delmas S, Duggin IG, Allers T (2013) DNA damage induces nucleoid compaction via the Mre11-Rad50 complex in the archaeon Haloferax volcanii. Mol Microbiol 87:168–179. https://doi.org/10.1111/mmi.12091

35. Alarcón-Schumacher T, Naor A, Gophna U et al. (2022) Isolation of a virus causing a chronic infection in the archaeal model organism Haloferax volcanii reveals antiviral activities of a provirus. Proc Natl Acad Sci U S A 119:e2205037119. https://doi.org/10.1073/pnas.2205037119

36. Babski J, Tjaden B, Voss B et al. (2011) Bioinformatic prediction and experimental verification of sRNAs in the haloarchaeon Haloferax volcanii. RNA Biol 8:806–816. https://doi.org/10.4161/rna.8.5.16039

37. Laass S, Monzon VA, Kliemt J et al. (2019) Characterization of the transcriptome of Haloferax volcanii, grown under four different conditions, with mixed RNA-Seq. PLoS One 14:e0215986. https://doi.org/10.1371/journal.pone.0215986

38. Martins SdT, Alves LR (2020) Extracellular Vesicles in Viral Infections: Two Sides of the Same Coin? Front Cell Infect Microbiol 10:593170. https://doi.org/10.3389/fcimb.2020.593170

39. Gomes-Filho JV, Zaramela LS, Italiani VCdS et al. (2015) Sense overlapping transcripts in IS1341-type transposase genes are functional non-coding RNAs in archaea. RNA Biol 12:490–500. https://doi.org/10.1080/15476286.2015.1019998

40. Duggin IG, Aylett CHS, Walsh JC et al. (2015) CetZ tubulin-like proteins control archaeal cell shape. Nature 519:362–365. https://doi.org/10.1038/nature13983

41. Brown HJ, Duggin IG (2023) Diversity and Potential Multifunctionality of Archaeal CetZ Tubulin-like Cytoskeletal Proteins. Biomolecules 13. https://doi.org/10.3390/biom13010134

42. Liao Y, Ithurbide S, Evenhuis C et al. (2021) Cell division in the archaeon Haloferax volcanii relies on two FtsZ proteins with distinct functions in division ring assembly and constriction. Nat Microbiol 6:594–605. https://doi.org/10.1038/s41564-021-00894-z

43. Wolters M, Borst A, Pfeiffer F et al. (2019) Bioinformatic and genetic characterization of three genes localized adjacent to the major replication origin of Haloferax volcanii. FEMS Microbiol Lett 366. https://doi.org/10.1093/femsle/fnz238

44. Zimmermann L, Stephens A, Nam S-Z et al. (2018) A Completely Reimplemented MPI Bioinformatics Toolkit with a New HHpred Server at its Core. J Mol Biol 430:2237–2243. https://doi.org/10.1016/j.jmb.2017.12.007

45. Braun F, Thomalla L, van der Does C et al. (2019) Cyclic nucleotides in archaea: Cyclic di-AMP in the archaeon Haloferax volcanii and its putative role. Microbiologyopen 8:e00829. https://doi.org/10.1002/mbo3.829

46. Fournier D, Palidwor GA, Shcherbinin S et al. (2013) Functional and genomic analyses of alpha-solenoid proteins. PLoS One 8:e79894. https://doi.org/10.1371/journal.pone.0079894

47. Dyall-Smith M, Pfeiffer F, Chiang P-W et al. (2021) The Novel Halovirus Hardycor1, and the Presence of Active (Induced) Proviruses in Four Haloarchaea. Genes (Basel) 12. https://doi.org/10.3390/genes12020149

48. Jumper J, Evans R, Pritzel A et al. (2021) Highly accurate protein structure prediction with AlphaFold. Nature 596:583–589. https://doi.org/10.1038/s41586-021-03819-2

49. Speth DR, Orphan VJ (2018) Metabolic marker gene mining provides insight in global mcrA diversity and, coupled with targeted genome reconstruction, sheds further light on metabolic potential of the Methanomassiliicoccales. PeerJ 6:e5614. https://doi.org/10.7717/peerj.5614

50. Choi DH, Kwon YM, Chiura HX et al. (2015) Extracellular Vesicles of the Hyperthermophilic Archaeon "Thermococcus onnurineus" NA1T. Appl Environ Microbiol 81:4591–4599. https://doi.org/10.1128/AEM.00428-15

51. Evans R, O'Neill M, Pritzel A et al. (2021) Protein complex prediction with AlphaFold-Multimer

52. Diestelkoetter-Bachert P, Beck R, Reckmann I et al. (2020) Structural characterization of an Arf dimer interface: molecular mechanism of Arf-dependent membrane scission. FEBS Letters 594:2240–2253. https://doi.org/10.1002/1873-3468.13808

53. Chen X, Court DL, Ji X (1999) Crystal structure of ERA: a GTPase-dependent cell cycle regulator containing an RNA binding motif. Proc Natl Acad Sci U S A 96:8396–8401. https://doi.org/10.1073/pnas.96.15.8396

54. Goldberg J (1998) Structural basis for activation of ARF GTPase: mechanisms of guanine nucleotide exchange and GTP-myristoyl switching. Cell 95:237–248. https://doi.org/10.1016/S0092-8674(00)81754-7

55. Tsatsaronis JA, Franch-Arroyo S, Resch U et al. (2018) Extracellular Vesicle RNA: A Universal Mediator of Microbial Communication? Trends Microbiol 26:401–410. https://doi.org/10.1016/j.tim.2018.02.009

56. O'Brien K, Breyne K, Ughetto S et al. (2020) RNA delivery by extracellular vesicles in mammalian cells and its applications. Nat Rev Mol Cell Biol 21:585–606. https://doi.org/10.1038/s41580-020-0251-y

57. Ghosal A, Upadhyaya BB, Fritz JV et al. (2015) The extracellular RNA complement of Escherichia coli. Microbiologyopen 4:252–266. https://doi.org/10.1002/mbo3.235

58. Gelsinger DR, DiRuggiero J (2018) Transcriptional Landscape and Regulatory Roles of Small Noncoding RNAs in the Oxidative Stress Response of the Haloarchaeon Haloferax volcanii. Journal of Bacteriology 200. https://doi.org/10.1128/JB.00779-17

59. Park SY, Guo X (2014) Adaptor protein complexes and intracellular transport. Biosci Rep 34. https://doi.org/10.1042/BSR20140069

60. Nielsen E, Cheung AY, Ueda T (2008) The regulatory RAB and ARF GTPases for vesicular trafficking. Plant Physiol 147:1516–1526. https://doi.org/10.1104/pp.108.121798

61. Hsu VW, Yang J-S (2009) Mechanisms of COPI vesicle formation. FEBS Letters 583:3758–3763. https://doi.org/10.1016/j.febslet.2009.10.056

62. Szul T, Sztul E (2011) COPII and COPI traffic at the ER-Golgi interface. Physiology (Bethesda) 26:348–364. https://doi.org/10.1152/physiol.00017.2011

63. Beck R, Sun Z, Adolf F et al. (2008) Membrane curvature induced by Arf1-GTPase is essential for MV formation 105:11731–11736. https://doi.org/10.1073/pnas.0805182105

64. Yu X, Breitman M, Goldberg J (2012) A structure-based mechanism for Arf1-dependent recruitment of coatomer to membranes. Cell 148:530–542. https://doi.org/10.1016/j.cell.2012.01.015

65. Biller SJ, Lundeen RA, Hmelo LR et al. (2022) Prochlorococcus extracellular vesicles: molecular composition and adsorption to diverse microbes. Environ Microbiol 24:420–435. https://doi.org/10.1111/1462-2920.15834

66. Fadeev E, Bastos CC, Hennenfeind J et al. (2022) Characterization of membrane vesicles in Alteromonas macleodii indicates potential roles in their copiotrophic lifestyle

67. Kellermann MY, Yoshinaga MY, Valentine RC et al. (2016) Important roles for membrane lipids in haloarchaeal bioenergetics. Biochim Biophys Acta 1858:2940–2956. https://doi.org/10.1016/j.bbamem.2016.08.010

68. Sprott GD, Larocque S, Cadotte N et al. (2003) Novel polar lipids of halophilic eubacterium Planococcus H8 and archaeon Haloferax volcanii. Biochim Biophys Acta 1633:179–188. https://doi.org/10.1016/j.bbalip.2003.08.001

69. Tashiro Y, Inagaki A, Shimizu M et al. (2011) Characterization of phospholipids in membrane vesicles derived from Pseudomonas aeruginosa. Biosci Biotechnol Biochem 75:605–607. https://doi.org/10.1271/bbb.100754

70. Ellen AF, Albers S-V, Huibers W et al. (2009) Proteomic analysis of secreted membrane vesicles of archaeal Sulfolobus species reveals the presence of endosome sorting complex components. Extremophiles 13:67–79. https://doi.org/10.1007/s00792-008-0199-x

71. Wuichet K, Søgaard-Andersen L (2014) Evolution and diversity of the Ras superfamily of small GTPases in prokaryotes. Genome Biol Evol 7:57–70. https://doi.org/10.1093/gbe/evu264

72. Baum B, Baum DA (2020) The merger that made us. BMC Biol 18:72. https://doi.org/10.1186/s12915-020-00806-3

73. Cukierman E, Huber I, Rotman M et al. (1995) The ARF1 GTPase-activating protein: zinc finger motif and Golgi complex localization. Science 270:1999–2002. https://doi.org/10.1126/science.270.5244.1999

74. Randazzo PA, Hirsch DS (2004) Arf GAPs: multifunctional proteins that regulate membrane traffic and actin remodelling. Cell Signal 16:401–413. https://doi.org/10.1016/j.cellsig.2003.09.012

75. Northup JK, Jian X, Randazzo PA (2012) Nucleotide exchange factors: Kinetic analyses and the rationale for studying kinetics of GEFs. Cell Logist 2:140–146. https://doi.org/10.4161/cl.21627

76. Dyall-Smith, Michael (2009) The Halohandbook: Protocols for haloarchaeal genetics

77. Pfeiffer F, Losensky G, Marchfelder A et al. (2020) Whole-genome comparison between the type strain of Halobacterium salinarum (DSM 3754T) and the laboratory strains R1 and NRC-1. Microbiologyopen 9:e974. https://doi.org/10.1002/mbo3.974

78. Allers T, Ngo H-P, Mevarech M et al. (2004) Development of additional selectable markers for the halophilic archaeon Haloferax volcanii based on the leuB and trpA genes. Appl Environ Microbiol 70:943–953. https://doi.org/10.1128/AEM.70.2.943-953.2004

79. Mills J, Erdmann S (2022) Isolation, Purification, and Characterization of Membrane Vesicles from Haloarchaea. Methods Mol Biol 2522:435–448. https://doi.org/10.1007/978-1-0716-2445-6_30

80. Schneider CA, Rasband WS, Eliceiri KW (2012) NIH Image to ImageJ: 25 years of image analysis. Nature Methods 9:671–675. https://doi.org/10.1038/nmeth.2089

81. Rio DC, Ares M, Hannon GJ et al. (2010) Purification of RNA using TRIzol (TRI reagent). Cold Spring Harb Protoc 2010:pdb.prot5439. https://doi.org/10.1101/pdb.prot5439

82. Bailey TL, Elkan C (1994) Fitting a Mixture Model By Expectation Maximization To Discover Motifs In Biopolymer. Proceedings of the Second International Conference on Intelligent Systems for Molecular Biology:28–36

83. Raden M, Ali SM, Alkhnbashi OS et al. (2018) Freiburg RNA tools: a central online resource for RNA-focused research and teaching. Nucleic Acids Res 46:W25-W29. https://doi.org/10.1093/nar/gky329

84. Will S, Joshi T, Hofacker IL et al. (2012) LocARNA-P: accurate boundary prediction and improved detection of structural RNAs. RNA 18:900–914. https://doi.org/10.1261/rna.029041.111

85. Will S, Reiche K, Hofacker IL et al. (2007) Inferring noncoding RNA families and classes by means of genome-scale structure-based clustering. PLoS Comput Biol 3:e65. https://doi.org/10.1371/journal.pcbi.0030065

86. Adams PP, Flores Avile C, Popitsch N et al. (2017) In vivo expression technology and 5' end mapping of the Borrelia burgdorferi transcriptome identify novel RNAs expressed during mammalian infection. Nucleic Acids Res 45:775–792. https://doi.org/10.1093/nar/gkw1180

87. Gebhard LJ, Duggin IG, Erdmann S (2023) Improving the genetic system for Halorubrum lacusprofundi to allow in-frame deletions. Front Microbiol 14:1095621. https://doi.org/10.3389/fmicb.2023.1095621

88. Cline SW, Schalkwyk LC, Doolittle WF (1989) Transformation of the archaebacterium Halobacterium volcanii with genomic DNA. Journal of Bacteriology 171:4987–4991. https://doi.org/10.1128/jb.171.9.4987-4991.1989

89. Allers T, Barak S, Liddell S et al. (2010) Improved strains and plasmid vectors for conditional overexpression of His-tagged proteins in Haloferax volcanii. Appl Environ Microbiol 76:1759–1769. https://doi.org/10.1128/AEM.02670-09

90. Gamble-Milner R Genetic analysis of the Hel308 helicase in the archaeon Haloferax volcanii

91. Arne Smits , Wolfgang Huber (2017) DEP. Bioconductor

92. Buchfink B, Reuter K, Drost H-G (2021) Sensitive protein alignments at tree-of-life scale using DIAMOND. Nature Methods 18:366–368. https://doi.org/10.1038/s41592-021-01101-x

93. Parks DH, Chuvochina M, Chaumeil P-A et al. (2020) A complete domain-to-species taxonomy for Bacteria and Archaea. Nat Biotechnol 38:1079–1086. https://doi.org/10.1038/s41587-020-0501-8

94. Nayfach S, Roux S, Seshadri R et al. (2021) A genomic catalog of Earth's microbiomes. Nat Biotechnol 39:499–509. https://doi.org/10.1038/s41587-020-0718-6

95. Jain C, Rodriguez-R LM, Phillippy AM et al. (2018) High throughput ANI analysis of 90K prokaryotic genomes reveals clear species boundaries. Nat Commun 9:5114. https://doi.org/10.1038/s41467-018-07641-9

96. Rasko DA, Myers GSA, Ravel J (2005) Visualization of comparative genomic analyses by BLAST score ratio. BMC Bioinformatics 6:2. https://doi.org/10.1186/1471-2105-6-2

97. Price MN, Dehal PS, Arkin AP (2010) FastTree 2--approximately maximum-likelihood trees for large alignments. PLoS One 5:e9490. https://doi.org/10.1371/journal.pone.0009490

98. Edgar RC (2004) MUSCLE: multiple sequence alignment with high accuracy and high throughput. Nucleic Acids Res 32:1792–1797. https://doi.org/10.1093/nar/gkh340

99. Trifinopoulos J, Nguyen L-T, Haeseler A von et al. (2016) W-IQ-TREE: a fast online phylogenetic tool for maximum likelihood analysis. Nucleic Acids Res 44:W232-5. https://doi.org/10.1093/nar/gkw256

100. Hoang DT, Chernomor O, Haeseler A von et al. (2018) UFBoot2: Improving the Ultrafast Bootstrap Approximation. Mol Biol Evol 35:518–522. https://doi.org/10.1093/molbev/msx281

101. Kalyaanamoorthy S, Minh BQ, Wong TKF et al. (2017) ModelFinder: fast model selection for accurate phylogenetic estimates. Nature Methods 14:587–589. https://doi.org/10.1038/nmeth.4285

102. Letunic I, Bork P (2021) Interactive Tree Of Life (iTOL) v5: an online tool for phylogenetic tree display and annotation. Nucleic Acids Res 49:W293-W296. https://doi.org/10.1093/nar/gkab301

103. Perez-Riverol Y, Bai J, Bandla C et al. (2022) The PRIDE database resources in 2022: a hub for mass spectrometry-based proteomics evidences. Nucleic Acids Res 50:D543-D552. https://doi.org/10.1093/nar/gkab1038

FIGURES

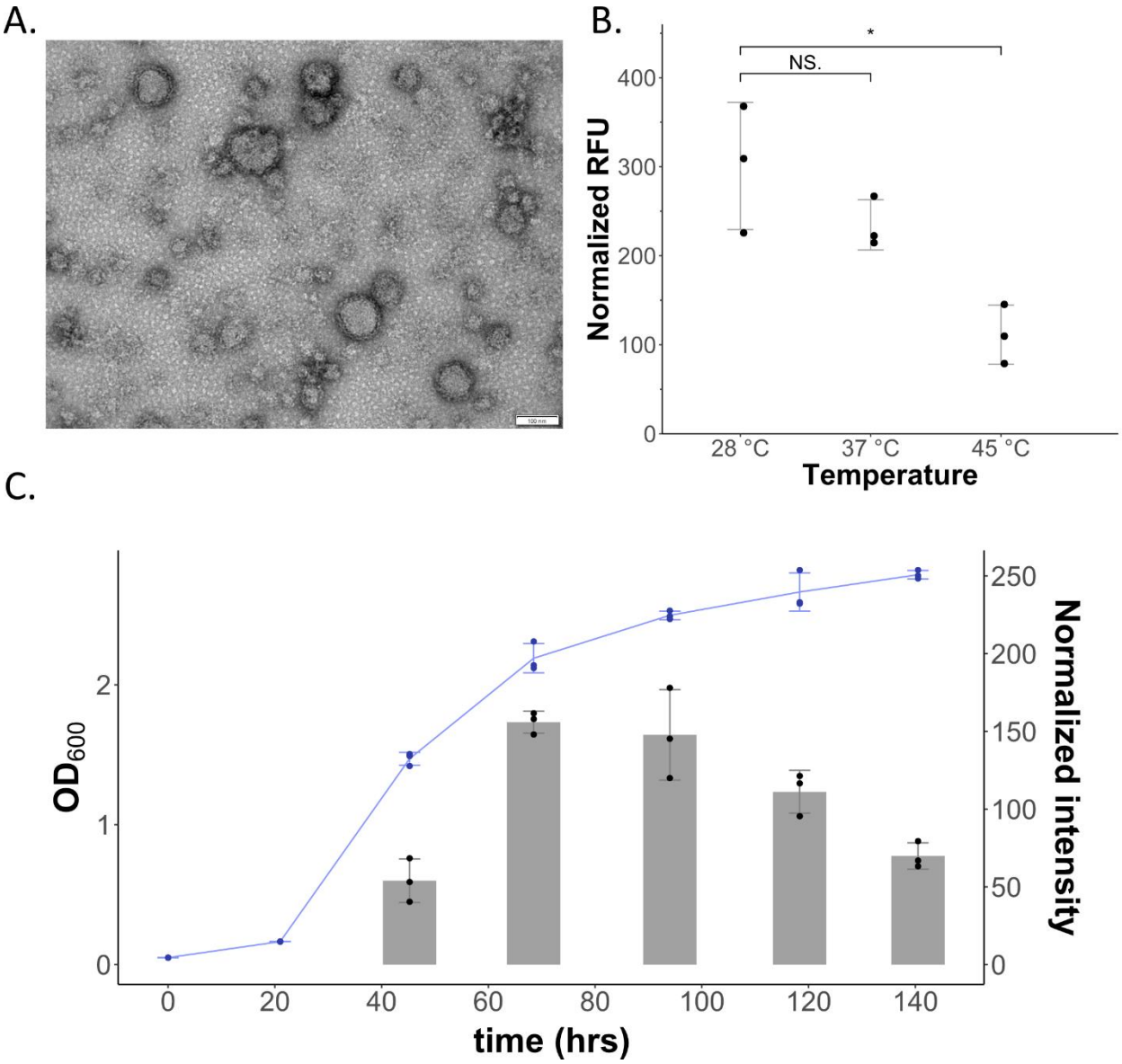

Figure 1. EV production in *H. volcanii DS2*. **(A)** Transmission electron micrograph of EVs. Size bar represents 100 nm. EVs were quantified from the supernatants of cultures **(B)** grown at different temperatures and **(C)** from different stages of growth at 28 °C. Each point indicates one biological replicate (n=3). Error bars indicate the average of three biological replicates ± standard deviation. Temperature-dependent EV production **(B)** was measured using relative fluorescence units (RFU) normalized to culture OD_{600}. Significance is indicated above the graph (NS. indicates "not significant", * indicates "$p \leq 0.05$"). Growth-dependent EV production **(C)** was quantified by immunodetection measuring the intensity of signals on spot blot (original spot blot in Supplementary Figure 2C), normalized to OD_{600}. Growth of cultures indicated in blue follows left axis, while EV production follows right axis.

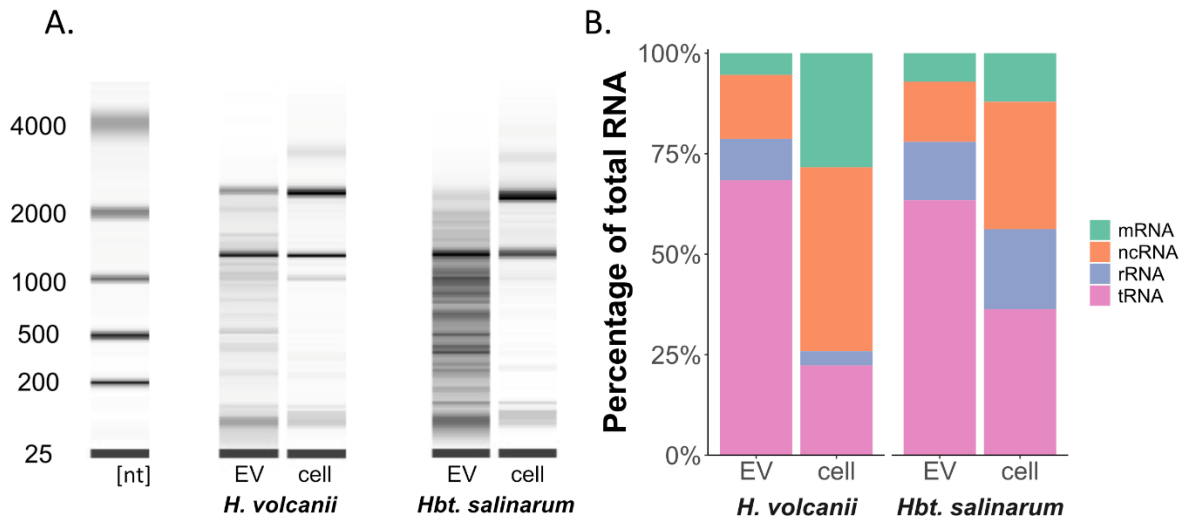

Figure 2. RNA composition of haloarchaeal EVs. (A) Analysis of the size distribution of RNA extracted from one replicate of purified EVs and whole cells of *H. volcanii* and *Hbt. salinarum*. **(B)** Expression levels of different RNA subpopulations calculated in percentage from total RNA expression (using TPM values) comparing cellular and EV-associated RNA for *H. volcanii* (average of three replicates) and *Hbt. salinarum* (one replicate).

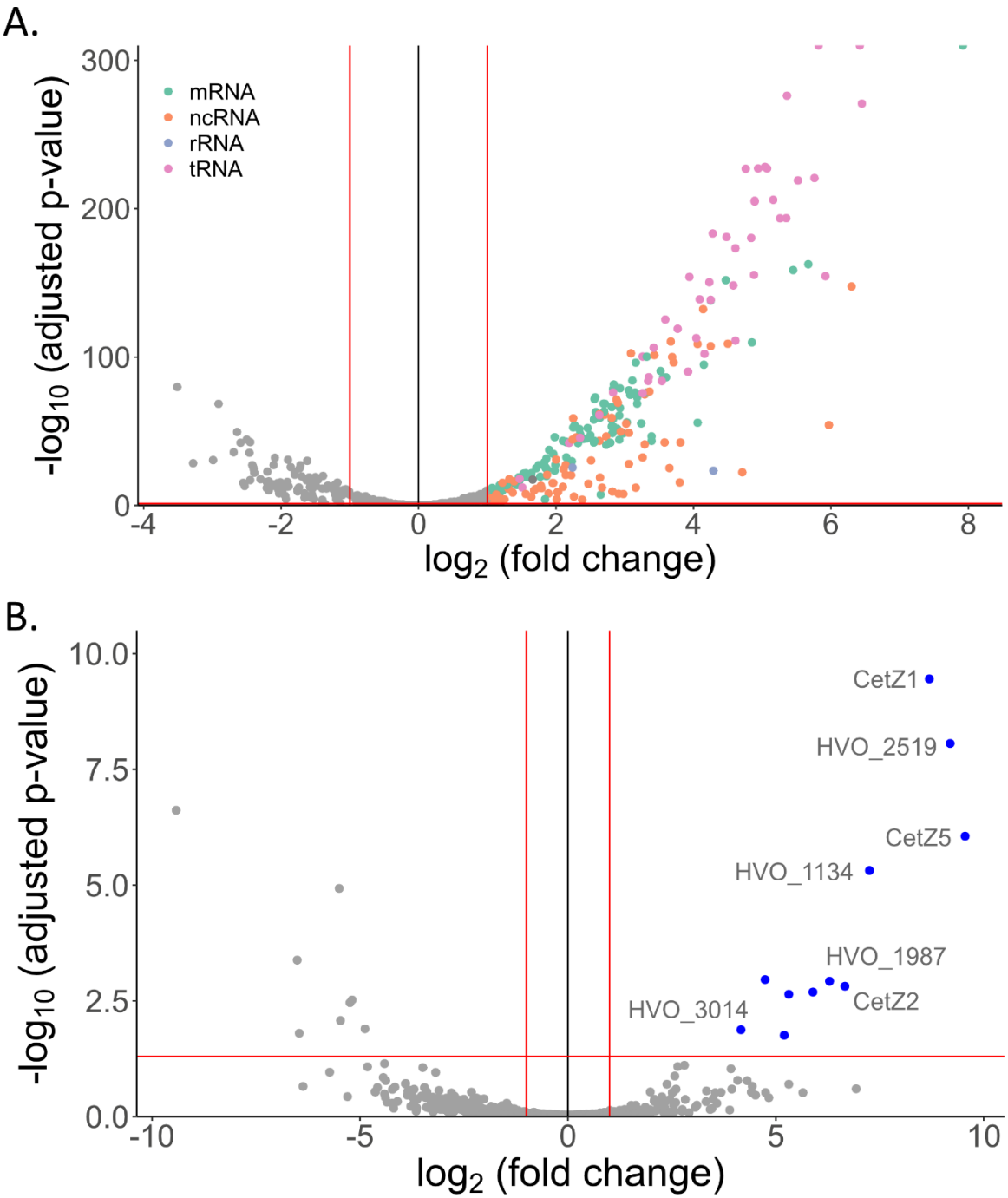

Figure 3. EV associated RNA and proteins. Volcano plots of RNA (**A**) and protein (**B**) abundance in EVs in comparison to cellular RNA abundance and protein abundances from cell membranes. Differential RNA abundancies and adjusted p-values were calculated using DESeq2, and only transcripts with TPM > 10 are represented in this plot. Differential protein abundancies and adjusted p-values were calculated with DEP (see methods). Raw data are presented in Supplementary Tables 6 and 10. Red asymptotes indicate thresholds for enrichment (p = 0.05 and |fold change| = 2)

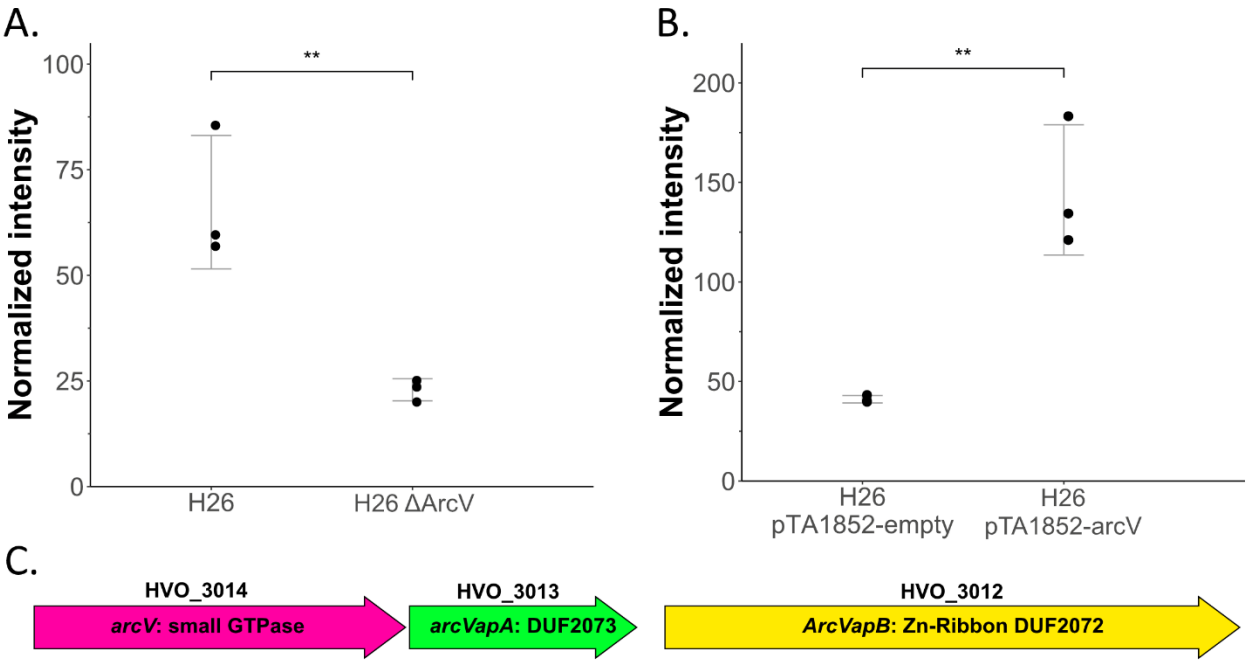

Figure 4. Analysis of *H. volcanii* EV-associated GTPase, ArcV. (A) Quantification of EVs in the culture supernatant of the ArcV knockout strain and the respective parental strain. **(B)** Quantification of EVs in the culture supernatant of a strain overexpressing ArcV (pTA1852-arcV) compared to control empty vector (pTA1852-empty). EVs were quantified by immunodetection and were averaged over three replicates with error bars denoting one standard deviation from the average value. Original spot blots are presented in Supplementary Figure 11A and B. **(C)** Map of the *arcV* operon in *H. volcanii*.

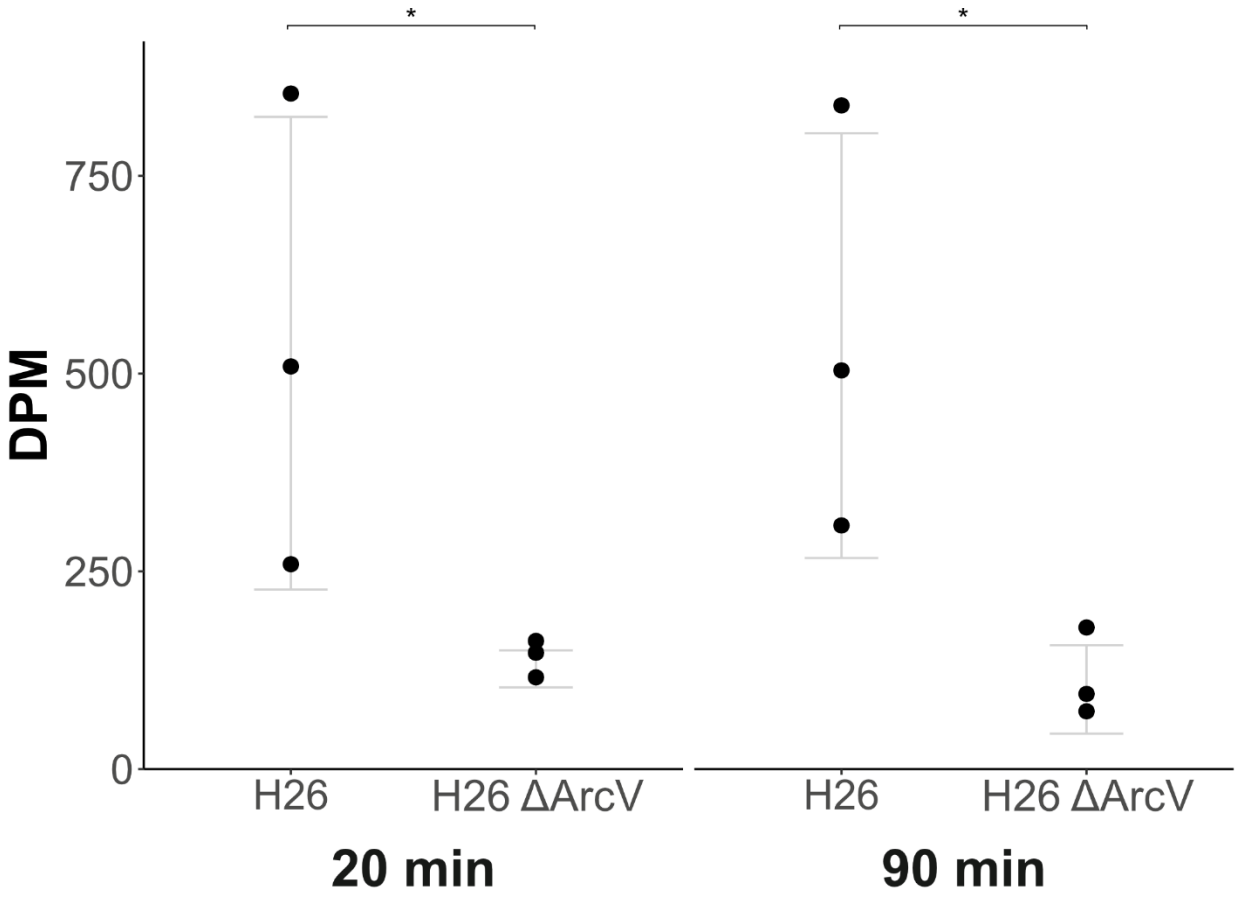

Figure 5. Transfer of radioactively labelled RNA by EVs. EVs were isolated from cells (H26 and H26 ΔarcV) that were incubated with radiolabeled uracil, resulting in EVs associated with radiolabeled RNA. EVs were then incubated with non-labelled wild-type cells and the intracellular radioactivity in decays per minute (DPM) was measured 20 and 90 minutes post incubation, and normalized by subtracting background radiation (~15 DPM). Significance was calculated using a one-tailed t-test (* indicates "$p < 0.05$).

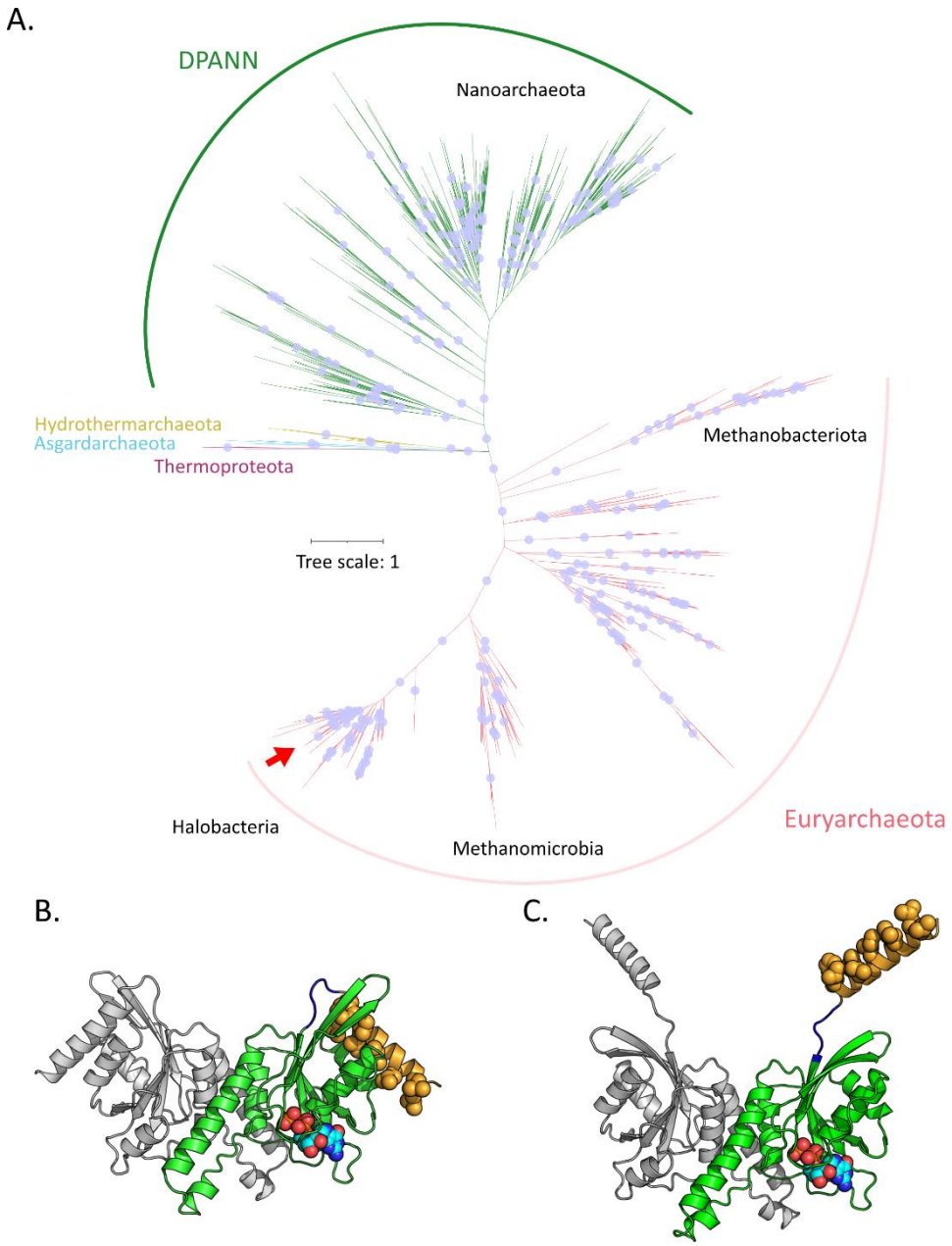

Figure 6. The new family of archaeal vesiculating GTPases, ArcV. (A) Unrooted phylogenetic tree of the identified ArcV homologs across the archaeal domain. Red arrow indicates position of *H. volcanii* ArcV. Blue dots represent branches with bootstrap value greater than 95. Structural prediction of tertiary structure of the ArcV dimer (monomer depicted in green) with **(B)** closed and **(C)** open conformations (AlphaFold v2 [41, 42]). The modelled GDP ligand (displayed as balls), comes from the distant structural homolog EngA from *Thermus thermophilus* HB8 (root-mean-square deviation of 3.29-Å out of 69 C-alphas, PDB 2DYK). Hydrophobic residues on N-terminal α-helix (displayed in yellow) are highlighted as balls.

SUPPLEMENTARY METHODS

Isolation and purification of EVs

For isolation of EVs from *H. volcanii*, cultures were grown at 45 °C in minimal media with serial dilution (two times in exponential growth to OD_{600} = 0.05) before being transferred into nutrient rich media and grown at 28 °C (unless otherwise specified). EVs were isolated and purified as described in [1]. Briefly, cells were removed at late stationary (~ 144 hours growth) by centrifugation (4,500 x *g*, 40 min), and EVs were precipitated with the addition of polyethylene glycol (PEG) 6000 and incubation at 4 °C. EVs were subsequently pelleted by centrifugation (14,000 x *g*, 50 min, 4 °C) and after resuspending the pellet, remaining cell contaminations were removed by an additional centrifugation (14,000 x *g*, 10 min) and filtration (1 x 0.45 µm filter, 1 x 0.2 µm filter). Extracellular nucleic acids were removed with DNase I (New England Biolabs, 20 U/mL) and RNase A (New England Biolabs, 20 U/mL) [2]. The samples were further purified through an OptiPrep™ density gradient, yielding two bands containing EVs.

EV quantification

Two different quantification methods were used, because each of them proved unsuitable for some conditions tested. We assume that enclosing CetZ1 into EVs can be influenced by particular conditions. Using CetZ1 [3] as a reporter gene for detection of EVs in culture supernatants (immunodetection) was unsuitable when testing temperatures dependencies (Supplementary Figure 2A and B) and did also not reflect results that we obtained for EVs from the *aglB* knockout strain (Supplementary Figure 17D and E). The fluorescence-based method proved unsuitable for quantification of EVs in virus infected cultures, because viral particles also appeared to be stained with the fluorescent dye (Supplementary Figure 2F). P-values are calculated by unpaired, two-tailed t-test.

RNA extraction and transcriptomic analysis

RNA was extracted from cell pellets or EV pellets using TRIzol™ (Thermo Fischer Scientific). 1 mL TRIzol™ reagent was added to the pellet, homogenized by pipetting, and incubated at room temperature for 5 min. 0.2 mL chloroform was added to the sample, gently mixed via inversion, and incubated at room temperature for 10 min. The sample was then centrifuged at 4 °C for 10 min at maximal speed (~20,000 x *g*). Upper phase was transferred to a new tube, and 500 mL isopropanol was added, mixed gently by inversion, and incubated at room temperature for 10 min. The sample was then centrifuged at 4 °C for 15 min at maximal speed. The supernatant was removed and pellets washed twice with ice-cold 75% ethanol. The remaining liquid was removed and the pellet was air-dried for 10 min. Pellets were resuspended in RNase/DNase free water.

Northern blot

The Northern blotting protocol was adapted from [4]. Briefly, RNA was extracted as described above and separated on formaldehyde-MOPS agarose gels, with a final concentration of 2% formaldehyde and 2% NuSieve 3:1 agarose (Lonza). 5 µg RNA was denatured for 10 min at 70 °C with 1 X MOPS buffer (20 mM MOPS, 5 mM NaOAc, 1 mM EDTA, pH 7.0), 3.7% formaldehyde and loading dye (67 nM EDTA pH 8, bromophenol blue and xylene cyanol in deionized formamide).

Samples were heat denatured for 10 min at 70 °C then placed on ice for 3 min before loading onto gel. The gel was run at 125 V for 3 to 4 hours and the RNA was then transferred to a Zeta-Probe GT membrane (Bio-Rad) by capillary action with 20 x SSC buffer (3 M NaCl, 300 mM Sodium Citrate, pH 7.0) and 2 x SSC buffer. The oligonucleotide probe is listed in Supplementary Table 2, and was labelled with [γ-^{32}P] ATP using polynucleotide kinase (Thermo Fisher).

Plasmid construction and expression of OapA

The plasmid, pTA1852 (provided by Thorsten Allers), is derived from pTA1392 [5] with a replacement of the 112 bp *Nde*I and *Not*I region containing an N-terminal 6 x His tag and a C-terminal 1 x StrepII tag with an N-terminal 7 x His tag and 2 x StrepII tag. Expression of tagged OapA ($OapA_t$) on pTA1852 is controlled by tryptophan-inducible promoter, p.tnaA.

For Expression of $OapA_t$ cultures were grown in Hv-YPC supplemented with 200 µg/mL tryptophan at 28 °C until OD_{600} of approximately 1. Cultures were then supplemented with tryptophan by adding 18% BSW containing 5 mg/mL tryptophan (final concentration of 450 µg/mL tryptophan). Cultures were grown for 2 hrs at 28 °C before EVs were quantified as described.

Affinity purification of $OapA_t$ was modified from [6]. Cells from 500 mL culture were pelleted (11,000 x *g*, 40 min) and resuspended in 7 mL Binding Buffer (20 mM HEPES pH 7.5, 2 M NaCl, 1 mM PMSF). Cells were lysed by sonication (6 x 30 seconds at 35% amplitude) on ice, and treated with 20 µL DNase I (New England Biolabs, 20 U/mL) for 1 hr at 28 °C. Lysates were centrifuged (20,000 x *g*, 15 min, 4 °C) and filtered through 0.8 µm, 0.45 µm and 0.22 µm pore-size filters. The remaining flow through was incubated overnight with 1 mL Strep-Tactin® Sepharose® beads (iba-lifesciences) equilibrated with Binding Buffer and applied to a Poly-Prep chromatography column (Bio-Rad). Flow through was run twice on the column, and the column was then washed 5 x with Binding Buffer. The column was then incubated with 3 mL Elution Buffer (Binding buffer with 5 mM D-desthiobiotin) for 30 min, and flow through was concentrated using Vivaspin® 500 centrifugal concentrator (10,000 MWCO, Sartorius). Expression of $OapA_t$ was then confirmed using Western blot (Supplementary Figure 11C).

Lipid extraction and analysis

For the total cell and cell membrane fraction, three biological replicates of cells pellets from *H. volcanii* cultures were dissolved in DBCM2 salt solution [7] and half of each replicate was used for total cell analysis and half for cell membrane extraction. For extraction of cell membranes, the dissolved cell pellet was sonicated with a microtip sonicator (MS 73 Sonoplus, Bandelin electronic, Germany) 3 times for 30 s on ice at 35% output. The lysate was treated with DNase I (30 min at 28°C, 10 µL per mL), and spun down (8,000 x *g*, 30 min, 4 °C) to remove cell debris. Cell membranes were pelleted from the supernatant by ultracentrifugation (248,000 x *g* for 15 min) and dissolved in DBCM2 salt solution. EVs from three biological replicates (200 mL cultures) were treated with DNase and RNase and purified with an Optiprep™ gradient (4 hr at 150,920 x *g*). The resulting EV bands were extracted separately from gradients. The samples were concentrated (Vivaspin 6, 100,000 MWCO PES, Sartorius, Germany) at 4 °C and washed twice with

DBCM2 salt solution. Each gradient band was concentrated to 900 µL, from which 3 x 300 µL technical replicates were aliquoted.

For lipid extraction, samples in DBCM2 salt solution were sonicated for 1 h in an ice-cooled ultrasonication bath and treated with a protocol based on [8]. Phase separation after the final centrifugation resulted in an upper lipid-containing organic phase, a lower metabolite-containing aqueous phase and a protein-containing pellet. The separate phases were isolated into combusted glass LC-MS vials, dried under constant N_2 flow and stored at -20 °C until further analysis. Three 300 µL aliquots of sterile DBCM2 salt solution were treated with the same protocol as negative controls.

For ultrahigh performance liquid chromatography (UHPLC) coupled to mass spectrometry (MS) analysis, dried samples were resuspended in a solvent mixture of dichloromethane:methanol (1:9). Measurements were performed on a Dionex Ultimate 3000 RS UHPLC system coupled to a maXis ultrahigh-resolution quadrupole time of flight tandem mass spectrometer (Q-TOF MS, Bruker Daltonics). Separation of archaeal lipids was achieved on a Waters Acquity UHPLC BEH C18 column (1.7 µm, 2.1 x 150 mm) at 65 °C using reverse phase chromatography [9]. Briefly, a 26 min gradient was run at a flow rate of 400 µL min^{-1} beginning with 100% A (held for 2 min), followed by an increase to 15% B within 0.1 min and ramping to 85% B in 19 min, followed by 8 min re-equilibration with eluent B. Eluent A was MeOH:H_2O (85:15) and eluent B was IPA:MeOH (50:50), both with addition of 0.04% HCO_2H and 0.1% NH_3. Analysis was performed in positive ionization mode, scanning from m/z 100 to 2000. MS2 scans were obtained in data dependent mode.

Output data were analyzed with the manufacturer's software (DataAnalysis 4.4.2, Bruker Daltonics). Lipid compounds were identified based on retention time, fractionation pattern and exact masses [10–12]. Several technical replicates were measured for each sample type, of which representative replicates were selected for each biological replicate. Since the EV samples showed minimal differences in lipid distribution between bands after ultracentrifugation (Supplementary Figure 18B), gradient bands were pooled for each biological replicate for further analysis. The samples were compared with respect to their relative abundance distributions without absolute quantification.

The relative abundances were normalized per replicate and averages for each fraction were calculated from three biological replicates (total cells and cell membrane fraction) and from the upper bands after density gradient centrifugation from three biological replicates (EV fraction). Figures were created in R Statistical Software (v4.1.2; R Core Team 2021) with the ggplot2 [13], plyr [14] and dplyr packages [15].

SUPPLEMENTARY RESULTS

EV-associated RNA is best analyzed when using small RNA libraries and normalizing EV RNA content with host cell RNA content

To determine the nature of the EV enclosed RNA, total RNA and small RNA (enriching for transcripts below 150 nt in length) libraries were prepared from EV-extracted RNA. When comparing sequencing results from both libraries, we observed a drastically different transcriptional profile (Supplementary Table 3). Around 95% of reads from total

RNAseq mapped to ribosomal RNA (rRNA) and only 17 transcripts recruited enough reads to reach the threshold (TPM > 10). In contrast, the small RNA library revealed a more diverse array of transcripts with transfer RNA (tRNA) being the most dominant RNA species (around 85% of reads) and 264 transcripts identified within the threshold. Further, over 2000 transcripts were only identified in the small RNA library and not in the total RNA library, the majority of them being tRNAs and non-coding RNAs (ncRNA), indicating that the total RNA library excludes important smaller transcripts. Therefore, we decided to use small RNA libraries for further analysis of EV-associated RNAs, as this seems to yield a more accurate picture of the RNA composition of EVs.

We also compared transcripts from EVs in the upper and lower bands in density gradients to determine whether the bands represented different subpopulations of EVs with respect to RNA content (Supplementary Table 4). Indeed, we identified transcripts that were only present in the upper band (app. 200) or only in the lower band (80). However, the abundance of these transcripts was below the threshold (TPM > 10) and they were disregarded. Overall, the RNA composition between both bands was mostly identical, with few outliers. We concluded that the RNA composition alone is not the differentiating factor between the two subpopulations of EVs in different density gradient bands, and pooling the bands for further sequencing analysis is acceptable.

Since vesicle production could be linked to UV exposure [16], we aimed to determine whether subjecting cultures to UV radiation would alter the RNA composition of EVs. Indeed, 145 transcripts appeared to be present in a higher abundance (log2 fold change > 1) in the UV-treated sample, and 32 transcripts were present in a higher abundance (log 2 fold change < -1) in the untreated sample (Supplementary Table 5). This population of EV-associated RNA from UV-treated cultures included all forms of RNA, including mRNAs, tRNAs, rRNAs and ncRNAs. Nevertheless, we realized that without determining transcriptional changes within the cells, it is difficult to distinguish transcripts that are associated with EVs as a response to UV exposure and transcripts that are present in EVs simply due to changes in intracellular levels. In order to differentiate between random packaging and potentially selective packaging of RNA into EVs, it became clear that sequencing intracellular RNA at the time of EV harvesting was imperative for any kind of analysis.

Analysis of EV-associated RNA under infection with a virus reveals viral transcripts associated with EVs

Direct interactions between EVs and viruses have been documented, demonstrating the capacity for EVs to act as a viral defense mechanism [17] or to facilitate viral propagation [18]. While we detected only minor changes to EV quantities under infection with the virus HFPV-1 (Figure 2B), we wanted to test whether infection with HFPV-1 would influence the RNA composition of EVs and thereby possibly indirectly influence virus-host interactions.

While it was shown that infection with HFPV-1 drastically altered the transcriptomic landscape of the cell during exponential and early stationary growth [19], sRNAseq in late exponential growth revealed a nearly identical transcriptional profile when comparing infected and uninfected cells (Supplementary Figure 6A). Only two genes showed a significant upregulation (log2 > 1) in the infected cells, HVO_2657 and HVO_0272; however, both are in

general rather weakly expressed (TPM < 15). When comparing the RNA content of EVs between infected and uninfected cells, two transcripts were found to be significantly higher in abundance in EVs of infected cells: HVO_A0466 and HVO_0272 (Supplementary Figure 6A). While HVO_0272 mRNA was about 4-fold upregulated in infected cells (log2 ~ 2), it was about 10-fold upregulated (log2 ~ 5) in EVs of infected cells (Supplementary Figure 6B), indicating that the packaging of this transcript into EVs increases significantly upon infection. Surprisingly, it appeared that the majority of reads mapping to HVO_0272 only map to two short regions of about 30 nt within the coding region of the gene that are identical to a region on the viral genome. Therefore, we conclude that the upregulation of HVO_0272 is due to viral transcripts mapping to the host genome.

Subsequently, when mapping reads to the virus genome, we detected a significant amount of viral transcripts in EVs. While only 1.7 ± 0.07% of intracellular RNA mapped to the HFPV-1 genome, 4.0 ± 0.10% of EV-associated RNA mapped to the viral genome, suggesting a slight enrichment of virus-derived transcripts in EVs. Both cellular and EV-associated RNA mapped the entire HFPV-1 genome, and no enrichment of particular viral RNAs could be detected in EVs (Supplementary Figure 7). However, the detection of viral transcripts within EVs shows that they are also exported in EVs together with host RNA.

Analysis of proteins in EVs from UV-treated cultures did not reveal significant differences

We also analyzed the protein composition of EVs from UV-treated cells and compared them with membrane-associated proteins isolated from their respective cells, to determine whether UV treatment would alter protein composition of the EVs. We identified 377 proteins associated with EVs and 668 proteins associated with their respective cell membranes. We identified 11 proteins to be enriched in EVs from UV-treated cells (Supplementary Table 9, Supplementary Figure 10A). All proteins identified as enriched in EVs from untreated cells were also identified as enriched in EVs from UV-treated cells, except for the small GTPase, HVO_3014, that was calculated as equally enriched but did not pass the p-value threshold. Instead, one additional ABC transport protein (HVO_2399) was identified as enriched. In comparing EV-associated proteins between untreated and UV-treated cultures, we did not identify major differences (Supplementary Figure 10B). Only one protein (HVO_B0027) was identified to be more enriched in EVs from untreated cultures, while two proteins (HVO_1751 and HVO_2529) were identified to be more enriched in EVs from UV-treated cultures. None of the enriched proteins from either culture held functions that appear significant to EV production.

Testing other knockout mutants provides further insight into the mechanisms of EV formation

CetZ1 and CetZ2 were amongst the most abundant proteins in EVs; however, we were able to isolate EVs from the supernatant of both CetZ1 and CetZ2 knockout strains (Supplementary Figure 16). While quantification of EVs by the immunodetection-based method was not possible for the CetZ1 knockout strain, we did not have any indication when purifying EVs that EV production was drastically altered for CetZ1 and CetZ2 knockout strains (Supplementary Figure 16). RNA could also be isolated from EVs of this strain, and the size distribution of EV-associated RNA was nearly identical when compared to the parental strain.

Previous studies in Bacteria have shown that destabilization of the cell envelope results in a 'hypervesiculation' phenotype [20, 21]. To investigate whether changes in cell envelope stability would similarly affect EV production in *H. volcanii*, we assessed EV production in an *aglB* knockout strain. Cells lacking AglB are unable to N-glycosylate the S-layer glycoprotein and absence of AglB results in enhanced release of the S-layer glycoprotein [22]. Thus, deletion of this protein causes a destabilization of the structural integrity of the cell envelope. Indeed, we observed a noticeable increase in EV production from the *aglB* knockout strain during the purification process as well as by TEM (Supplementary Figure 17A and B). While we could not confirm this result when using the immunodetection-based assay for quantifying EVs (Supplementary Figure 17D and E), EV quantification by fluorescence staining revealed a 1.52-fold ($p = 0.003$) increase in EV production (Supplementary Figure 17F), indicating that CetZ1 incorporation into EVs is altered in this mutant. Interestingly, we observed a drastic change to the morphology of EVs in the mutant. The surface of EVs isolated from the AglB knockout strain was significantly different from EVs of the parental strain, appearing very fuzzy (Supplementary Figure 17B and C), likely due to the instability of the S-layer. Further, while we isolated a significantly larger amount of EVs from the mutant, the RNA yield remained the same (Supplementary Figure 17G), indicating that RNA distribution in EVs is altered.

Lipid analysis reveals differences in the relative abundance of distinct lipids between cells and EVs

To determine whether EVs selectively enclose particular lipids, we analyzed the lipid content of EVs and compared the relative abundances of different lipid compounds in EVs to that of cell membranes and total cells of *H. volcanii*. We only detected minimal differences in proportions of lipid types between EVs deriving from upper and lower bands of a density gradient (Supplementary Figure 19B), indicating that the lipid content alone is not the differentiating factor between the two subpopulations. We therefore chose to pool samples from different bands of each replicate for comparison.

Lipids with phosphate-based polar head groups were dominant across all samples. Methylated-phosphatidylglycerolphosphate-archaeol (Me-PGP-ARP) both in saturated and unsaturated form (:n) represented the most abundant lipid across samples, with relative abundances of 53.9 ± 2% in whole cells, 66.4 ± 8.81% in cell membranes and 46.8± 1.91% in EVs (Supplementary Figure 20, Supplementary Figure 19A). The ratio of unsaturated to total Me-PGP-AR abundance was identical in cells and cell membranes (28 ± 1.64% and 29 ± 3.6%), but the comparative amount of unsaturated Me-PGP-AR was lower in the vesicle fraction (11.1 ± 3%) (Supplementary Table 11). Phosphatidylglycerol-archaeol (PG-AR) was the second most abundant lipid in all fractions (18.8 ± 5.3%, 17 ± 3.7% and 32.6 ± 2.9% for cells, cell membranes and EVs respectively) and showed the highest degree of unsaturation (either 4 or 6 double bonds). The ratio of unsaturated to total PG-AR did not show a large variation between cellular (36.1 ± 4.1%), cell membrane (38.9 ± 6.4%) and extracellular fractions (31.3 ± 9%). Sulfated-diglycosyl-archaeol (S-2G-AR) showed relative abundances of 5.75 ± 4.4% (whole cells), 6.8 ± 3.9% (cell membrane) and 12.9 ± 1.5% (EVs) respectively, with negligible amounts of unsaturated lipids detected in the whole cell and cell membrane fraction.

Lipids with a neutral headgroup, such as diglycosyl-archaeol (2G-AR) or no head group, such as core-archaeol (C-AR), were detected in all fractions but showed higher relative abundances in the EV samples (2.57 ± 0.19% and 4.1 ± 1%)

compared to lipid extracts from cells and cell membranes (<1.2 ± 0.2%). A notable difference was also observed for dimeric phospholipids (or cardiolipins, CL). While they contributed 20.1 ± 9.7% and 9.04 ± 8.1% of the total lipids in whole cells and cell membrane samples respectively, they were almost undetectable in the EV samples (0.91 ± 0.41%). Interestingly, we were not able to detect any extended archaeol lipids (C_{25} instead of C_{20} isoprenoidal chains) with relevant concentrations in any of the samples, despite how common they are among many haloarchaea [23].

We could not detect any lipid compounds which were only present in the vesicular fraction but not in cells or cell membranes. However, the lipid composition of EVs differed significantly to that of cells and cell membranes when comparing the relative abundance patterns of different lipid groups (Supplementary Figure 20, Supplementary Figure 19B). The distribution between unsaturated and saturated compounds shifts towards saturated lipids from 67.5 ± 2.7% and 68.7 ± 1.7% in whole cell and cell membrane extracts, to 84.4 ± 4.7% in EVs (Supplementary Table 11). In the vesicle fraction this is likely attributable to the absence of cardiolipins and the lower abundance of unsaturated Me-PGP-ARs.

SUPPLEMENTARY DISCUSSION

We were able to detect the major bilayer forming lipids PG-AR, Me-PGP-AR, S-2G-AR, C-AR, 2G-AR and cardiolipins, that were previously described for *H. volcanii* [11, 24] in all samples, albeit in different relative amounts.. Me-PGP-AR and PG-AR were the two most abundant lipid species across all samples, while the cardiolipins (CL) contributed to a notable portion of the intact polar lipids (IPLs) in cells and cell membranes and were surprisingly only detected in low abundances in EVs. CLs are considered to be important for membrane curvature [25]; therefore, we expected them to be essential in EVs due to the high degree of bilayer curvature in the vesicles. However, Kellermann et al [11] observed that changing extracellular Mg^{2+} levels influence CL and Me-PGP ratios in *H. volcanii* and proposed that changes to the ratio of the two compounds are used to control membrane permeability in neutrophilic haloarchaea, in response to extracellular Mg^{2+} levels. As we cultivated *H. volcanii* in medium with a constant high Mg^{2+} concentration (174 mM) it is not surprising that Me-PGP-AR was the most prominent phospholipid species across all samples. This could also explain the absence of CLs in EVs, as Me-PGP-AR may be sufficient to ensure membrane stability in the smaller-sized EVs under high Mg^{2+} concentrations. C-ARs and 2G-AR showed the opposite trend to cardiolipins, with an increase in their relative abundance in EVs compared to the cellular fraction.

SUPPLEMENTARY FIGURES

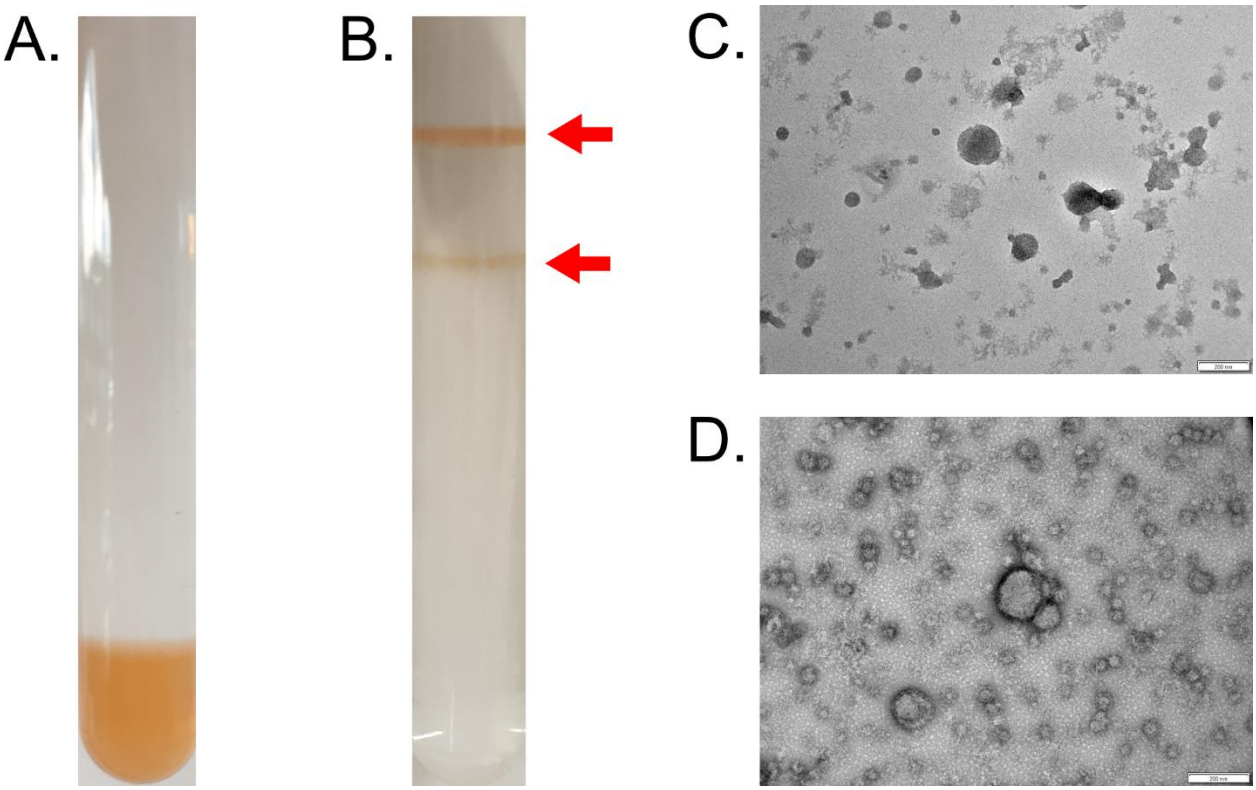

Supplementary Figure 1. Purification of *H. volcanii* H26 EVs by Optiprep™ density gradient purification. Gradient before **(A)** and after **(B)** ultracentrifugation. Red arrows indicate upper and lower band. Transmission electron micrograph of EVs isolated from upper **(C)** and lower **(D)** bands. Size bar: 200 nm.

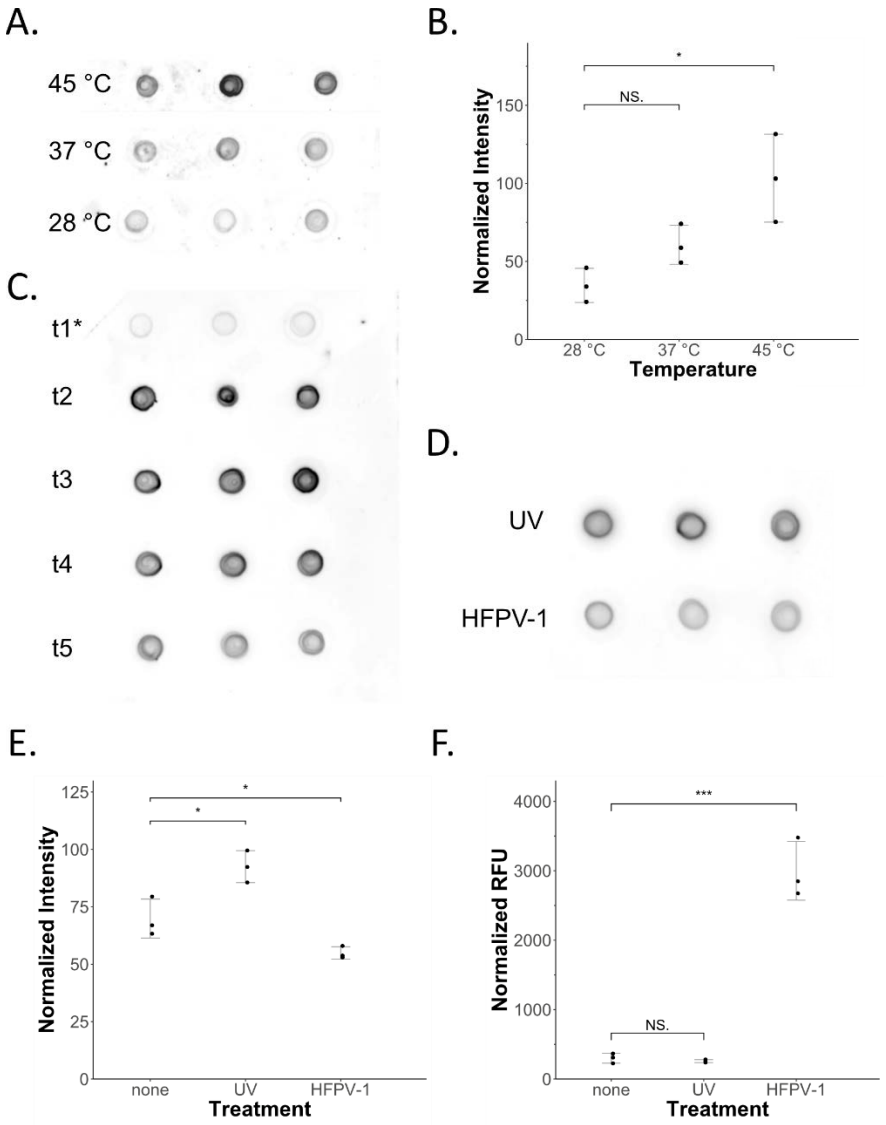

Supplementary Figure 2. EV quantification of *H. volcanii* cultures grown under different conditions and through growth. (A) Spot blot for quantification of EVs in *H. volcanii* culture supernatants grown at 45, 37 and 28 °C. **(B)** Plot representing EV production in different temperatures quantified by immunodetection (original spot blot in **A**). Intensity of spot blot signal was normalized to OD_{600} of culture. **(C)** Spot blot for quantification of *H. volcanii* grown at 28 °C with time points taken at 45.3, 68.5, 94, 118.3, and 140.5 hours. Asterisk on time point 1 represents sample diluted by a factor of 2. **(D)** Spot blot for quantification of *H. volcanii* grown with either UV or viral stress. **(E)** Plot representing EV production with either UV or viral stress, quantified by immunodetection (original spot blot in **D**). **(F)** Plot representing EV production with either UV or viral stress, quantified by fluorescence labeling. Significance is indicated above the graph (NS. indicates "not significant", * indicates "$p \leq 0.05$", *** indicates "$p \leq 0.001$"). Spot blot images were modified by subtracting background on ImageJ (rolling ball radius = 25).

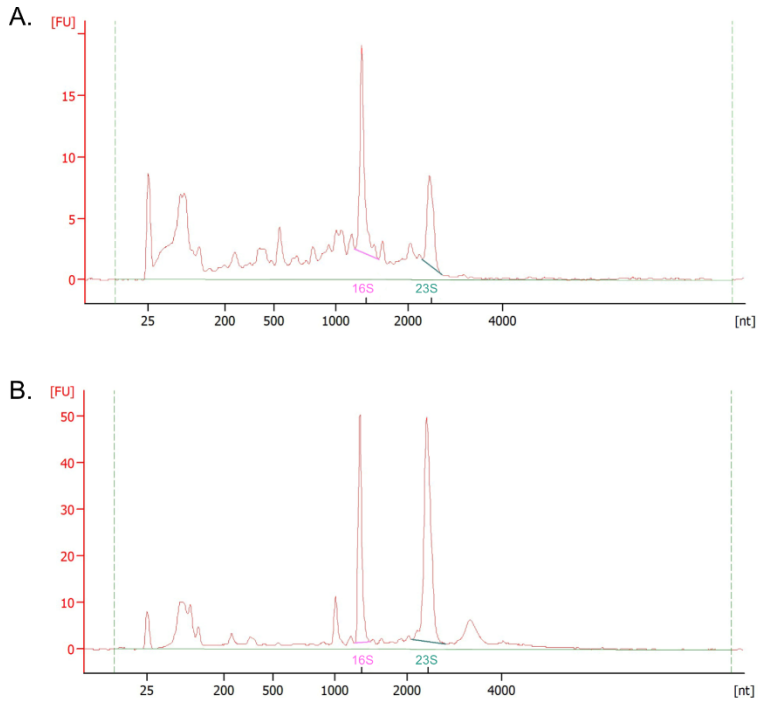

Supplementary Figure 3. Electropherograms of EV-associated RNA (A) and cellular RNA (B). Capillary electrophoresis demonstrates differences in size distribution between RNA isolated from EVs and cells of *H. volcanii*.

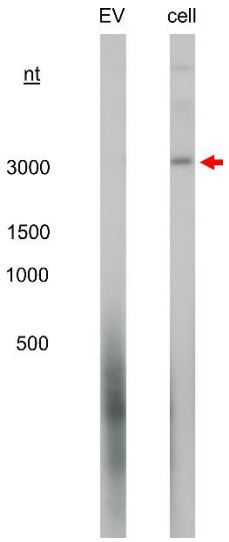

Supplementary Figure 4. Northern blot with EV and cellular RNA probed for HVO_2072. Red arrow indicates full-length transcript. Northern was conducted in duplicates, but only one replicate is presented here.

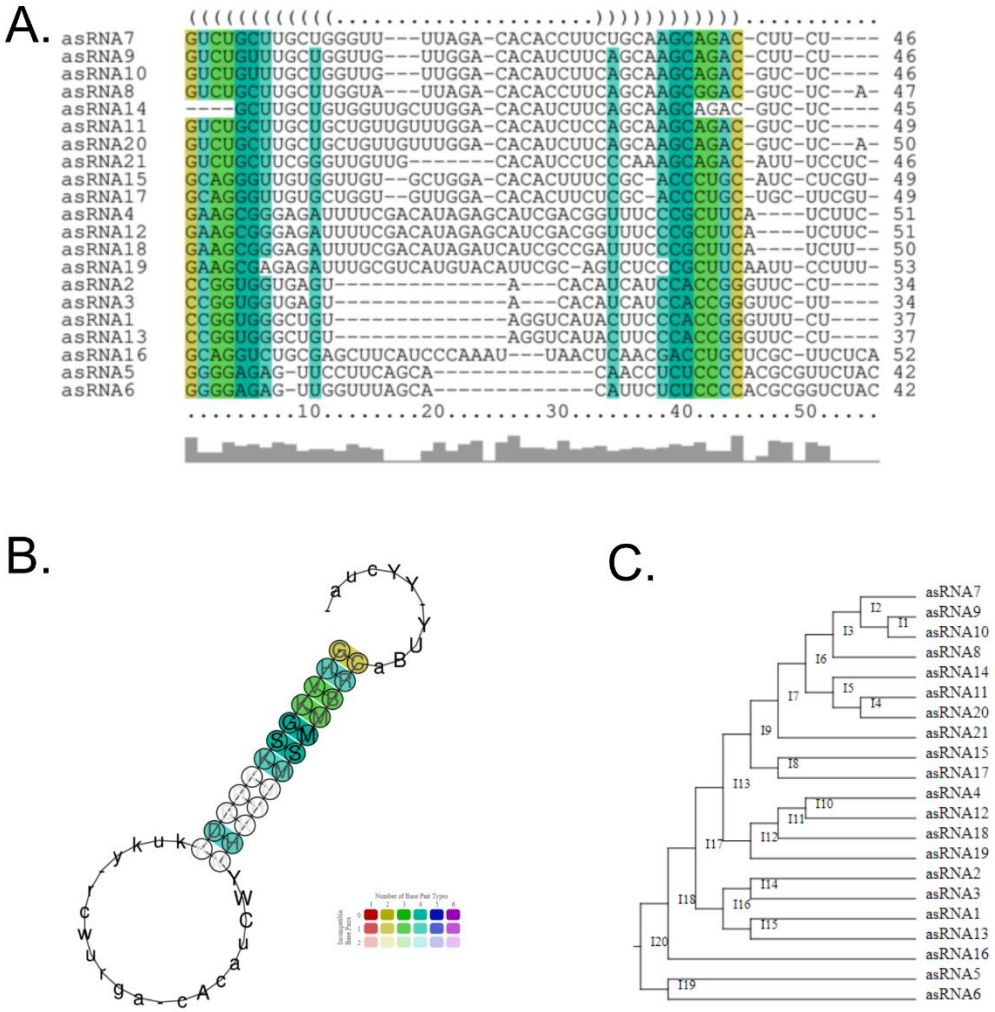

Supplementary Figure 5. Secondary structure alignment prediction of EV-associated asRNA from LocARNA [26–28]. (A) Sequence alignment with RNAalifold consensus structure. **(B)** Predicted consensus secondary structure with legend. **(C)** Hierarchical clustering based on similarities of sequences.

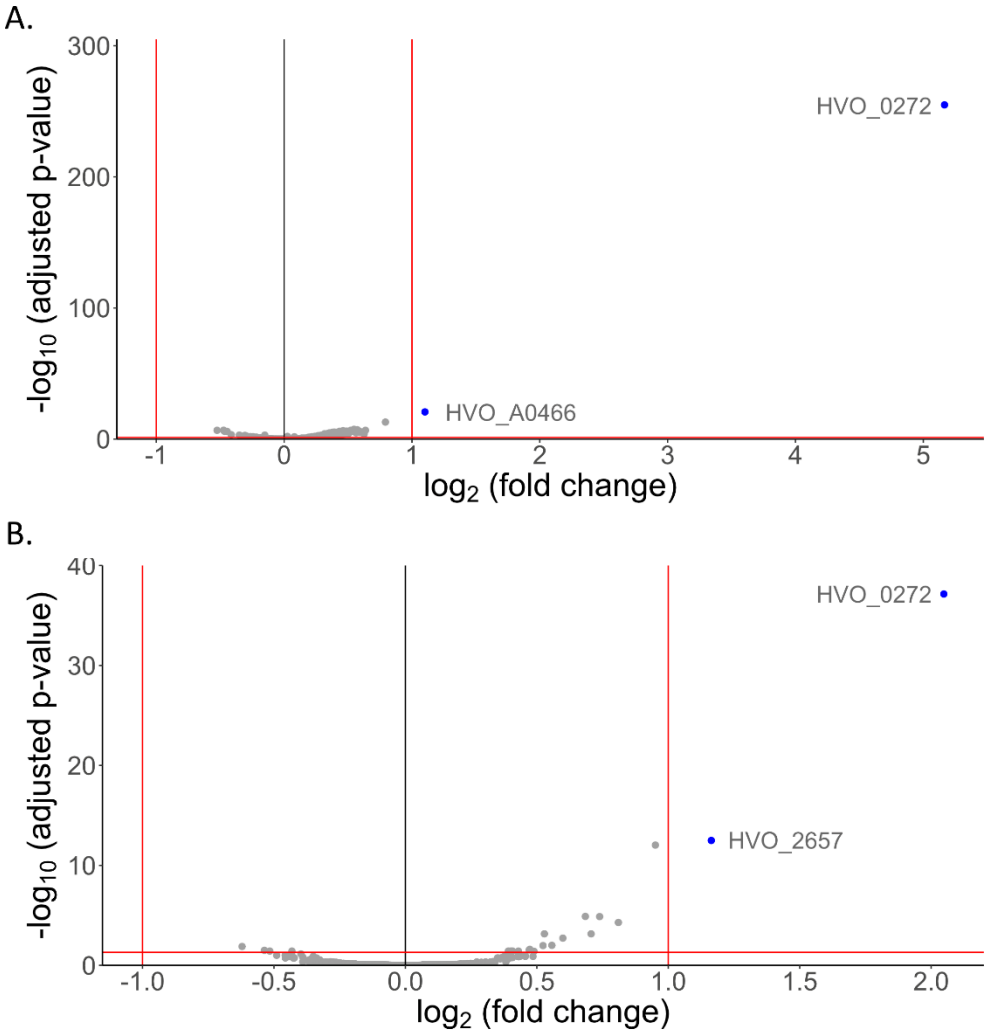

Supplementary Figure 6. Volcano plots of intracellular and EV-associated transcripts comparing cultures infected with HFPV-1 and uninfected control cultures. **(A)** Differential expression of transcripts in EVs from infected versus uninfected cultures. **(B)** Differential expression of intracellular transcripts from infected versus uninfected cultures. Cells and EVs were isolated at late stationary phase of growth. Volcano plots only depict transcripts that had an average TPM greater than 10 in either infected or uninfected samples. Red asymptotes indicate thresholds for enrichment ($p = 0.05$ and $|\text{fold change}| = 2$).

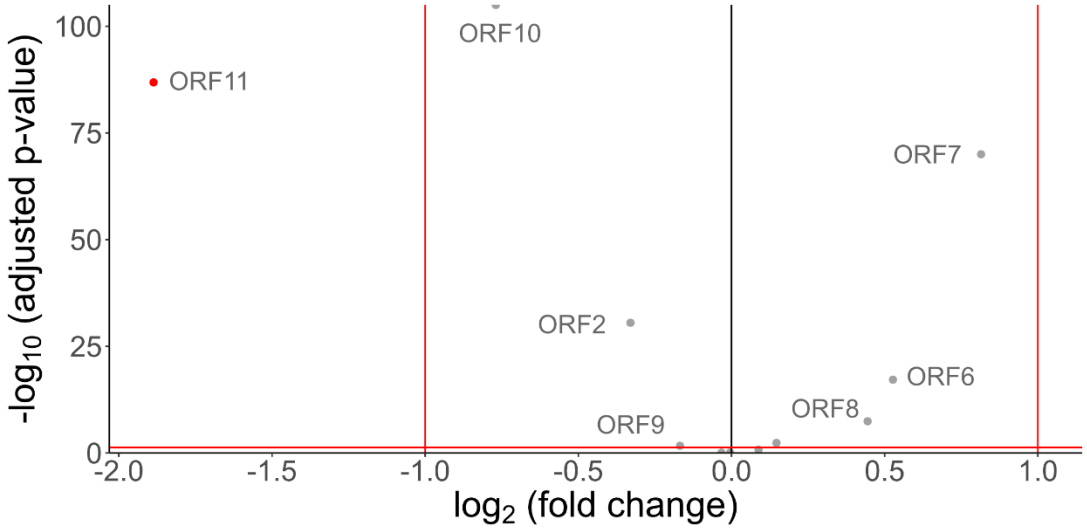

Supplementary Figure 7. Volcano plot comparing viral transcript abundance between EV-associated RNA and cellular RNA. RNA isolated from EVs and cells of cultures infected with HFPV-1 during late stationary phase. Red asymptotes indicate thresholds for enrichment ($p = 0.05$ and $|\text{fold change}| = 2$).

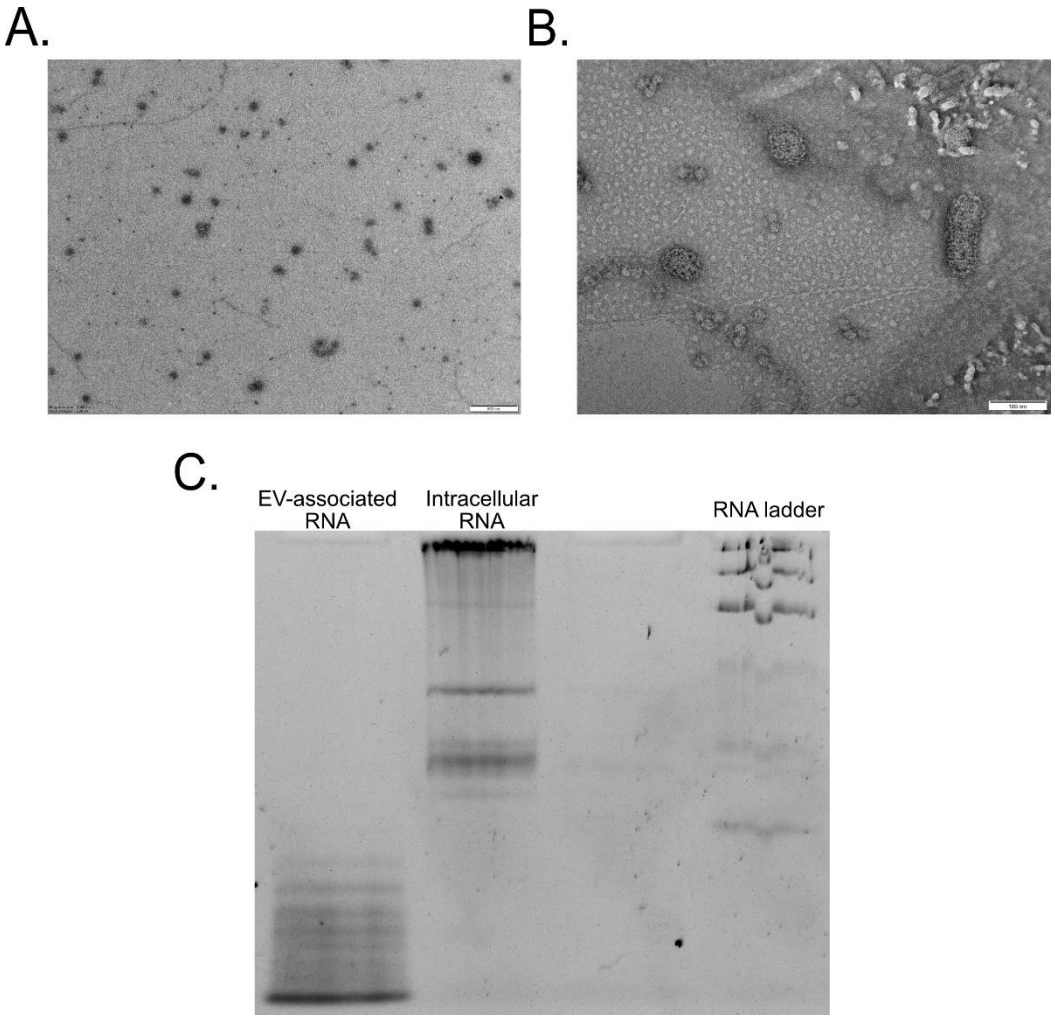

Supplementary Figure 8. EVs from other haloarchaea. (A) Transmission electron micrograph of purified EV from *Hbt. salinarum.* Scale bar: 500 nm. **(B)** Transmission electron micrograph of purified EVs from *Hrr. lacusprofundi.* Scale bar = 100 nm. **(C)** RNA extracted from gradient purified EVs and cells of *Hrr. lacusprofundi* on a 12.5% Urea-PAGE gel.

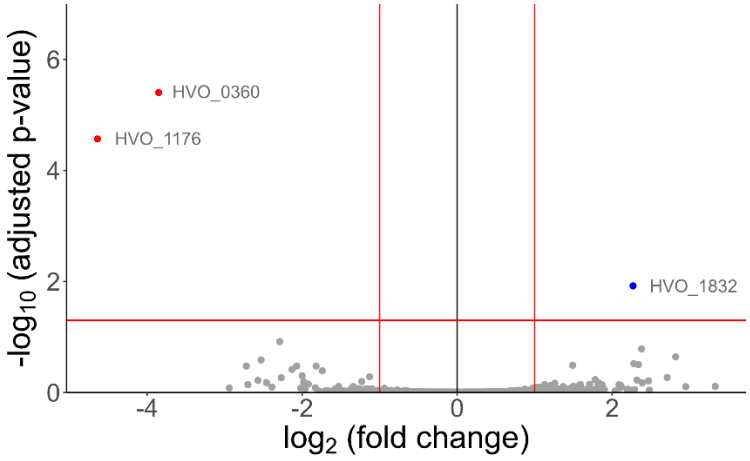

Supplementary Figure 9. Volcano plot comparing protein content from *H. volcanii* EVs isolated from upper and lower bands of Optiprep™ density gradient. EVs were isolated from three replicates at stationary phase of growth. Red asymptotes indicate thresholds for enrichment (p = 0.05 and |fold change| = 2). Differential protein abundancies and adjusted p-values were calculated by DEP (see methods).

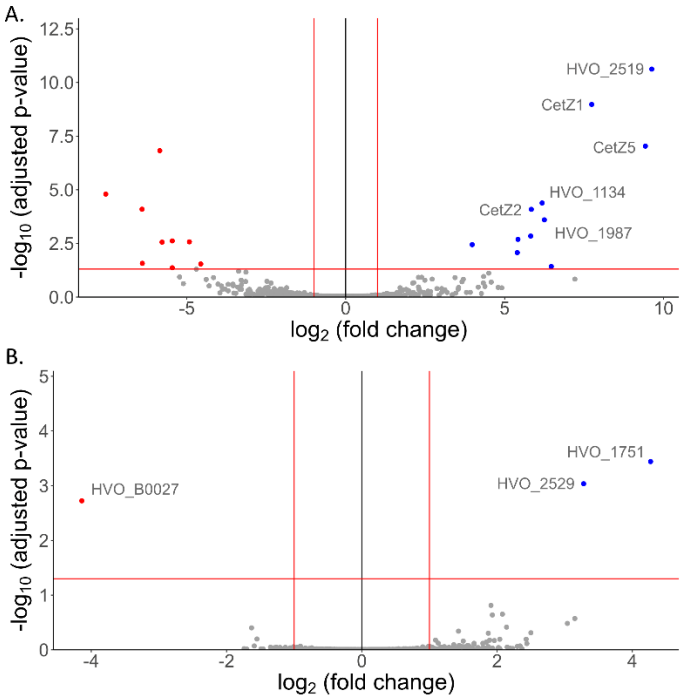

Supplementary Figure 10. Volcano plots depicting differences in protein abundance from UV-treated cultures. **(A)** Proteins isolated from EVs of UV-treated cultures are compared to their respective cell membrane protein content. **(B)** EV-associated proteins from UV-treated cultures are compared to EV-associated proteins from untreated cultures. Raw data found in Supplementary Table 9. Red asymptotes indicate thresholds for enrichment (p = 0.05 and |fold change| = 2).

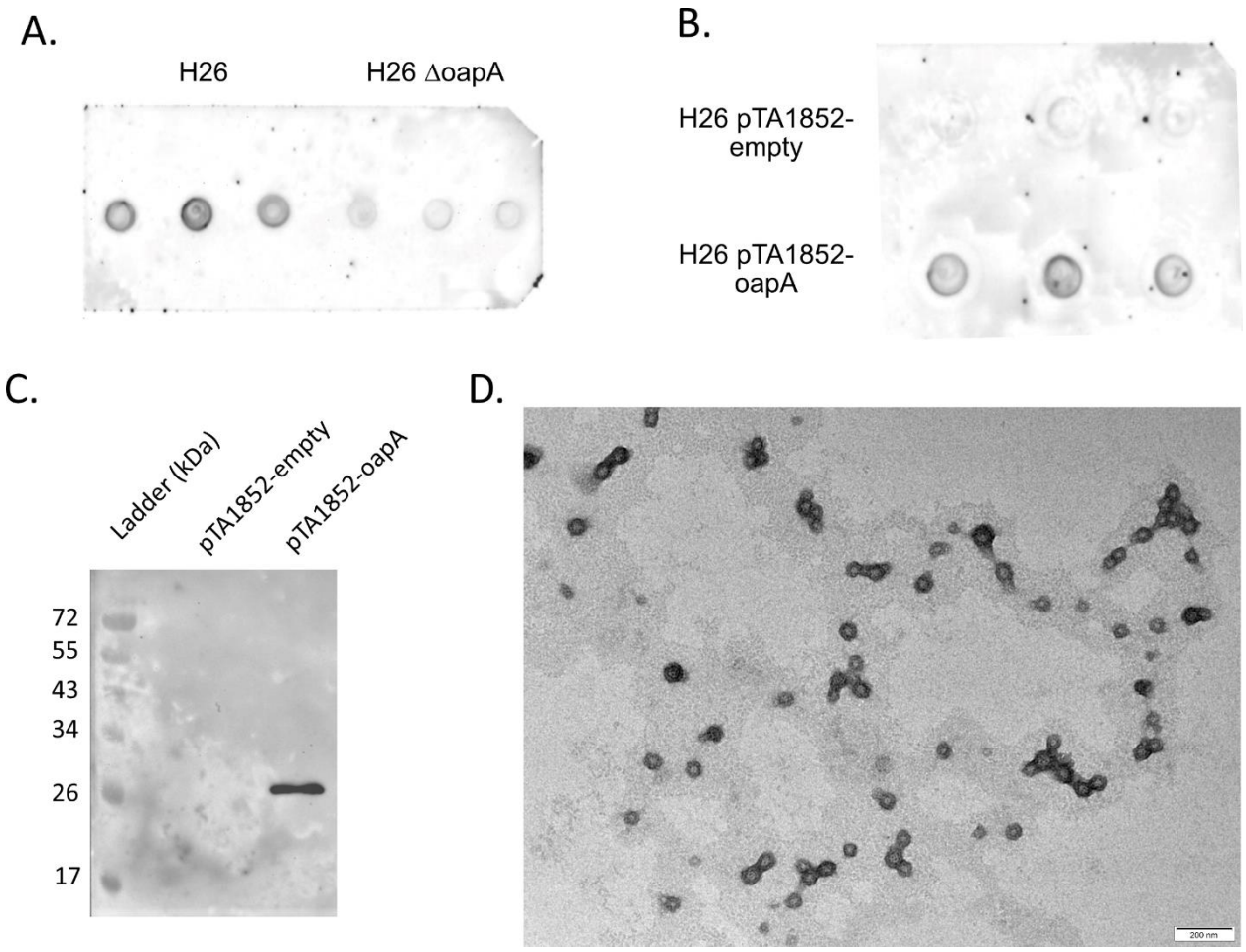

Supplementary Figure 11. Knockout and overexpression of OapA. Original spot blots of EV production from culture supernatants of strains with knockout **(A)** and overexpression **(B)** of OapA (quantifications found in Figure 4A and B). Spot blots were modified by subtracting background on ImageJ (rolling ball radius = 25). **(C)** Western blot with an anti-Strep tag antibody on affinity purified OapA expressed in H26, compared to an affinity purification from H26 with the empty vector (see methods). **(D)** Transmission electron micrographs of EVs isolated from strains overexpressing OapA. Scale bar 200 nm.

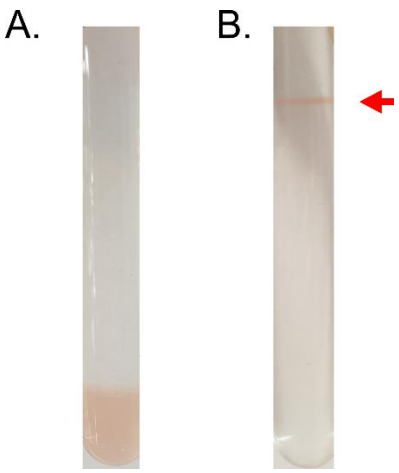

Supplementary Figure 12. Optiprep™ density gradient of OapA knockout strain. EVs **(A)** before and **(B)** after ultracentrifugation. Red arrow indicates where particles concentrated. For comparison with parental strain, see Supplementary Figure 1A.

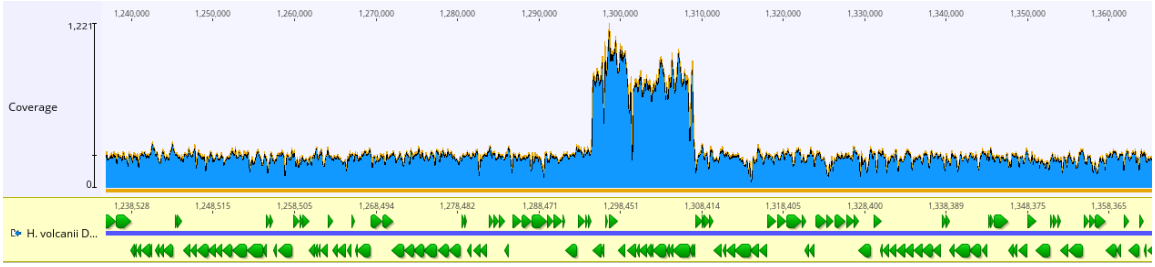

Supplementary Figure 13. Resequencing of OapA knockout strain shows activation of proviral region. Coverage blot of the genomic region including the provirus region. Image created in Geneious™.

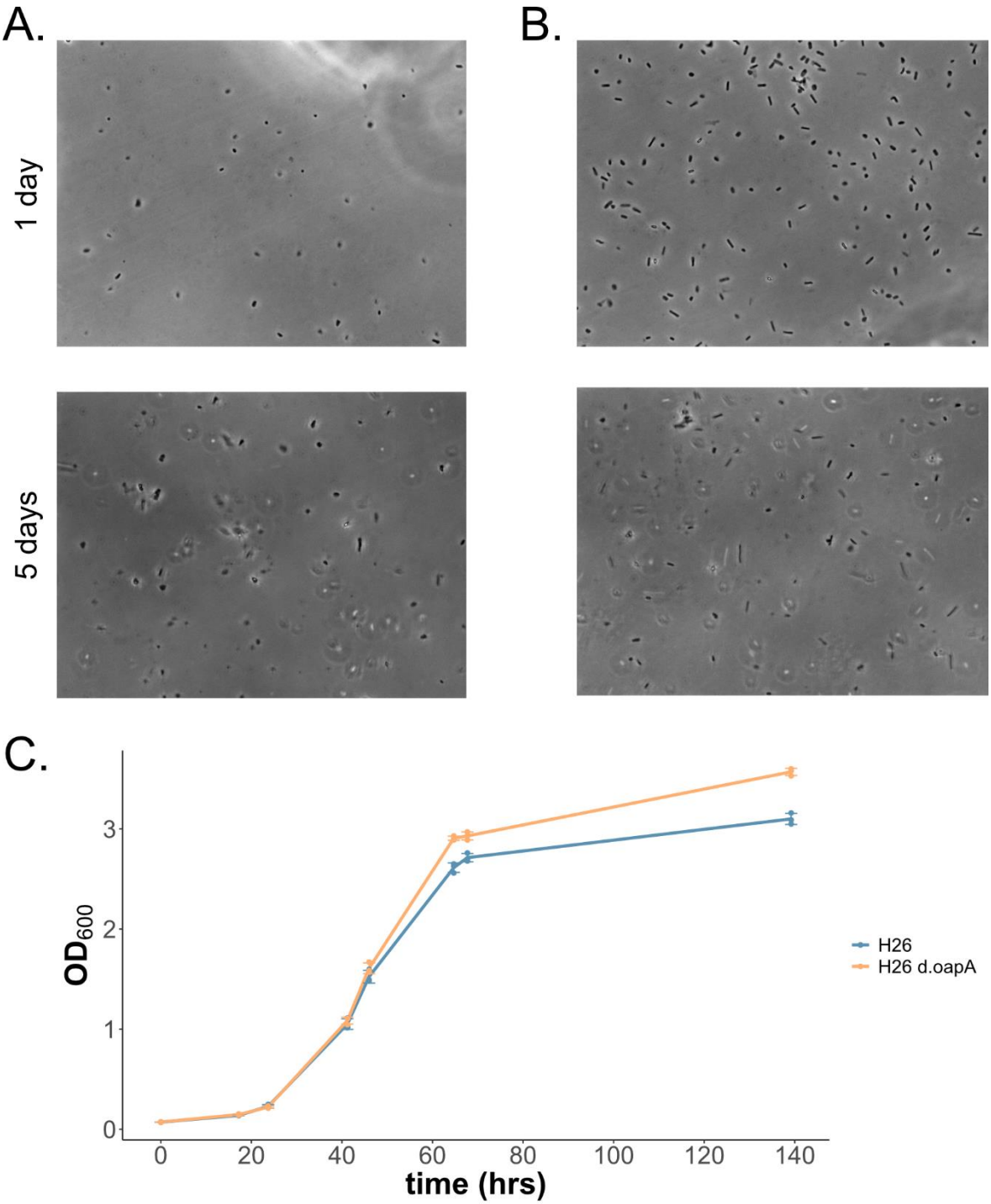

Supplementary Figure 14. Phenotypes of OapA knockout strain in comparison to parental strain. Phase contrast microscopy images of cells from OapA knockout strain **(A)** and parental strain **(B)** after 1 day (top) and 5 days (bottom) of growth. Samples were fixed with 1% glutaraldehyde and visualized with Axiophot Zeiss microscope. **(C)** Growth curve of parental strain (H26) and OapA knockout strain (H26 ΔoapA). Error bars represent standard deviation from three replicates.

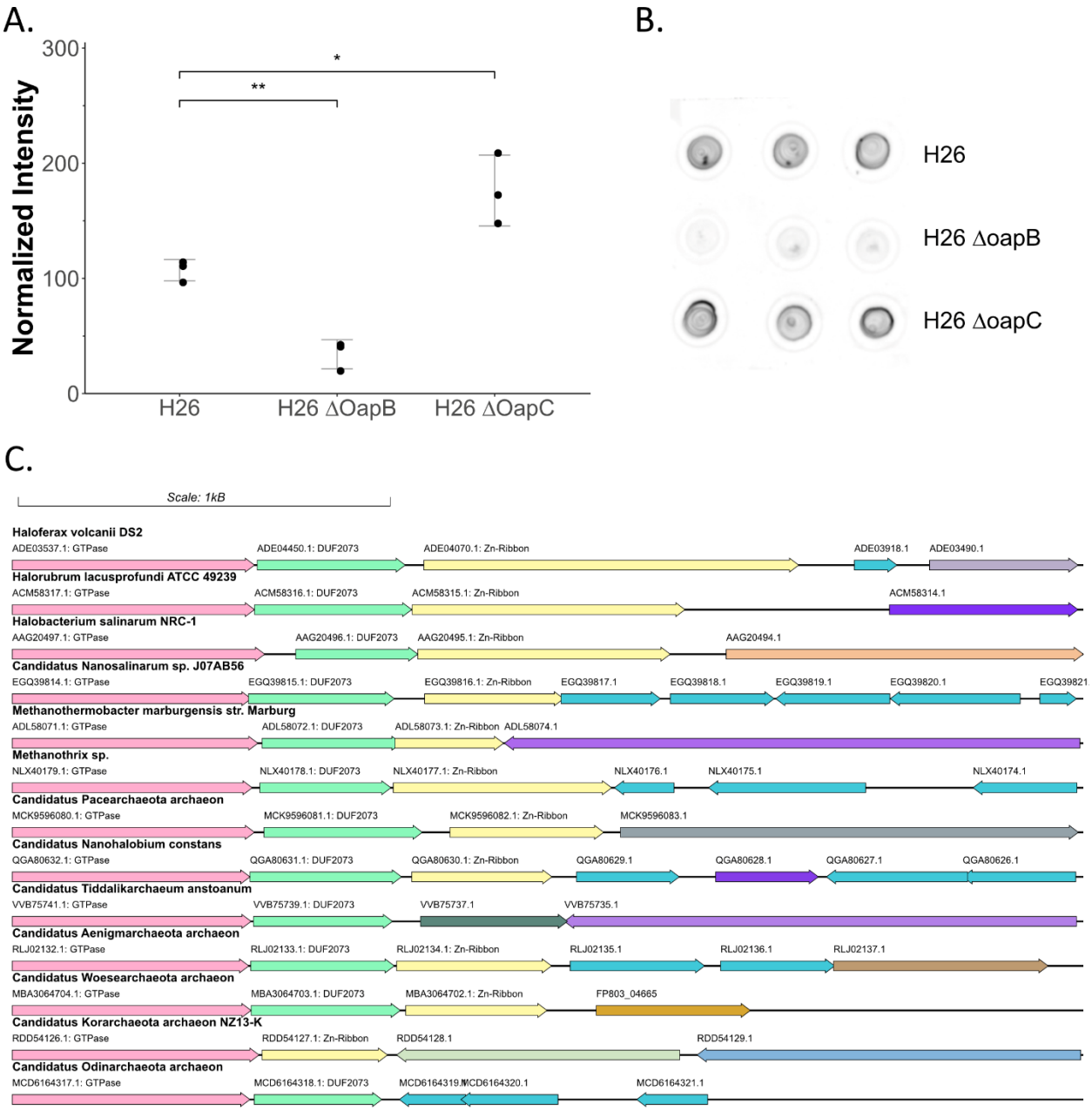

Supplementary Figure 15. The gene neighborhood of the archaeal vesiculating GTPase, ArcV. (A) Immunodetection-based quantification of EV production from the supernatant of knockout strains of OapB and OapC. **(B)** Original spot blot for **(A)**. Spot blots were modified by subtracting background on ImageJ (rolling ball radius = 25). **(C)** The gene neighborhoods of other Archaea that have a conserved ArcV homolog. Gene map generated by Gene Graphics [29].

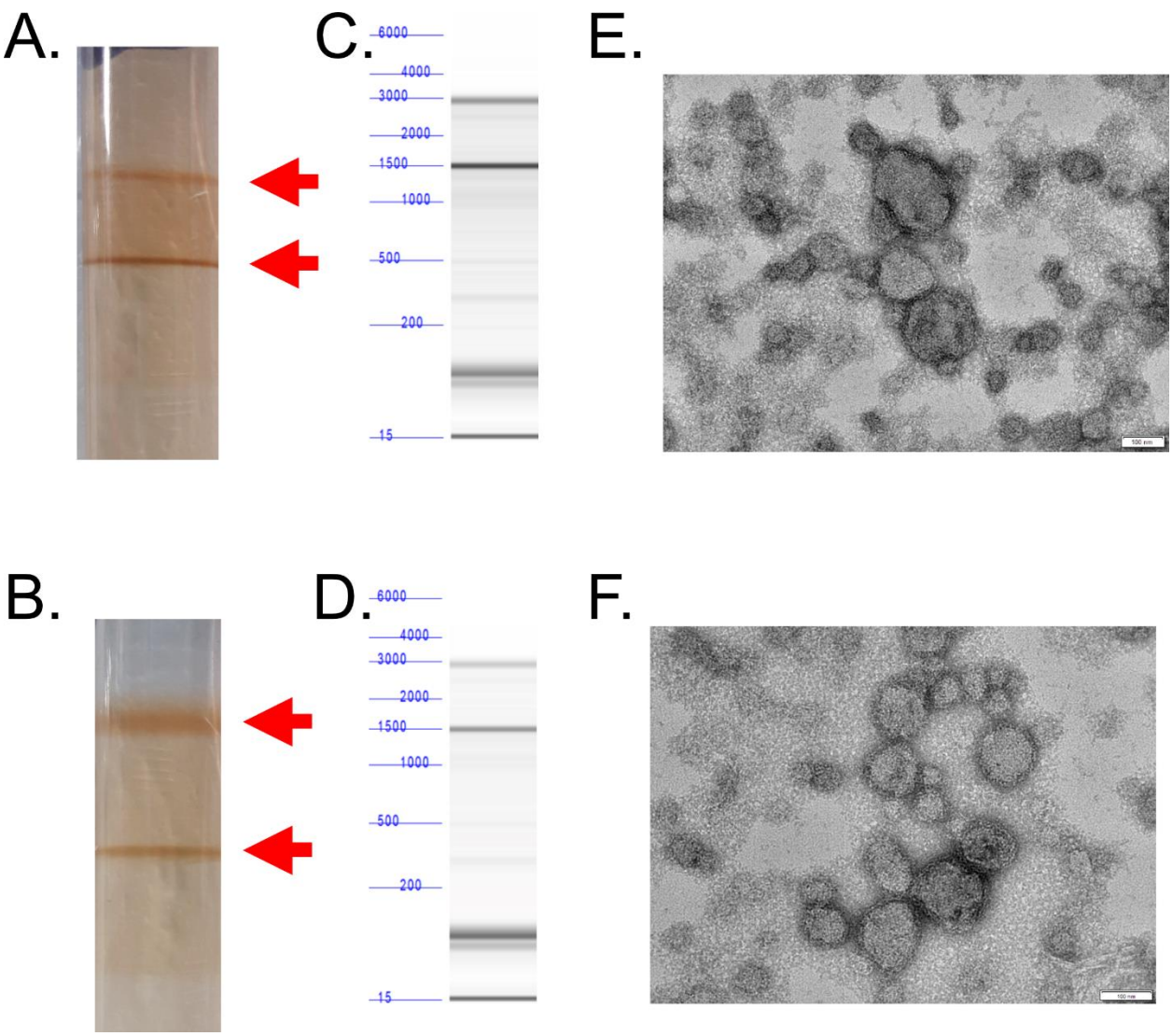

Supplementary Figure 16. EVs isolated from CetZ1 and CetZ2 knockout strains. Optiprep™ density gradients of EVs isolated from CetZ1 **(A)** and CetZ2 **(B)** knock out strains after ultracentrifugation. Red arrows indicate the upper and lower bands where particles had concentrated. **(C and D)** RNA was isolated from both strains and run on a fragment analyzer to observe the size distribution. For comparison to wild type, see Figure 2. **(E and F)** EVs could also be observed through TEM. Scale bars: 100 nm.

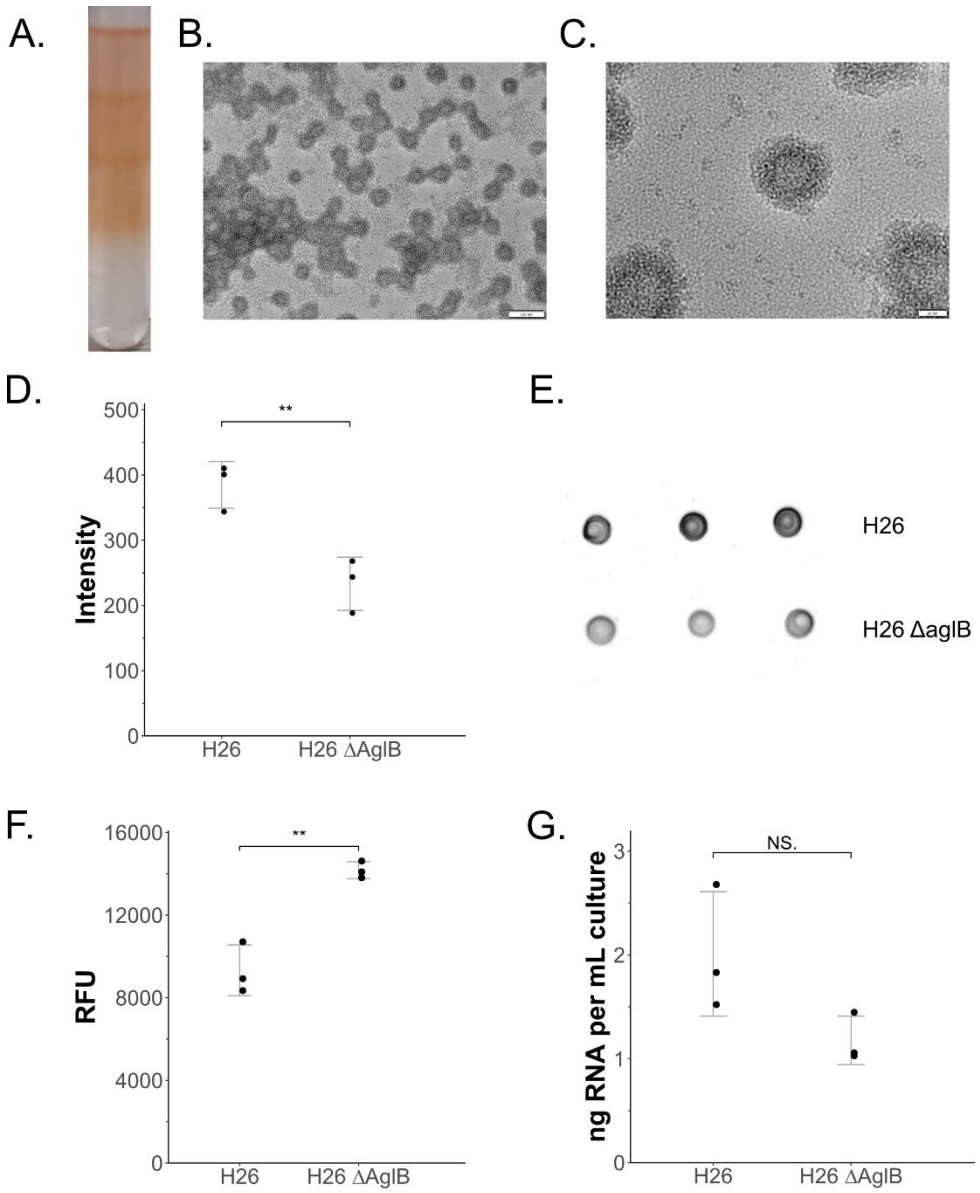

Supplementary Figure 17. Phenotypes of EVs from AglB knockout strain. (A) Bands of concentrated EVs after ultracentrifugation in Optiprep™ density gradient. Transmission electron microscopy of EVs isolated from AglB knockout strain with size bar 100 nm **(B)** and 20 nm **(C)**. **(D)** Quantification of EV production of AglB knockout strain compared to parental strain by immunodetection and the corresponding spot blot **(E). (F)** Quantification of EV production from cultures of AglB knockout strain compared to parental strain by fluorescence staining, measured in relative fluorescence units (RFU) **(G)** Quantification of EV-associated RNA in culture supernatants of AglB knockout strain compared to parental strain normalized to OD (nm = 600). Error bars represent one standard deviation from the mean value. Significance calculated using a two-tailed t-test (** indicates "$p < 0.01$, NS indicates "not significant").

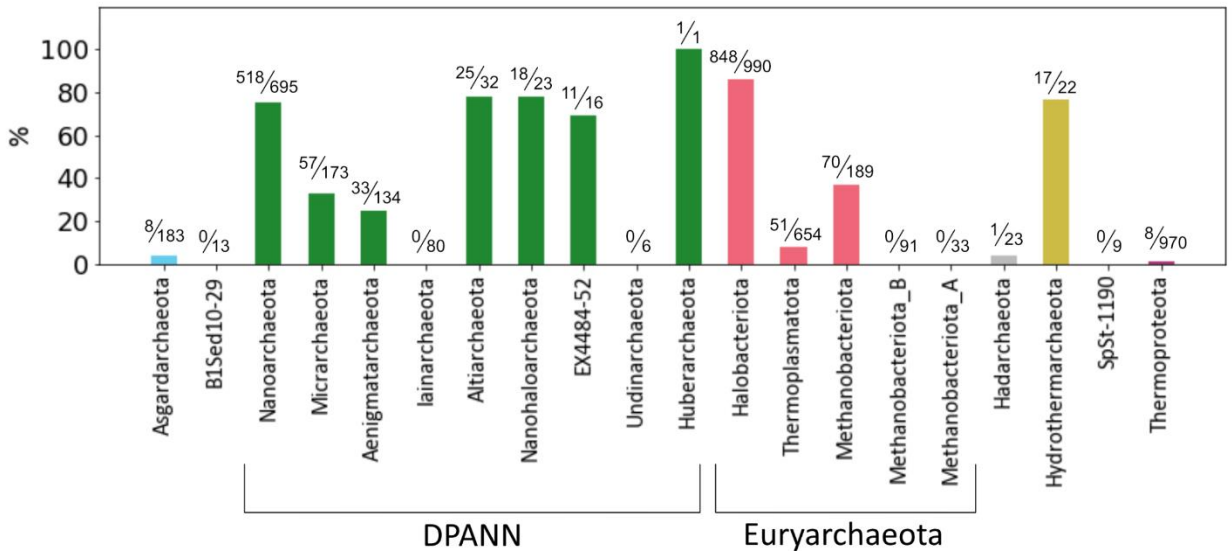

Supplementary Figure 18. Archaeal vesiculating GTPase, ArcV, is conserved among specific archaeal lineages. Percentage of species identified containing an ArcV homolog within each phylum. Fraction above each bar denotes the number of species identified over the number of species surveyed.

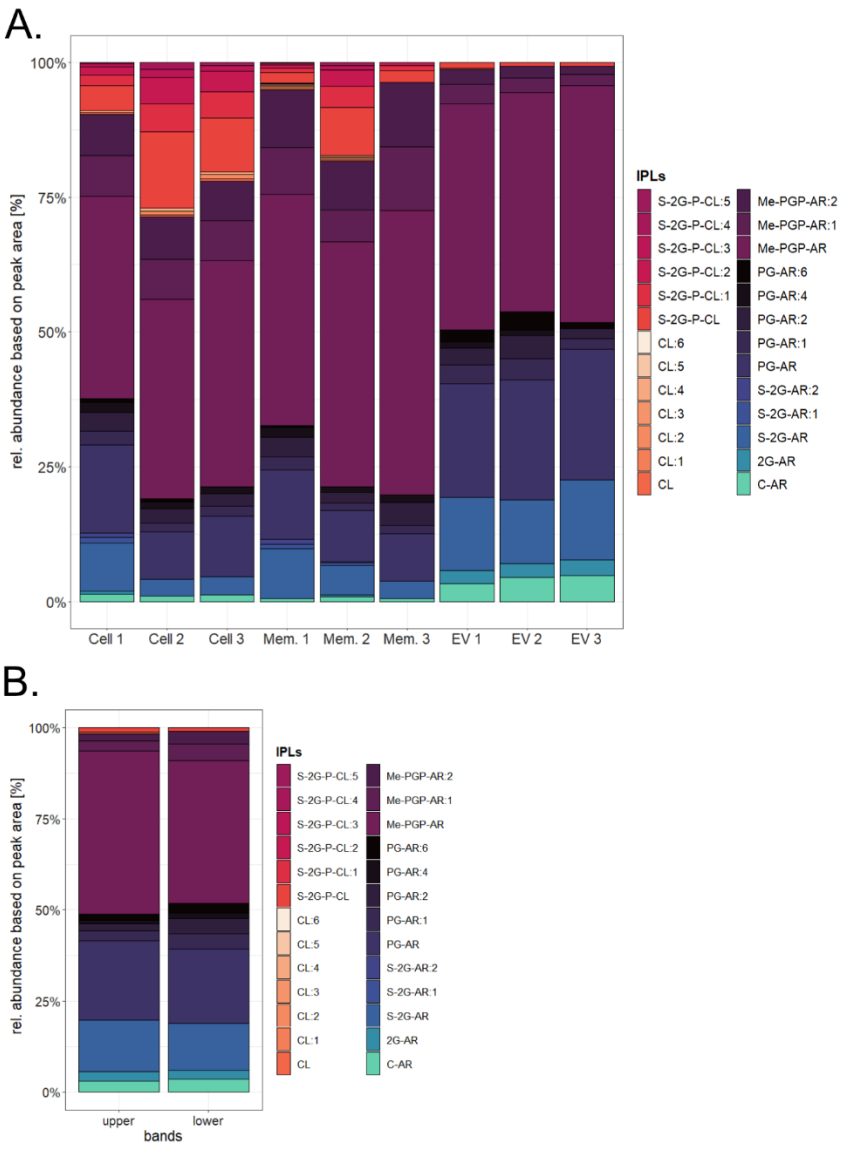

Supplementary Figure 19. Distribution of lipid compounds comparing whole cells, cell membranes and EVs of H. volcanii. (A) Individual replicates used to calculate the average relative abundances in Figure 6. Cell 1-3: whole cells, Mem. 1-3: membrane fraction and EV 1-3: extracellular vesicles after ultracentrifugation in Optiprep™ density gradients and bands pooled together for each biological replicate. **(B)** The lipid distribution in the upper (left column) and lower band (right column) after ultracentrifugation from one biological replicate. Relative abundances were calculated based on the peak area of the most abundant adduct for each compound. Lipids were identified based on their retention time, fractionation pattern and exact mass.

Compound abbreviations: AR = archaeol (C20-C20 isoprenoidal chains), CL = cardiolipin, :nUS = lipid with n number of unsaturations, UK = unknown compound. Lipids with neutral headgroups: 1G = monoglycosyl, 2G = diglycosyl, C-AR = core-AR. Lipids with anionic headgroups: PGP-Me = phosphatidylglycerophosphate methyl esters, PG = phosphatidylglycerol, S-2G =sulfated diglycosyl, S-GP = sulfoglycophospho, 2-PGLY = diphosphoglycerol.

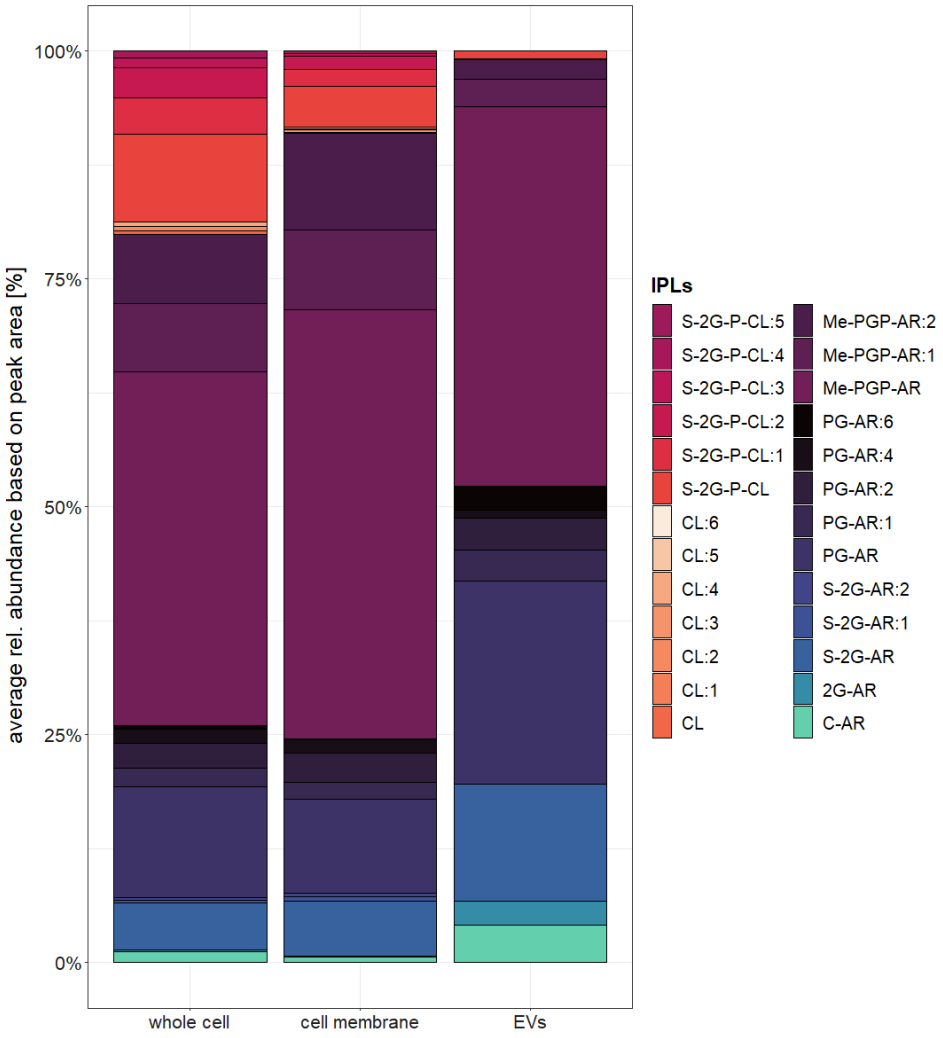

Figure 20. Average distribution of lipid compounds comparing whole cells, cell membranes and EVs of *H. volcanii*. The average (n = 3) relative abundance of lipids was calculated for each preparation; whole cells, cell membrane and EVs based on the peak area of the most abundant adduct for each compound. The distribution in the individual samples is shown in Supplementary Figure 18A. For the EV fraction, bands after density gradient purification were pooled together from 3 biological replicates. Lipids were identified based on their retention time, fractionation pattern and exact mass.

Compound abbreviations: AR = archaeol (C_{20}-C_{20} isoprenoidal chains), CL = cardiolipin, :nUS = lipid with n number of unsaturations, UK = unknown compound. Lipids with neutral headgroups: 1G = monoglycosyl, 2G = diglycosyl, C-AR = core-AR. Lipids with anionic headgroups: Me-PGP = phosphatidylglycerophosphate methyl esters, PG = phosphatidylglycerol, S-2G =sulfated diglycosyl, S-GP = sulfoglycophospho, 2P-GLY = diphosphoglycerol.

SUPPLEMENTARY TABLES

Abbreviated versions of supplementary tables are provided below. Subset criteria are presented in the table captions.

Supplementary Table 1. Strains used in this study

Name	Reference	Organism	Description	Media	Supplement
H. volcanii DS2	[30]	*H. volcanii DS2*	Wild type strain	HV-cab/YPC	none
H26	[31]	*H. volcanii*	ΔpyrE2	HV-cab/YPC	uracil
H26 ΔoapA	[32]	*H. volcanii*	ΔpyrE2, ΔoapA	HV-cab/YPC	uracil
H26 ΔaglB	[22]	*H. volcanii*	ΔpyrE2, ΔaglB	HV-cab/YPC	uracil
H53	[31]	*H. volcanii*	ΔpyrE2, ΔtrpA	HV-cab/YPC	uracil, tryptophan
H53 ΔcetZ1	[3]	*H. volcanii*	ΔpyrE2, ΔtrpA, ΔcetZ1	HV-cab/YPC	uracil, tryptophan
H53 ΔcetZ2	[3]	*H. volcanii*	ΔpyrE2, ΔtrpA, ΔcetZ2	HV-cab/YPC	uracil, tryptophan
Halobacterium salinarum	[33]	*Halobacterium salinarum*	Wild type strain	HS-Media	none
Halorubrum lacusprofundi DL18	[34]	*Halorubrum lacusprofundi DL18*	Wild type strain	DBCM2	none

Supplementary Table 2. Primer Sequences

Name	Oligonucleotide sequence 5'-3'	Description
HFPV1F	CACGAACGAGAACACCGACC	Forward primer to test infection of HFPV-1
HFPV1R	TGATGACGAATCCAACGAGCAG	Reverse primer to test infection of HFPV-1
AglB_US_F	CCGGCCAAGCTTGGTTTGCGAGCGACCCAGTCG	Forward primer for upstream flank of aglB with HindIII restriction sites
AglB_US_R	GAATTCGCCGCCCGAAGATCTTGTGACCAACAACCGCCAAG	Reverse primer for upstream flank of aglB with EcoRI and BglII restriction sites
AglB_DS_F	AGATCTTCGGGCGGCGAATTCCACGAGCCGAGACGGCGACGA	Forward primer of downstream flank of aglB with BglII and EcoRI restriction sites
AglB_DS_R	CCGGCCGGATCCGCGCGTCGCCGTGCTCGGAC	Reverse primer for downstream flank of AglB with BamHI restriction sites
csg probe	GCTGTCAGCGTCGAGGTTTCC	Northern blot probe for the 5' end of S-layer mRNA

Supplementary Table 3: Differential expression calculated for transcripts from total vs small RNA libraries of EV associated RNA. One replicate of RNA associated with EVs isolated from the upper band of a density gradient was sequenced using a total RNA library and a small RNA library. Read mapping (90% minimum overlap identity, TPM) and differential expression (log2 ratio) performed with Geneious™ (2021.0.1). (Excel file available at https://www.biorxiv.org/content/10.1101/2023.03.03.530948v1 as Supplementary Table 3)

Supplementary Table 4: Differential expression calculated for transcripts from EVs of upper versus lower band of a density gradient. One replicate of RNA associated with EVs isolated from the upper band and the lower band of

a density gradient. Read mapping (90% minimum overlap identity, TPM) and differential expression (log2 ratio) performed with Geneious™ (2021.0.1).

(Excel file available at https://www.biorxiv.org/content/10.1101/2023.03.03.530948v1 as Supplementary Table 4)

Supplementary Table 5: Differential expression calculated for transcripts from EVs from untreated and UV treated cells. One replicate of RNA associated with EVs isolated from untreated and UV treated cells. Read mapping (99% minimum overlap identity, TPM) and differential expression (log2 ratio) performed with Geneious™ (2021.0.1).

(Excel file available at https://www.biorxiv.org/content/10.1101/2023.03.03.530948v1 as Supplementary Table 5)

Supplementary Table 6. Differential expression calculated for EV associated transcript normalized with intracellular levels. RNA was extracted from purified EVs and the respective cells in triplicates. Read mapping (99% minimum overlap identity, TPM) and differential expression (log2 ratio, p-value) were calculated with DESeq2 in Geneious™ (2021.0.1). Only transcripts with Average TPM EV > 10, Log2 Ratio > 1, and adjusted p-value > 0.05 are shown. "Genome" denotes the genomic element of the gene; min and max denote minimum or maximum nucleotide in the genome.

Source	Replicate	Reads Generated	Reads Mapped
Cell	1	7227507	2669488
Cell	2	7101387	2530662
Cell	3	7266071	2492686
EV	1	7306836	1697153
EV	2	7235360	3951375
EV	3	7296896	4014429

HVO_XXXX	Gene ID	Gene description	Genome	Min	Max	RNA Type	Average TPM EV	Average TPM Cell	Log2 Ratio	Adjusted p-value
HVO_2072	WP_013035656.1	major cell surface glycoprotein	CHR	1923913	1926396	mRNA	738.98	21.23	7.92	0
HVO_0640	#N/A	#N/A	CHR	575668	575752	tRNA	4944.04	383.17	6.45	2.81E-274
HVO_2719	#N/A	#N/A	CHR	2564774	2564858	tRNA	4530.38	365.15	6.42	0
HVO_2488s	#N/A	#N/A	CHR	2357769	2357840	ncRNA	180.71	15.92	6.30	3.00E-150
HVO_1083s	#N/A	#N/A	CHR	988804	988820	ncRNA	161.99	15.76	5.97	3.04E-56
HVO_2854	#N/A	#N/A	CHR	2693483	2693566	tRNA	228.77	25.36	5.92	2.87E-157
HVO_0458	#N/A	#N/A	CHR	408343	408423	tRNA	3119.44	388.81	5.82	0
HVO_2785	#N/A	#N/A	CHR	2620287	2620371	tRNA	2321.95	287.88	5.76	8.75E-224
HVO_1988	WP_004041870.1	hypothetical protein	CHR	1834767	1835816	mRNA	14.59	1.98	5.67	2.29E-165
HVO_1029	#N/A	#N/A	CHR	937864	937934	tRNA	4041.82	599.18	5.52	3.86E-222
HVO_1987	WP_004041869.1	proteinase IV-like protein	CHR	1833881	1834780	mRNA	14.82	2.40	5.45	2.13E-161
HVO_1689	#N/A	#N/A	CHR	1546150	1546223	tRNA	2958.35	507.94	5.36	1.02E-279
HVO_2780	#N/A	#N/A	CHR	2617832	2617916	tRNA	3212.10	532.30	5.35	1.46E-196
HVO_2352	#N/A	#N/A	CHR	2217987	2218060	tRNA	5643.12	1027.50	5.26	2.00E-196
HVO_0361	#N/A	#N/A	CHR	329507	329578	tRNA	6550.14	1257.75	5.16	5.10E-209
HVO_0499	#N/A	#N/A	CHR	441236	441309	tRNA	5279.39	1091.99	5.07	2.47E-230
HVO_0495	#N/A	#N/A	CHR	439239	439312	tRNA	5275.33	1110.94	5.04	1.57E-231

HVO_2927	#N/A	#N/A	CHR	2759237	2759311	tRNA	5599.56	1271.67	4.94	2.25E-230
HVO_0584	#N/A	#N/A	CHR	518441	518514	tRNA	2157.81	508.37	4.89	8.31E-208
HVO_1722	#N/A	#N/A	CHR	1590379	1590452	tRNA	2157.82	509.02	4.89	2.38E-208
HVO_1663	#N/A	#N/A	CHR	1526268	1526350	tRNA	328.79	76.84	4.88	3.82E-158
HVO_2755	WP_004043001.1	50S ribosomal protein P1	CHR	2594860	2595201	mRNA	22.46	5.31	4.85	2.10E-112
HVO_0928	#N/A	#N/A	CHR	840913	840985	tRNA	5070.57	1258.22	4.84	4.03E-183
HVO_1881	#N/A	#N/A	CHR	1736209	1736280	tRNA	2536.76	657.98	4.76	4.63E-230
HVO_C0036s	#N/A	#N/A	pHV1	30413	30450	ncRNA	2623.95	580.51	4.71	5.16E-24
HVO_1833	#N/A	#N/A	CHR	1692867	1692939	tRNA	1153.10	337.04	4.61	3.65E-176
HVO_2794	#N/A	#N/A	CHR	2626534	2626617	tRNA	221.30	60.91	4.61	1.30E-113
HVO_1149	#N/A	#N/A	CHR	1048559	1048630	tRNA	58206.90	16461.49	4.58	5.59E-151
HVO_1026_R	#N/A	#N/A	CHR	936055	936360	ncRNA	6337.17	1859.56	4.50	1.75E-111
HVO_1877	#N/A	#N/A	CHR	1733316	1733386	tRNA	1236.21	388.71	4.48	8.67E-184
HVO_2804	#N/A	GNAT family N-acetyltransferase	CHR	2636111	2636184	mRNA	620.57	194.30	4.47	1.48E-154
HVO_1731	#N/A	#N/A	CHR	1603075	1603196	rRNA	35508.14	11412.19	4.29	4.29E-25
HVO_1732	#N/A	#N/A	CHR	1603383	1603459	tRNA	3721.50	1338.63	4.28	3.40E-186
HVO_A0352	#N/A	ISH3 family transposase	pHV4	364513	364575	mRNA	1477.55	531.46	4.25	9.96E-141
asRNA18	#N/A	#N/A	pHV4	131911	131960	ncRNA	194.14	69.85	4.25	6.98E-110
HVO_2458	#N/A	#N/A	CHR	2328336	2328410	tRNA	26837.58	9666.58	4.25	4.57E-141
HVO_2457	#N/A	#N/A	CHR	2328216	2328290	tRNA	26838.41	9670.55	4.25	3.38E-141
HVO_0503	#N/A	#N/A	CHR	443018	443091	tRNA	884.02	325.99	4.23	3.98E-153
HVO_2217	#N/A	#N/A	CHR	2082040	2082124	tRNA	163.26	61.95	4.16	1.29E-104
HVO_A0134	#N/A	IS5/IS1182 family transposase	pHV4	131940	132431	mRNA	13.07	5.10	4.15	3.03E-97
asRNA20	#N/A	#N/A	pHV4	364549	364598	ncRNA	2611.27	1014.95	4.14	7.09E-135
HVO_2566	#N/A	#N/A	CHR	2420585	2420655	tRNA	15995.78	6559.62	4.09	1.43E-141
asRNA16	#N/A	#N/A	pHV1	62764	62815	ncRNA	406.24	165.86	4.06	2.96E-111
HVO_A0007_A	#N/A	hypothetical protein	pHV4	7920	9687	mRNA	37.97	14.88	4.06	8.70E-58
HVO_0524	#N/A	#N/A	CHR	458021	458095	tRNA	625.67	261.59	4.04	2.52E-115
HVO_1846	#N/A	#N/A	CHR	1706125	1706198	tRNA	1037.86	475.38	3.94	9.61E-157
HVO_1729	#N/A	#N/A	CHR	1599762	1599833	tRNA	3336.95	1512.30	3.92	1.62E-92
HVO_2938	#N/A	#N/A	CHR	2769994	2770065	tRNA	3336.95	1512.30	3.92	1.62E-92
HVO_2565s	#N/A	#N/A	CHR	2420311	2420327	ncRNA	117.80	58.00	3.81	2.35E-44
H62	#N/A	#N/A	CHR	1781262	1781347	ncRNA	676.09	288.28	3.80	5.33E-17
HVO_0523	#N/A	#N/A	CHR	457852	457924	tRNA	12099.10	6142.44	3.77	1.19E-121
asRNA4	#N/A	#N/A	pHV4	115698	115748	ncRNA	291.10	153.48	3.71	9.34E-99
asRNA21	#N/A	#N/A	pHV4	413589	413634	ncRNA	445.28	242.37	3.69	1.93E-102
asRNA6	#N/A	#N/A	CHR	1010936	1010977	ncRNA	1956.84	1079.38	3.67	5.36E-113
HVO_2006s	#N/A	#N/A	CHR	1852367	1852383	ncRNA	68.89	35.90	3.65	6.66E-27
HVO_0381	WP_004044542.1	CopG family transcriptional regulator	CHR	339904	340089	mRNA	50.25	29.64	3.60	1.10E-88
HVO_1435	#N/A	#N/A	CHR	1307487	1307561	tRNA	3213.10	1857.21	3.59	6.74E-128

H124	#N/A	#N/A	CHR	311835	311885	ncRNA	50.60	29.04	3.58	2.29E-44
HVO_2777	WP_004043023.1	30S ribosomal protein S9	CHR	2616629	2617027	mRNA	30.36	17.93	3.56	2.40E-88
HVO_2567	#N/A	#N/A	CHR	2420668	2420738	tRNA	12196.93	7187.40	3.54	3.52E-86
HVO_A0408	#N/A	ISH3 family transposase	pHV4	413614	414760	mRNA	13.16	8.05	3.52	5.67E-93
asRNA10	#N/A	#N/A	pHV1	70152	70197	ncRNA	4318.51	2778.06	3.43	8.65E-104
HVO_0345	#N/A	#N/A	CHR	311755	311827	tRNA	5297.56	3505.78	3.42	8.12E-109
HVO_A0008	WP_004043314.1	transposase	pHV4	8150	9448	mRNA	13.13	8.19	3.39	1.86E-45
HVO_2940	#N/A	hypothetical protein	CHR	2772189	2772305	mRNA	249.04	155.73	3.39	1.55E-48
asRNA13	#N/A	#N/A	pHV1	80995	81031	ncRNA	946.92	634.83	3.36	4.62E-79
HVO_2393	#N/A	#N/A	CHR	2264001	2264075	tRNA	3301.76	2297.35	3.35	8.28E-89
HVO_0130	#N/A	#N/A	CHR	121223	121296	tRNA	169.82	118.50	3.34	2.92E-86
HVO_C0080_A	#N/A	ISH5 family transposase	pHV1	80936	81022	mRNA	404.16	277.69	3.32	2.35E-78
HVO_2519	#N/A	hypothetical protein	CHR	2384839	2384987	mRNA	1503.78	1053.04	3.32	1.15E-102
asRNA1	#N/A	#N/A	CHR	243867	243903	ncRNA	2434.77	1618.38	3.29	5.02E-43
asRNA15	#N/A	#N/A	CHR	780347	780395	ncRNA	217.54	153.60	3.29	4.69E-77
HVO_0706	#N/A	#N/A	CHR	633681	633755	tRNA	3016.55	2247.13	3.26	6.05E-78
HVO_0288	#N/A	#N/A	CHR	259298	259370	tRNA	787.37	575.60	3.26	9.79E-103
HVO_2821s	#N/A	#N/A	CHR	2655103	2655119	ncRNA	498.45	335.51	3.26	3.68E-34
HVO_2565	WP_004042620.1	hypothetical protein	CHR	2419453	2420295	mRNA	13.53	9.67	3.24	2.55E-57
HVO_2117	WP_004042001.1	sugar ABC transporter permease	CHR	1981148	1982068	mRNA	17.81	13.69	3.18	9.63E-71
HVO_2160	WP_004042044.1	PGF-CTERM sorting domain-containing protein	CHR	2025177	2031950	mRNA	23.98	19.16	3.18	4.96E-75
HVO_0987	WP_004043956.1	oxidoreductase	CHR	896613	898142	mRNA	24.60	19.51	3.16	1.28E-98
HVO_2908s	#N/A	#N/A	CHR	2745602	2745678	ncRNA	1788.68	1226.67	3.16	2.35E-13
HVO_0972	WP_004043971.1	hypothetical protein	CHR	882969	883490	mRNA	25.89	20.77	3.15	2.03E-78
HVO_0263	WP_013035611.1	ISH3 family transposase ISH51	CHR	235110	236276	mRNA	151.55	122.12	3.11	1.66E-86
asRNA8	#N/A	#N/A	CHR	1698155	1698201	ncRNA	1115.67	928.63	3.09	5.22E-105
HVO_0985	WP_004043958.1	NADH-quinone oxidoreductase subunit K	CHR	894274	894576	mRNA	34.63	28.91	3.08	8.29E-77
HVO_2784	WP_004043029.1	30S ribosomal protein S13	CHR	2619760	2620263	mRNA	47.78	40.53	3.06	7.34E-80
HVO_2073s	#N/A	#N/A	CHR	1928023	1928062	ncRNA	163.72	125.96	3.06	1.09E-29
H225.1	#N/A	#N/A	CHR	1597695	1598068	ncRNA	344.37	279.65	3.06	6.78E-51
HVO_0983	WP_004043960.1	NADH dehydrogenase subunit J	CHR	893649	893909	mRNA	25.29	21.95	3.03	5.08E-58
HVO_1802_R	#N/A	#N/A	CHR	1665493	1665927	ncRNA	213.19	177.77	3.02	3.81E-57
HVO_2737	WP_004042964.1	50S ribosomal protein L7ae	CHR	2583344	2583706	mRNA	10.44	9.46	2.98	1.11E-50
HVO_2412s	#N/A	#N/A	CHR	2281530	2281546	ncRNA	16.77	13.55	2.98	6.16E-09
asRNA5	#N/A	#N/A	pHV1	68727	68768	ncRNA	265.28	239.24	2.94	8.80E-52
HVO_0944	WP_004044001.1	cytochrome c oxidase subunit II	CHR	855836	856375	mRNA	29.89	28.15	2.93	8.71E-68
HVO_2773	WP_004043019.1	30S ribosomal protein S2	CHR	2614266	2615048	mRNA	32.44	30.46	2.93	3.12E-81
HVO_2775	WP_004043021.1	DNA-directed RNA polymerase subunit K/omega	CHR	2616249	2616425	mRNA	24.94	23.43	2.92	2.81E-46

HVO_0984	WP_004043959.1	hypothetical protein	CHR	893906	894274	mRNA	20.84	19.46	2.92	1.09E-62
HVO_2718s2	#N/A	#N/A	CHR	2564860	2564876	ncRNA	17.58	15.34	2.91	4.24E-09
CRISPR3	#N/A	#N/A	pHV4	217812	218566	ncRNA	314.39	293.82	2.90	2.47E-71
HVO_C0065	N/A	IS6 family transposase	pHV1	62797	63476	mRNA	11.12	10.28	2.89	1.09E-53
asRNA9	#N/A	#N/A	pHV4	264268	264313	ncRNA	2522.05	2384.95	2.88	1.66E-73
HVO_2776	WP_004043022.1	DNA-directed RNA polymerase subunit N	CHR	2616422	2616616	mRNA	35.60	34.86	2.87	5.07E-53
HVO_2073	WP_004041957.1	LacI family transcriptional regulator	CHR	1926766	1927521	mRNA	11.16	10.93	2.84	6.60E-55
HVO_0986	WP_004043957.1	NADH-quinone oxidoreductase subunit L	CHR	894580	896616	mRNA	19.71	19.51	2.84	7.95E-84
HVO_0517	#N/A	#N/A	CHR	452351	452423	tRNA	774.92	770.53	2.83	2.11E-78
HVO_0196	WP_004045310.1	DUF1931 domain-containing protein	CHR	176934	177101	mRNA	105.87	105.43	2.83	9.62E-81
HVO_2778	WP_004043024.1	50S ribosomal protein L13	CHR	2617021	2617458	mRNA	41.75	40.99	2.83	2.26E-60
HVO_2116	WP_013035569.1	sugar ABC transporter permease	CHR	1980207	1981151	mRNA	15.70	15.73	2.82	1.04E-50
HVO_0480s	#N/A	#N/A	CHR	429875	429891	ncRNA	23.18	21.64	2.82	1.08E-10
HVO_2782	WP_004043027.1	30S ribosomal protein S11	CHR	2618847	2619239	mRNA	34.30	34.63	2.81	2.96E-55
asRNA2	#N/A	#N/A	pHV4	438839	438872	ncRNA	494.66	490.46	2.81	4.00E-61
HVO_A0117	WP_013035143.1	IS5 family transposase ISHvo1	pHV4	115728	116552	mRNA	10.02	9.95	2.81	8.62E-60
HVO_2783	WP_004043028.1	30S ribosomal protein S4	CHR	2619236	2619763	mRNA	33.72	34.08	2.81	1.92E-68
HVO_1518	#N/A	ISH5 family transposase	CHR	1382710	1385466	mRNA	70.10	68.40	2.79	3.58E-44
HVO_A0137s	#N/A	#N/A	pHV4	135199	135340	ncRNA	68.40	70.87	2.73	1.89E-48
HVO_0275	WP_013035249.1	IS4 family transposase	CHR	243876	245228	mRNA	71.79	73.16	2.73	1.04E-42
HVO_2774	WP_004043020.1	phosphopyruvate hydratase	CHR	2615045	2616244	mRNA	19.80	21.63	2.71	8.75E-71
CRISPR2	#N/A	#N/A	pHV4	204975	207584	ncRNA	211.09	224.74	2.71	2.73E-63
HVO_A0354	N/A	ISH3 family transposase	pHV4	365276	365704	mRNA	253.90	272.70	2.70	1.97E-65
HVO_0062	WP_004045090.1	peptide ABC transporter substrate-binding protein	CHR	61296	63134	mRNA	23.30	25.89	2.69	8.00E-71
HVO_2451s	#N/A	#N/A	CHR	2319814	2319830	ncRNA	42.50	43.05	2.67	2.22E-13
HVO_2822	WP_013035380.1	hypothetical protein	CHR	2655111	2655413	mRNA	13.00	12.63	2.65	1.81E-08
HVO_A0035s	#N/A	#N/A	pHV4	33964	33980	ncRNA	63.83	70.14	2.64	2.20E-20
HVO_0979	WP_004043964.1	NADH dehydrogenase	CHR	889665	890366	mRNA	18.04	20.63	2.64	2.86E-61
CRISPR1	#N/A	#N/A	CHR	2385045	2386660	ncRNA	289.09	324.70	2.63	1.45E-63
HVO_2491	#N/A	#N/A	CHR	2358758	2358828	tRNA	625.28	713.39	2.63	5.22E-63
H25	#N/A	#N/A	CHR	2499841	2500057	ncRNA	172.44	190.64	2.63	1.92E-45
HVO_0945	WP_004044000.1	cytochrome c oxidase subunit I	CHR	856375	858144	mRNA	20.32	23.84	2.61	1.56E-61
HVO_2817	#N/A	ISH3 family transposase	CHR	2648777	2649943	mRNA	101.64	118.04	2.59	5.45E-64
HVO_2070	WP_049941511.1	sialidase	CHR	1919938	1921572	mRNA	14.36	16.98	2.58	4.73E-65
HVO_1837	N/A	ISH3 family transposase	CHR	1697021	1698178	mRNA	46.67	55.45	2.57	4.19E-75
HVO_A0364	WP_013035046.1	ISH3 family transposase ISHvo20	pHV4	375384	376550	mRNA	46.18	55.39	2.56	5.55E-74
HVO_1276	#N/A	hypothetical protein	CHR	1165740	1165916	mRNA	671.75	781.02	2.56	2.41E-45
HVO_0946	WP_004043999.1	hypothetical protein	CHR	858141	858335	mRNA	29.10	34.84	2.55	2.43E-44

HVO_C0013	WP_013035120.1	IS4 family transposase ISHvo12	pHV1	9798	11096	mRNA	53.72	64.91	2.55	6.38E-60
asRNA3	#N/A	#N/A	CHR	2650374	2650407	ncRNA	1030.28	1211.23	2.51	4.13E-32
HVO_2757	WP_004043003.1	50S ribosomal protein L1	CHR	2596266	2596904	mRNA	17.13	20.99	2.50	2.62E-49
HVO_0942s	#N/A	#N/A	CHR	855543	855559	ncRNA	60.22	71.14	2.47	4.41E-16
HVO_0982	WP_004043961.1	(4Fe-4S)-binding protein	CHR	893082	893543	mRNA	25.94	33.35	2.46	3.45E-54
HVO_2779	WP_004043025.1	50S ribosomal protein L18e	CHR	2617455	2617805	mRNA	52.08	66.85	2.45	3.90E-47
HVO_A0353	N/A	ISH3 family transposase	pHV4	364986	365228	mRNA	58.22	76.44	2.40	8.74E-47
H51	#N/A	#N/A	CHR	1891968	1892001	ncRNA	241.44	265.90	2.38	6.41E-05
HVO_0981	WP_004043962.1	NADH dehydrogenase	CHR	892036	893085	mRNA	14.60	20.13	2.35	3.91E-50
HVO_0012	#N/A	#N/A	CHR	11661	11733	tRNA	780.98	1085.29	2.35	1.52E-47
HVO_2103	WP_004041986.1	PTS galactitol enzyme II, C component	CHR	1965879	1967369	mRNA	21.05	30.08	2.34	1.66E-53
HVO_2062	WP_004041947.1	flagellin	CHR	1911379	1911816	mRNA	102.04	142.23	2.32	6.18E-44
asRNA11	#N/A	#N/A	pHV1	30739	30787	ncRNA	341.90	496.76	2.29	8.61E-48
HVO_0907	WP_004044032.1	cox-type terminal oxidase subunit I	CHR	824054	825853	mRNA	60.32	88.63	2.27	4.48E-56
HVO_2718s	#N/A	#N/A	CHR	2564654	2564774	ncRNA	373.82	488.20	2.26	4.03E-07
HVO_0988	WP_004043955.1	oxidoreductase	CHR	898143	899663	mRNA	18.61	27.93	2.25	1.37E-54
asRNA14	#N/A	#N/A	pHV1	15169	15213	ncRNA	3988.01	5990.89	2.25	7.89E-61
HVO_1730	#N/A	#N/A	CHR	1600056	1602963	rRNA	2558.13	3650.92	2.24	2.99E-27
asRNA12	#N/A	#N/A	pHV4	364964	365009	ncRNA	360.90	534.80	2.24	2.62E-46
HVO_2818	#N/A	ISH5 family transposase	CHR	2650123	2650398	mRNA	133.98	195.03	2.23	1.47E-31
H226.7	#N/A	#N/A	CHR	442805	442946	ncRNA	27.22	39.33	2.22	4.92E-22
HVO_2816	#N/A	#N/A	CHR	2646860	2646934	tRNA	312.64	488.33	2.19	4.88E-44
HVO_0359	WP_004044564.1	elongation factor 1-alpha	CHR	327676	328941	mRNA	22.87	36.74	2.15	1.59E-44
HVO_0763	WP_049941502.1	quinol oxidase	CHR	684671	685198	mRNA	16.46	26.13	2.15	3.12E-34
HVO_0864	#N/A	IS5 family transposase ISHvo7	CHR	781200	781303	mRNA	278.26	440.48	2.14	5.44E-45
HVO_2757s	#N/A	#N/A	CHR	2596927	2596971	ncRNA	307.46	466.66	2.14	3.11E-22
HVO_1422s	#N/A	#N/A	CHR	1296161	1296238	ncRNA	219.68	341.53	2.14	5.80E-29
H3.2	#N/A	#N/A	CHR	2163482	2163629	ncRNA	97.50	153.52	2.11	3.72E-26
HVO_B0092s	#N/A	#N/A	pHV3	104714	104732	ncRNA	68.36	108.02	2.10	5.62E-14
HVO_C0037	WP_013035684.1	ISH3 family transposase ISHvo21	pHV1	30761	31930	mRNA	18.86	31.05	2.10	1.99E-45
HVO_2583s	#N/A	#N/A	CHR	2436253	2436271	ncRNA	50.32	82.42	2.03	1.70E-10
HVO_2736s	#N/A	#N/A	CHR	2583222	2583238	ncRNA	43.35	75.28	2.02	3.49E-10
HVO_B0272s	#N/A	#N/A	pHV3	325593	325609	ncRNA	13.28	21.97	2.01	3.20E-05
asRNA7	#N/A	#N/A	pHV4	379434	379479	ncRNA	1717.92	3005.22	2.00	1.07E-32
HVO_B0091	WP_004041064.1	ABC transporter permease	pHV3	102695	103717	mRNA	10.50	19.32	1.99	4.86E-29
HVO_B0152	WP_013034963.1	IS4 family transposase	pHV3	170084	171253	mRNA	135.36	243.68	1.98	5.42E-48
HVO_1422_A	#N/A	pHK2-ORF12 homolog	CHR	1296078	1296386	mRNA	56.34	97.73	1.98	3.80E-25
HVO_0763s	#N/A	#N/A	CHR	685198	685214	ncRNA	102.57	182.85	1.96	1.27E-16
HVO_2781	WP_004043026.1	DNA-directed RNA polymerase subunit D	CHR	2618061	2618840	mRNA	23.40	42.54	1.96	1.29E-36
HVO_C0073s	#N/A	#N/A	pHV1	72253	72276	ncRNA	79.25	143.92	1.95	1.18E-16

HVO_A0349	WP_013035196.1	ISH3 family transposase ISHvo22	pHV4	361704	362870	mRNA	17.78	33.66	1.90	3.03E-39
HVO_A0633s	#N/A	#N/A	pHV4	631327	631347	ncRNA	33.57	60.06	1.89	2.55E-09
HVO_2051	WP_013035619.1	IS4 family transposase	CHR	1897872	1899221	mRNA	31.00	58.43	1.87	5.21E-26
HVO_2779s	#N/A	#N/A	CHR	2617815	2617831	ncRNA	397.25	754.69	1.87	2.61E-22
HVO_0947	WP_004043998.1	hypothetical protein	CHR	858517	858738	mRNA	15.62	31.07	1.86	2.15E-21
HVO_0980	WP_004043963.1	NADH-quinone oxidoreductase subunit C	CHR	890363	892036	mRNA	15.10	30.06	1.86	2.01E-33
HVO_0360	WP_004044563.1	30S ribosomal protein S10	CHR	328944	329252	mRNA	18.92	36.76	1.85	8.21E-27
HVO_0943	WP_004044002.1	hypothetical protein	CHR	855608	855835	mRNA	32.31	63.79	1.85	2.85E-27
HVO_3011	#N/A	hypothetical protein	CHR	2844315	2844428	mRNA	61.78	108.66	1.84	3.34E-05
HVO_2466	WP_013035323.1	IS4 family transposase	CHR	2335167	2336333	mRNA	74.68	147.20	1.83	8.86E-31
HVO_C0030s	#N/A	#N/A	pHV1	20663	20679	ncRNA	584.96	1121.23	1.79	4.88E-13
HVO_2522s	#N/A	#N/A	CHR	2388676	2388758	ncRNA	36.85	72.82	1.78	1.15E-14
HVO_C0072	WP_013035731.1	ABC transporter permease	pHV1	70334	71227	mRNA	28.26	60.71	1.77	5.47E-21
HVO_0988s	#N/A	#N/A	CHR	899676	899692	ncRNA	251.27	490.34	1.76	2.32E-13
HVO_A0431	WP_013035212.1	IS4 family transposase	pHV4	438848	440197	mRNA	15.93	33.39	1.75	5.34E-29
HVO_0864	WP_004044073.1	IS5 family transposase ISHvo7	CHR	779373	780371	mRNA	10.65	22.83	1.71	1.02E-26
H226.11	#N/A	#N/A	CHR	1526132	1526231	ncRNA	16.31	34.20	1.70	2.00E-12
HVO_A0204s	#N/A	#N/A	pHV4	207662	207678	ncRNA	89.79	189.32	1.68	2.18E-11
HVO_1728	#N/A	#N/A	CHR	1598192	1599664	rNRA	1597.82	3445.76	1.66	6.05E-19
HVO_A0548	WP_049941497.1	quinol oxidase	pHV4	549629	550156	mRNA	13.98	30.79	1.65	1.17E-19
HVO_2881s	#N/A	#N/A	CHR	2718383	2718399	ncRNA	32.53	70.20	1.64	6.87E-07
HVO_B0092	WP_004041063.1	peptide ABC transporter permease	pHV3	103720	104724	mRNA	15.57	35.61	1.64	2.46E-23
HVO_A0378	WP_004043279.1	N-methylhydantoinase	pHV4	387218	388993	mRNA	42.45	98.53	1.59	6.39E-21
HVO_1749	WP_004041632.1	hypothetical protein	CHR	1619596	1620450	mRNA	13.06	31.42	1.56	2.49E-23
HVO_1991s	#N/A	#N/A	CHR	1838651	1838667	ncRNA	472.96	1037.57	1.56	6.32E-09
HVO_A0155	WP_004043084.1	sodium:solute symporter	pHV4	153466	153903	mRNA	25.08	62.21	1.54	5.18E-21
HVO_A0154	WP_004043083.1	cation acetate symporter	pHV4	151820	153469	mRNA	25.67	63.90	1.53	3.81E-23
HVO_1161	#N/A	#N/A	CHR	1061493	1061565	tRNA	48.99	118.26	1.51	1.76E-13
HVO_0281	#N/A	#N/A	CHR	252026	252098	tRNA	157.18	400.31	1.47	1.78E-19
HVO_1014	WP_004043928.1	cytochrome c oxidase subunit II	CHR	923045	923803	mRNA	15.86	40.53	1.47	1.49E-18
HVO_0860	WP_004044077.1	Fe-S cluster assembly protein SufB	CHR	775569	776999	mRNA	14.18	36.34	1.46	1.25E-20
HVO_0312	WP_004044611.1	F0F1 ATP synthase subunit C	CHR	281153	281410	mRNA	14.53	38.05	1.45	1.26E-16
HVO_C0073	WP_004045462.1	ABC transporter	pHV1	71227	72192	mRNA	34.00	91.48	1.43	3.35E-15
H226.17	#N/A	#N/A	CHR	2263863	2263979	ncRNA	66.44	178.34	1.39	1.12E-17
HVO_A0153	WP_004043082.1	universal stress protein UspA	pHV4	151328	151816	mRNA	21.19	58.48	1.38	1.48E-16
HVO_1148s	#N/A	#N/A	CHR	1048636	1048804	ncRNA	17.30	45.80	1.37	6.24E-10
HVO_1187s	#N/A	#N/A	CHR	1080199	1080376	ncRNA	938.40	2628.31	1.32	2.57E-19
asRNA19	#N/A	#N/A	pHV4	244540	244592	ncRNA	129.22	362.90	1.31	1.26E-12
HVO_0908	WP_004064260.1	hypothetical protein	CHR	825916	826275	mRNA	13.08	37.45	1.30	7.36E-14

HVO_1992	WP_004041873.1	cold-shock protein	CHR	1838678	1838872	mRNA	232.77	670.20	1.28	5.26E-15
HVO_A0379	WP_013035057.1	N-methylhydantoinase	pHV4	388990	391035	mRNA	28.67	82.92	1.26	8.77E-13
HVO_A0377	WP_004043278.1	hypothetical protein	pHV4	386436	387218	mRNA	38.09	112.28	1.26	4.18E-14
HVO_1885s	#N/A	#N/A	CHR	1739827	1739843	ncRNA	32.54	94.75	1.25	4.26E-05
asRNA17	#N/A	#N/A	pHV3	297120	297168	ncRNA	293.13	895.22	1.22	8.45E-17
HVO_B0249	#N/A	ISH11 family transposase	pHV3	296165	297144	mRNA	14.04	42.73	1.22	4.17E-16
HVO_A0637	WP_013035036.1	translation initiation factor 1A	pHV4	634653	634937	mRNA	64.83	190.18	1.22	3.04E-11
HVO_A0547s	#N/A	#N/A	pHV4	549560	549576	ncRNA	24.39	69.81	1.21	0.000646764
HVO_0841	WP_004044095.1	cytochrome b	CHR	757686	758450	mRNA	30.00	92.53	1.19	3.23E-15
HVO_1831s	#N/A	#N/A	CHR	1691173	1691189	ncRNA	45.76	140.80	1.19	8.02E-06
HVO_0701	WP_004044234.1	50S ribosomal protein L44e	CHR	629175	629456	mRNA	12.60	39.21	1.19	3.48E-10
HVO_0842	WP_004044094.1	cytochrome b6	CHR	758461	759255	mRNA	25.21	79.02	1.18	4.86E-15
HVO_A0376	WP_004043277.1	peptidase	pHV4	385336	386439	mRNA	40.08	123.58	1.17	3.05E-11
HVO_2351s	#N/A	#N/A	CHR	2218063	2218169	ncRNA	179.71	558.98	1.13	1.24E-08
HVO_1106s	#N/A	#N/A	CHR	1011067	1011083	ncRNA	17.86	55.09	1.11	0.007306836
HVO_0861	WP_004044076.1	Fe-S cluster assembly protein SufD	CHR	777003	778211	mRNA	11.22	37.36	1.10	1.48E-10
HVO_0783	WP_004044154.1	ATP-dependent protease LonB	CHR	702504	704588	mRNA	54.69	182.56	1.07	3.69E-13
HVO_1954s	#N/A	#N/A	CHR	1804444	1804462	ncRNA	108.25	355.26	1.06	4.20E-06

Supplementary Table 7: Differential expression calculated for transcripts from *Hbt. salinarum* EVs normalized to intracellular levels. RNA was extracted from purified EVs (duplicates) and the respective cells (one replicate). Read mapping (90% minimum overlap identity, TPM) and differential expression (log2 ratio) performed with Geneious™ (2021.0.1).

(Excel file available at https://www.biorxiv.org/content/10.1101/2023.03.03.530948v1 as Supplementary Table 7)

Supplementary Table 8. Proteins enriched in EVs after normalization with the protein content of cell membranes. Protein content of EVs was pooled from upper and lower bands in three replicates (total of 6 EV replicates) and quantities were compared with three replicates from host cell membrane preparations. Quantity was estimated using MaxQuant (v. 1.6.10.43) and differential expression analysis (log2 fold change, adjusted p-value) was calculated with DEP (v. 1.21.0) [35]. Only proteins with log2 ratio > 1 and adjusted p-value > 0.05 are shown (Full Excel file with raw data can be found at https://www.biorxiv.org/content/10.1101/2023.03.03.530948v1 as Supplementary Table 8)

Protein ID	HVO_XXXX	Description	arCOG	log2 ratio	Adjusted p-value	cellular localisation
WP_004041897.1	HVO_2013	CetZ5	D	9.55	0.000000877	indirectly associated with the cell membrane (De Castro et al. 2022)
WP_004042501.1	HVO_2519	hypothetical protein	S	9.19	8.71E-09	no transmembrane regionin detected
ADE04578.1	HVO_2204	CetZ1	D	8.69	3.51E-10	indirectly associated with the cell membrane (Duggin et al. 2015)
WP_004043803.1	HVO_1134	hypothetical protein	S	7.25	0.00000484	no transmembrane region detected
WP_004044352.1	HVO_0581	FtsZ2	D	6.66	0.00153	indirectly associated with the cell membrane (Liao et al. 2021)

WP_004041869.1	HVO_1987	proteinase IV-like protein	O	6.29	0.00119	Signal peptide and transmembran region
WP_004041843.1	HVO_1964	photosystem reaction center subunit H	R	5.89	0.00204	no transmembrane region detected
WP_004044192.1	HVO_0745	CetZ2	D	5.31	0.00228	indirectly associated with the cell membrane (Brown et al. 2023)
WP_004044872.1	HVO_2985	hypothetical protein	V	5.2	0.0175	no transmembrane region detected
WP_004041076.1	HVO_B007	ABC transporter ATP-binding protein	E	4.74	0.0011	no transmembrane region detected
WP_004044952.1	HVO_3014	GTP-binding protein	R	4.16	0.0133	no transmembrane region detected

Supplementary Table 9: Proteins enriched in EVs from UV-treated cells after normalization with the protein content of respective cell membranes. Protein content of EVs from UV treated cells was pooled from upper and lower bands in three replicates (total of 6 EV replicates) and quantities were compared with three replicates from respective host cell membrane preparations. Quantity was estimated using MaxQuant (v. 1.6.10.43) and differential expression analysis (log2 fold change, adjusted p-value) was calculated with DEP (v. 1.21.0) [35].

(Excel file can be viewed at https://www.biorxiv.org/content/10.1101/2023.03.03.530948v1 as Supplementary Table 9)

Supplementary Table 10. Proteins identified as present in all EV samples. Protein content of EVs from untreated cells (3 replicates from upper and lower bands of density gradient each) and UV treated cells (3 replicates from upper and lower bands of density gradient each) was pooled (total of 12 EV replicates). Label-free quantities (LFQ) were calculated using MaxQuant (v. 1.6.10.43) and averaged over all replicates. Proteins were only considered present if peptide count was greater than or equal to 2 in all replicates and all replicates had a corresponding LFQ value.

Protein IDs	HVO_XXXX	Description	arCOG	Average LFQ intensity
ADE04578.1	HVO_2204	CetZ1	D	1929791667
ELY33665.1	HVO_2072	major cell surface glycoprotein	T	1746082500
WP_004045090.1	HVO_0062	peptide ABC transporter substrate-binding protein	E	916335833.3
ELY32287.1	HVO_2695	sugar ABC transporter substrate-binding protein	G	638015833.3
WP_004043971.1	HVO_0972	hypothetical protein	N	525204166.7
WP_004043803.1	HVO_1134	hypothetical protein	S	475101666.7
WP_004044872.1	HVO_2985	hypothetical protein	V	457697500
ADE02586.1	HVO_2126	peptide ABC transporter substrate-binding protein	E	446278333.3
WP_004044135.1	HVO_0801	phosphoesterase	O	424017500
WP_004041897.1	HVO_2013	CetZ5	D	382883416.7
WP_004043537.1	HVO_1401	BMP family ABC transporter substrate-binding protein	R	363347500
WP_004044307.1	HVO_0628	ABC transporter substrate-binding protein	E	212107166.7
WP_004042044.1	HVO_2160	PGF-CTERM sorting domain-containing protein	S	201645000
WP_004042501.1	HVO_2519	hypothetical protein	S	197842083.3
ADE03035.1	HVO_0763	quinol oxidase	S	190519000
WP_004041916.1	HVO_2031	BMP family ABC transporter substrate-binding protein	R	187271500
WP_004041769.1	HVO_1888	molybdenum transporter	H	176909750
ADE01499.1	HVO_B0082	peptide ABC transporter substrate-binding protein	E	146354166.7
WP_004041775.1	HVO_1894	hypothetical protein	S	134678416.7
WP_049941511.1	HVO_2070	sialidase	M	125886583.3
ELY32157.1	HVO_A0133	Tat (twin-arginine translocation) pathway signal sequence domain protein	S	125199666.7
WP_004043922.1	HVO_1020	PBS lyase HEAT-like repeat domain-containing protein	S	118896833.3
WP_004044607.1	HVO_0316	ATP synthase subunit A	C	113604250
WP_004042036.1	HVO_2153	membrane protein	Q	111740166.7
WP_004044564.1	HVO_0359	elongation factor 1-alpha	J	108387833.3
WP_004042286.1	HVO_2397	adhesin	P	106958250
WP_004042262.1	HVO_2373	30S ribosomal protein S8e	J	106240833.3
WP_004041336.1	HVO_B0198	iron ABC transporter substrate-binding protein	P	101337000

WP_004044567.1	HVO_0356	elongation factor EF-2	J	93035500
WP_004044823.1	HVO_2960	branched-chain alpha-keto acid dehydrogenase subunit E2	C	90253333.33
WP_004044400.1	HVO_0530	sugar ABC transporter substrate-binding protein	G	89559666.67
ADE01713.1	HVO_A0548	quinol oxidase	S	87995000
WP_004045197.1	HVO_0106	hypothetical protein	S	84348166.67
WP_004044192.1	HVO_0745	CetZ2	D	79767833.33
WP_013035363.1	HVO_1530	MFS transporter	M	75016916.67
WP_004044606.1	HVO_0317	V-type ATP synthase subunit B	C	72820500
WP_004042940.1	HVO_2724	ribonuclease J	J	71380500
WP_004041424.1	HVO_1546	dihydroxyacetone kinase subunit DhaK	G	70506333.33
WP_004041481.1	HVO_1590	molecular chaperone DnaK	O	70455500
WP_004044609.1	HVO_0314	ATP synthase subunit C	C	70427416.67
ELY28087.1	HVO_1228	cytochrome Fbr	C	70209916.67
WP_004043963.1	HVO_0980	NADH-quinone oxidoreductase subunit C	C	69684500
WP_004043835.1	HVO_1103	hypothetical protein	S	67152083.33
WP_004044718.1	HVO_2900	fumarase	C	67080250
WP_004044820.1	HVO_2959	2-oxoisovalerate dehydrogenase subunit beta	C	63911666.67
WP_004042273.1	HVO_2384	CBS domain-containing protein	R	63371000
WP_004044825.1	HVO_2961	dihydrolipoamide dehydrogenase	C	61895000
WP_004042325.1	HVO_2432	basic amino acid ABC transporter substrate-binding protein	S	60522000
ELY35686.1	HVO_1673	hypothetical protein	S	57473083.33
WP_004043700.1	HVO_1241	photosynthetic protein synthase I	R	57030875
WP_004041107.1	HVO_B0047	iron ABC transporter substrate-binding protein	P	56856500
WP_004044818.1	HVO_2958	pyruvate dehydrogenase (acetyl-transferring) E1 component subunit alpha	C	55475833.33
WP_004042658.1	HVO_2588	isocitrate dehydrogenase (NADP(+))	C	54533583.33
WP_004043964.1	HVO_0979	NADH dehydrogenase	C	52595416.67
WP_004042268.1	HVO_2379	phosphate transport system regulatory protein PhoU	P	51864333.33
WP_004044093.1	HVO_0843	hypothetical protein	S	49737416.67
WP_004042616.1	HVO_2563	50S ribosomal protein L4	J	49675083.33
WP_004042287.1	HVO_2398	ABC transporter ATP-binding protein	P	48654833.33
WP_004045327.1	HVO_0213	rubrerythrin	R	47987500
WP_004041835.1	HVO_1955	aconitate hydratase	C	47038166.67
ADE01609.1	HVO_B0135	hypothetical protein	S	44420583.33
WP_004043050.1	HVO_2808	succinate dehydrogenase	C	43540500
WP_004044952.1	HVO_3014	Era-like GTP binding protein, oapA	R	43503083.33
WP_013035331.1	HVO_2889	nuclease	L	43181416.67
WP_004042006.1	HVO_2122	ABC transporter ATP-binding protein	E	41926675
WP_004043005.1	HVO_2758	50S ribosomal protein L11	J	41821000
WP_004044604.1	HVO_0319	V-type ATP synthase subunit D	C	41746750
WP_004043028.1	HVO_2783	30S ribosomal protein S4	J	40564025
ELY33434.1	HVO_2205	NADH dehydrogenase	R	39342416.67
WP_004044569.1	HVO_0354	30S ribosomal protein S7	J	39151833.33

WP_004044637.1	HVO_0285	metalloprotease	R	38823916.67
WP_004041171.1	HVO_B0363	dimethylsulfoxide reductase	C	38244083.33
WP_004041062.1	HVO_B0093	peptide ABC transporter substrate-binding protein	E	37982833.33
WP_004044352.1	HVO_0581	FtsZ2	D	37763666.67
WP_004043701.1	HVO_1240	Tat pathway signal protein	P	37480250
WP_004042101.1	HVO_2209	2-oxo acid dehydrogenase	C	35712000
WP_004041843.1	HVO_1964	photosystem reaction center subunit H	R	35670416.67
WP_004042542.1	HVO_2537	hypothetical protein	S	34985850
WP_004041964.1	HVO_2081	hypothetical protein	S	34952000
WP_004043696.1	HVO_1245	DSBA oxidoreductase	O	34886083.33
WP_004045186.1	HVO_0102	zinc metalloprotease HtpX	O	34727583.33
WP_004044965.1	HVO_0009	L-cysteine desulfhydrase	E	34348166.67
WP_004043847.1	HVO_1091	proteasome endopeptidase complex,subunit alpha	O	34245416.67
WP_004043029.1	HVO_2784	30S ribosomal protein S13	J	33218466.67
WP_013035375.1	HVO_2913	superoxide dismutase	P	33106916.67
WP_013035585.1	HVO_1495	PTS sugar transporter subunit IIC	G	33034166.67
WP_004043632.1	HVO_1305	2-ketoglutarate ferredoxin oxidoreductase subunit alpha	C	32590416.67
WP_004044212.1	HVO_0725	short-chain dehydrogenase/reductase	I	32336458.33
WP_004043804.1	HVO_1133	hypothetical protein	K	32271866.67
ADE04559.1	HVO_2015	hypothetical protein	D	31856541.67
WP_004043743.1	HVO_1198	universal stress protein UspA	T	31414916.67
WP_004043023.1	HVO_2777	30S ribosomal protein S9	J	30462450
WP_004043051.1	HVO_2809	succinate dehydrogenase	C	29269166.67
ADE03416.1	HVO_0455	thermosome subunit 2	O	29073750
WP_004043025.1	HVO_2779	50S ribosomal protein L18e	J	28744958.33
WP_004044124.1	HVO_0812	phosphoenolpyruvate synthase	G	28414416.67
WP_004043020.1	HVO_2774	phosphopyruvate hydratase	G	28308416.67
ELY35097.1	HVO_1831	(2Fe-2S)-binding protein	C	28054916.67
WP_004045034.1	HVO_0035	stomatin-prohibitin-like protein	O	27175008.33
WP_004041551.1	HVO_1660	diadenylate cyclase	T	26918100
WP_004044199.1	HVO_0738	hypothetical protein	S	26736358.33
WP_004041869.1	HVO_1987	proteinase IV-like protein	O	26277833.33
WP_004044046.1	HVO_0892	copper ABC transporter substrate-binding protein	P	25836750
WP_004043003.1	HVO_2757	50S ribosomal protein L1	J	25807991.67
ELY32386.1	HVO_2798	branched-chain amino acid ABC transporter substrate-binding protein	E	25799091.67
WP_004040809.1	HVO_A0451	SLC13 family permease	P	25789833.33
WP_004041022.1	HVO_B0134	multidrug ABC transporter ATP-binding protein	V	25433166.67
WP_004044112.1	HVO_0824	glycosyl transferase family 1	M	25370583.33
ADE04124.1	HVO_2694	ABC transporter permease	G	25270583.33
WP_004042606.1	HVO_2558	30S ribosomal protein S3	J	24955250
WP_004041855.1	HVO_1976	preprotein translocase subunit SecD	U	24640066.67
WP_004044369.1	HVO_0564	sugar ABC transporter substrate-binding protein	G	24597491.67

WP_004042269.1	HVO_2380	ATPase	O	24353058.33
WP_004041795.1	HVO_1916	potassium transporter	P	24221833.33
WP_004042128.1	HVO_2239	universal stress protein UspA	T	24079500
WP_004042456.1	HVO_2495	HTR-like protein	U	24045333.33
WP_004044000.1	HVO_0945	cytochrome c oxidase subunit I	C	23405016.67
ADE01809.1	HVO_A0380	peptide ABC transporter substrate-binding protein	E	23181666.67
WP_004044610.1	HVO_0313	ATP synthase subunit E	C	23043750
WP_004044608.1	HVO_0315	ATP synthase subunit F	C	23024950
WP_004041430.1	HVO_1552	transcriptional regulator	K	22926416.67
WP_004041457.1	HVO_1577	TrmB family transcriptional regulator	K	22646100
WP_004043924.1	HVO_1018	hypothetical protein	L	22522083.33
ADE02701.1	HVO_0002	S26 family signal peptidase	U	22341425
WP_013035666.1	HVO_1145	30S ribosomal protein S3ae	J	22193083.33
WP_004044154.1	HVO_0783	ATP-dependent protease LonB	O	22164691.67
WP_004045088.1	HVO_0060	peptide ABC transporter permease	E	22113841.67
WP_004043776.1	HVO_1165	mechanosensitive ion channel protein	M	22048833.33
WP_004042753.1	HVO_2636	phage shock protein A	K	21989933.33
WP_004044047.1	HVO_0891	copper ABC transporter ATP-binding protein	V	21850308.33
WP_004043948.1	HVO_0995	hypothetical protein	S	21844333.33
WP_004043454.1	HVO_1481	universal stress protein UspA	T	21789808.33
WP_004042597.1	HVO_2554	50S ribosomal protein L14	J	21527750
WP_004041953.1	HVO_2068	CetZ6	D	21432050
WP_004045245.1	HVO_0133	thermosome subunit 1	O	21213791.67
WP_004041077.1	HVO_B0078	ABC transporter ATP-binding protein	E	21137000
WP_144064030.1	HVO_A0432	hypothetical protein	S	20756375
WP_004042381.1	HVO_2464	succinate--CoA ligase subunit alpha	C	20264341.67
WP_004045086.1	HVO_0059	ABC transporter ATP-binding protein	E	20092825
WP_004043637.1	HVO_1300	triose-phosphate isomerase	G	19776300
WP_004042618.1	HVO_2564	50S ribosomal protein L3	J	19215650
ADE05264.1	HVO_C0075	peptide ABC transporter substrate-binding protein	E	19056066.67
WP_004042573.1	HVO_2547	50S ribosomal protein L32e	J	18948841.67
WP_004042875.1	HVO_2693	sugar ABC transporter permease	G	18761383.33
WP_004040858.1	HVO_A0507	phenylacetate-CoA oxygenase subunit PaaA	Q	18537941.67
WP_004041580.1	HVO_1691	photosystem reaction center subunit H	R	18497366.67
WP_004044095.1	HVO_0841	cytochrome b	C	18470575
WP_004044001.1	HVO_0944	cytochrome c oxidase subunit II	C	18270958.33
WP_004043019.1	HVO_2773	30S ribosomal protein S2	J	18228441.67
WP_004042966.1	HVO_2738	30S ribosomal protein S28e	J	18186433.33
WP_004042131.1	HVO_2242	translation initiation factor IF-2	J	18166000
WP_004041975.1	HVO_2091	aspartate aminotransferase family protein	E	18143916.67
WP_004044078.1	HVO_0859	ABC transporter ATP-binding protein	O	17953083.33
WP_004041932.1	HVO_2046	N-acetylgalactosamine-6-sulfatase	P	17809600

WP_004064311.1	HVO_0850	peptidase	O	17737916.67
WP_004044927.1	HVO_3008	hypothetical protein	R	17727791.67
WP_004041423.1	HVO_1545	dihydroxyacetone kinase subunit L	G	17681733.33
WP_004040981.1	HVO_A0627	hypothetical protein	P	17367316.67
WP_004041740.1	HVO_1858	30S ribosomal protein S19e	J	17120225
WP_004043699.1	HVO_1242	Tat pathway signal protein	C	17084983.33
WP_004043682.1	HVO_1257	ATPase AAA	N	16765250
ADE03135.1	HVO_0311	ATP synthase subunit I	C	16720833.33
WP_004041049.1	HVO_B0106	sugar ABC transporter substrate-binding protein	G	16483883.33
WP_004044194.1	HVO_0743	nucleotide pyrophosphatase	R	16282591.67
WP_004041515.1	HVO_1625	hypothetical protein	S	16271933.33
WP_004045343.1	HVO_0229	hypothetical protein	S	16246783.33
WP_004043565.1	HVO_1374	long-chain-fatty-acid--CoA ligase	I	15530383.33
WP_004042558.1	HVO_2541	preprotein translocase subunit SecY	U	15436658.33
WP_004044044.1	HVO_0894	acetyl-coenzyme A synthetase	I	15366900
WP_004041075.1	HVO_B0080	cytochrome c550	E	15273000
WP_004040849.1	HVO_A0496	universal stress protein UspA	T	15269000
WP_004042565.1	HVO_2544	30S ribosomal protein S5	J	15204441.67
WP_004040978.1	HVO_A0624	cadmium-translocating P-type ATPase	P	15062450
WP_004041594.1	HVO_1705	iron ABC transporter substrate-binding protein	P	15044016.67
WP_004042007.1	HVO_2123	ABC transporter ATP-binding protein	E	14928475
WP_004044742.1	HVO_2916	short-chain dehydrogenase	I	14903366.67
WP_004042874.1	HVO_2692	ABC transporter ATP-binding protein	E	14366500
WP_004042039.1	HVO_2156	universal stress protein UspA	T	14292958.33
WP_004042029.1	HVO_2147	cytochrome b	P	14275358.33
WP_004042991.1	HVO_2749	50S ribosomal protein L21e	J	14201125
WP_004044616.1	HVO_0307	hypothetical protein	N	14180100
WP_004042593.1	HVO_2553	50S ribosomal protein L24	J	14130516.67
WP_004043730.1	HVO_1212	circadian clock protein KaiC	T	14078991.67
WP_004044258.1	HVO_0677	aspartate--tRNA(Asn) ligase	J	14054716.67
WP_004044390.1	HVO_0541	aconitate hydratase	C	13571091.67
WP_004043752.1	HVO_1189	hypothetical protein	C	13262408.33
ADE04716.1	HVO_1375	2-succinylbenzoate-CoA ligase	I	13207216.67
WP_004042226.1	HVO_2336	pyridoxal 5'-phosphate synthase lyase subunit PdxS	H	13099716.67
ELY26379.1	HVO_0758	small zinc finger protein	S	13042808.33
WP_004044487.1	HVO_0437	preprotein translocase subunit Sec61beta	U	12917000
WP_004045193.1	HVO_0104	DNA repair and recombination protein RadA	L	12746358.33
WP_004043944.1	HVO_0999	hypothetical protein	R	12691216.67
WP_004044756.1	HVO_2923	proteasome subunit alpha	O	12478608.33
WP_004041586.1	HVO_1697	FAD-dependent oxidoreductase	C	12386481.67
WP_004041074.1	HVO_B0081	peptide ABC transporter	E	12385883.33
WP_004042193.1	HVO_2300	translation initiation factor IF-5A	J	12355566.67

WP_004042571.1	HVO_2546	50S ribosomal protein L19e	J	12232050
WP_004042017.1	HVO_2135	hypothetical protein	C	12115850
WP_004041954.1	HVO_2069	RND transporter	R	11927825
WP_004044296.1	HVO_0639	ATPase AAA	N	11880575
WP_013035311.1	HVO_0627	ABC transporter ATP-binding protein	E	11783383.33
WP_004043943.1	HVO_1000	acetyl-CoA synthetase	C	11730966.67
WP_004041717.1	HVO_1827	30S ribosomal protein S6e	J	11710650
WP_004042255.1	HVO_2366	universal stress protein UspA	T	11682091.67
WP_004045195.1	HVO_0105	pyridine nucleotide-disulfide oxidoreductase	R	11678741.67
WP_004043562.1	HVO_1377	hypothetical protein	P	11578916.67
WP_004042733.1	HVO_2625	GMP synthase	F	11563216.67
WP_004043002.1	HVO_2756	50S ribosomal protein L10	J	11378808.33
WP_004042267.1	HVO_2378	phosphate ABC transporter ATP-binding protein	P	11346550
WP_004042563.1	HVO_2543	50S ribosomal protein L30	J	11231741.67
WP_004043525.1	HVO_1413	NADH dehydrogenase	C	11024625
WP_004041419.1	HVO_1541	glycerol kinase	C	10979941.67
WP_004041753.1	HVO_1871	hypothetical protein	R	10953058.33
WP_004044914.1	HVO_3002	copper ABC transporter ATP-binding protein	V	10916716.67
WP_004043024.1	HVO_2778	50S ribosomal protein L13	J	10792741.67
WP_004042115.1	HVO_2226	anthranilate phosphoribosyltransferase	E	10679858.33
WP_004045083.1	HVO_0058	peptide ABC transporter ATP-binding protein	E	10229616.67
WP_004041752.1	HVO_1870	metalloprotease	O	10050241.67
WP_004043675.1	HVO_1264	membrane protein	S	9991333.333
WP_004041777.1	HVO_1896	30S ribosomal protein S24e	J	9949441.667
WP_004044036.1	HVO_0903	ABC transporter ATP-binding protein	E	9930658.333
WP_004044267.1	HVO_0668	TPP-dependent acetoin dehydrogenase complex, E1 protein subunit beta	C	9852350
WP_004044050.1	HVO_0888	oxoglutarate--ferredoxin oxidoreductase	C	9811483.333
WP_004044479.1	HVO_0445	phosphonate ABC transporter, permease protein PhnE	P	9675883.333
WP_004043807.1	HVO_1130	hypothetical protein	S	9624825
WP_004042436.1	HVO_2486	carbamoyl phosphate synthase	I	9595975
WP_004043962.1	HVO_0981	NADH dehydrogenase	C	9066641.667
WP_004044100.1	HVO_0836	peptidase M28	O	8891841.667
WP_004044162.1	HVO_0775	amidohydrolase	R	8823125
WP_004045089.1	HVO_0061	peptide ABC transporter permease	E	8550916.667
WP_004042612.1	HVO_2561	50S ribosomal protein L2	J	8536741.667
WP_004043027.1	HVO_2782	30S ribosomal protein S11	J	8521141.667
WP_004043279.1	HVO_A0378	N-methylhydantoinase	E	8354991.667
WP_004044695.1	HVO_2879	ornithine cyclodeaminase	E	8198000
WP_004043974.1	HVO_0970	type III ribulose-bisphosphate carboxylase	G	8074433.333
WP_004044129.1	HVO_0807	hypothetical protein	S	8058033.333
ELY26169.1	HVO_0570	ATP-binding protein	T	7832200
WP_049914885.1	HVO_0954	hypothetical protein	S	7781800

WP_004044061.1	HVO_0876	methylglyoxal synthase	G	7768783.333
WP_004044397.1	HVO_0534	ABC transporter ATP-binding protein	E	7768341.667
WP_004043936.1	HVO_1007	PQQ-dependent glucose dehydrogenase	G	7730300
WP_004044440.1	HVO_0481	type I glyceraldehyde-3-phosphate dehydrogenase	E	7583883.333
ELY23357.1	HVO_0250	DNA-binding protein	R	7171316.667
WP_004043667.1	HVO_1271	DNA-binding protein	T	6880141.667
WP_004044456.1	HVO_0466	citrate (Si)-synthase	C	6862000
WP_004040921.1	HVO_A0562	urocanate hydratase	E	6853891.667
WP_004043851.1	HVO_1087	universal stress protein	T	6847083.333
WP_004042048.1	HVO_2163	ABC transporter ATP-binding protein	V	6445900
WP_004044168.1	HVO_0769	deoxyribonuclease	O	6335925
WP_004041799.1	HVO_1920	sodium-dependent transporter	P	6333350
WP_004040973.1	HVO_A0619	hypothetical protein	S	6317175
WP_004044159.1	HVO_0778	thermosome subunit 3	O	6257008.333
WP_004041447.1	HVO_1568	alpha/beta hydrolase	R	6235475
WP_004044911.1	HVO_3001	ABC transporter permease	O	6207975.833
WP_004045354.1	HVO_0239	glutamine synthetase	E	6172750
WP_004044048.1	HVO_0890	copper ABC transporter permease	R	6083425
WP_004041895.1	HVO_2011	hypothetical protein	S	6044850
WP_004044130.1	HVO_0806	pyruvate kinase	G	6002066.667
WP_004041076.1	HVO_B0079	ABC transporter ATP-binding protein	E	5995800
WP_004041905.1	HVO_2020	hypothetical protein	S	5993908.333
WP_004042060.1	HVO_2168	ATPase	N	5733708.333
WP_004042217.1	HVO_2325	amphi-Trp domain-containing protein	S	5713025
WP_004044305.1	HVO_0630	peptide ABC transporter permease	E	5581075
WP_004043957.1	HVO_0986	NADH-quinone oxidoreductase subunit L	C	5362200
ADE03394.1	HVO_1914	acetyl-CoA acetyltransferase	I	5338408.333
WP_004044614.1	HVO_0309	SAM-dependent methyltransferase	Q	5122358.333
WP_004044522.1	HVO_0401	universal stress protein	T	4988608.333
WP_004042886.1	HVO_2700	ATPase AAA	O	4858058.333
WP_004041410.1	HVO_1532	DUF368 domain-containing protein	S	4834008.333
WP_004044925.1	HVO_3007	malate dehydrogenase	C	4767800
WP_004042383.1	HVO_2465	succinate--CoA ligase subunit beta	C	4420350
WP_004041159.1	HVO_B0376	aryl-alcohol dehydrogenase	C	4285400
WP_004042968.1	HVO_2739	50S ribosomal protein L24e	J	4050341.667
WP_004043540.1	HVO_1398	ABC transporter permease	R	3902025
WP_004041469.1	HVO_1585	acetyl-CoA synthetase	I	3720783.333
ADE03884.1	HVO_0773	N-methyltransferase-like protein	Q	3606416.667
WP_004043985.1	HVO_0960	oxidoreductase	R	3525416.667
ADE01771.1	HVO_A0379	N-methylhydantoinase	E	3380326.667
WP_004044667.1	HVO_2849	serine protein kinase PrkA	T	3176219.167
WP_004044896.1	HVO_2993	peptidase A24	N	3115016.667

WP_004044617.1	HVO_0306	hypothetical protein	K	2949383.333
WP_004043481.1	HVO_1454	aspartate carbamoyltransferase	F	2267472.5
WP_004044491.1	HVO_0433	NADPH-dependent F420 reductase	R	1905196.667
ELY36918.1	HVO_B0292	ABC transporter substrate-binding protein	G	1672920
WP_004044574.1	HVO_0349	DNA-directed RNA polymerase subunit A'	K	760651.6667

Supplementary Table 11: Mass spectrometry peak areas and relative abundances of lipid compounds extracted from whole cells, cell membranes and EVs of *H. volcanii*. Intact polar lipids were extracted from whole cells, cell membranes and vesicles of *H. volcanii* and measured with a Q-TOF MS (Bruker Daltonics). Output data were analyzed with the manufacturer's software (DataAnalysis 4.4.2, Bruker Daltonics) and lipid compounds were identified based on retention time, fractionation pattern and exact masses and quantified via mass spectrometry peak area.

(Excel file can be viewed at https://www.biorxiv.org/content/10.1101/2023.03.03.530948v1 as Supplementary Table 11)

Supplementary Table 12: Taxonomy of Archaea identified to contain archaeal vesiculating GTPase, ArcV. 1,666 archaeal organisms out of 78,738 archaeal and bacterial genomes were identified to contain an ArcV homolog (see Methods). Taxonomy listed according to genome taxonomy database release (r207). (Excel file available upon request)

SUPPLEMENTARY REFERENCES

1. Mills J, Erdmann S (2022) Isolation, Purification, and Characterization of Membrane Vesicles from Haloarchaea. Methods Mol Biol 2522:435–448. https://doi.org/10.1007/978-1-0716-2445-6_30
2. Witte A, Baranyi U, Klein R et al. (1997) Characterization of Natronobacterium magadii phage ΦCh1, a unique archaeal phage containing DNA and RNA. Mol Microbiol 23:603–616
3. Duggin IG, Aylett CHS, Walsh JC et al. (2015) CetZ tubulin-like proteins control archaeal cell shape. Nature 519:362–365. https://doi.org/10.1038/nature13983
4. Adams PP, Flores Avile C, Popitsch N et al. (2017) In vivo expression technology and 5' end mapping of the Borrelia burgdorferi transcriptome identify novel RNAs expressed during mammalian infection. Nucleic Acids Res 45:775–792. https://doi.org/10.1093/nar/gkw1180
5. Haque RU, Paradisi F, Allers T (2020) Haloferax volcanii for biotechnology applications: challenges, current state and perspectives. Appl Microbiol Biotechnol 104:1371–1382. https://doi.org/10.1007/s00253-019-10314-2
6. Gamble-Milner R Genetic analysis of the Hel308 helicase in the archaeon Haloferax volcanii
7. Dyall-Smith, Michael (2009) The Halohandbook: Protocols for haloarchaeal genetics
8. Giavalisco P, Li Y, Matthes A et al. (2011) Elemental formula annotation of polar and lipophilic metabolites using (13) C, (15) N and (34) S isotope labelling, in combination with high-resolution mass spectrometry. Plant J 68:364–376. https://doi.org/10.1111/j.1365-313X.2011.04682.x
9. Wörmer L, Lipp JS, Schröder JM et al. (2013) Application of two new LC–ESI–MS methods for improved detection of intact polar lipids (IPLs) in environmental samples. Organic Geochemistry 59:10–21. https://doi.org/10.1016/j.orggeochem.2013.03.004

10. Bale NJ, Sorokin DY, Hopmans EC et al. (2019) New Insights Into the Polar Lipid Composition of Extremely Halo(alkali)philic Euryarchaea From Hypersaline Lakes. Front Microbiol 10:377. https://doi.org/10.3389/fmicb.2019.00377

11. Kellermann MY, Yoshinaga MY, Valentine RC et al. (2016) Important roles for membrane lipids in haloarchaeal bioenergetics. Biochim Biophys Acta 1858:2940–2956. https://doi.org/10.1016/j.bbamem.2016.08.010

12. Yoshinaga MY, Kellermann MY, Rossel PE et al. (2011) Systematic fragmentation patterns of archaeal intact polar lipids by high-performance liquid chromatography/electrospray ionization ion-trap mass spectrometry. Rapid Commun Mass Spectrom 25:3563–3574. https://doi.org/10.1002/rcm.5251

13. Wickham H (2009) ggplot2: Elegant graphics for data analysis / by Hadley Wickham. Use R! Springer, New York, London

14. Wickham H (2011) The Split-Apply-Combine Strategy for Data Analysis. Journal of Statistical Software 40

15. Wickham H, François R, Henry L, Müller K (2022) dplyr: A Grammar of Data Manipulation

16. Delmas S, Duggin IG, Allers T (2013) DNA damage induces nucleoid compaction via the Mre11-Rad50 complex in the archaeon Haloferax volcanii. Mol Microbiol 87:168–179. https://doi.org/10.1111/mmi.12091

17. Manning AJ, Kuehn MJ (2011) Contribution of bacterial outer membrane vesicles to innate bacterial defense. BMC Microbiol 11:258. https://doi.org/10.1186/1471-2180-11-258

18. Martins SdT, Alves LR (2020) Extracellular Vesicles in Viral Infections: Two Sides of the Same Coin? Front Cell Infect Microbiol 10:593170. https://doi.org/10.3389/fcimb.2020.593170

19. Alarcón-Schumacher T, Naor A, Gophna U et al. (2022) Isolation of a virus causing a chronic infection in the archaeal model organism Haloferax volcanii reveals antiviral activities of a provirus. Proc Natl Acad Sci U S A 119:e2205037119. https://doi.org/10.1073/pnas.2205037119

20. Bernadac A, Gavioli M, Lazzaroni J-C et al. (1998) Escherichia coli tol-pal Mutants Form Outer Membrane Vesicles. Journal of Bacteriology 180:4872–4878

21. McBroom AJ, Johnson AP, Vemulapalli S et al. (2006) Outer membrane vesicle production by Escherichia coli is independent of membrane instability. Journal of Bacteriology 188:5385–5392. https://doi.org/10.1128/JB.00498-06

22. Abu-Qarn M, Yurist-Doutsch S, Giordano A et al. (2007) Haloferax volcanii AglB and AglD are involved in N-glycosylation of the S-layer glycoprotein and proper assembly of the surface layer. J Mol Biol 374:1224–1236. https://doi.org/10.1016/j.jmb.2007.10.042

23. Dawson KS, Freeman KH, Macalady JL (2012) Molecular characterization of core lipids from halophilic archaea grown under different salinity conditions. Organic Geochemistry 48:1–8. https://doi.org/10.1016/j.orggeochem.2012.04.003

24. Sprott GD, Larocque S, Cadotte N et al. (2003) Novel polar lipids of halophilic eubacterium Planococcus H8 and archaeon Haloferax volcanii. Biochim Biophys Acta 1633:179–188. https://doi.org/10.1016/j.bbalip.2003.08.001

25. Mileykovskaya E, Dowhan W (2009) Cardiolipin membrane domains in prokaryotes and eukaryotes. Biochim Biophys Acta 1788:2084–2091. https://doi.org/10.1016/j.bbamem.2009.04.003

26. Raden M, Ali SM, Alkhnbashi OS et al. (2018) Freiburg RNA tools: a central online resource for RNA-focused research and teaching. Nucleic Acids Res 46:W25-W29. https://doi.org/10.1093/nar/gky329

27. Will S, Joshi T, Hofacker IL et al. (2012) LocARNA-P: accurate boundary prediction and improved detection of structural RNAs. RNA 18:900–914. https://doi.org/10.1261/rna.029041.111

28. Will S, Reiche K, Hofacker IL et al. (2007) Inferring noncoding RNA families and classes by means of genome-scale structure-based clustering. PLoS Comput Biol 3:e65. https://doi.org/10.1371/journal.pcbi.0030065

29. Harrison KJ, Crécy-Lagard V de, Zallot R (2018) Gene Graphics: a genomic neighborhood data visualization web application. Bioinformatics 34:1406–1408. https://doi.org/10.1093/bioinformatics/btx793

30. Hartman AL, Norais C, Badger JH et al. (2010) The complete genome sequence of Haloferax volcanii DS2, a model archaeon. PLoS One 5:e9605. https://doi.org/10.1371/journal.pone.0009605

31. Allers T, Ngo H-P, Mevarech M et al. (2004) Development of additional selectable markers for the halophilic archaeon Haloferax volcanii based on the leuB and trpA genes. Appl Environ Microbiol 70:943–953. https://doi.org/10.1128/AEM.70.2.943-953.2004

32. Wolters M, Borst A, Pfeiffer F et al. (2019) Bioinformatic and genetic characterization of three genes localized adjacent to the major replication origin of Haloferax volcanii. FEMS Microbiol Lett 366. https://doi.org/10.1093/femsle/fnz238

33. Ng WV, Kennedy SP, Mahairas GG et al. (2000) Genome sequence of Halobacterium species NRC-1. Proc Natl Acad Sci U S A 97:12176–12181. https://doi.org/10.1073/pnas.190337797

34. Erdmann S, Tschitschko B, Zhong L et al. (2017) A plasmid from an Antarctic haloarchaeon uses specialized membrane vesicles to disseminate and infect plasmid-free cells. Nat Microbiol 2:1446–1455. https://doi.org/10.1038/s41564-017-0009-2

35. Arne Smits , Wolfgang Huber (2017) DEP. Bioconductor

CHAPTER IV.

The Regulatory Impact of Archaeal Extracellular Vesicles on Microbe-Microbe Interactions

Joshua Mills[1] and Susanne Erdmann[1]

[1]Max Planck Institute for Marine Microbiology, Archaeal Virology, Celsiusstrasse 1, 28359, Bremen, Germany

*manuscript is in preparation

Author contributions: J.M. and S.E. conceived the study, J.M. performed the majority of the experimental work, the analysis, and drafted the manuscript with support from S.E. S.E. led the study.

ABSTRACT

Extracellular vesicles (EV) that enclose RNA are known to be produced by organisms in all three domains. However, the impact of prokaryotic EV-associated RNA on microbial community dynamics remains unresolved. Here we explore the EV-associated transcriptome of the halophilic archaeon, *Halorubrum lacusprofundi* ACAM34_UNSW, and how these exported transcripts are able to influence gene expression. We determine that intracellular and EV-associated transcriptomes represent distinct subpopulations, which change upon the introduction of viral stress. EVs are demonstrated to export specific RNAs with regulatory potential, dependent on the growth conditions. We also observe small transcriptomic changes in response to EV exposure, suggesting that the EVs are able to induce gradual changes to specific gene expression. Though many questions remain about how haloarchaea are able to utilize this mechanism to influence each other or other organisms, the work presented here provides a starting point into decrypting the nature of EV-mediated cross-talk among prokaryotic organisms.

INTRODUCTION

Extracellular vesicles (EV) are nanoscale, membrane-bound structures that derive from the cellular envelope, and have been observed in all three domains of life [1, 2]. They are able to contain various compounds including DNA, RNA, proteins and signaling molecules, export them into the extracellular milieu and potentially deliver them to a recipient cell [3]. This form of intercellular transport provides specific advantages for the communication of signaling compounds, such as providing protection from environmental factors that may degrade the cargo [2]. This is especially relevant for the trafficking of RNA, as RNases in the extracellular space are ubiquitous and quickly eliminate extracellular RNA [4].

The EV-mediated transport of RNA has been observed in both bacterial [5] and archaeal [6, 7] organisms, though investigations into the function of prokaryotic EV-associated RNA is still ongoing. Bacterial and archaeal EV-associated RNA have been demonstrated to derive from all RNA functional classes: messenger RNA (mRNA), ribosomal RNA (rRNA), transfer RNA (tRNA) and noncoding RNA (ncRNA). Here we define ncRNA as transcripts that do not contain an open reading frame, including small RNA (sRNA), but excluding rRNA and tRNA. sRNA are transcripts that are generally smaller than 250 nucleotides and are able to regulate mRNA translation through imperfect base-pairing [8, 9]. The RNA population, including sRNA, that is exported in EVs has been shown to be dependent on environmental stress in both the bacterial organism, *Staphylococcus aureus* [10], and the archaeal organism, *Haloferax volcanii* [6]. Therefore, it is speculated that the conditionally-dependent trafficking of sRNA though EVs are able to alter gene expression of the recipient organism [4].

There are several recent examples of this type of interaction between bacterial and eukaryotic organisms [11]. For example, during the colonization of the squid, *Euprymna scolopes*, by its symbiont, *Vibrio fischeri*, downregulation of host immune response genes was triggered by the transfer of a *V. fischeri*-encoded sRNA through EVs [12]. In another study, EV-associated sRNAs from *Legionella pneumophilia* were similarly shown to downregulate the expression of key defense signaling genes in human cells [13]. In both cases, EV-associated RNA was shown to be internalized by the host organism and consequentially alter gene expression of the host. Therefore, it is suggested that EV-mediated

RNA "cross talk" represents a common mechanism deployed in inter-domain communication and likely plays a key role in pathogenesis [4]. However, this mechanism of intercellular communication between microbial organisms and to what extent they drive microbial population dynamics has not been investigated.

Here, we investigate the role of EV-mediated transport of RNA in hypersaline environments using the halophilic archaeaon (haloarchaeaon) *Halorubrum lacusprofundi* ACAM34. Using the lytic virus, HRTV-DL1 [14], we show that viral stress induces a shift in the subpopulation of exported RNA, including ncRNA with regulatory potential. We also investigate cells after exposure to EVs and observe gradual changes in the transcriptome. Therefore, we propose that EVs of haloarchaea can alter gene expression in recipient organisms in a condition-dependent manner.

METHODS

Strains and growth conditions

Halorubrum lacusprofundi strain ACAM34_UNSW [14] ΔpyrE2 [15] was grown in DBCM2+ media [16] supplemented with 50 µg/mL uracil at 28 °C in glass flasks aerobically (120 rpm).

Isolation and purification of extracellular vesicles

EV isolation and purification was adapted from Mills and Erdmann 2022 [17]. ACAM34_UNSW ΔpyrE2 was grown in triplicate with serial dilution (two times in exponential growth with starting OD_{600} = 0.05) before being transferred to 500 mL media with starting OD_{600} = 0.05. HRTV-DL1 at a virus:host ratio of 0.01:1 was added directly to cultures and they were grown as stated above. After ~50 hours of growth (OD_{600} between 0.7 and 1), cultures were centrifuged (4,500 x *g*, 30 min, RT) to pellet cells. EVs were precipitated from the supernatant with the addition of polyethylene glycol (PEG) 6000 at a final concentration of 10% at 4 °C overnight. EVs were pelleted through centrifugation (14,000 x *g*, 50 min, 4 °C) and pellets resuspended in DBCM2 salt solution [16]. Remaining cellular contaminations were removed by additional centrifugation (14,000 x *g*, 10 min, RT) and filtration (0.45 µm and 0.2 µm). Samples were treated with DNase I (New England Biolabs, 20 U/mL) and RNase A (New England Biolabs, 20 U/mL) for 2 hours at 37 °C with supplemented $CaCl_2$ (final concentration 1 mM) and with intermittent mixing to remove extracellular nucleic acids. EVs were precipitated with PEG 6000 as described above and purified further with either a CsCl density gradient (0.5 g/mL CsCl, 38,000 x *g*, 4 °C, 20 hours) or Optiprep™ density gradient as described previously [6]. EV band was extracted from the CsCl gradient. EVs were precipitated with PEG 6000, resuspended in 150 µL DBCM2 salt solution, and stored at 4 °C. Presence of viral contamination in the EV preparation was determined by plaque assay, which confirmed the absence of active viral particles. Methods for transmission electron microscopy of purified EVs was the same as previously described [6].

EV treatment of cells

ACAM34_UNSW was grown after serial dilution (two times in exponential growth with starting OD_{600} = 0.05) until exponential phase (OD_{600} ~1). Each culture was concentrated to three 1 mL aliquots in media. 125 µL of either DBCM2 salt solution, EV preparations from uninfected cultures, or EV preparations from infected cultures was mixed with the cells in three replicates. Samples were incubated for 2 hours at 28 °C with intermittent shaking. 200 µL of the sample

was removed, centrifuged to pellet cells (14,000 x *g*, 2 min, RT), washed twice with DBCM2 salt solution to remove excess EVs, and final cell pellet used for RNA extraction and subsequent transcriptomic analysis.

Each of the three EV-cell mixtures and the control (only cells) was subsequently split into 2 x 400 µL, and each was used to inoculate 2 x 50 mL of media with starting OD_{600} = 0.05 (total of 18 cultures). HRTV-DL1 was added to nine of the cultures (3 x control, 3 x cells mixed with EVs uninfected, 3 x cells mixed with EV infected) at a virus:host ratio of 1000:1, while the others remained uninfected to serve as the control. Growth was monitored over the course of 5 days post-infection. Cells were harvested as described above after 12 hours of growth.

RNA extraction and transcriptomic analysis

RNA extraction was performed using TRIzol™ (Thermo Fischer Scientific) [18] as described previously [6]. Total RNA libraries (NEBNext® Ultra™ II RNA Library Prep Kit for Illumina) and Small RNA libraries (RealSeq®-AC miRNA Library Kit) were prepared and sequenced (1x 150bp, 1 Gb per sample) at the Max Planck-Genome-Center (Cologne, Germany). Samples prepared with Total RNA libraries were rRNA depleted (Pan-Prokaryote riboPOOLkit, siTOOLs).

Read mapping and differential expression analysis were conducted using Geneious Prime® (2021.0.1). Reads were mapped to the *Hrr. lacusprofundi* ACAM34_UNSW genome using the Geneious RNA mapper, with trimmed paired read overhangs and minimum overlap identity of 80%. Differential expression analysis of EVs and cells from infected and uninfected cultures was conducted with DESeq2 mostly in triplicates. One replicate of cellular RNA (uninfected cultures) and one replicate of EV-associated RNA (infected cultures) were removed after failing quality control.

Prediction of potential mRNA targets of enriched ncRNA was conducted using IntaRNA (3.3.1) [19–22] against the genome of *Hrr. lacusprofundi* ATCC 49239 (GCF_000022205.1), with search region limited to 50 bp before and after the start codon.

RESULTS

Extracellular vesicles of Hrr. lacusprofundi ACAM34_UNSW are enriched with small RNAs

Hrr. lacusprofundi was cultivated and assessed for EV production during exponential growth (OD_{600} ~ 0.7) under standard conditions. EV-like particles were observed in the cell-free supernatant between 50 and 80 nm in diameter (Figure 1). Similar to EVs from other Archaea [7, 23, 24], the surface of *Hrr. lacusprofundi* EVs appeared decorated with a protein-like layer that we assume to be the host-derived S-layer.

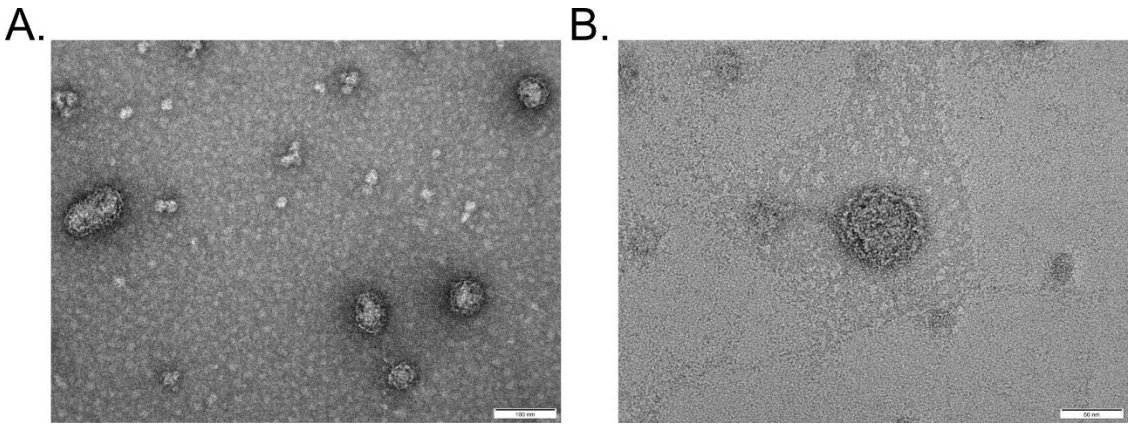

Figure 1. Transmission electron micrographs of *Hrr. lacusprofundi* ACAM34_UNSW EVs. Scale bar is 100 nm in **(A)**, and 50 nm in **(B)**.

In order to identify the RNA population exported by *Hrr. lacusprofundi* EVs, RNA was isolated from EVs and their respective cells. In a previous study, we determined that sequencing of haloarchaeal EVs only provided a comprehensive profile of EV-associated RNA when using small RNA libraries, because haloarchaeal EVs were found to be enriched in smaller transcripts [6]. The RNA content of *Hrr. lacusprofundi* appeared to be enriched in smaller transcripts as well (Figure 2A); therefore, we used the same approach. For EV-associated reads, only 39 ± 13% of the genome was covered with at least one read (73 ± 4% for intracellular reads). 3,129 genes were identified to be associated with EVs, representing nearly all genes in the *Hrr. lacusprofundi* genome (Supplementary Table 1). However, the majority of EV-associated genes were present with transcripts per million (TPM) lower than 10, which we consider transcriptional noise. Only 463 of EV-associated genes were identified with TPM greater than 10. Ribosomal RNAs (rRNA) constituted the majority of reads of EV-associated RNA (52%) followed by transfer RNAs (tRNA), noncoding RNAs (ncRNA) and messenger RNAs (mRNA) (29%, 13% and 6% respectively). This distribution of different RNA types did not reflect intracellular levels (Figure 2B), similar to what has been observed for other haloarchaeal EV-associated RNA [6]. Surprisingly, unlike in *H. volcanii* and *Hbt. salinarum* [6], none of the two S-layer mRNAs (ACAM34UNSW_01892 and ACAM34UNSW_01982) were identified as one of the most abundant EV-associated transcripts. The transcripts with the highest abundance in EVs were mostly rRNA subunits, tRNAs, and ncRNAs. The ncRNAs included both intergenic RNAs and antisense RNAs (asRNA).

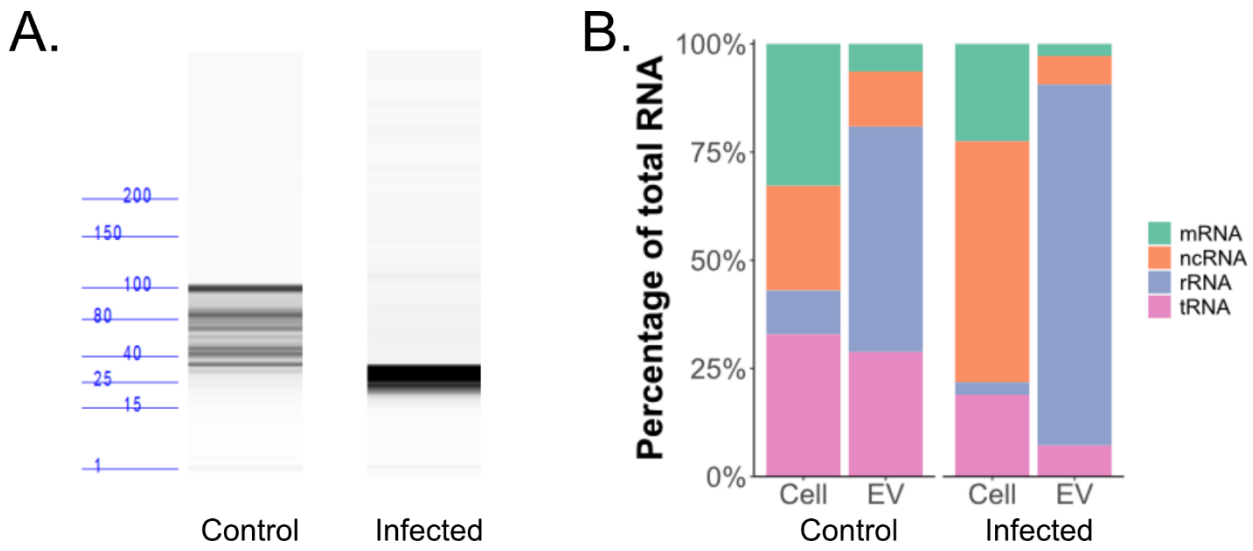

Figure 2. RNA content of *Hrr. lacusprofundi* EVs. (A) Analysis of the size distribution of EV-associated RNA from cultures uninfected and infected with HRTV-DL1, measured by Fragment analyzer. **(B)** Expression of RNA functional groups in cells and EVs from cultures uninfected or infected with HRTV-DL1. Expression levels were calculated as percentage of total transcripts per million (TPM), and averaged over the replicates.

Differential expression analysis revealed 169 genes that were enriched (TPM > 10, log2 > 1, adjusted p-value < 0.05) in EVs with respect to intracellular levels (Figure 3A, Supplemental Table 2). We also identified 11 ncRNAs to be enriched in EVs, including RNase P and the 7S subunit of the signal recognition particle (Table 1). We found two of the ncRNAs to be asRNAs that derived from the 5' end of IS6-like transposases (asRNA1 and asRNA2). Small RNAs antisense to transposases similar to what had already been observed in EV-associated RNA from *H. volcanii* [6]. Interestingly, ncRNA2 was identified to contain a small 123 base pair open reading frame (ORF) with no predicted function. We predicted mRNA targets for the EV-enriched ncRNA and identified 14 statistically significant matches (p-value < 0.05, false detection rate < 0.5) (Supplementary Table 3). As expected, both asRNAs were only predicted to target IS6 family or IS6-like transposases. The small ORF-containing ncRNA2 was predicted to interact with 4 mRNA, including a CinA family protein. The same CinA family protein was also the only predicted target of ncRNA1, both sharing the same predicted region of interaction on the mRNA. Only one target was predicted for ncRNA3, a 129 aa hypothetical protein of unknown function.

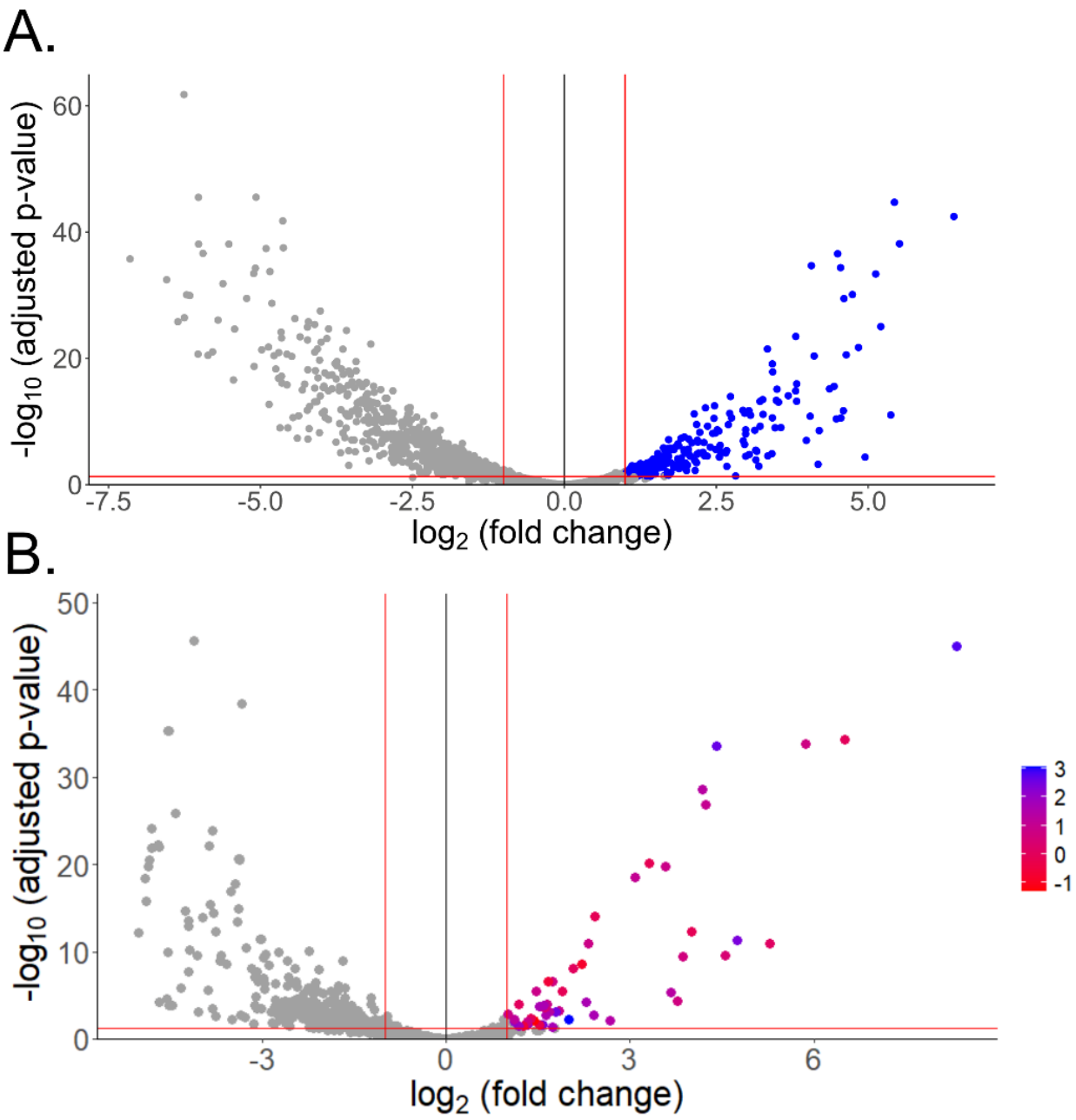

Figure 3. Differential expression of RNA between cells and EVs, from uninfected (A) and infected (B) cultures. Differential RNA abundancies and adjusted p-values were calculated using DESeq2, and only transcripts with TPM > 10 are represented in this plot. Red lines represent the threshold for differential expression ($p < 0.05$ and fold change > 2). Gradient legend in **(B)** represents the differential expression of transcripts between uninfected and infected cells in log2 fold change. Raw data is presented in Supplementary Table 2 and 5.

Table 1. EV-enriched ncRNA. Descriptions for newly annotated ncRNA show the intergenic region (IGR) in the *Hrr. lacusprofundi* ACAM34UNSW genome that the ncRNA is located.

Name	Description	Length [nt]
ncRNA1	ACAM34UNSW_ - ACAM34UNSW_01067 IGR	84
RNaseP	RNase P	382
asRNA1	antisense to ISH6-like transposase	69
ncRNA2	ACAM34UNSW_01444 - ACAM34UNSW_01445 IGR, small ORF WP_272931215.1	204
ncRNA3	ACAM34UNSW_01961 - ACAM34UNSW_01962 IGR	44
asRNA2	ACAM34UNSW_00942 - ACAM34UNSW_00943 IGR, overlaps an ORF for IS6-like transposase	54
ncRNA4	ACAM34UNSW_00708 - ACAM34UNSW_00709 IGR	91
7S	7S SRP RNA	359
ncRNA5	ACAM34UNSW_01407 - ACAM34UNSW_01408 IGR	63
ncRNA6	ACAM34UNSW_01570 - ACAM34UNSW_01571 IGR	38
ncRNA7	ACAM34UNSW_00612 - ACAM34UNSW_00613 IGR	44
ncRNA8	encoded within ORF of *tfb2 7*	31

Infection with lytic virus alters EV-associated RNA composition

Changes to EV-associated RNA were previously tested during infection with a chronic virus [25], and no significant changes were observed. Therefore, we wanted to test changes to EV-associated RNA in response to a lytic virus infection. We infected cultures of ACAM34_UNSW with the lytic virus, HRTV-DL1 [14], with a very low cell to virus ratio (0.01:1) as to prevent immediate lysis of the cultures. EVs were harvested at exponential phase of growth (OD_{600} ~ 0.7), and RNA was extracted and sequenced. We observed 13.8-fold higher amounts of RNA present in EVs from the infected cultures when compared to untreated cultures (p-value = 0.02), which we attribute to an increased production of EVs as observed during density gradient purification (Supplementary Figure 1). Interestingly, the composition of EV-associated RNA from infected cultures also appeared to be altered (Figure 2A). We observed a shift in the sizes of packaged transcripts from 25-100 nt in EVs from uninfected cultures to 25-40 nt in EVs from infected cultures. Sequencing of the EVs from infected cultures also proved difficult, as most did not pass quality checks and appeared more degraded than normal. Nevertheless, we sequenced the EV-associated RNA from infected cultures, which revealed that intracellular transcripts and transcripts from EVs of infected and uninfected cultures all represent distinct populations (Supplementary Figure 2). The RNA enclosed in EVs was dramatically altered under infection with HRTV-DL1. We identified 245 genes associated with EVs with TPM above 10 (Supplementary Table 4). EVs from infected cultures enclosed five-fold less tRNAs (p-value = 0.002) and 1.3-fold more rRNA (p-value = 0.02), while no significant changes were detected for the mRNA and ncRNA populations (Figure 2B). While changes were also detected in the intracellular transcriptome, these changes did not reflect the changes in EV-associated RNA.

When normalized to intracellular levels, only 35 genes were identified as enriched in EV-associated RNAs from infected cultures (Figure 3B, Supplementary Table 5). Of those, 14 were also identified as enriched in EVs from uninfected

cultures. Only two ncRNA were identified as enriched in EVs from infected cultures, RNaseP and intergenic transcript, ncRNA3. Both were also identified as enriched in EVs from uninfected cultures, but the level of enrichment in EVs differed when comparing between treatments. The RNaseP RNA subunit increased from 7.5-fold enrichment to 39-fold enrichment and the intergenic transcript increased from 8.9-fold enrichment to 16-fold enrichment upon infection. Intracellular levels between uninfected and infected cells remained the same for both ncRNA. This was not observed for the other shared enriched transcripts (except 16S and 5S rRNA), as for most the abundance decreased or remained the same upon infection.

Surprisingly, the most enriched transcript in EVs from infected cultures was the mRNA for transcription initiation factor IIB family protein, Tfb2 (WP_015911428), which was about 322-fold higher in abundance in EVs than in cells, but only 7-fold increased when comparing between uninfected and infected cells. Upon inspection of the read mapping, we observed that the vast majority of reads mapped to a 31 bp section within the coding region of the *tfb2* gene (ncRNA8, Table 1). In the absence of viral infection, this transcript was far below the threshold for transcriptional noise in both EVs and intracellularly, and is presumed to be not expressed. Therefore, we suggest that upon infection, *Hrr. lacusprofundi* selectively packages a sRNA derived from *tfb2* into EVs. It should also be noted that 13 nt of this transcript align with the HRTV-DL1 genome, specifically to the coding region of ORF43 (transcription initiation factor IIB). However, mapping the EV-associated reads to the HRTV-DL1 genome did not result in a similar peak, suggesting that the transcript was not derived from the viral genome. Prediction of potential targets of this ncRNA revealed only one mRNA for b(o/a)3-type cytochrome-c oxidase subunit 1 (Supplementary Table 3), implying a potential impact on ATP synthesis or oxidative stress.

Incubation of EVs with cells induced slight changes in the intracellular transcriptome

EVs isolated from uninfected and infected cultures were incubated with naïve cells to determine whether the uptake of EV-associated RNA would alter the transcriptomic landscape of recipient cells. After two hours of incubation with EVs, using the small RNA library preparation kit, we were unable to measure any intracellular transcriptomic fold change greater than 2 or less than 0.5 (Figure 4). However, the rate of sRNA-mediated mRNA deactivation is dependent on the ratio of sRNA to the target mRNA and the rate of RNA turnover in the cell [26], and is therefore specific to each sRNA. Further, sRNA-mediated mRNA degradation, unlike in Bacteria and Eukaryotes, is only assumed but not confirmed in the archaeal domain [27]. Therefore, these effects may more likely be observable at the proteomic level, especially if a transcriptional regulator is not the target of sRNA regulation. It is possible that the effects of EV-associated RNA at the transcriptomic level would be subtle at the time of measurement and with the amount of EVs used. Therefore, in order to gain a higher resolution on more subtle changes to transcript levels, we lowered the fold change threshold from 2 to 1.5. We also increased the significance threshold from an adjusted p-value of 0.05 to 0.02 to compensate for the changes in fold change threshold.

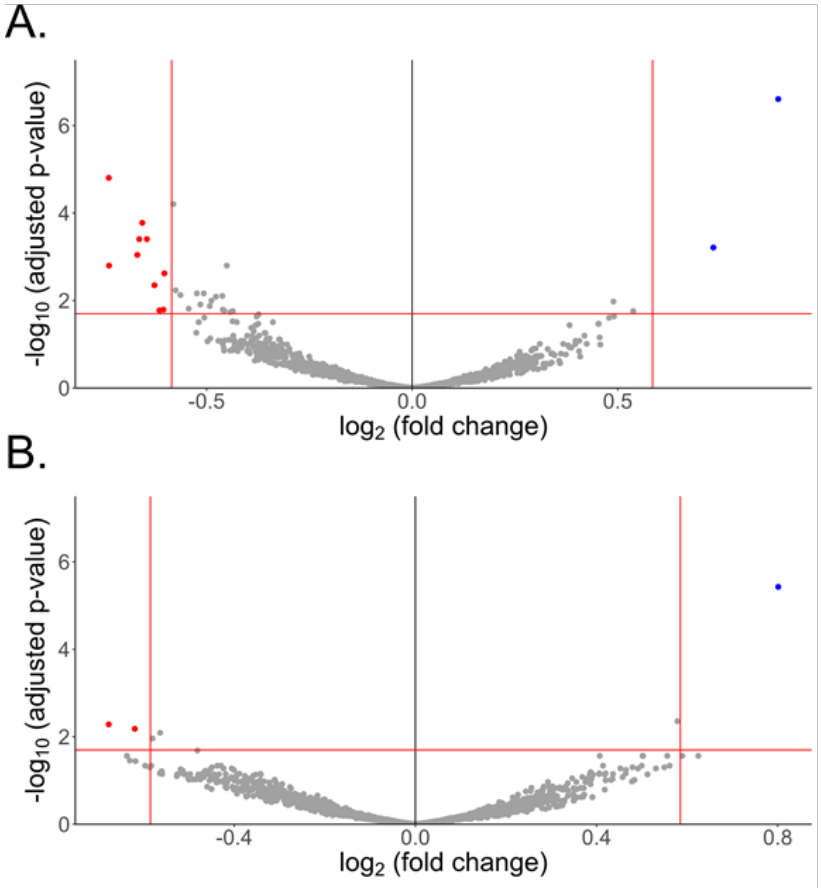

Figure 4. Differential expression of RNA between cells incubated with EVs from uninfected (A) and infected (B) cultures versus no treatement. Blue dots indicate slight upregulation and red dots indicate slight down regulation. Differential RNA abundancies and adjusted p-values were calculated using DESeq2, and only transcripts with TPM > 10 are represented in this plot. Red lines represent the threshold for differential expression ($p < 0.02$ and fold change > 1.5 and < -1.5). Data is presented in Supplementary Table 6.

With these changes, we detected two slightly upregulated and ten slightly downregulated genes after incubation with EVs from uninfected cultures (Supplementary Table 6). The two upregulated genes were ncRNA5, which was also identified as enriched in EVs, and a conserved hypothetical protein of unknown function, ACAM34_UNSW_02188. However, it should be noted that the expression level of the hypothetical protein was relatively low (TPM < 20) in both control and EV-incubated cells. The downregulated genes included a chemoreceptor, beta-galactosidase and an extracellular solute binding protein, suggesting a functional connection to chemotaxis and metabolism. We also observed a slight downregulation of an integrase/recombinase, a transposase, a translation initiation factor, an osmotic stress protein and two hypothetical proteins, as well as the tRNA for glycine. After incubation with EVs from infected cultures, we only detected the same ncRNA as slightly upregulated, and the same chemoreceptor and osmotic stress protein as slightly downregulated.

To gain clues as to whether the downregulation of these genes were related to the enriched ncRNA in the EVs, we predicted base-pairing regions between the ncRNA and genes using TargetRNA3 [28]. However, none of the searches identified significant interactions between the ncRNA and the slightly downregulated genes.

Cells grown after incubation with EVs show transcriptional changes

After cells were incubated with EVs, the cells were grown in fresh media and their growth was monitored. However, no significant changes in growth were detected following adsorption of EVs from uninfected or infected cultures (Supplementary Figure 3A). The same was done with the addition of HRTV-DL1 (virus:host = 1000:1) to determine whether infectivity of the virus would be affected as a result of exposure to EVs from a culture already experiencing infection. Lysis progressed similarly to the control with no significant differences detected (Supplementary Figure 3B).

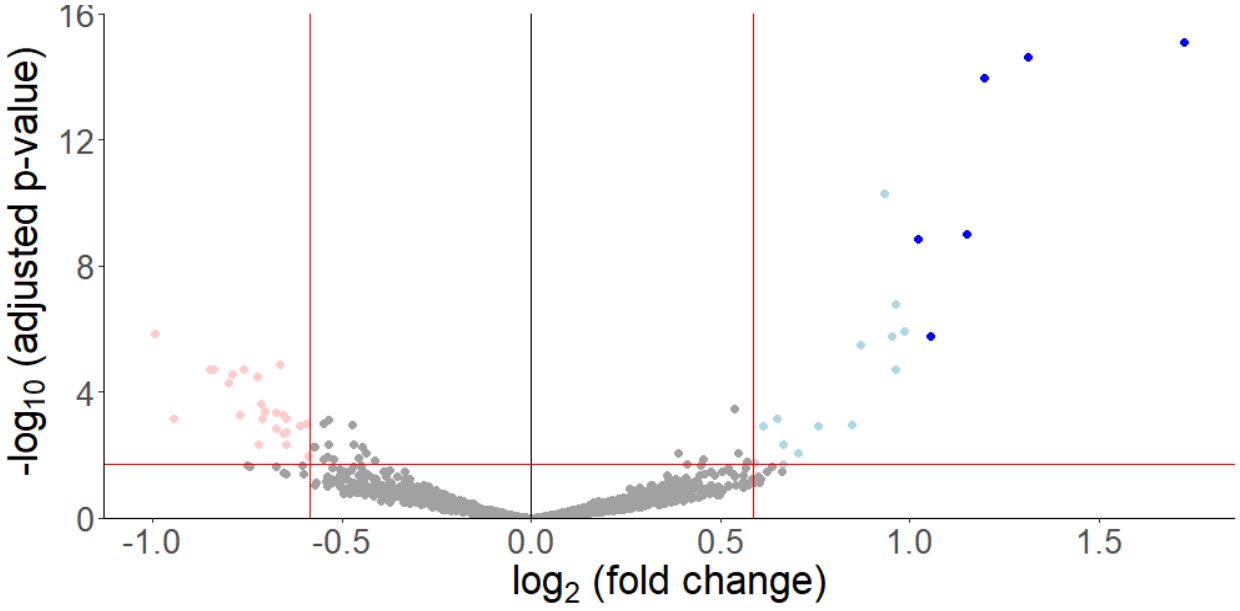

Figure 5. Differential expression of RNA 12 hours after incubation with EVs. Fold change determined between cells incubated with EVs versus no treatment. Blue dots indicate upregulation (with dark blue indicating log2 fold change greater than 1) and light red dots indicate slight down regulation. Differential RNA abundancies and adjusted p-values were calculated using DESeq2, and only transcripts with TPM > 10 are represented in this plot. Red lines represent the threshold for differential expression ($p < 0.02$ and fold change > 1.5 and < -1.5). Data is presented in Supplementary Table 7.

Samples of cells were taken after 12 hours of growth after incubation with EVs from uninfected cultures, and RNA was sequenced to determine if significant changes in the transcriptome were still observable. Using the small RNA library preparation kit, we did not detect any significantly differentially expressed transcripts. However, when using the Total RNA library preparation kit, we detected 45 differentially expressed transcripts (fold change threshold 1.5, p-value < 0.02), with 6 transcripts being highly upregulated (fold change > 2) (Figure 5, Supplementary Table 7). Out of the 20 upregulated mRNAs, four are involved in lipid biosynthesis and three encode for proteins containing a signal peptide. Out of the 25 downregulated mRNAs, eight are associated with chemotaxis and six are involved in cell motility. Unlike the transcriptomes from 2 hours post-EV incubation, we did not detect any downregulation of the mRNA for chemotaxis protein, CheD, after 12 hours of growth.

DISCUSSION

In this study, we investigate the potential roles of RNA-associated EVs that are produced by various haloarchaeal organisms [6]. Using the haloarchaeal organism, *Hrr. lacusprofundi* ACAM34_UNSW, we identify and compare the

intracellular and EV-associated transcriptomes and how these change upon the introduction of viral stress with a lytic virus, as well as the subsequent effects on cells receiving EVs.

EV-associated RNA and intracellular RNA in *Hrr. lacusprofundi* were demonstrated to represent significantly distinct RNA populations, similar to what was observed in *H. volcanii* and *Hbt. salinarum* [6]. This further supports the prediction that the export of RNA in EVs is a conserved phenomenon among haloarchaea. During infection with the lytic virus, HRTV-DL1 [14], we observed that the intracellular transcriptome and the exported EV-associated RNA populations change dramatically, suggesting that EV-associated RNA composition is strongly influenced by growth conditions. Specifically, upon infection, the length/size range of the exported RNA was noticeably smaller. The decrease in RNA size in EVs from infected cultures could be a result of RNA degradation from virus-induced increased transcriptomic turnover within the cell. However, it is also possible that specific smaller sized RNAs were enclosed into EVs upon virus infection. The majority of reads in EVs derived from infected cultures was rRNA. Without further experimental evidence it is uncertain whether the rRNA was intact or degraded, and whether this is an indicator of changes to the number of ribosomes within the cell during infection. The export of degraded rRNA could potentially function as a defense mechanism, in that ribosomal degradation could stall the viral replication machinery and prevent cells from internally recycling the RNA product. Increased EV production could also increase the chances of EV-virus interaction, a phenomenon that has been observed in Bacteria and predicted to hinder viral activity [29–31]. Therefore, apart from of the RNA content itself, EV production could function as a defense mechanism against viral infection.

The majority of changes in the composition of EV-associated RNAs cannot be explained by the intracellular changes upon infection. Conditional changes of EV-associated RNA have been observed in Bacteria [10], and recently also have been suggested for EVs of *H. volcanii* [6]. Considering that the majority of the genome of the producing organism was represented as transcriptome in the EV-associated RNA population, we predict that RNA is enclosed randomly, but with a preference for smaller transcripts as has been suggested for *H. volcanii*. However, the drastic enrichment of specific ncRNAs in EVs (such as ncRNA8), suggests that mechanisms for active RNA packaging may be present and are conditionally dependent. It should be noted, though, that since some sequencing yielded low sequencing depth, in particular of RNA from EVs of infected cultures, it is likely that some enriched RNAs with lower expressions were missed during this analysis.

The enrichment of the 31 nt ncRNA8 in EVs from infected cultures was intriguing, since the size fits the observed size distribution of EV-associated RNA (Figure 2). The average relative abundance of ncRNA8 (readjusted for the smaller gene length) was one to two magnitudes lower than the highly abundant rRNA and tRNA, yet ncRNA8 was one of the most abundant ncRNAs in EVs. The gene that ncRNA8 derives from is one of seven isoforms in the *Hrr. lacusprofundi* genome of a specific family of general transcription initiation factors (TFIIB, IPR023484). Each of the multiple isoforms of *tfb2* differ in amino acid sequence identity (from 81% to 37%), suggesting that they likely individually regulate specific functions for the cell. While it could be hypothesized that ncRNA8 regulates the expression of this specific transcription initiation factor and the subsequent genes of the associated regulon, it is also possible that ncRNA8 interacts with other mRNA. For example, we identified 13 nt shared between ncRNA8 and ORF43 in the HRTV-DL1

genome, suggesting that ncRNA8 could potentially regulate expression of this viral gene. We were unable to detect any effect in growth curves of infected cultures after they have been treated with EVs from infected cultures. However, the viral titer used for this experiment was much higher (100x) than usually used for infection experiments with HRTV-DL1 [14]. Using lower virus-to-host ratios and determining virus copy numbers within cells might allow to detect effects of EV-associated RNA on the viral life cycle.

We can also infer some potential functions of the other ncRNAs enriched in EVs from both uninfected and infected cultures. Two ncRNAs enriched in EVs are predicted to interact with the mRNA of CinA, suggesting the potential for EVs to regulate CinA expression. The CinA family of proteins has been characterized in Bacteria to be related to cell competence and the uptake of extracellular DNA, though the exact mechanism is unknown [32]. However, after incubation of cells with EVs, we did not detect any changes to CinA expression or any other predicted targets of the ncRNA enriched in EVs under the conditions tested (time points and chosen RNA libraries). Whether the EV-associated ncRNAs are able to upregulate or downregulate CinA expression, or whether CinA is related to EV-cell interactions remains to be determined. However, the export of ncRNAs that could influence the uptake of extracellular nucleic acids is interesting and should be investigated further.

When incubating cells with EVs for two hours, we did not detect any major changes to the transcriptome of the receiving cells. It has been shown that *H. volcanii* is able to transfer RNA between *H. volcanii* cells within two hours of incubation [6], but this has not been determined for ACAM34_UNSW. Therefore, it is possible that the time point chosen was too early to observe larger effects on the transcriptome. Nevertheless, we did detect slight changes in the transcriptome of the recipient cells, which could be a reaction to the presence of EVs themselves rather than to the associated ncRNA. Both conditions (incubation with EVs from uninfected cultures and EVs from infected cultures) resulted in a downregulation of the mRNA for CheD, a regulatory component of the chemotaxis system [33]. Deletion of CheD in *Bacillus subtilis* leads to deactivation of the chemotaxis system [34]. Downregulation of CheD upon exposure to EVs would therefore lead to a decreased chemotactic response, similar to what was observed from the deletion of CheD interacting partner, CheC, in *Hrr. salinarum* [35]. Additionally, a number of chemotaxis- and motility-related transcripts were downregulated 12 hours after incubation with EVs, indicating an effect on motility upon EV exposure. Downregulation of genes involved in motility has also been observed upon virus infection in *H. volcanii* [25], indicating that this could be a general response to invading elements. However, it is also possible that this could be an effect of specific RNA signals communicated by EVs, or EVs could be carriers of signaling compounds, such as quorum sensing compounds influencing motility, similar to what has been observed for some bacterial organisms [36–38].

Another hypothesis for the function of prokaryotic EVs in microbial communities is that they are used as “public goods” [39], in that they provide benefits for the entire community. Under this hypothesis, the enclosed nucleic acids and lipids could be utilized as a food source, which has been shown with EVs from the bacterial organism, *Prochlorococcus* [31]. Perhaps the availability of nutrients supplied by the EVs could lead to the downregulation of motility and chemotaxis. Nutrient availability and cell motility have been shown to be connected in *E. coli* [40], though it is undetermined if motility and chemotaxis in Archaea are similarly regulated. Further, we did not detect any changes to the growth of the

organism following exposure to EVs, suggesting that the EVs were not used as a nutrient source under the conditions tested. Therefore, additional experimental evidence is required to conclude whether chemotaxis and motility is indeed affected by EVs, and what component of EV-cell interaction mediates this regulation.

We also observed effects on other transcripts. Two hours after incubation with EVs from uninfected and infected cultures, we observed a slight upregulation of asRNA2 that is undetectable after 12 hours. It remains to be determined whether this increased presence is caused by asRNA2 delivered by EVs or endogenous expression. We did not detect a similar upregulation of the other RNAs enriched in EVs, suggesting that it is likely not higher in abundance due to EV-mediated delivery. We also observed the upregulation of several lipid biosynthesis-related mRNAs after incubation with EVs. Acyl-CoA dehydrogenases and long chain fatty acyl-CoA ligases are both involved in the metabolism of fatty acids [41, 42], which could be a response to the supplemented source of saturated lipids in the EVs [6].

In searching for direct effects of EV-associated RNA on gene expression, we did not uncover any evidence that the specific RNA cargo had any effects on EV-receiving cells. However, the possibility for effects of this nature should not be ruled out. Apart from the possibility that the conditions or the time frame chosen for the EV exposure were not optimal, it is possible that at the transcriptomic level, the effect of EV-associated ncRNA regulation is not visible. Typically a canonical sRNA interacts with the target mRNA to increase or decrease the rate of translation [8, 27]. In Bacteria, the effect that an sRNA has on the transcriptome is highly dependent on the individual sRNA [26]. This includes factors such as whether the sRNA regulates the translation of global transcriptional regulators or whether the target RNA is degraded or remains in complex with the sRNA. We did detect the slight downregulation of one PadR family transcriptional regulator 12 hours post-incubation with EVs, though it remains to be determined if this could explain the other transcriptomic changes we observed or if this was a direct result of RNA-based communication. Another possibility is that the enriched ncRNAs could act as non-canonical sRNAs. Rather than post-transcriptionally regulating gene expression, they could convey their function through interacting with specific proteins, as it has been observed in Bacteria [43] but not yet in Archaea. It should be noted though that the mechanisms and diversity of ncRNA function in Archaea are still relatively unknown [27], and it is likely that most mechanisms of ncRNA-mediated regulation are still uncharacterized. Therefore, a proper assessment of transcriptome- and proteome-level, and perhaps even phenotypic changes, could possibly allow for the detection of temporary changes caused by EV-associated ncRNA.

From our investigation into whether EVs derived from infected cultures would be able to act as a type of warning system for naïve cells, we detected no such immunity or resistance transferred through EVs. Considering the high virus-to-host ratio, the early lysis of cultures, and the infrequency of measurements of growth that were taken, it is likely that infection progressed too fast to be able to detect slight changes in the infection. Perhaps using a lower virus to cells ratio during infection to allow a slower progression of the infection in the culture would allow us to better detect any deviations as a result of EV exposure. The presence of an ncRNA with sequential homology to a region of the viral genome, specifically a transcriptional regulator, suggests that viral gene expression could potentially be targeted. Though, a proper investigation into the activity of the enriched ncRNA would be required to make more conclusive statements. Additionally, the effects of exposure to EVs on intracellular and extracellular viral genome copies should be considered.

Considering the conditionally dependent changes in EV-associated transcriptome and the targeted effects on the transcriptomes of cells that have interacted with EVs, we propose that haloarchaea are able to use EVs as a signaling mechanism. Though both the transcriptome and proteome of haloarchaeal EVs have been demonstrated to change depending on the growth conditions [6], the conditionality of other EV-associated compounds such as signaling compounds or toxins should also be taken into consideration. Both the function of EVs and ncRNA regulation in Archaea are still relatively in their infancy [44, 27]. From the work presented here, it is clear that additional experiments are necessary to properly assess the regulatory nature of EVs in archaeal systems.

REFERENCES

1. Deatherage BL, Cookson BT (2012) Membrane vesicle release in bacteria, eukaryotes, and archaea: a conserved yet underappreciated aspect of microbial life. Infect Immun 80:1948–1957. https://doi.org/10.1128/IAI.06014-11
2. Gill S, Catchpole R, Forterre P (2019) Extracellular membrane vesicles in the three domains of life and beyond. FEMS Microbiol Rev 43:273–303. https://doi.org/10.1093/femsre/fuy042
3. Schatz D, Vardi A (2018) Extracellular vesicles - new players in cell-cell communication in aquatic environments. Curr Opin Microbiol 43:148–154. https://doi.org/10.1016/j.mib.2018.01.014
4. Tsatsaronis JA, Franch-Arroyo S, Resch U et al. (2018) Extracellular Vesicle RNA: A Universal Mediator of Microbial Communication? Trends Microbiol 26:401–410. https://doi.org/10.1016/j.tim.2018.02.009
5. Dauros-Singorenko P, Blenkiron C, Phillips A et al. (2018) The functional RNA cargo of bacterial membrane vesicles. FEMS Microbiol Lett 365. https://doi.org/10.1093/femsle/fny023
6. Mills J, Gebhard LJ, Schubotz F et al. (2023) Extracellular vesicles of Euryarchaeida: precursor to eukaryotic membrane trafficking. BioRxiv
7. Choi DH, Kwon YM, Chiura HX et al. (2015) Extracellular Vesicles of the Hyperthermophilic Archaeon "Thermococcus onnurineus" NA1T. Appl Environ Microbiol 81:4591–4599. https://doi.org/10.1128/AEM.00428-15
8. Storz G, Vogel J, Wassarman KM (2011) Regulation by small RNAs in bacteria: expanding frontiers. Mol Cell 43:880–891. https://doi.org/10.1016/j.molcel.2011.08.022
9. Wagner EGH, Romby P (2015) Small RNAs in bacteria and archaea: who they are, what they do, and how they do it. Adv Genet 90:133–208. https://doi.org/10.1016/bs.adgen.2015.05.001
10. Da Luz BSR, Nicolas A, Chabelskaya S et al. (2021) Environmental Plasticity of the RNA Content of Staphylococcus aureus Extracellular Vesicles. Front Microbiol 12:634226. https://doi.org/10.3389/fmicb.2021.634226
11. Ahmadi Badi S, Bruno SP, Moshiri A et al. (2020) Small RNAs in Outer Membrane Vesicles and Their Function in Host-Microbe Interactions. Front Microbiol 11:1209. https://doi.org/10.3389/fmicb.2020.01209
12. Moriano-Gutierrez S, Bongrand C, Essock-Burns T et al. (2020) The noncoding small RNA SsrA is released by Vibrio fischeri and modulates critical host responses. PLoS Biol 18:e3000934. https://doi.org/10.1371/journal.pbio.3000934
13. Sahr T, Escoll P, Rusniok C et al. (2022) Translocated Legionella pneumophila small RNAs mimic eukaryotic microRNAs targeting the host immune response. Nat Commun 13:762. https://doi.org/10.1038/s41467-022-28454-x
14. Mercier C, Thies D, Zhong L et al. (2023) Characterization of an archaeal virus-host system reveals massive genomic rearrangements in a laboratory strain. Front Microbiol 14:1274068. https://doi.org/10.3389/fmicb.2023.1274068
15. Gebhard LJ, Duggin IG, Erdmann S (2023) Improving the genetic system for Halorubrum lacusprofundi to allow in-frame deletions. Front Microbiol 14:1095621. https://doi.org/10.3389/fmicb.2023.1095621
16. Dyall-Smith, Michael (2009) The Halohandbook: Protocols for haloarchaeal genetics
17. Mills J, Erdmann S (2022) Isolation, Purification, and Characterization of Membrane Vesicles from Haloarchaea. Methods Mol Biol 2522:435–448. https://doi.org/10.1007/978-1-0716-2445-6_30
18. Rio DC, Ares M, Hannon GJ et al. (2010) Purification of RNA using TRIzol (TRI reagent). Cold Spring Harb Protoc 2010:pdb.prot5439. https://doi.org/10.1101/pdb.prot5439

19. Mann M, Wright PR, Backofen R (2017) IntaRNA 2.0: enhanced and customizable prediction of RNA-RNA interactions. Nucleic Acids Res 45:W435-W439. https://doi.org/10.1093/nar/gkx279
20. Wright PR, Georg J, Mann M et al. (2014) CopraRNA and IntaRNA: predicting small RNA targets, networks and interaction domains. Nucleic Acids Res 42:W119-23. https://doi.org/10.1093/nar/gku359
21. Busch A, Richter AS, Backofen R (2008) IntaRNA: efficient prediction of bacterial sRNA targets incorporating target site accessibility and seed regions. Bioinformatics 24:2849–2856. https://doi.org/10.1093/bioinformatics/btn544
22. Raden M, Ali SM, Alkhnbashi OS et al. (2018) Freiburg RNA tools: a central online resource for RNA-focused research and teaching. Nucleic Acids Res 46:W25-W29. https://doi.org/10.1093/nar/gky329
23. Erdmann S, Tschitschko B, Zhong L et al. (2017) A plasmid from an Antarctic haloarchaeon uses specialized membrane vesicles to disseminate and infect plasmid-free cells. Nat Microbiol 2:1446–1455. https://doi.org/10.1038/s41564-017-0009-2
24. Prangishvili D, Holz I, Stieger E et al. (2000) Sulfolobicins specific proteinaceous toxins produced by strains of the extremely thermophilic archaeal genus Sulfolobus. Journal of Bacteriology 182:2985–2988
25. Alarcón-Schumacher T, Naor A, Gophna U et al. (2022) Isolation of a virus causing a chronic infection in the archaeal model organism Haloferax volcanii reveals antiviral activities of a provirus. Proc Natl Acad Sci U S A 119:e2205037119. https://doi.org/10.1073/pnas.2205037119
26. Mitarai N, Benjamin J-AM, Krishna S et al. (2009) Dynamic features of gene expression control by small regulatory RNAs. Proc Natl Acad Sci U S A 106:10655–10659. https://doi.org/10.1073/pnas.0901466106
27. Gelsinger DR, DiRuggiero J (2018) The Non-Coding Regulatory RNA Revolution in Archaea. Genes (Basel) 9. https://doi.org/10.3390/genes9030141
28. Kery MB, Feldman M, Livny J et al. (2014) TargetRNA2: identifying targets of small regulatory RNAs in bacteria. Nucleic Acids Res 42:W124-9. https://doi.org/10.1093/nar/gku317
29. Augustyniak D, Olszak T, Drulis-Kawa Z (2022) Outer Membrane Vesicles (OMVs) of Pseudomonas aeruginosa Provide Passive Resistance but Not Sensitization to LPS-Specific Phages. Viruses 14. https://doi.org/10.3390/v14010121
30. Manning AJ, Kuehn MJ (2011) Contribution of bacterial outer membrane vesicles to innate bacterial defense. BMC Microbiol 11:258. https://doi.org/10.1186/1471-2180-11-258
31. Biller SJ, Schubotz F, Roggensack SE et al. (2013) Bacterial Vesicles in Marine Ecosystems. Science 343:183–186
32. Martin B, García P, Castanié MP et al. (1995) The recA gene of Streptococcus pneumoniae is part of a competence-induced operon and controls lysogenic induction. Mol Microbiol 15:367–379. https://doi.org/10.1111/j.1365-2958.1995.tb02250.x
33. Quax TEF, Albers S-V, Pfeiffer F (2018) Taxis in archaea. Emerg Top Life Sci 2:535–546. https://doi.org/10.1042/ETLS20180089
34. Glekas GD, Plutz MJ, Walukiewicz HE et al. (2012) Elucidation of the multiple roles of CheD in Bacillus subtilis chemotaxis. Mol Microbiol 86:743–756. https://doi.org/10.1111/mmi.12015
35. Rudolph J, Oesterhelt D (1996) Deletion analysis of the che operon in the archaeon Halobacterium salinarium. J Mol Biol 258:548–554. https://doi.org/10.1006/jmbi.1996.0267
36. Pesci EC, Milbank JB, Pearson JP et al. (1999) Quinolone signaling in the cell-to-cell communication system of Pseudomonas aeruginosa. Proc Natl Acad Sci U S A 96:11229–11234. https://doi.org/10.1073/pnas.96.20.11229
37. Toyofuku M, Morinaga K, Hashimoto Y et al. (2017) Membrane vesicle-mediated bacterial communication. ISME J 11:1504–1509. https://doi.org/10.1038/ismej.2017.13
38. Brameyer S, Plener L, Müller A et al. (2018) Outer Membrane Vesicles Facilitate Trafficking of the Hydrophobic Signaling Molecule CAI-1 between Vibrio harveyi Cells. Journal of Bacteriology 200. https://doi.org/10.1128/JB.00740-17
39. Caruana JC, Walper SA (2020) Bacterial Membrane Vesicles as Mediators of Microbe - Microbe and Microbe - Host Community Interactions. Front Microbiol 11:432. https://doi.org/10.3389/fmicb.2020.00432

40. Thomason MK, Fontaine F, Lay N de et al. (2012) A small RNA that regulates motility and biofilm formation in response to changes in nutrient availability in Escherichia coli. Mol Microbiol 84:17–35. https://doi.org/10.1111/j.1365-2958.2012.07965.x
41. Thorpe C, Kim JJ (1995) Structure and mechanism of action of the acyl-CoA dehydrogenases. FASEB J 9:718–725. https://doi.org/10.1096/fasebj.9.9.7601336
42. Hisanaga Y, Ago H, Nakagawa N et al. (2004) Structural basis of the substrate-specific two-step catalysis of long chain fatty acyl-CoA synthetase dimer. J Biol Chem 279:31717–31726. https://doi.org/10.1074/jbc.M400100200
43. Pichon C, Felden B (2007) Proteins that interact with bacterial small RNA regulators. FEMS Microbiol Rev 31:614–625. https://doi.org/10.1111/j.1574-6976.2007.00079.x
44. Liu J, Soler N, Gorlas A et al. (2021) Extracellular membrane vesicles and nanotubes in Archaea. Microlife 2:uqab007. https://doi.org/10.1093/femsml/uqab007

SUPPLEMENTARY FIGURES

Supplementary Figure 1. Optiprep density gradient of EVs from uninfected and infected cultures.

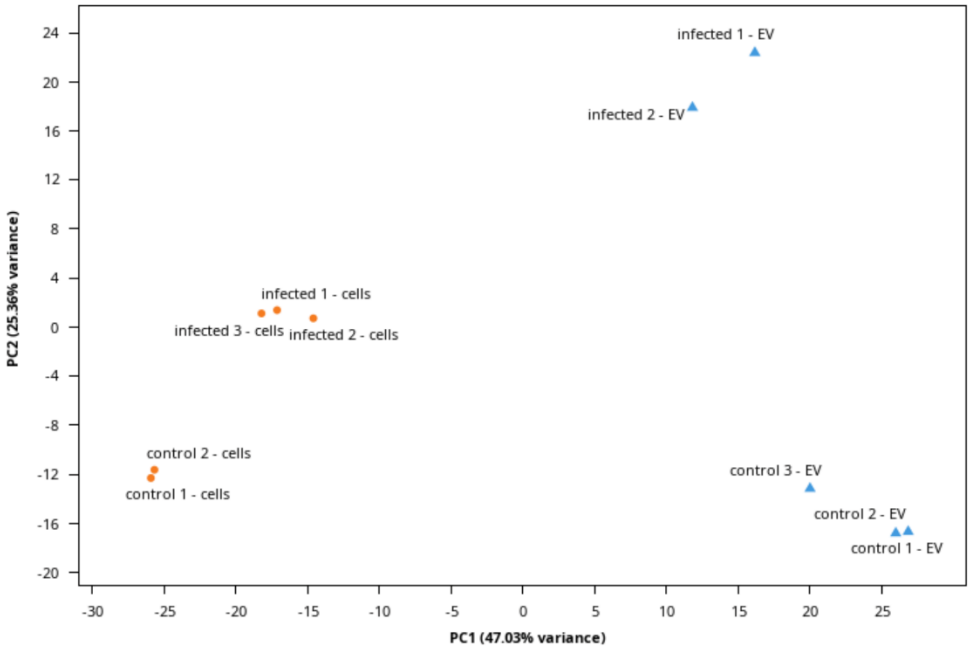

Supplementary Figure 2. Principle component analysis of intracellular and EV-associated transcriptomes from infected and uninfected cultures. Blue triangles represent EV-associated transcriptomes and orange circles represent intracellular transcriptomes. Plot generated on Geneious Prime (2021.0.1).

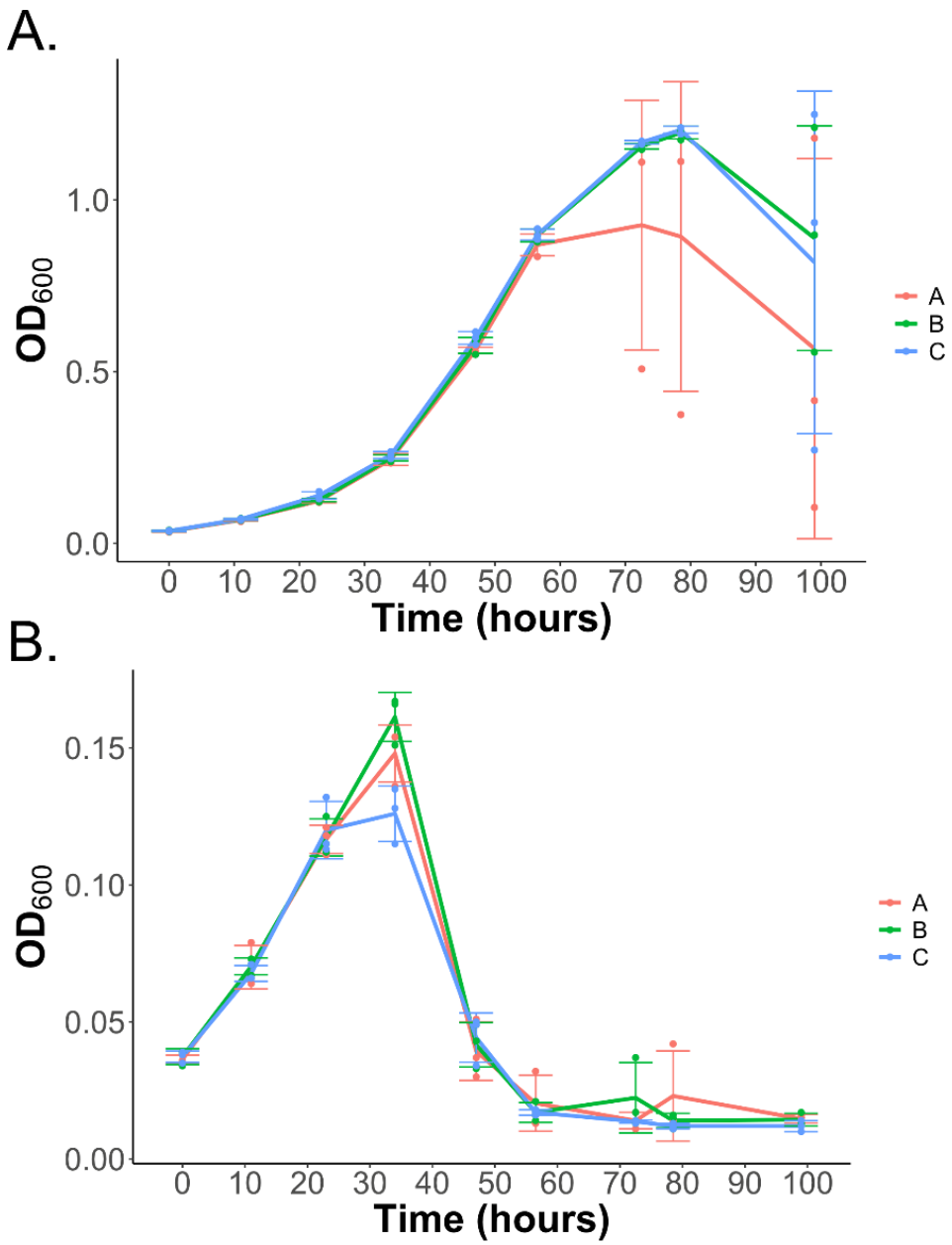

Supplementary Figure 3. Growth curve of uninfected (A) and HRTV-DL1 infected (B) cells after incubation with EVs. In uninfected cultures (**A**) biofilm formation was observed after hour 60, resulting in the large variations between replicates. Figure legends indicate the EV treatment of the cells: A – no treatment, B – EVs from uninfected cultures, C – EVs from infected cultures. Lines plot the average between three replicates, with error bars indicating the standard deviation. Dots plot the individual replicate values.

SUPPLEMENTARY TABLES

Abbreviated versions of supplementary tables are provided below. Subset criteria are presented in the table captions.

Supplementary Table 1. RNA sequencing of EV-associated RNA from uninfected cultures. RNA was isolated from EVs in triplicate and mapped to the Hrr. lacusprofundi ACAM34_UNSW genome using Geneious Prime (2021.0.1). Relative abundance was calculated by transcripts per million (TPM). Only transcripts with TPM > 100 are presented. Min and Max denote minimum or maximum nucleotide in the genome.

Replicate	Reads Generated	Reads Mapped
1	12,542,814	8,683,378
2	12,748,336	9,397,436
3	14,548,720	10,153,710

locus_tag	Name	Min	Max	RNA type	TPM 1	TPM 2	TPM 3	Average TPM
ACAM34_UNSW_01545	23S rRNA	1535206	1538105	rRNA	123252.2	135226.9	133307.8	130595.6433
ACAM34_UNSW_00026	5S rRNA	25629	25744	rRNA	94455.78	97260.08	82880.1	91531.98667
ACAM34_UNSW_02597	tRNA-Glu	2543858	2543932	tRNA	48206.52	38210.1	35950.33	40788.98333
ACAM34_UNSW_00023	16S rRNA	20596	22064	rRNA	42699.92	38079.82	12649.7	31143.14667
ACAM34_UNSW_02715	tRNA-Val	2670975	2671049	tRNA	34414.14	39937.35	3583.66	25978.38333
ACAM34_UNSW_00933	tRNA-Ala	912708	912780	tRNA	3632.54	3449.34	37684.86	14922.24667
	asRNA	1932024	1932051	ncRNA	9532.47	4824.09	29338.64	14565.06667
ACAM34_UNSW_02165	tRNA-Pro	2151555	2151625	tRNA	14868.51	13426.55	4826.3	11040.45333
	asRNA	1015806	1015844	ncRNA	8823.21	4525.66	17946.32	10431.73
ACAM34_UNSW_01917	tRNA-Ala	1901341	1901414	tRNA	9020.49	11204.22	1168.02	7130.91
	ncRNA	1976995	1977036	ncRNA	4714.32	4241.65	9146.91	6034.293333
	ncRNA	2771129	2771510	ncRNA	6742.1	7528.02	485.01	4918.376667
ACAM34_UNSW_02154	tRNA-His	2140510	2140583	tRNA	4351.39	4802.63	4397.77	4517.263333
ACAM34_UNSW_00836	tRNA-Met	817377	817452	tRNA	4593.99	6208.64	1327.23	4043.286667
	ncRNA	1566573	1566610	ncRNA	3029.4	2258.7	6577.98	3955.36
ACAM34_UNSW_01693	tRNA-Gly	1684848	1684919	tRNA	365.67	289.53	9729.69	3461.63
	asRNA	1223934	1223964	ncRNA	2387.1	1243.7	6238.5	3289.766667
	ncRNA	1292889	1292977	ncRNA	1742.66	960.21	7022.71	3241.86
ACAM34_UNSW_03069	tRNA-Gln	3020453	3020525	tRNA	3191.74	2935.77	1653.68	2593.73
ACAM34_UNSW_00349	tRNA-Asn	359516	359588	tRNA	1168.05	780.2	5617.94	2522.063333
ACAM34_UNSW_00115	tRNA-Asp	114519	114591	tRNA	1216.29	1755.63	4228.75	2400.223333
ACAM34_UNSW_02240	tRNA-Leu	2208593	2208677	tRNA	3293.7	2670.21	974.41	2312.773333
	ncRNA	2540081	2540238	ncRNA	1602.9	1070.98	4021.21	2231.696667
	ncRNA	922183	922236	ncRNA	919.93	449.07	3618.95	1662.65
	ncRNA	369492	369521	ncRNA	1188.19	600.92	3052.55	1613.886667
	ncRNA	1397233	1397295	ncRNA	762.72	478.61	3168.55	1469.96
	ncRNA	875429	875787	ncRNA	1701.54	1363.99	1189.11	1418.213333
	ncRNA	1945630	1945673	ncRNA	1329.69	964.47	1860.85	1385.003333
ACAM34_UNSW_01047	tRNA-Gly	1018454	1018524	tRNA	247.97	152.8	3659.76	1353.51
ACAM34_UNSW_01769	tRNA-Tyr	1752408	1752482	tRNA	923.1	750.18	2324.75	1332.676667
ACAM34_UNSW_02170	tRNA-Ser	2155029	2155115	tRNA	1420.94	872.87	1594.98	1296.263333
ACAM34_UNSW_01839	hypothetical protein CDS	1826794	1827123	mRNA	802.58	409.32	2306.02	1172.64
ACAM34_UNSW_00369	tRNA-Ala	376154	376226	tRNA	669.37	634.5	2134.46	1146.11
	ncRNA	2561924	2561992	ncRNA	1503.49	678.22	872.81	1018.173333
ACAM34_UNSW_00061	tRNA-Pro	56692	56762	tRNA	1171.2	621.67	1046.46	946.4433333
ACAM34_UNSW_02344	hypothetical protein CDS	2305222	2305416	mRNA	959.27	776.68	1006.57	914.1733333
ACAM34_UNSW_01668	tRNA-Val	1661563	1661638	tRNA	459.04	339.37	1833.55	877.32
ACAM34_UNSW_02175	tRNA-Leu	2157538	2157623	tRNA	706.14	641.24	1234.27	860.55
ACAM34_UNSW_01384	tRNA-Ile	1377714	1377789	tRNA	485.42	357.56	1730.27	857.75
	ncRNA	707534	707624	ncRNA	673.29	466.34	1274.03	804.5533333
ACAM34_UNSW_03045	tRNA-Arg	2990268	2990340	tRNA	179.59	177.02	2015.19	790.6

ACAM34_UNSW_02816	tRNA-Gly	2753764	2753834	tRNA	679.07	508.57	1152.57	780.07
ACAM34_UNSW_00060	tRNA-Phe	56281	56354	tRNA	170.57	118.57	1949.55	746.23
ACAM34_UNSW_00116	tRNA-Asp	114620	114694	tRNA	222.47	413.38	1433.35	689.7333333
ACAM34_UNSW_01066	tRNA-Leu	1037500	1037584	tRNA	587.61	407.29	1038.63	677.8433333
	ncRNA	1435548	1435751	ncRNA	801.17	831.57	375.27	669.3366667
ACAM34_UNSW_01616	tRNA-Pro	1609519	1609592	tRNA	200.59	120.73	1559.4	626.9066667
ACAM34_UNSW_01658	hypothetical protein CDS	1653135	1653341	mRNA	706.08	521.26	642.24	623.1933333
ACAM34_UNSW_00501	tRNA-Gln	502186	502258	tRNA	633.75	597.35	597.57	609.5566667
ACAM34_UNSW_00756	tRNA-Thr	750705	750777	tRNA	120.96	88.87	1596.21	602.0133333
ACAM34_UNSW_02890	tRNA-Val	2827791	2827864	tRNA	542.46	584.25	660.21	595.64
	ncRNA	1037604	1037687	ncRNA	463.05	279.82	1043.47	595.4466667
ACAM34_UNSW_01344	hypothetical protein CDS	1336847	1337152	mRNA	764.61	773.7	136.22	558.1766667
ACAM34_UNSW_01913	hypothetical protein CDS	1896858	1897253	mRNA	308.48	156.58	1177.91	547.6566667
	ncRNA	614019	614062	ncRNA	321.34	314.24	879.68	505.0866667
	ncRNA	1967830	1968033	ncRNA	327.16	251.04	931.86	503.3533333
ACAM34_UNSW_00022	hypothetical protein CDS	20374	20517	mRNA	622.61	433.93	410.39	488.9766667
ACAM34_UNSW_01680	tRNA-Ser	1672377	1672463	tRNA	575.35	417.48	407.04	466.6233333
ACAM34_UNSW_01988	malE 2 CDS	1981645	1982490	mRNA	321.96	164.19	909.8	465.3166667
ACAM34_UNSW_00434	tRNA-Ser	438501	438582	tRNA	92.49	51.88	1105.23	416.5333333
ACAM34_UNSW_01332	hypothetical protein CDS	1324048	1324242	mRNA	409.77	300.8	513.81	408.1266667
	ncRNA	629884	629980	ncRNA	367.48	276.31	567.85	403.88
	ncRNA	1815428	1815486	ncRNA	165.27	91.04	877.76	378.0233333
	ncRNA	1222503	1222686	ncRNA	227.29	203.18	677.9	369.4566667
ACAM34_UNSW_01925	hypothetical protein CDS	1908670	1909836	mRNA	209.36	103.67	714.63	342.5533333
ACAM34_UNSW_01914	hypothetical protein CDS	1897274	1898440	mRNA	209.77	103.03	714.56	342.4533333
ACAM34_UNSW_01787	hypothetical protein CDS	1772996	1774162	mRNA	209.03	102.62	714.56	342.07
ACAM34_UNSW_02110	hypothetical protein CDS	2098602	2099768	mRNA	208.8	102.58	714.63	342.0033333
ACAM34_UNSW_01838	hypothetical protein CDS	1825623	1826789	mRNA	208.8	102.53	714.63	341.9866667
ACAM34_UNSW_02067	hypothetical protein CDS	2065190	2066356	mRNA	208.8	102.53	714.63	341.9866667
ACAM34_UNSW_02103	hypothetical protein CDS	2094631	2095797	mRNA	208.8	102.53	714.63	341.9866667
ACAM34_UNSW_02451	hypothetical protein CDS	2405313	2406479	mRNA	208.85	102.53	714.56	341.98
ACAM34_UNSW_01867	hypothetical protein CDS	1852646	1853812	mRNA	208.8	102.53	714.56	341.9633333
ACAM34_UNSW_01949	hypothetical protein CDS	1932046	1933212	mRNA	208.8	102.53	714.56	341.9633333
ACAM34_UNSW_01984	hypothetical protein CDS	1977526	1978692	mRNA	208.8	102.53	714.56	341.9633333
ACAM34_UNSW_01989	hypothetical protein CDS	1982495	1983661	mRNA	208.8	102.53	714.56	341.9633333
ACAM34_UNSW_01829	hypothetical protein CDS	1816384	1817550	mRNA	208.8	102.44	714.32	341.8533333
ACAM34_UNSW_00058	hypothetical protein CDS	53180	54352	mRNA	283.01	145.21	595.68	341.3
ACAM34_UNSW_01044	hypothetical protein CDS	1015830	1017002	mRNA	281.99	144.17	595.68	340.6133333
ACAM34_UNSW_01634	hypothetical protein CDS	1625059	1626231	mRNA	281.99	144.17	595.68	340.6133333

ACAM34_UNSW_01869	hypothetical protein CDS	1855610	1856782	mRNA	281.99	144.17	595.68	340.6133333
ACAM34_UNSW_01802	hypothetical protein CDS	1793729	1794901	mRNA	281.99	144.17	594.87	340.3433333
ACAM34_UNSW_02196	hypothetical protein CDS	2171268	2172440	mRNA	281.99	144.17	594.87	340.3433333
ACAM34_UNSW_00605	tRNA-Ser	604795	604880	tRNA	103.94	39.57	831.94	325.15
ACAM34_UNSW_01982	hypothetical protein CDS	1972787	1975429	mRNA	182.28	104.06	669.42	318.5866667
ACAM34_UNSW_01887	hypothetical protein CDS	1876924	1878090	mRNA	188.93	93.6	664.69	315.74
ACAM34_UNSW_02124	tRNA-Lys	2114119	2114193	tRNA	71.51	56.02	816.22	314.5833333
ACAM34_UNSW_01494	tRNA-Leu	1482015	1482099	tRNA	178.45	122.62	587.51	296.1933333
ACAM34_UNSW_00027	tRNA-Cys	25892	25968	tRNA	137.89	85.64	653.83	292.4533333
ACAM34_UNSW_00120	tRNA-Arg	118230	118303	tRNA	196.93	168.16	500.49	288.5266667
ACAM34_UNSW_00543	nikR 2 CDS	545534	545713	mRNA	257.92	196.17	410.77	288.2866667
ACAM34_UNSW_02556	tRNA-Thr	2502859	2502930	tRNA	52.67	60.56	728.05	280.4266667
ACAM34_UNSW_01809	hypothetical protein CDS	1799609	1800754	mRNA	216.64	117.91	457.1	263.8833333
ACAM34_UNSW_02024	hypothetical protein CDS	2014435	2015580	mRNA	216.03	116.71	457.26	263.3333333
ACAM34_UNSW_02997	hypothetical protein CDS	2939999	2940166	mRNA	287.95	296.6	204.08	262.8766667
ACAM34_UNSW_03028	tRNA-Lys	2971426	2971501	tRNA	302.94	176.33	309.25	262.84
ACAM34_UNSW_02112	tRNA-Arg	2100936	2101010	tRNA	118.46	107.78	503.45	243.23
ACAM34_UNSW_02814	hypothetical protein CDS	2751324	2752190	mRNA	306.35	205.91	152.92	221.7266667
	ncRNA	1762337	1762525	ncRNA	116.94	58.24	419.85	198.3433333
ACAM34_UNSW_00052	hypothetical protein CDS	49494	49688	mRNA	208.91	162.81	164.72	178.8133333
ACAM34_UNSW_02214	tRNA-Arg	2184886	2184960	tRNA	148.79	74.45	250.82	158.02
ACAM34_UNSW_02333	hypothetical protein CDS	2296152	2296901	mRNA	156.88	135.85	178.94	157.2233333
ACAM34_UNSW_02404	50S ribosomal protein L37e CDS	2359611	2359787	mRNA	191.29	192.89	47.41	143.8633333
ACAM34_UNSW_00348	tRNA-Met	359303	359377	tRNA	132.18	91.47	169.02	130.89
ACAM34_UNSW_02199	30S ribosomal protein S28e CDS	2173554	2173778	mRNA	108.1	109.43	167.01	128.18
ACAM34_UNSW_01983	hypothetical protein CDS	1975703	1976956	mRNA	113.01	75.4	192.5	126.97
ACAM34_UNSW_00568	hypothetical protein CDS	573076	573348	mRNA	123.23	64.09	192.51	126.61
ACAM34_UNSW_01516	tfb2 5 CDS	1502243	1503196	mRNA	172.57	127.71	25.77	108.6833333
ACAM34_UNSW_02043	hypothetical protein CDS	2039178	2040176	mRNA	72.18	38.65	214.63	108.4866667
ACAM34_UNSW_00940	hypothetical protein CDS	919601	920599	mRNA	71.74	38.17	214.68	108.1966667
ACAM34_UNSW_01232	hypothetical protein CDS	1222942	1223940	mRNA	71.74	38.17	214.58	108.1633333
ACAM34_UNSW_02051	hypothetical protein CDS	2047296	2048294	mRNA	71.74	38.17	214.58	108.1633333
ACAM34_UNSW_01009	tatA CDS	979288	979572	mRNA	109.68	107.85	93.07	103.5333333

Supplementary Table 2. Differential expression of EV-associated RNA of Hrr. Lacusprofundi ACAM34_UNSW from uninfected cultures normalized to intracellular levels. RNA was isolated from EVs in triplicate and cells in duplicate. Reads were mapped to the Hrr. lacusprofundi

ACAM34_UNSW genome and differential expression calculated using DESeq2 on Geneious Prime (2021.0.1). Only transcripts with TPM > 10 in EVs, log2 fold ratio > 2 and adjusted p-value < 0.05 are presented. Min and Max denote minimum or maximum nucleotide in the genome.

Source	Replicate	Reads Generated	Reads Mapped
EV	1	12,542,814	8,683,378
EV	2	12,748,336	9,397,436
EV	3	14,548,720	10,153,710
Cell	1	10,277,888	7,482,103
Cell	2	14,613,672	11,800,512

locus_tag	Name	Min	Max	RNA type	Average TPM EV	Average TPM cell	Log2 Ratio	Adjusted p-value
ACAM34_UNSW_01545	23S rRNA	1535206	1538105	rRNA	130595.6433	8873.995	6.41034975	3.38237E-43
ACAM34_UNSW_02802	50S ribosomal protein L24 CDS	2744987	2745343	mRNA	17.71	1.86	5.515492249	6.9086E-39
ACAM34_UNSW_02199	30S ribosomal protein S28e CDS	2173554	2173778	mRNA	128.18	16.09	5.432031772	1.89968E-45
ACAM34_UNSW_01344	hypothetical protein CDS	1336847	1337152	mRNA	558.1766667	70.405	5.372138466	9.0324E-12
ACAM34_UNSW_02794	50S ribosomal protein L18 CDS	2740925	2741482	mRNA	21.72	3.365	5.207815229	8.99846E-26
ACAM34_UNSW_02795	50S ribosomal protein L19e CDS	2741482	2741943	mRNA	32.69	5.36	5.124129528	4.20752E-34
ACAM34_UNSW_02715	tRNA-Val	2670975	2671049	tRNA	25978.38333	2509.015	4.9489561	4.23732E-05
ACAM34_UNSW_02793	rps5 CDS	2740285	2740932	mRNA	19.63	4.045	4.840809943	1.84723E-22
ACAM34_UNSW_02796	50S ribosomal protein L32e CDS	2741936	2742646	mRNA	32.41333333	6.855	4.7411045	7.78353E-31
ACAM34_UNSW_02597	tRNA-Glu	2543858	2543932	tRNA	40788.98333	9473.475	4.638990374	2.68775E-21
ACAM34_UNSW_00369	tRNA-Ala	376154	376226	tRNA	1146.11	217.695	4.601374554	3.29743E-30
ACAM34_UNSW_02956	hypothetical protein CDS	2894103	2894456	mRNA	31.96333333	7.945	4.591885896	1.91627E-12
ACAM34_UNSW_02240	tRNA-Leu	2208593	2208677	tRNA	2312.773333	588.07	4.551567519	2.68552E-11
ACAM34_UNSW_02800	rpl5 CDS	2743751	2744275	mRNA	12.76333333	2.87	4.54589998	4.2537E-35
	ncRNA	1037604	1037687	ncRNA	595.4466667	131.38	4.498123504	2.66235E-37
ACAM34_UNSW_02809	30S ribosomal protein S19 CDS	2748156	2748581	mRNA	32.88666667	8.755	4.475953465	3.78284E-11
ACAM34_UNSW_02808	50S ribosomal protein L22 CDS	2747688	2748152	mRNA	25.13333333	6.67	4.439158209	2.62101E-16
ACAM34_UNSW_02797	rpl6 CDS	2742650	2743183	mRNA	24.84333333	4.865	4.363220079	6.6394E-16
ACAM34_UNSW_02806	50S ribosomal protein L29 CDS	2746540	2746749	mRNA	27.80333333	7.975	4.194350433	2.65813E-09
ACAM34_UNSW_01917	tRNA-Ala	1901341	1901414	tRNA	7130.91	1364.255	4.17548366	0.000587002
ACAM34_UNSW_00115	tRNA-Asp	114519	114591	tRNA	2400.223333	667.105	4.110592562	4.1296E-21
ACAM34_UNSW_02898	50S ribosomal protein L10 CDS	2832297	2833334	mRNA	33.84333333	10.215	4.065954014	2.03106E-35
ACAM34_UNSW_02396	hypothetical protein CDS	2353692	2353781	mRNA	15.05	4.23	4.045145407	1.42029E-11
ACAM34_UNSW_02556	tRNA-Thr	2502859	2502930	tRNA	280.4266667	60.415	3.982624717	9.59883E-08
ACAM34_UNSW_02804	30S ribosomal protein S17 CDS	2745744	2746088	mRNA	20.38	8.445	3.824310158	1.05286E-16
ACAM34_UNSW_02810	rpl2 CDS	2748578	2749300	mRNA	15.09	6.25	3.822745309	6.06647E-14
ACAM34_UNSW_02791	50S ribosomal protein L15 CDS	2739327	2739824	mRNA	14.07333333	5.465	3.808713862	3.32543E-24

ACAM34_UNSW_02799	hypothetical protein CDS	2743581	2743754	mRNA	19.72666667	8	3.806851428	1.40674E-15
ACAM34_UNSW_02312	hypothetical protein CDS	2276238	2277245	mRNA	15.44333333	7.06	3.685298292	8.015E-15
ACAM34_UNSW_02897	hypothetical protein CDS	2831940	2832278	mRNA	57.15666667	29.925	3.563787019	8.84624E-10
ACAM34_UNSW_02792	50S ribosomal protein L30 CDS	2739821	2740285	mRNA	14.71	7.6	3.524445449	8.43595E-14
ACAM34_UNSW_02805	hypothetical protein CDS	2746079	2746537	mRNA	11.79333333	5.37	3.499624426	7.42752E-16
ACAM34_UNSW_01288	Desampylase CDS	1279918	1280346	mRNA	13.21333333	6.725	3.488195935	4.3325E-14
ACAM34_UNSW_00449	samp2 CDS	451095	451313	mRNA	11.09333333	4.845	3.467471098	9.6376E-10
ACAM34_UNSW_02807	hypothetical protein CDS	2746750	2747688	mRNA	16.77666667	8.85	3.428564677	1.35065E-18
ACAM34_UNSW_00290	atpF CDS	303324	303653	mRNA	23.44333333	11.915	3.423616803	2.5563E-11
ACAM34_UNSW_02175	tRNA-Leu	2157538	2157623	tRNA	860.55	419.57	3.423303506	7.26853E-20
ACAM34_UNSW_00023	16S rRNA	20596	22064	rRNA	31143.14667	15429.08	3.416501314	1.21793E-05
ACAM34_UNSW_01516	tfb2 5 CDS	1502243	1503196	mRNA	108.6833333	63.765	3.348534452	2.74006E-05
ACAM34_UNSW_02790	secY CDS	2737845	2739323	mRNA	15.02	7.56	3.341644264	3.18807E-22
ACAM34_UNSW_00730	hypothetical protein CDS	723286	723645	mRNA	20.26	10.18	3.271263935	7.21496E-12
ACAM34_UNSW_01753	btuD 21 CDS	1741318	1742292	mRNA	22.87	12.825	3.263985111	3.25886E-14
ACAM34_UNSW_00026	5S rRNA	25629	25744	rRNA	91531.98667	56835.655	3.2221936	5.37136E-10
ACAM34_UNSW_02506	btuD 24 CDS	2458446	2459246	mRNA	10.22	6.155	3.219572983	6.38553E-14
ACAM34_UNSW_01962	hypothetical protein CDS	1945683	1946072	mRNA	10.88666667	3.42	3.199931925	0.001167257
	ncRNA	1435548	1435751	ncRNA	669.3366667	417.53	3.167736617	5.10554E-06
ACAM34_UNSW_00434	tRNA-Ser	438501	438582	tRNA	416.5333333	146.32	3.152640766	0.000116767
ACAM34_UNSW_00470	hypothetical protein CDS	469344	470267	mRNA	81.99666667	55.21	3.150769695	3.41762E-06
ACAM34_UNSW_00884	hypothetical protein CDS	857424	857621	mRNA	37.20666667	20.13	3.134754211	2.37554E-09
ACAM34_UNSW_02172	rps4 CDS	2155693	2156220	mRNA	15.91666667	10.795	3.064765004	1.00488E-11
ACAM34_UNSW_00933	tRNA-Ala	912708	912780	tRNA	14922.24667	6900.77	3.043518331	1.64186E-05
ACAM34_UNSW_00061	tRNA-Pro	56692	56762	tRNA	946.4433333	654.96	3.038238282	1.88949E-12
ACAM34_UNSW_02760	spt4 CDS	2711568	2711765	mRNA	25.15	17.2	2.984064502	2.02217E-09
ACAM34_UNSW_02975	argF CDS	2915284	2916183	mRNA	16.68666667	7.72	2.98404625	3.12133E-05
ACAM34_UNSW_02173	30S ribosomal protein S11 CDS	2156227	2156616	mRNA	23.86	16.44	2.983616718	9.08728E-09
ACAM34_UNSW_00119	hypothetical protein CDS	116382	117887	mRNA	13.11	9.43	2.967076955	4.77492E-12
ACAM34_UNSW_00427	hypothetical protein CDS	429353	432544	mRNA	35.95666667	28.29	2.966190726	4.22877E-07
ACAM34_UNSW_02997	hypothetical protein CDS	2939999	2940166	mRNA	262.8766667	208.79	2.945184434	1.12327E-07
ACAM34_UNSW_01067	ssuD 2 CDS	1037852	1039000	mRNA	12.34	8.94	2.939514121	1.66983E-12
	ncRNA	2771129	2771510	ncRNA	4918.376667	2462.48	2.819120239	0.040057139
ACAM34_UNSW_00291	atpA CDS	303655	305430	mRNA	15.81	13.89	2.752265476	2.6131E-11
ACAM34_UNSW_02438	Digeranylgeranylglyceryl phosphate synthase CDS	2389412	2390275	mRNA	15.22	12.47	2.734961106	1.06705E-14
ACAM34_UNSW_02170	tRNA-Ser	2155029	2155115	tRNA	1296.263333	1082.375	2.721828967	5.03284E-12
ACAM34_UNSW_02174	rpoD CDS	2156618	2157370	mRNA	16.34666667	13.35	2.698615022	3.03403E-10

ACAM34_UNSW_00836	tRNA-Met	817377	817452	tRNA	4043.286667	3625.66	2.674271099	0.001243088
ACAM34_UNSW_00883	hypothetical protein CDS	857257	857427	mRNA	20.65333333	19.885	2.671956873	4.041E-06
ACAM34_UNSW_02814	hypothetical protein CDS	2751324	2752190	mRNA	221.7266667	211.155	2.662153776	4.78133E-06
ACAM34_UNSW_02176	50S ribosomal protein L18e CDS	2157662	2158015	mRNA	52.88333333	51.95	2.655866536	9.46313E-06
	ncRNA	2561924	2561992	ncRNA	1018.173333	947.55	2.572311003	5.63282E-06
ACAM34_UNSW_02641	hypothetical protein CDS	2589059	2589415	mRNA	43.81666667	43.19	2.563998228	5.70226E-07
ACAM34_UNSW_01494	tRNA-Leu	1482015	1482099	tRNA	296.1933333	201.365	2.551862713	4.32342E-05
ACAM34_UNSW_02200	50S ribosomal protein L24e CDS	2173782	2173970	mRNA	64.95333333	65.88	2.551551608	3.84716E-05
ACAM34_UNSW_00728	ndhI 2 CDS	722512	722973	mRNA	19.37666667	15.91	2.54142594	3.16383E-09
ACAM34_UNSW_02811	50S ribosomal protein L23 CDS	2749302	2749556	mRNA	22.36666667	21.36	2.54127358	1.87569E-06
ACAM34_UNSW_00277	ProteinC CDS	290733	291029	mRNA	27.98	26.85	2.516056074	2.00539E-09
ACAM34_UNSW_01913	hypothetical protein CDS	1896858	1897253	mRNA	547.6566667	433.65	2.491721337	2.56885E-06
ACAM34_UNSW_01197	hypothetical protein CDS	1183292	1183579	mRNA	13.40333333	12.4	2.483367646	6.72496E-09
ACAM34_UNSW_00072	btuD 2 CDS	68569	69657	mRNA	10.47	10.235	2.471452702	3.10755E-13
ACAM34_UNSW_00635	30S ribosomal protein S15 CDS	634706	635167	mRNA	22.59666667	23.035	2.4628655	3.085E-11
ACAM34_UNSW_00292	atpB CDS	305432	306856	mRNA	18.07666667	19.75	2.442090177	7.38999E-09
ACAM34_UNSW_00428	50S ribosomal protein L15e CDS	433017	433607	mRNA	34.45666667	38.55	2.400748193	1.0995E-06
ACAM34_UNSW_02201	ndk CDS	2173971	2174450	mRNA	19.97333333	21.135	2.357078171	5.3489E-10
ACAM34_UNSW_00116	tRNA-Asp	114620	114694	tRNA	689.7333333	600.51	2.350345613	2.92648E-05
ACAM34_UNSW_00285	hypothetical protein CDS	298719	299075	mRNA	56.97	62.89	2.322660346	6.75978E-13
ACAM34_UNSW_00349	tRNA-Asn	359516	359588	tRNA	2522.063333	2166.555	2.304266609	2.54669E-05
ACAM34_UNSW_00823	hypothetical protein CDS	806492	807415	mRNA	32.49666667	39.23	2.297106945	2.0904E-07
ACAM34_UNSW_01031	50S ribosomal protein L44e CDS	1005706	1005891	mRNA	39.77333333	49.96	2.281517109	7.26104E-06
ACAM34_UNSW_00844	eif6 CDS	822042	822707	mRNA	10.62333333	10.325	2.210308258	9.5106E-06
ACAM34_UNSW_01809	hypothetical protein CDS	1799609	1800754	mRNA	263.8833333	301.88	2.201866033	1.45483E-07
ACAM34_UNSW_02024	hypothetical protein CDS	2014435	2015580	mRNA	263.3333333	301.82	2.197100299	1.78204E-07
ACAM34_UNSW_01169	hypothetical protein CDS	1156133	1157446	mRNA	12.34	14.02	2.189320815	9.17661E-08
ACAM34_UNSW_00606	hypothetical protein CDS	604931	605242	mRNA	17.53	22.34	2.184970049	1.47805E-05
ACAM34_UNSW_00476	hypothetical protein CDS	475825	476349	mRNA	16.25	19.685	2.176807341	2.86003E-10
ACAM34_UNSW_00584	rpoP CDS	586219	586353	mRNA	20.54	19.165	2.174208114	0.000325469
ACAM34_UNSW_02124	tRNA-Lys	2114119	2114193	tRNA	314.5833333	268.965	2.152544988	0.005481636
	ncRNA	1566573	1566610	ncRNA	3955.36	4711.4	2.136863648	6.092E-12
ACAM34_UNSW_00845	50S ribosomal protein L31e CDS	822709	822987	mRNA	19.44666667	25.29	2.099509615	2.28204E-07
ACAM34_UNSW_00966	hypothetical protein CDS	943501	944025	mRNA	12.46333333	13.635	2.072708135	3.14622E-05
ACAM34_UNSW_00885	IMPDH 2 CDS	857682	858221	mRNA	20.81333333	30.845	2.048524346	1.40771E-05
ACAM34_UNSW_01708	putative ribosome biogenesis protein CDS	1697201	1697704	mRNA	24.79333333	34.5	2.045559707	5.63948E-08

ACAM34_UNSW_02344	hypothetical protein CDS	2305222	2305416	mRNA	914.1733333	1293.015	2.038912413	2.38303E-06
ACAM34_UNSW_02178	rps9 CDS	2158455	2158853	mRNA	13.04333333	20.83	2.024899218	0.000785559
ACAM34_UNSW_02899	rpl1 CDS	2833331	2833969	mRNA	32.65666667	48.83	2.013188748	4.90463E-06
ACAM34_UNSW_02544	hypothetical protein CDS	2493034	2494365	mRNA	17.00333333	16.225	2.010462834	0.005757071

Supplementary Table 3. Predicted mRNA targets of EV-enriched ncRNA. Targets were predicted against Hrr. lacusprofundi ATCC 49239 (GCF_000022205.1) using IntaRNA (Version 3.3.1) (Mann et al. 2017, Wright et al. 2014, Busch et al. 2008, Raden et al. 2018). Target searches were restricted to 50 nt before and after the start codon (denoted by start and end in the table). Complementary base pairing is denoted by seedStart and seedEnd. Targets were only presented with p-value < 0.05 and false discovery rate (fdr) < 0.5. E represents the energy score of the interaction (kcal/mol), E_hybrid the hybridization free energy (kcal/mol), and E_norm the energy score normalized to the length.

id1	start1	end1	seedStart1	seedEnd1	ED1	id2	start2	end2	seedStart2	seedEnd2	ED2	E	E_hybrid	E_norm	p-value	fdr	annotation
HLAC_RS07760	60	93	64	70	7.06	ncRNA1	24	56	45	51	4.92	-26.25	-38.23	-2.90505	0.0001595	0.27753	CinA family protein
HLAC_RS05565	26	93	87	93	17.25	ncRNA2	96	178	96	102	23.22	-33.39	-73.86	-3.36481	0.0001496	0.229395	anaerobic glycerol-3-phosphate dehydrogenase subunit C
HLAC_RS07760	34	95	63	69	17.06	ncRNA2	94	174	122	128	23.02	-32.32	-72.4	-3.25698	0.0002158	0.229395	CinA family protein
HLAC_RS06310	6	88	6	12	12.99	ncRNA2	114	199	193	199	25.7	-30.52	-69.21	-3.07559	0.0003983	0.295939	tryptophan synthase subunit beta
HLAC_RS19450	62	94	87	93	9.72	ncRNA2	83	120	84	90	9.13	-30.07	-48.92	-3.03024	0.000464	0.295939	PGF-CTERM sorting domain-containing protein
HLAC_RS14570	1	41	12	18	22.51	ncRNA3	1	41	24	30	25.63	-53.06	-101.2	-6.32468	2.80E-06	0.003942	Derived by automated computational analysis using gene prediction method: GeneMarkS-2+.
HLAC_RS15710	9	77	10	16	34.22	asRNA1	1	69	62	68	30	-94.81	-159.03	-10.726	0.0000028	0.000873	ISH6-like element ISHla10 family transposase
HLAC_RS15095	9	77	10	16	34.22	asRNA1	1	69	62	68	30	-94.81	-159.03	-10.726	0.0000028	0.000873	ISH6-like element ISHla10 family transposase
HLAC_RS11180	9	77	10	16	34.22	asRNA1	1	69	62	68	30	-94.81	-159.03	-10.726	0.0000028	0.000873	ISH6-like element ISHla10 family transposase
HLAC_RS13805	9	77	10	16	34.22	asRNA1	1	69	62	68	30	-94.81	-159.03	-10.726	0.0000028	0.000873	ISH6-like element ISHla10 family transposase
HLAC_RS18925	9	77	59	65	25.52	asRNA1	1	69	13	19	30	-47.45	-102.97	-5.36809	0.0000671	0.016735	ISH6 family transposase
HLAC_RS04555	18	71	47	53	34.2	asRNA2	1	54	19	25	25.96	-53.22	-113.38	-6.19258	0.000204	0.028584	IS6 family transposase
HLAC_RS17780	18	71	19	25	30.36	asRNA2	1	54	47	53	25.96	-49.45	-105.77	-5.75391	0.0002745	0.028584	IS6 family transposase
HLAC_RS17770	19	71	19	25	30.15	asRNA2	1	53	47	53	25.96	-48.79	-104.9	-5.67711	0.0002897	0.028584	IS6 family transposase
HLAC_RS11985	9	26	9	15	5.97	ncRNA8	10	28	22	28	1.26	-19.26	-26.49	-2.39577	0.00029	0.36656	b(o/a)3-type cytochrome-c oxidase subunit 1

Supplementary Table 4. RNA sequencing of EV-associated RNA from infected cultures. RNA was isolated from EVs in duplicate from cultures infected with HRTV-DL1 and mapped to the Hrr. lacusprofundi ACAM34_UNSW genome using Geneious Prime (2021.0.1). Relative abundance was calculated by transcripts per million (TPM). Only transcripts with TPM > 100 are presented. Min and Max denote minimum or maximum nucleotide in the genome.

Replicate	Reads Generated	Reads Mapped
1	9,144,584	6,516,464
2	4,001,091	677,194

locus_tag	Name	Min	Max	RNA type	TPM 1	TPM 2	Average TPM - EV
ACAM34_UNSW_00026	5S rRNA	25629	25744	rRNA	66381.78	239560.2	152971
ACAM34_UNSW_00023	16S rRNA	20596	22064	rRNA	170881.5	60385.93	115633.7
ACAM34_UNSW_01545	23S rRNA	1535206	1538105	rRNA	85846.44	36675.77	61261.11
ACAM34_UNSW_02597	tRNA-Glu	2543858	2543932	tRNA	19909.82	4266.77	12088.3
	ncRNA	2771129	2771510	ncRNA	16801.57	3384.45	10093.01
	ncRNA	1976995	1977036	ncRNA	14504.03	3156.29	8830.16
ACAM34_UNSW_00836	tRNA-Met	817377	817452	tRNA	6276.92	2377.27	4327.095
	asRNA	1932024	1932051	ncRNA	1315.33	3894.46	2604.895
ACAM34_UNSW_02715	tRNA-Val	2670975	2671049	tRNA	3365.83	674.7	2020.265
ACAM34_UNSW_02165	tRNA-Pro	2151555	2151625	tRNA	1254.93	1887.18	1571.055
ACAM34_UNSW_02170	tRNA-Ser	2155029	2155115	tRNA	2819	184.32	1501.66
ACAM34_UNSW_02154	tRNA-His	2140510	2140583	tRNA	499.92	1473.58	986.75
	ncRNA	875429	875787	ncRNA	1356.19	325.58	840.885
	ncRNA	1967830	1968033	ncRNA	1231.37	323.17	777.27
ACAM34_UNSW_03069	tRNA-Gln	3020453	3020525	tRNA	649.3	766.41	707.855
ACAM34_UNSW_01008	tRNA-Arg	979161	979234	tRNA	928.43	462.3	695.365
ACAM34_UNSW_01007	tRNA-Arg	979143	979218	tRNA	904	450.13	677.065
	asRNA	1015806	1015844	ncRNA	389.59	804.08	596.835
	asRNA	1223934	1223964	ncRNA	612.67	425.33	519
ACAM34_UNSW_00933	tRNA-Ala	912708	912780	tRNA	562.2	458.87	510.535
	ncRNA	1435548	1435751	ncRNA	693.4	235.82	464.61
ACAM34_UNSW_02333	hypothetical protein CDS	2296152	2296901	mRNA	519.46	228.54	374
ACAM34_UNSW_02344	hypothetical protein CDS	2305222	2305416	mRNA	437.45	239.4	338.425
ACAM34_UNSW_01047	tRNA-Gly	1018454	1018524	tRNA	309.37	316.2	312.785
ACAM34_UNSW_00060	tRNA-Phe	56281	56354	tRNA	188.59	399.7	294.145
	ncRNA	1566573	1566610	ncRNA	147.77	318.84	233.305
ACAM34_UNSW_01839	hypothetical protein CDS	1826794	1827123	mRNA	129.37	333.68	231.525
ACAM34_UNSW_01066	tRNA-Leu	1037500	1037584	tRNA	391.51	71.27	231.39
ACAM34_UNSW_02240	tRNA-Leu	2208593	2208677	tRNA	428.43	33.54	230.985
ACAM34_UNSW_01917	tRNA-Ala	1901341	1901414	tRNA	263.35	192.62	227.985
ACAM34_UNSW_01693	tRNA-Gly	1684848	1684919	tRNA	159.42	262.32	210.87
	ncRNA	1945630	1945673	ncRNA	208.32	202.47	205.395
ACAM34_UNSW_01769	tRNA-Tyr	1752408	1752482	tRNA	146.44	256.58	201.51
ACAM34_UNSW_01890	tfb2 7 CDS	1880721	1881647	mRNA	281.94	94.57	188.255
ACAM34_UNSW_01332	hypothetical protein CDS	1324048	1324242	mRNA	204.96	140.71	172.835
	ncRNA	1037604	1037687	ncRNA	268.37	42.42	155.395
ACAM34_UNSW_02890	tRNA-Val	2827791	2827864	tRNA	218.72	86.68	152.7
	ncRNA	629884	629980	ncRNA	115.78	176.34	146.06
ACAM34_UNSW_02816	tRNA-Gly	2753764	2753834	tRNA	73.27	215.82	144.545

	ncRNA	1222503	1222686	ncRNA	203.75	85.22	144.485
	ncRNA	2540081	2540238	ncRNA	129.61	148.86	139.235
ACAM34_UNSW_02903	hypothetical protein CDS	2836639	2837709	mRNA	222.21	51.91	137.06
ACAM34_UNSW_02545	hypothetical protein CDS	2494468	2494581	mRNA	88.37	184.43	136.4
ACAM34_UNSW_01983	hypothetical protein CDS	1975703	1976956	mRNA	207.3	64.79	136.045
ACAM34_UNSW_00369	tRNA-Ala	376154	376226	tRNA	208.14	48.82	128.48
ACAM34_UNSW_00501	tRNA-Gln	502186	502258	tRNA	115.38	141.57	128.475
ACAM34_UNSW_00022	hypothetical protein CDS	20374	20517	mRNA	182.93	64.34	123.635
ACAM34_UNSW_01668	tRNA-Val	1661563	1661638	tRNA	98.87	135.98	117.425
ACAM34_UNSW_01968	hypothetical protein CDS	1951430	1952497	mRNA	180.08	53.39	116.735
ACAM34_UNSW_01959	hypothetical protein CDS	1943241	1944494	mRNA	174.83	44.33	109.58
ACAM34_UNSW_00349	tRNA-Asn	359516	359588	tRNA	110.86	107.39	109.125
ACAM34_UNSW_00433	hypothetical protein CDS	438077	438250	mRNA	89.22	118.79	104.005

Supplementary Table 5. Differential expression of EV-associated RNA of Hrr. Lacusprofundi ACAM34_UNSW from HLTV-DL1 infected cultures normalized to intracellular levels. RNA was isolated from EVs in duplicate and cells in triplicate. Reads were mapped to the Hrr. lacusprofundi ACAM34_UNSW genome and differential expression calculated using DESeq2 on Geneious Prime (2021.0.1). Only transcripts with TPM > 10 in EVs, log2 fold ratio > 1 and adjusted p-value < 0.05 are presented. Min and Max denote minimum or maximum nucleotide in the genome.

Source	Replicate	Reads Generated	Reads Mapped
EV	1	9,144,584	6,516,464
EV	2	4,001,091	677,194
Cell	1	9,239,664	6,302,231
Cell	2	14,532,142	10,701,568
Cell	3	7,260,371	4,031,615

locus_tag	Name	Min	Max	Average TPM EV	Average TPM Cell	Log2 Ratio	Adjusted p-value
ACAM34_UNSW_01890	tfb2 7 CDS	1880721	1881647	94.57	1.06	8.326974333	8.64E-46
ACAM34_UNSW_00023	16S rRNA	20596	22064	60385.93	3160.8	6.510414393	4.59E-35
ACAM34_UNSW_01545	23S rRNA	1535206	1538105	36675.77	3374.37	5.866012244	1.65E-34
	ncRNA	2771129	2771510	3384.45	561.32	5.278180896	1.23E-11
ACAM34_UNSW_01966	hypothetical protein CDS	1949296	1949718	14.32	4.12	4.740436456	4.24E-12

ACAM34_UNSW_00026	5S rRNA	25629	25744	239560.18	8647.93	4.557917666	2.36E-10
ACAM34_UNSW_02018	hypothetical protein CDS	2008122	2008562	18.59	1.84	4.419711301	2.51E-34
ACAM34_UNSW_02076	hypothetical protein CDS	2073627	2074313	37.35	7.57	4.237496187	1.50E-27
ACAM34_UNSW_02004	hypothetical protein CDS	1998032	1998355	20.9	4.72	4.190288258	2.36E-29
	ncRNA	1435548	1435751	235.82	73.77	3.998247858	5.05E-13
ACAM34_UNSW_01007	tRNA-Arg	979143	979218	450.13	86.03	3.859599027	3.61E-10
ACAM34_UNSW_01008	tRNA-Arg	979161	979234	462.3	87.83	3.859077377	3.46E-10
ACAM34_UNSW_02012	hypothetical protein CDS	2002804	2003205	11.52	1.4	3.77277362	4.99E-05
ACAM34_UNSW_01560	hypothetical protein CDS	1555270	1557246	27.22	24.08	3.65991013	4.00E-06
ACAM34_UNSW_00433	hypothetical protein CDS	438077	438250	118.79	34.02	3.579993135	1.61E-20
ACAM34_UNSW_01861	hypothetical protein CDS	1847540	1847824	36.26	13.71	3.309457767	7.92E-21
ACAM34_UNSW_01797	DNA repair protein Mre11 CDS	1787628	1788560	20.24	10.1	3.083754455	3.01E-19
ACAM34_UNSW_02170	tRNA-Ser	2155029	2155115	184.32	588.98	2.672756059	0.00889362
ACAM34_UNSW_03063	hypothetical protein CDS	3013383	3014231	16.79	10.05	2.432646506	8.46E-15
ACAM34_UNSW_01921	hypothetical protein CDS	1905747	1906136	12.79	4.22	2.409403743	0.00188632
ACAM34_UNSW_01955	hypothetical protein CDS	1940206	1941216	11.63	9.87	2.313245104	1.13E-11
ACAM34_UNSW_00836	tRNA-Met	817377	817452	2377.27	3023.71	2.279512978	5.54E-05
ACAM34_UNSW_01217	hypothetical protein CDS	1204289	1204990	10.66	4.77	2.220763675	2.59E-09
ACAM34_UNSW_01810	hypothetical protein CDS	1800808	1801164	26.95	56.73	2.008133907	0.005334922
ACAM34_UNSW_02070	hypothetical protein CDS	2068405	2068533	16.57	30.29	1.834688429	0.000567932
ACAM34_UNSW_02333	hypothetical protein CDS	2296152	2296901	228.54	350.84	1.787310664	0.000724365
ACAM34_UNSW_02715	tRNA-Val	2670975	2671049	674.7	1421.37	1.738266266	0.043848766
ACAM34_UNSW_00470	hypothetical protein CDS	469344	470267	21.21	15.64	1.735270542	2.48E-07
ACAM34_UNSW_00588	hypothetical protein CDS	587581	587778	10.8	11.53	1.686912841	0.000782773
ACAM34_UNSW_00293	atpD CDS	306978	307664	14.01	16.81	1.660794948	2.42E-07
ACAM34_UNSW_02344	hypothetical protein CDS	2305222	2305416	239.4	351.26	1.604146689	0.000246644
ACAM34_UNSW_01836	hypothetical protein CDS	1822890	1825094	10.34	19.98	1.381195285	0.004210223
ACAM34_UNSW_01788	hypothetical protein CDS	1774320	1775642	11.85	19.93	1.186153151	0.033237457
ACAM34_UNSW_02760	spt4 CDS	2711568	2711765	10.8	16.12	1.121478633	0.01009549
ACAM34_UNSW_01963	hypothetical protein CDS	1946193	1946594	18.62	18.72	1.117410442	0.005762106

Supplementary Table 6. Transcriptomic differential expression 2 hours after incubation with EVs. RNA was isolated from cells after incubation with EVs in triplicate and RNA library was prepared using small RNA library preparation kit. Reads were mapped to the Hrr. lacusprofundi ACAM34_UNSW genome and differential expression calculated using DESeq2 on Geneious Prime (2021.0.1). Only transcripts with TPM > 10 in at least one condition, fold ratio > |1.5|, and adjusted p-value < 0.02 are presented. Condition A: cells not incubated with EVs. Condition B: cells incubated with EVs from uninfected cultures. Condition C: cells incubated with EVs from infected cultures.

Source	Replicate	Reads Generated	Reads Mapped
A	1	13,492,886	8,666,998
A	2	14,202,774	8,750,602
A	3	14,532,242	10,432,729
B	1	14,601,400	9,862,860
B	2	11,120,318	6,597,985
B	3	12,161,724	7,737,466
C	1	15,566,118	11,080,450
C	2	15,536,998	10,799,980
C	3	14,455,014	10,522,622

Condition B normalized to A: Upregulated

locus_tag	Name	arCOG	Minimum	Maximum	Average A	Average B	Log2 Ratio	Adjusted p-value
	ncRNA		922183	922236	513.90	1069.83	0.890677784	2.48E-07
ACAM34_UNSW_02188	hypothetical protein	S	2165400	2165738	10.10	19.67	0.732752618	0.000614

Condition B normalized to A: Downregulated

locus_tag	Name	arCOG	Minimum	Maximum	Average A	Average B	Log2 Ratio	Adjusted p-value
ACAM34_UNSW_02927	Chemoreceptor glutamine deamidase, CheD	T	2862255	2862782	26.62	13.36	-0.73791796	1.57E-05
ACAM34_UNSW_02654	hypothetical protein CDS	S	2605461	2605931	17.93	9.79	-0.65634598	0.000167
ACAM34_UNSW_01879	Beta-galactosidase Bga CDS	G	1865950	1868052	100.16	50.72	-0.6637177	0.000394
ACAM34_UNSW_01673	integrase/recombinase XerC 2	L	1666167	1667168	53.36	28.08	-0.64521229	0.000394
ACAM34_UNSW_00599	transposase, IS605 OrfB family	X	597223	598536	163.04	79.86	-0.66838623	0.000904
ACAM34_UNSW_01817	hypothetical protein CDS	S	1806614	1806976	385.75	157.42	-0.73722764	0.001592
ACAM34_UNSW_02567	OsmC family protein	R	2512844	2513350	36.99	19.82	-0.60259106	0.00239
ACAM34_UNSW_02553	tRNA-Gly		2501210	2501280	51971.75	27981.49	-0.62676666	0.004477
ACAM34_UNSW_01990	extracellular solute-binding protein	R	1983829	1984374	78.59	37.52	-0.60499895	0.016153
ACAM34_UNSW_02437	Protein translation factor SUI1 CDS	J	2389001	2389294	1975.70	902.01	-0.61466463	0.016796

Condition C normalized to A: Upregulated

locus_tag	Name	arCOG	Minimum	Maximum	Average A	Average C	Log2 Ratio	Adjusted p-value
	ncRNA		922183	922236	513.9	793.9433	0.801170305	3.74E-06

Condition C normalized to A: Downregulated

locus_tag	Name	arCOG	Minimum	Maximum	Average A	Average C	Log2 Ratio	Adjusted p-value
ACAM34_UNSW_02927	Chemoreceptor glutamine deamidase, CheD	T	2862255	2862782	26.62	11.61667	-0.67689537	0.005204
ACAM34_UNSW_02567	OsmC family protein	R	2512844	2513350	36.99	16.77333	-0.61946144	0.006569

Supplementary Table 7. Transcriptomic differential expression 12 hours after incubation with EVs from uninfected cultures. RNA was isolated from cells 12 hours after incubation with EVs in triplicate. Libraries were prepared using normal RNA library preparation kit. Reads were mapped to the Hrr. lacusprofundi ACAM34_UNSW genome and differential expression calculated using DESeq2 on Geneious Prime (2021.0.1). Only transcripts with TPM > 10 in at least one condition, fold ratio > |1.5|, and adjusted p-value < 0.02 are presented. Condition A: cells not incubated with EVs. Condition B: cells incubated with EVs from uninfected cultures.

Source	Replicate	Reads Generated	Reads Mapped
A	1	10,176,050	10,070,678
A	2	11,864,374	11,782,110
A	3	11,474,874	11,333,883
B	1	12,898,504	12,679,258
B	2	9,528,840	9,348,859
B	3	11,254,412	11,025,081

locus_tag	Name	arCOG	Min	Max	Average A	Average B	Log2 Ratio	Adjusted p-value
ACAM34_UNSW_00868	zinc ABC transporter substrate-binding protein	R	844182	845195	13.73667	97.82333	1.72451358	7.81E-16
ACAM34_UNSW_00130	hypothetical membrane bound protein	S	127514	128425	72.64667	293.52	1.31323724	2.33E-15
ACAM34_UNSW_01519	acyl-CoA dehydrogenase family protein	I	1505887	1507035	51.86667	186.94	1.19761363	1.06E-14
ACAM34_UNSW_03047	CARDB domain-containing protein	R	2993008	2994837	4.196667	15.13	1.15186548	9.71E-10
ACAM34_UNSW_00137	signal peptidase I	U	136537	137598	40.22667	148.4733	1.05485973	1.67E-06
ACAM34_UNSW_01338	acyl-CoA dehydrogenase family protein	I	1329857	1331011	59.22	182.4467	1.02264227	1.42E-09
ACAM34_UNSW_00131	hypothetical, DNA-binding, membrane bound protein	S	128659	129222	24.53	77.39333	0.98704889	1.17E-06
ACAM34_UNSW_00136	SipW-dependent-type signal peptide-containing protein	R	135458	136537	58.78	198.7333	0.96350367	1.85E-05
ACAM34_UNSW_01520	YeeE/YedE family protein	R	1507119	1507607	34.76667	102.1867	0.96319682	1.60E-07
ACAM34_UNSW_00135	hypothetical signal peptide-containing protein	S	134667	135461	66.89333	206.4733	0.95209402	1.67E-06
ACAM34_UNSW_02573	long-chain fatty acid--CoA ligase	I	2517829	2519886	19.33	54.42333	0.93130424	4.84E-11
ACAM34_UNSW_00745	MTH865 family protein	S	741149	741406	95.65667	262.46	0.87068568	3.06E-06
ACAM34_UNSW_00138	hypothetical signal peptide-containing protein	S	137598	138137	41.96	134.8067	0.84680195	0.0011031
ACAM34_UNSW_01154	hypothetical protein	S	1142311	1142616	15.67667	41.50333	0.7590296	0.0011508 6
ACAM34_UNSW_01774	tRNA-Leu		1757705	1757793	74.28333	192.38	0.70479065	0.0087881 3
ACAM34_UNSW_00834	hypothetical protein	S	816355	816507	27.9	69.05667	0.66590035	0.0199271 4
ACAM34_UNSW_02749	hypothetical protein	S	2702811	2703071	140.46	327.6633	0.66472099	0.0044352 2
ACAM34_UNSW_02302	hypothetical protein	S	2267276	2267695	167.1833	371.6933	0.64993356	0.0006829 5
ACAM34_UNSW_02559	PadR family transcriptional regulator	K	2505124	2505399	379.5033	839.5167	0.61243626	0.0011508 6

ACAM34_UNSW_02206	thiolase family protein	I	2177667	2178809	88.10333	188.6233	0.58872688	0.0180550 3
ACAM34_UNSW_02928	FlaD/FlaE family flagellar protein	N	2862902	2864764	854.13	753.7167	-0.5878917	0.0100069 2
ACAM34_UNSW_02926	chemotaxis protein CheC	T	2861059	2862258	239.6933	199.47	-0.5898674	0.0107878 9
ACAM34_UNSW_02627	protein-glutamate O-methyltransferase CheR	T	2575256	2576065	571.84	513.8133	-0.5935318	0.0009512 9
ACAM34_UNSW_03049	PAS domain-containing protein	T	2996015	2997565	339.5367	290.0333	-0.6110176	0.0011508 6
ACAM34_UNSW_00511	hypothetical protein	S	510543	511595	1067.7	934.6333	-0.6483265	0.0006661 1
ACAM34_UNSW_02093	hypothetical protein	S	2086616	2087101	49.59	42.70333	-0.6486523	0.0044352 2
ACAM34_UNSW_00090	methyl-accepting chemotaxis protein	T	87996	89711	834.16	704.06	-0.6487217	0.0018693 4
ACAM34_UNSW_01449	ABC transporter permease	C P	1440530	1441585	67.91333	57.21667	-0.65397	0.0005078 3
ACAM34_UNSW_03092	methyl-accepting chemotaxis sensory transducer with Pas/Pac sensor	T	3040470	3042194	385.49	322.7067	-0.6544944	0.0021277 7
ACAM34_UNSW_02931	Archaellum biogenesis protein FlaH	N	2865722	2866471	518.99	442.9167	-0.6626726	1.29E-05
ACAM34_UNSW_01448	ABC transporter permease	C P	1438585	1440537	87.63333	68.35	-0.6726493	0.0014045 8
ACAM34_UNSW_03063	hypothetical protein	S	3013383	3014231	180.8267	147.36	-0.6744936	0.0004503 4
ACAM34_UNSW_02626	chemotaxis protein CheA	T	2573034	2575259	656.51	523.53	-0.7055303	0.0004164 3
ACAM34_UNSW_02929	Archaellum component FlaG	N	2864754	2865221	822.5833	666.9967	-0.7092047	0.0006829 5
ACAM34_UNSW_02591	MscS Mechanosensitive ion channel	M	2537262	2538482	70.84667	55.04667	-0.7128399	0.0002406 6
ACAM34_UNSW_02094	ParA family protein	D N	2087094	2087966	58.96	48.34	-0.7193772	0.0047590 6
ACAM34_UNSW_02930	Archaellum component FlaG	N	2865222	2865719	600.0833	484.82	-0.7243903	3.19E-05
ACAM34_UNSW_01712	hypothetical protein	S	1701896	1702135	639.8533	488.89	-0.760729	1.85E-05
ACAM34_UNSW_02399	Rad50 ATPase-containing protein	R	2356041	2357048	695.6967	538.8067	-0.7712123	0.0005078 3
ACAM34_UNSW_02400	hypothetical protein	S	2357045	2357665	886.82	668.0433	-0.7899206	2.62E-05
ACAM34_UNSW_02517	HAMP domain-containing sensor histidine kinase	T	2469187	2470362	63.08	45.84667	-0.7987974	4.92E-05
ACAM34_UNSW_01711	methyl-accepting chemotaxis sensory transducer	T	1700138	1701871	546.2933	392.9467	-0.8401511	1.85E-05
ACAM34_UNSW_02653	methyl-accepting chemotaxis protein	T	2603614	2605425	168.6267	116.37	-0.8491138	1.99E-05
ACAM34_UNSW_00022	hypothetical protein	S	20374	20517	4583.547	2736.617	-0.9440985	0.0006661 1
ACAM34_UNSW_02921	archaellin/type IV pilin N-terminal domain-containing protein	N	2855959	2856690	4946.223	3081.11	-0.9935252	1.40E-06

CHAPTER V. DISCUSSION AND PERSPECTIVES

5.1 A STANDARDIZED METHOD FOR THE ISOLATION AND ANALYSIS OF ARCHAEAL EXTRACELLULAR VESICLES

In the process of characterizing EVs from various haloarchaea, we developed a method for the purification and further downstream analysis of EVs [1]. As interest into EVs is increasing, with few publications regarding EVs in the archaeal domain [2], we thought that it would be relevant to establish a common work flow for the purification of archaeal EVs. In this way, results from each study could be comparable with one another. The method described involves the removal of cells through centrifugation and filtration, and the concentration of EVs through precipitation and density gradient purification. Other methods have relied on ultracentrifugation of cell-free supernatants to concentrate EVs from Archaea [3, 4]. However, it has been shown that ultracentrifugation of EV preparations can sometimes result in damaged EVs [5]. To investigate the interactions between EVs and cells, we required a method that minimally affected the natural structure and composition of EVs. We therefore opted for a gentler method of purification involving the precipitation of EVs by the addition of polymers followed by low-speed centrifugation [6]. The method has so far been successful for the characterization of EVs from haloarchaeal organisms, such as *Haloferax volcanii*, *Halorubrum lacusprofundi* and *Halobacterium salinarum*. EVs from *H. volcanii* that were isolated using this approach were demonstrated to transfer RNA, confirming that the EV purification method results in viable EVs. While EV preparations from *Thermococcales* species have also been shown to transfer nucleic acids, even though they were purified through ultracentrifugation [4], it remains unknown whether a large proportion of the EVs might have been damaged. Therefore, I would recommend to test several purification methods and their effects on the ability for EVs to transfer compounds. The advantage of our described method is the ability to quickly process large volumes of sample. Polyethylene glycol (PEG)-based precipitation can pellet around 900 mL of supernatant over 50 min, while ultracentrifugation can process less than 100 mL over a longer period of time. This is advantageous when high amounts of biomass are needed, or for organisms that do not reach high cell densities.

I also developed two additional methods to quantify EV production. Typically, others have used nanoparticle tracking analysis or high resolution flow cytometry to provide exact numbers of EV particles [7, 8]. However, as both methods require expensive and highly specialized machinery, we needed to find an alternative solution to characterize the rate of EV production. The first method was based on immunodetection, using a highly abundant EV-associated protein, CetZ1. The second method utilized a fluorescent stain. Both showed their own advantages and disadvantages, which required us to deploy one method over the other depending on the conditions we were testing. The first method proved unsuccessful when comparing between different temperatures. Since the first method is dependent on the amount of CetZ1 that is packaged into EVs, we presume that temperature affects the packaging of CetZ1, making this method of enumeration unreliable. However, it remains to be tested if there is an actual difference in the amount of CetZ1 packaged in different temperatures. Further, the first method requires prior knowledge of the protein composition of EVs for the respective organism and the production of antibodies for these proteins. The second method proved unsuccessful for quantifying EVs during viral infection, as viral particles were also stained by the fluorescent dye. It was successful in

quantifying EV production in all other conditions though, and was a reliable alternative to the first method. Therefore, when possible, we used both methods and determined whether a similar result was obtained. While both methods do not provide exact quantities of EVs in culture supernatants, they still provided valuable information for quantifying the relative abundancies across the different conditions tested.

In principle, the methods discussed should also be adaptable to other Archaea, provided that the respective buffers are used and that one takes into consideration the possible introduction of biases. PEG precipitation has been successfully utilized for the purification of viruses from thermophilic archaea [9], acidophilic archaea [10], as well as the isolation of EVs from marine environments [11]. Since EVs often end up in the same population as viruses during purification [12], I would predict that the EV purification method described here would also work for the isolation of EVs from Archaea that inhabit a diverse range of environments. Though the particular fluorescent stain that we used in our studies has not been confirmed to work in organisms from other non-moderate conditions, there are other alternative stains for lipids and proteins [13] that could be deployed for the enumeration of EVs from other Archaea. While EV production in other culturable archaeal organisms remains uncharacterized, hopefully the work flow that we have provided will stimulate additional explorations into this field.

5.2 New perspectives on extracellular vesicle production in Archaea

Before our study on haloarchaeal EVs presented in Chapter III, the only other archaeal organism for which an EV production mechanism has been described comes from the *Thermoproteota* phylum. Specifically in *Sulfolobus*, it was shown that its ESCRT-like cell division system was involved in the production of EVs [3, 14]. However, ESCRT-like proteins are not encoded in all major branches of the archaeal tree, and are missing in lineages such as *Euryarchaeota* [15]. Nevertheless, euryarchaeotal organisms have been observed to produce EVs [4, 16, 17], suggesting that multiple mechanisms for EV production exist within the archaeal domain. Among haloarchaea, various proteins were identified in the EVs of both *H. volcanii* and *Hrr. lacusprofundi* [16] that provide some clues as to the mechanism behind EV production among haloarchaea. Further, I also identified other haloarchaeal proteins that are not present in EVs, but still are involved in EV-production. While many questions remain as to the exact roles of the proteins involved, the results presented in Chapter III provides a first glimpse into the mechanisms driving EV production in haloarchaea. Based on this, we can already start to construct a model based on what we have uncovered and what we know about other vesicle producing machineries.

5.2.1 Extracellular vesicle production is conditional in H. volcanii

Initial attempts to isolate EVs from *H. volcanii* at the optimal growth temperature (45 °C) yielded low amounts of EVs. Upon lowering the growth temperature, we observed increased amounts of EVs, which was also quantifiable. This suggested that the abundance of EVs in culture supernatants was linked to certain external factors. We also observed a slight induction of EV production when cultures were treated with UV radiation, similar to what was observed in a different study [18], though no significant changes upon viral infection. There are other external stimuli such as salt concentration, pH, or oxidative stress that could also be explored and likely also impact EV production.

The conditional production of EV trafficking suggests that it is a process that requires regulation to some extent. In Bacteria, gene knock out of different global transcriptional regulators has been observed to influence EV production [19–21]. Perhaps exploring the EV production of knock out strains for transcriptional regulators in *H. volcanii* could provide clues into this regulatory network and how it interacts with other cellular networks. The potential regulators could be further narrowed down by comparing gene expression between conditions that stimulate and repress EV production. Exploring these regulatory networks may also help determine other components of the EV production machinery that are not enclosed in EVs and were therefore not identified in our study.

The amount of EVs present in culture supernatants is related to the sum of the rate of EV production and the rate of EV uptake. Therefore changes detected in the quantity of EVs in culture supernatants could be explained by a change in either of these parameters. However, in order to address this question, one would require additional information about how the mechanisms for EV production and EV uptake work and how they are regulated. It is likely that specific external factors trigger specific nodes in the regulation network for EV trafficking. One could calculate the rate of production from the amount of EVs present and the rate of uptake, and observe how this changes throughout the course of growth or a gradient of specific stimuli.

5.2.2 The archaeal vesiculating GTPase, ArcV

The most striking discovery from the characterization of *H. volcanii* EVs was the involvement of a small GTPase that we have renamed, ArcV. ArcV was identified to be abundantly associated with EVs from two different haloarchaeal organisms [16, 17]. When compared with the relative abundance in the cell membrane, ArcV was identified to be enriched in EVs. Knocking out ArcV results in a severe deficiency in the production of RNA-associated EVs, strongly suggesting that ArcV plays a crucial role in EV production among haloarchaea. While ArcV could be regulating EV production indirectly through the activation of transcriptional regulators or other downstream effectors, the abundance of the protein in the EV fraction suggests that the GTPase is directly involved in EV production. Bacterial EV production has so far been observed to be stimulated by various indirect factors, such as for example the enrichment of saturated lipids [22, 23] or cell death [24]. So far, no bacterial proteins have been identified to be directly involved in EV production. In contrast, eukaryotic vesicle production involves extensive protein-mediated membrane remodeling [25, 26]. Considering our data, and data from *Sulfolobus* [3, 14], I propose that EV production in Archaea is driven protein-mediated membrane remodeling, as has been described for Eukaryota.

ArcV was observed to be present in the cell membrane fraction despite not being predicted to be an integral membrane or a transmembrane protein. Based on the structural prediction of the ArcV dimer, I predict that ArcV functions in a similar manner as Arf-family GTPases, in that activation by GTP allows for membrane interaction through an N-terminal α-helix [27]. While we were able to induce EV overproduction with an N-terminal tagged ArcV, we were unable to recover EV production with this construct in the knock out strain (unpublished), suggesting that the N-terminus of ArcV is critical for the EV producing machinery. Therefore, I suggest that ArcV is similarly both cytoplasmic and membrane-associated, depending on the bound nucleotide. Confirming this would require information regarding the proteins involved in activation and inactivation, and testing how this influences membrane binding of ArcV. The transition from

the inactive state to the active state of the GTPase would provide another node for the cell to regulate EV production. Something that we did not investigate was the ratio of membrane-bound and cytoplasmic form of ArcV in the cell, which would have required mass spectrometry analysis of the intracellular protein composition and how this changes depending on the growth conditions. It would be interesting to see whether these ratios align with what we observe for EV production, or if EV production is regulated by the translation of ArcV.

Since knocking out ArcV yields a hypovesiculation phenotype, I conclude that ArcV is a key component to the EV production machinery. However, we still observe particles in the culture supernatant and EV quantification from the ArcV knock out strain results in a non-zero value. This suggests that extracellular particles are still being produced, though at a much lower rate than before. There may be a redundant mechanism encoded for EV production in case ArcV is compromised. We have not attempted proteomics to verify the similarity between these particles and wild type EVs, but if there was an alternative mechanism, I would expect similar compositions, with the involvement of other proteins. However, other factors related to the ArcV mutant make me doubt that these are bona fide EVs. The particles were not associated with RNA, but contained DNA instead, implying a different biochemical composition to wild type EVs. Further, resequencing the genome of the knock out strain revealed increased activity in one of the proviral regions encoding for a pleolipovirus [28]. Pleolipoviruses have similar morphologies to EVs, in that both entities are membrane bound [29]. It is possible that the particles observed under transmission electron microscopy are in fact pleolipovirus particles rather than EVs. However, whether or not the induction of the provirus is related to the *arcV* deletion remains undetermined. Another possibility is that these particles are a result of cell death, similar to endolysin-dependent EV production in Bacteria [24, 30]. It is likely that the EV population in wild type cultures is a heterogeneous mixture of EVs with different compositions, so perhaps several routes of EV production occur in wild type cells.

The interaction partners of activated ArcV are currently unknown. The activation of small GTPases is typically followed by a cascade of protein-protein interactions, allowing for a specific function to be carried out [31]. For the example of Arf-family small GTPases, the activation of Arf1 triggers induces structural changes and subsequent membrane interaction, as well as the recruitment of other proteins to facilitate membrane curvature [32]. It is possible that ArcV functions in a similar way, in that activation leads to membrane interaction and protein recruitment. However, it has also been shown that Arf1-GTP alone can stimulate membrane curvature [33], suggesting that an interacting coat complex may not be necessary for the formation of EVs. One should also keep in mind that Arf-family GTPases mostly induce positive membrane curvature [33]. In other words, curvature in the same direction that the GTPase is oriented on the membrane. We do not know whether ArcV is bound on the cytoplasmic side or is exported in order to trigger membrane curvature, but this is something to consider when trying to reconstruct the mechanism for EV production in haloarchaea. Another possibility is that the S-layer subunit could function as a coat complex. We have both, through transmission electron microscopy and proteomic analysis, shown that EVs retain the S-layer. Recently, the S-layer has been shown to be able to adapt to multiple membrane curvatures [34], making it a much more flexible structure than is was previously considered. The cryo-electron tomography of purified *H. volcanii* EVs did not reveal the presence of other coat-like complexes besides the S-layer subunit. Further they identified periodic pentameric conformations in the highly curved EVs that interrupt the typical hexameric interfaces of S-layer subunits, which were also identified in

cellular regions with higher degrees of membrane curvature. Perhaps the localization of ArcV-GTP to the membrane forces the S-layer into a conformation that induces higher membrane curvature. One could test this hypothesis by determining whether ArcV interacts with the S-layer, or observing the S-layer lattice in the ArcV knockout strain and on their corresponding vesicle-like particles.

5.2.3 Extracellular vesicle-associated proteins

Besides ArcV, additional proteins were identified as enriched in EVs that could potentially be involved in EV production. Both *H. volcanii* and *Hrr. lacusprofundi* [16] EVs contained the same HEAT repeat-containing protein (HVO_1020 and Hlac_2402 respectively). HEAT repeats are a type of α-solenoid domain, which are elongated domains comprised of α-helical repeats [35]. They are key domains in the proteins that make up the coat complexes of intracellular vesicles in the eukaryotic cell [36]. It is therefore curious that two proteins similar to intracellular membrane trafficking components, a small GTPase and an α-solenoid-containing protein, were both identified as part of the core proteome of haloarchaeal EVs. However, it should be noted that the protein was not enriched in EVs, but had higher relative abundance in the cell membrane. I would expect that if the protein acted as a part of the coat complex, that it would be enriched in EVs. Perhaps characterizing the function of this protein in relation to EV production could help elucidate whether its presence is coincidental or integral to the EV production machinery.

Both profiled haloarchaeal EVs also contained a PQQ repeat protein (HVO_B0132 and Hlac_0271 respectively, 27.3% sequence identity). However, it should be noted that one out of the 12 *H. volcanii* EV replicates did not contain this protein. PQQ repeat proteins take on a distinctive β-propeller structure comprised of eight blades [37], which is also predicted in an AlphaFold2 [38] model of the protein structure of the EV-associated PQQ repeat protein (Figure 1A). ß-propeller domains are key components of the protocoatomer [36], and are found in the "outer coats" of COPI (α-and β'-subunits) [39], COPII (Sec31) [40] and clathrin-coated vesicles (heavy chain) [41]. Based on structural prediction, both the haloarchaeal EV-associated β-propeller protein and protocoatomer β-propellers are WD-repeat proteins. However, all vesicle-associated β-propellers in Eukaryotes are six- or seven-bladed, as opposed to the predicted eight-bladed β-propeller protein in haloarchaeal EVs. Therefore, while it is intriguing that we have identified both α-solenoid and β-propeller domain proteins in haloarchaeal EVs, I am not convinced that the β-propeller domain protein functions in the same manner as those found in the protocoatomer. Additional protein characterization would be needed to confirm its relevance to EV production.

Three highly enriched hypothetical proteins were also identified in *H. volcanii* EVs: HVO_2519, HVO_1134 and HVO_2985. Only a homologue of HVO_1134 was identified in all vesicle replicates from *Hrr. lacusprofundi* (Hlac_1325), while the other two were not present in all replicates [16]. Therefore, I would predict that HVO_2519 and HVO_2985 are likely not relevant components of the EV production machinery. Alternatively, they could represent species specific components for *H. volcanii*, but this requires additional experiments to verify. I predicted the structure of HVO_1134 using AlphaFold2 [38], which showed highly probable folds for the N and C terminal regions separated by a long disordered region (Figure 1B). Based on structural homology using DALI [42], the N-terminal domain showed similarities to cysteine peptidase family proteins (IPR038765), while the C-terminal domain showed similarities to

tRNA-endonuclease-like domain superfamily proteins (IPR011856). However, I cannot conclusively predict any functions from these predictions, and additional functional characterizations would need to be conducted in order to draw conclusions about HVO_1134 and its relation to EV production. The fact that it is present in EVs from two organisms suggests that it is relevant for EV production. However, it could also be a membrane associated protein that has a higher probability of being packaged into budding EVs due to its localization.

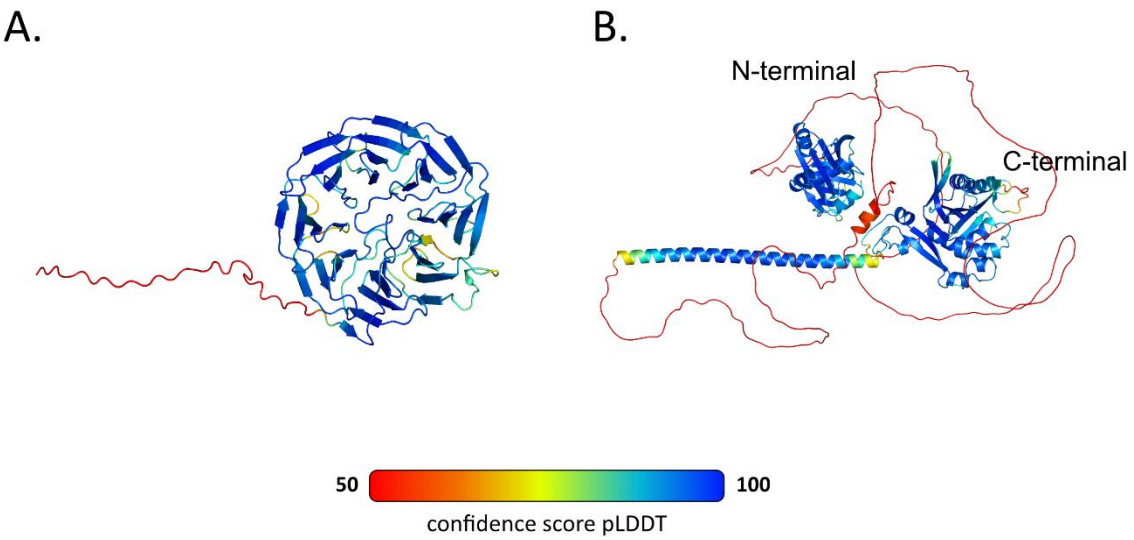

Figure 1. AlphaFold v2 [38] protein structure predictions of HVO_B0132 (A) and HVO_1134 (B). Protein models are color coded depending on confidence measured by predicted local-distance difference test (pLDDT).

Interestingly, certain components of the cell division machinery were enriched in EVs from both *H. volcanii* and *Hrr. lacusprofundi* [16]. CetZ1, CetZ2, CetZ5 and FtsZ2 were all identified as enriched, and CetZ6 was identified in all EV replicates in *H. volcanii*. However, I am not certain that their presence or enrichment in EVs indicates that they are responsible for EV production. The two FtsZ proteins encoded by most Euryarchaeota and DPANN are responsible for coordinating cell division [43]. Both are anchored to the membrane through interaction with SepF to form a ring structure at the central division plane [44]. FtsZ2 drives the constriction of the cell membrane , allowing division to occur [45]. The high abundance and enrichment of FtsZ2 could be a result of its localization in proximity to the membrane. However, I would then expect the other components of the division ring, such as SepF or FtsZ1, to be present as well. I did not test whether cell division is related to EV production, as this has been shown for the ESCRT-like mechanism in *Sulfolobus* [14]. By deleting one or more components of the division ring and quantifying EV production in both, one could perhaps determine if the two mechanisms are related. On the other hand, deletion of the CetZ homologues in *H. volcanii* had no observable impact on EV production in terms of quantity and morphology. The CetZ proteins are archaeal tubulin-like proteins that belong to the same tubulin superfamily as FtsZ [46]. Both CetZ1 and CetZ2 were shown to be involved in coordinating the transition from cocci to rod-shaped cells in *H. volcanii*, and CetZ1 is observed to be highly associated with the cell membrane [46, 47]. The cellular localization could explain their presence and enrichment in EVs.

5.2.4 ArcV operon-associated proteins

Deletion of two proteins directly downstream from *arcV* had opposite effects on EV production. Knocking out ArcV operon-associated protein A (ArcVapA) yielded a severe hypovesiculation phenotype, similar to the ΔarcV phenotype, while knocking out ArcVapB yielded a hypervesiculation phenotype. Neither of the proteins was enriched or detected in the EVs. The presence of both genes directly downstream of *arcV* was also shown to be conserved across ArcV-encoding Archaea, suggesting that their functions are closely related. ArcVapA structure was predicted using AlphaFold2 [38] (Figure 2A), and structurally similar proteins were identified using DALI [42]. The N-terminal domain showed structural similarities to SepF (IRP038594, RMSD = 3.442) and the C-terminal domain showed structural similarities to Alba-like proteins (IPR036882, RMSD = 3.335) (Figure 2B). SepF interacts with the GTPase, FtsZ, during cell division to anchor proteins to the cell membrane [44]. The high similarities between ArcVapA and SepF suggest that ArcVapA could similarly interact with a GTPase domain-containing protein, such as ArcV.

Based on the knock out phenotype and the domains identified, I predict that ArcVapA is the cognate guanine nucleotide exchange factor (GEF) for ArcV. During the process of activation of small GTPases, the corresponding GEF interacts with the GTPase to promote the exchange of GDP for GTP [48]. Deletion of the GEF would prevent the activation of ArcV and consequentially the formation of EVs. It is also compelling that the protein shares structural similarity to SepF, a protein that is known to interact with the GTPase, FtsZ [44]. It is possible that the SepF-like domain of ArcVapA coordinates the interaction between ArcVapA and ArcV, regulating the activation of the GTPase and thus the initiation of EV formation. On the other hand, I was unable to resolve a probable structure of ArcVapB. Based on the hypervesiculation phenotype of the knock out strain, ArcVapB could represent the cognate GTPase activating protein (GAP). Small GTPases tend to have low intrinsic GTP hydrolysis rates and require an additional protein to promote GTP hydrolysis and GTPase deactivation [48]. GAPs in COPI and COPII vesicles are responsible for de-coating and the recycling of coat components [25]. However, the recycling of coat components only makes sense in an intracellular context where specific coat complexes and associated proteins have specific subcellular localization. GTPase deactivation in Archaea could instead act as an additional node of regulation to prematurely terminate the formation of a budding vesicle. Therefore, deletion of *arcVapB* would prevent this failsafe, leading to a hypervesiculation phenotype. Further characterization of the interactions between ArcV and the downstream proteins, and the expression patterns of the ArcVaps could help elucidate their function.

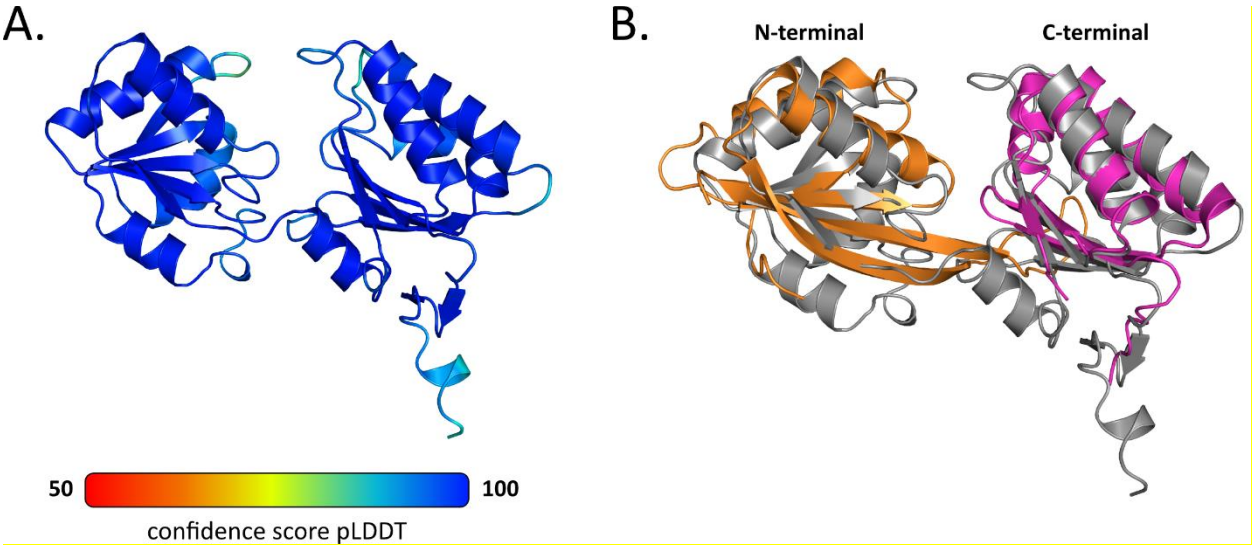

Figure 2. Predicted structure of ArcVapA and comparison to similar protein structures. (**A**) Structure was predicted using AlphaFold v2 [38], and color-coded depending on confidence measured by predicted local-distance difference test (pLDDT). Predicted structure shows two distinct domains at each end of the protein. (**B**) The predicted structure was used to identify structurally similar proteins using DALI [42], which identified SepF family proteins (IPR038594) and proteins that belonged to the Alba-like superfamily of proteins (IPR036882). ArcVapA was superimposed on SepF (7AL1, shown in pink) and Alba (3U6Y, shown in orange), showing that each protein structure corresponds to the two identified domains in the ArcVapA predicted structure. Superposition to SepF had an RMSD value of 3.442 (373 to 373 atoms) and superposition to Alba had an RMSD value of 3.335 (305 to 305 atoms).

5.2.5 A proposed model for extracellular vesicle production in haloarchaea

Considering the components identified in EVs from haloarchaea, I would propose the following speculative model for ArcV-dependent EV production. Upon external stimuli, EV production is initiated by the activation of the small GTPase, ArcV, exchanging GDP for GTP. This exchange could be mediated by the candidate GEF, ArcVapA. Once activated, a conformational change occurs in ArcV, releasing an amphipathic N-terminal α-helix that interacts with the membrane. Since EVs were determined to be selectively enriched in saturated lipids, ArcV could preferentially interact with regions in the cell membrane with saturated lipids. This interaction either takes place on the cytosolic side or the extracellular side of the cell membrane, depending on the curvature induced by ArcV. If the latter, a corresponding protein would be required to flip the GTPase to the extracellular side. While ArcV could be the sole protein responsible for inducing membrane curvature, other proteins could also be involved in this process, such as the hypothetical proteins or S-layer subunit. While we were unable to identify any common features among the RNA packaged in EVs, it is likely that smaller transcripts and those that are close to the cell periphery are either randomly packaged inside the budding vesicle or guided in through an unknown protein chaperone. EV production could be terminated by GTP hydrolysis facilitated by ArcVapB, resulting in the dissociation of ArcV from the membrane. With enough cumulative membrane curvature, the vesicle breaks off from the donor membrane either by an additional cytoplasmic protein, through activity of an EV-associated protein, or from the tension generated by membrane curvature.

The above model is based mostly on speculation and reflects a simplified version of protocoatomer-based vesicle production. Many of the steps mentioned would need extensive experimentation to verify, but I think this model provides

a foundation on which additional research can be built. For example, one can determine the curvature induced by ArcV by observing interactions between activated ArcV and artificial liposomes/lipid sheets, similar to what has been done for Arf1 [33]. Further components of the EV production machinery can be identified through pulldowns using tagged ArcV as the bait. Activity assays of the rate of hydrolysis of ArcV, with and without the candidate GEF and GAP, could verify their respective functions. Additionally, it is uncertain whether these steps are specific to haloarchaea, or extend to other Archaea that encode the ArcV operon. Further proteomic analysis of archaeal EVs outside of haloarchaea would be required to determine if the processes are similar, or if there are phylogenetically distinct mechanisms of ArcV-dependent EV production. While the work presented in this thesis represents a starting point, it is quite clear that there is still much work that needs to be done to construct a proper model of ArcV-dependent vesiculation in the archaeal domain.

5.3 Extracellular vesicles as mediators for microbe-microbe interactions

Multiple studies have previously demonstrated how bacterial EVs interact with eukaryotic host organisms [49], such as the transfer of immunogenic compounds [50] or RNAs to influence host gene expression [51]. However, the role of EVs in the context of microbe-microbe interactions is still an open question in microbiology [52, 53], with EV-mediated RNA communication among microbes being completely unexplored. The aqueous bacterium, *Paracoccus*, has been observed to export EV-associated quorum sensing compounds and transport them to other bacteria [54]. Though we did not characterize the smaller bioactive compounds enclosed in EVs, it is possible that Archaea are similarly able to transport signaling compounds in EVs. It has also been proposed that the trafficking of DNA in EVs can drive horizontal gene transfer within a microbial community [11, 16, 22]. However, as DNA was not found associated with haloarchaeal EVs under the conditions tested, we can exclude this possibility. Rather, I will focus on the compounds identified in the characterized EVs, the effects of EV-cell interactions, and the potential roles that EVs can play in microbial systems.

5.3.1 Haloarchaeal EV-associated RNA

EVs from three haloarchaeal species were demonstrated to contain a distinct subpopulation of RNA. Though the organisms certainly do not constitute the entire diversity of the archaeal class, *Halobacteria*, I would predict that EV-mediated export of RNA is a conserved process among haloarchaeal organisms. Based on the size profile of EV-associated RNA and the comparison of sequencing results using small and total RNA library preparation kits, EV-associated RNA mostly consisted of low-range RNA, including tRNA and noncoding RNA (ncRNA). Total RNA libraries revealed that the higher range population of EV-associated RNA was 98% rRNA. However, it is likely that these (along with other mRNA) are not the full annotated transcript lengths, but degraded products, similar to what was observed for the mRNA for the S-layer subunit. Two ribonucleases were identified in the proteome of all EV samples across all conditions tested. While the activity of the EV-associated ribonucleases in EVs has not been characterized, it is possible that the ribonucleases would degrade enclosed RNA, resulting in the observed length profile. Under this hypothesis, RNA that have more stable secondary structures would persist in EVs [55]. However, the possibility for longer transcripts to exhibit function in a receiving organism should not be excluded.

Since ncRNAs are known to regulate gene expression in all three domains of life [56–58], I wanted to explore whether EV-associated RNA are able to influence gene expression in receiving cells. After cells were incubated with EVs, I detected significant changes to the transcriptome of the receiving cell, including the downregulation of multiple chemotaxis- and motility-related genes. While this is not definitive evidence that the EV-associated RNAs were the cause of the observed effects, it is possible that one of the ncRNA affected a transcriptional regulator for motility and chemotaxis. The observed downregulation of genes would then be an indirect effect of gene regulation mediated by the EV-associated ncRNA. However, this would require additional characterization of the individual ncRNA and the mRNA that they are able to interact with in order to establish that these ncRNA are functional. Further, since I only meausred the cell transcriptome, the effects could have been more visible in the proteome or in phenotypical changes.

We showed that the EV-associated RNA population changes under different conditions in both *H. volcanii* and *Hrr. lacusprofundi*. Upon virus infection, EVs from both organisms contained virus-encoded transcripts. In *Hrr. lacusprofundi*, EVs were also observed to completely alter their RNA composition and package specific ncRNA that did not reflect the intracellular changes upon virus infection. The viruses used in these studies exhibit different lifestyles, one chronic and the other lytic. While the differences in the exported RNA could be explained by the different lifestyles, it should be noted that drastic changes to the host transcriptome under viral infection with the chronic virus mainly occur during exponential phase and do not appear into stationary phase [59]. Therefore, since I isolated the vesicles from the chronically-infected cultures during stationary phase, I would not expect to observe drastic changes in the transcriptomes of EVs. In contrast, the cultures infected with a lytic virus were harvested during exponential phase, which likely contributed to the large changes in the EV-associated transcriptome. Isolating EVs from chronically-infected cultures during exponential phase may have better revealed how the EV-exported transcriptomes would have shifted and allow us to properly compare the EV-associated transcriptomes under different types of viral stress. Focusing on the effects of EVs from lytic virus-infected cultures, we did not observe the transference of immunity or resistance through EVs. Our hypothesis was that viral infection would stimulate the expression of the host immune system, including ncRNAs that are active in the regulation of gene expression in this condition. These ncRNAs would then be preferentially enriched in EVs due to their length and stability, and be functional in receiving cells by stimulating expression of immune responses. A specific ncRNA that corresponds to the coding region of a transcription factor was uniquely enriched in EVs from infected cultures, suggesting that it is able to regulate expression of that transcription factor. Though no such effect was observed in the receiving cells, the virus-to-host ratio that was used may have been too high, obscuring the more subtle variations in growth that could have been caused by EVs. Perhaps a lower ratio to slow down the progression of lysis would grant the higher resolution needed to observe any resistance communicated by EVs.

Based on the results of this thesis, I cannot conclude that the EV-associated RNA influence gene expression in receiving organisms, though this hypothesis should not yet be excluded. The hypothesis could be further explored by using other conditions that are known to stimulate ncRNA expression in haloarchaea, such as oxidative stress [60], or in bacterial organisms with well-studied sRNA regulatory systems. By using a regulatory system that has been previously characterized, one could design a more targeted approach in the search for EV-mediated ncRNA regulation. Alternatively, one could overexpress characterized ncRNA and observe whether feeding EVs from the overexpressing

cultures to naïve cells would elicit similar effects. Such a system could prove useful in working with organisms without an established genetic system. For example, a microbe could be engineered to produce EVs containing specific asRNA to target corresponding genes in the non-model organism. By feeding asRNA-enriched EVs to the other organisms, RNA-based gene silencing could be achieved in the co-cultured organism, allowing for the characterization of specific genes.

5.3.2 EV-associated proteins

Outside of the RNA cargo of haloarchaeal EVs, the associated protein cargo could also convey the function of EVs. However, it is undetermined whether proteins remain functional in EVs or after they have been transferred to the receiving cell. The core set of EV proteins that were present in all replicates and conditions of EV preparations constituted 285 proteins, representing 20 different COG functional groups [61]. In terms of average relative abundance, about 13% of the total relative abundance of EV-associated proteins are hypothetical proteins. Since we still do not have any information regarding their characteristics, it is highly probable that these proteins convey an unknown function in EVs. The group with the highest relative abundance were cell cycle-related proteins (15%), which were comprised of four CetZ isoforms, FtsZ2, and FtsA. Their high abundance in EVs could be explained by their high cellular abundance, and a bias for proteins localized close to the cell membrane [46, 45]. This could explain why we also observe 23% of relative abundance corresponding to proteins related to ABC transport. However, the functionality of these proteins cannot entirely be ruled out and should be experimentally explored.

5.3.3 Potential roles for haloarchaeal EV production

The identification of an operon linked to haloarchaeal EV production suggests that EV production is a genome-encoded feature in haloarchaea. Therefore, it is likely that these organisms have evolved this mechanism to serve specific functions.

A proposed function for EVs is that they can serve as a source of nutrients. Whether the biochemical composition of EV is random or not, the RNA, lipids and proteins contained in EVs can serve as sources of carbon, nitrogen and phosphorous [62, 63]. In fact, bacterial EVs have been demonstrated to sustain the growth of heterotrophic bacteria [22]. However, after feeding EVs to haloarchaeal cells, we did not observe any growth benefit. Though, we observed the upregulation of genes associated with the metabolism of fatty acids after cells were incubated with EVs, which could suggest that the cells were responding to the supplemented EV-associated lipids. Nutrient rich media was used during incubation of cells and EVs, since preliminary experiments in *H. volcanii* only showed EV uptake when nutrients were available. Perhaps growth benefits would be more observable if the experiment was conducted using a more nutrient limiting media. However, it is still uncertain why cells would actively export these nutrient rich compounds rather than recycling them internally. The benefits of feeding a community are still unclear but some hypotheses have been proposed [49]. In the example of the gut bacteria, *Bacteroides ovatus* and *Bacteroides vulgatus*, *B. ovatus* was observed to export glycoside hydrolases in EVs that are able to extracellularly degrade polysaccharides [64]. The degradation products would then be available to both organisms, since these specific hydrolases are not encoded in *B. vulgatus*. This

mechanism of cooperativity was demonstrated to promote the growth of both the EV-producing organism and the organism utilizing the degradation products by an unknown interaction, perhaps through the stimulation of growth-promoting factors [49]. Under this hypothesis, haloarchaea releasing nutrient-rich EVs could stimulate the production of other beneficial factors in organisms participating in a cooperative relationship.

Alternatively, the enrichment of regulatory RNAs in EVs suggests that EVs could be a signaling mechanism, similar to the interactions between symbiotic or pathogenic Bacteria and their eukaryotic hosts [65, 51]. The export of regulatory RNAs among haloarchaea could represent a mechanism to control gene expression of an entire community. However, while EV-associated RNA was observed to be transferred between *H. volcanii* cells, we are unable to conclude that the RNA was indeed internalized. It is possible that EVs remained adhered to the cell surface without membrane fusion and the release of EV cargo into the cell interior. The internalization of EV-associated RNA has been demonstrated in the interaction between *Vibrio fischeri* and its eukaryotic host [66]. By using fluorescence in situ hybridization chain reaction to target a highly enriched EV-associated ncRNA, the authors observed the RNA signal within the cytoplasm of host cells, suggesting that the symbiont-derived RNA was taken up by host cells via EVs. Such an approach could be used to investigate the interaction between two different haloarchaeal organisms, and whether the EV-associated RNA enters the receiving cell. Other compounds exported in EVs, such as proteins or secondary messengers, could also be relevant for the transmission of signals. For example, an EV-associated diadenylate cyclase was observed in *H. volcanii* EVs. Diadenylate cyclases produce cyclic-di-AMP, a secondary messenger involved in osmoregulation in *H. volcanii* [67]. While it is unlikely that the secondary messenger is being produced in the EVs since the reaction requires two ATP, EVs could act as an external reservoir of diadenylate cyclase and uptake can therefore trigger the corresponding signal cascade.

5.4 The evolutionary implications of an archaeal vesiculating GTPase

The presence of a conserved small GTPase, ArcV, in EVs of haloarchaea and its functional connection to EV production was quite surprising. The only other known system that utilizes a small GTPase in the production of vesicles is the endomembrane system of eukaryotic cells [68]. Therefore, I think this requires us to take a deeper look into whether the two systems are related and whether this changes our understanding of the archaeal origins of eukaryotic features.

5.4.1 ArcV in the archaeal domain

Though ArcV was identified to be conserved in other archaeal lineages, it remains undetermined whether ArcV mediates EV production in other organisms. Since we only have characterized one example of ArcV-dependent EV production, investigations into EV production and ArcV from other cultivatable Archaea is necessary to verify the function of this novel protein family. Specifically, the identification of ArcV in the phylum, *DPANN*, raises some questions about its function. Most characterized *DPANN* are obligate symbionts with reduced cell mass and reduced genome sizes that utilize unique mechanisms of membrane remodeling to interact with their host organisms [69, 70]. Based on their reduced sizes and unique lifestyle, I would not predict that they expend energy to produce EVs. Rather, it could be possible that these membrane remodeling mechanisms utilize ArcV to mediate interaction between symbiont and host.

In the proteome of *Candidatus* Nanohaloarchaeum antarcticus and *Hrr. lacusprofundi* cocultures, the *DPANN* organism was demonstrated to express ArcV, suggesting that ArcV is indeed active during symbiosis [71]. By uncovering the range of functions that this novel protein family mediates, we can better reconstruct how ArcV emerged and evolved in evolutionary history.

The only other archaeal EV production mechanism that has been uncovered is linked to the archaeal ESCRT-like system [3, 14]. Such a system is not encoded in *Euryarchaeota* and *DPANN* [15], the lineages in which we identify ArcV. Additionally, the *Euryarchaeota* genus, *Thermococcus*, does not encode ArcV, but still produces EVs through an unknown mechanism [72, 73]. Therefore, it is certainly possible that multiple mechanisms for EV production have evolved separately within the archaeal domain. We also identified some *Asgardarchaeota* that encoded an ArcV homolog, though this is not the case in the majority of the surveyed asgardarchaeotal genomes. It is likely that these were horizontally inherited, but the presence of both the archaeal ESCRT-like system and ArcV system in one organism reflects the observed eukaryotic-like nature of the phylum [74, 75]. Whether the EV-producing capacity of ArcV is maintained in the asgardarchaeotal organisms should be experimentally investigated.

5.4.2 A closer look into small GTPases

GTP binding and hydrolyzing domains represent multiple classes of proteins, the main two being Rossmann NTPases and P-loop NTPases, which are characterized by specific structural architecture [76]. These proteins are comprised of a central β-sheet formed by β-strands connected by α-helices [77]. Rossmann NTPases consist of dinucleotide binding domains as well as tubulin/FtsZ family GTPases [78, 79]. P-loop NTPases are a much more diverse group of NTP binding proteins and represent up to 18% of encoded proteins across the domains of life [80]. Whether the two groups emerged through common ancestry pre-last universal common ancestor (LUCA) or through convergent evolution is still uncertain, but recent analysis points to common ancestry [76]. From the P-loop GTPases specifically, these can be categorized into two main classes: TRAFAC class GTPases (including Ras superfamily, Era GTPases, translation factors, signal transducers and some ATPases) and SIMIBI class GTPases (including signal recognition particle-associated GTPases, MinD superfamily and BioD superfamily) [77]. While all the described P-loop GTPases contain six or seven β-strands, TRAFAC GTPases distinguish themselves with one antiparallel strand [77]. It is clear from the structural prediction of an antiparallel β-strand that ArcV belongs to the TRAFAC class of GTPases.

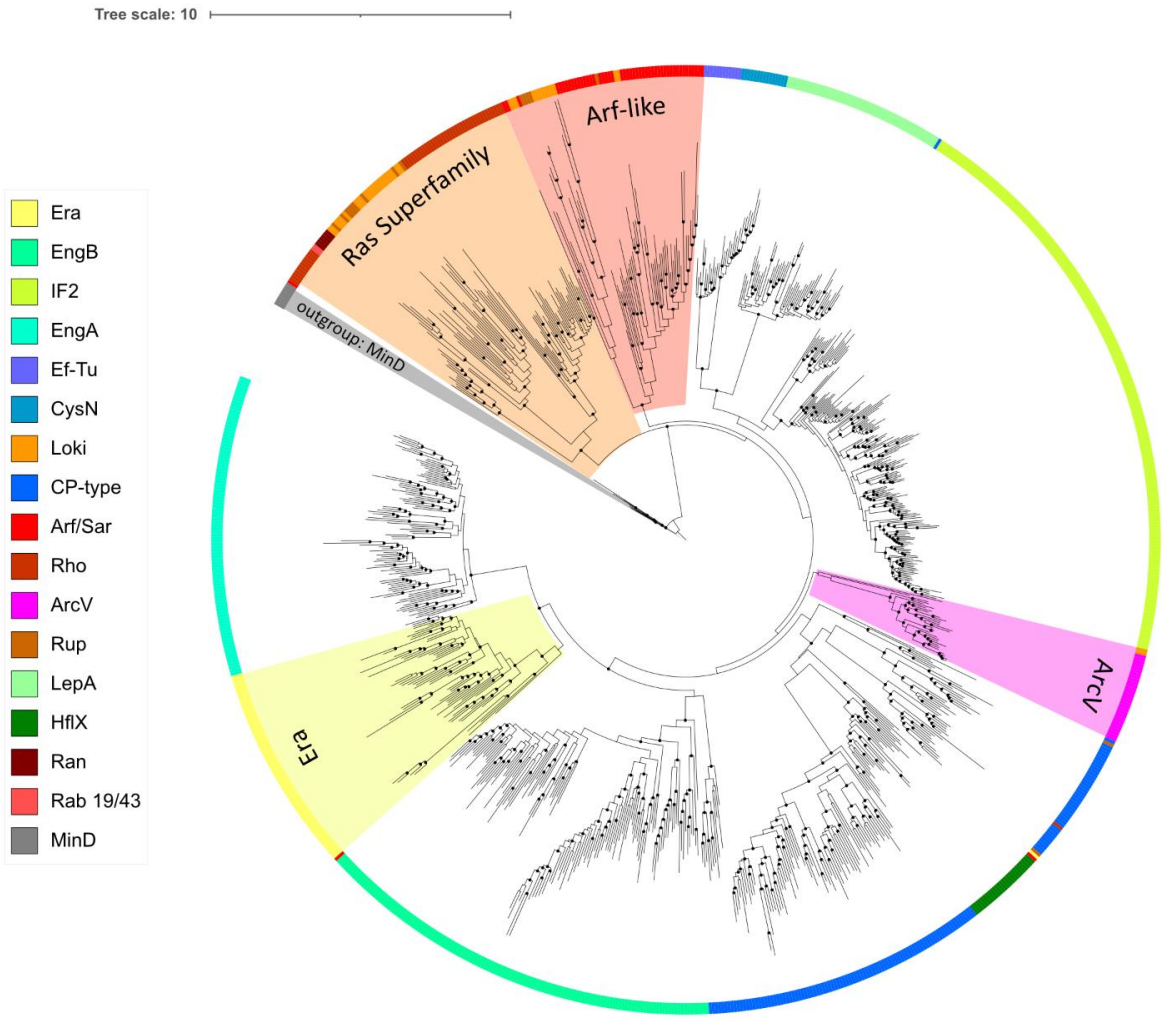

Figure 3. Phylogenetic tree of TRAFAC GTPase domains. Colors on the outer ring represent the subfamilies present in the phylogenetic tree, corresponding to the legend on the left. Uniprot-reviewed sequences of the InterPro families for TRAFAC GTPase domains (Ran: IPR002041, Rab 19/43: IPR048040, Rho: IPR003578, Arf/Sar: IPR006689, Ef-Tu: IPR041709, CysN: IPR041757, LepA: IPR013842, IF2: IPR015760, CP-type: IPR030378, HlfX: IPR016496, EngB: IPR030393, and EngA: IPR031166) and the outgroup SIMIBI class GTPase, MinD (IPR010223) were clustered using 60% sequence identity and number of sequences reduced using CD-HIT [81, 82]. The resulting sequences, 29 ArcV sequences, single domain GTPases from *Candidatus Lokiarchaeum B-35* [83], and Rup GTPases [84] were aligned using MAFFT v7 on default settings [85]. Tree was generated from the alignment using IQ-Tree [86] with ultrafast bootstrap analysis [87] using 10,000 bootstrap replicates on default settings, auto-detecting the substitution model [88]. Phylogenetic tree visualized on iTOL (v6) [89] rooted to the outgroup, MinD (https://itol.embl.de/shared/1ZJ4TuNJA1fcD). Black dots represent branches with bootstrap value greater than 90.

Most of the GTPases identified in our search for ArcV homologues were annotated as 50S ribosome binding GTPases (IPR01926) or more specifically Era GTPases (IPR005662). Era GTPases are uniquely characterized by having an N-terminal GTPase domain with a C-terminal KH domain (RNA binding), and have been shown to coordinate the assembly of ribosomes [90]. ArcV appears to be a single domain GTPase with no KH domain, making it unlikely that the proteins interact with ribosomes or carry out the same functions. The extended N-terminal α-helix predicted in ArcV are not present in Era GTPases, but are rather characteristic for Arf-family GTPases [91]. Canonical Era GTPases have also been shown to be essential genes in Bacteria [92], while ArcV-knockout strains are still viable. Therefore, I do not think ArcV is an Era homologue. Rather, when aligning ArcV against the Pfam database (Pfam-A_v36) on HHpred, 177

different P-loop NTPase protein families show over 90% probability matches to ArcV. The top-most hit is for Arf-family GTPases (99.75% probability, 94.31 score), suggesting that ArcV is closer matched to Arf than 50S ribosome binding GTPases (99% probability, 54.71 score). Superposing the structures of ArcV and Era (from *Aquifex aeolicus* PDB: 3IEV, and *E. coli* PDB: 3IEU), I obtain RMSD values of 2.101 and 2.845 respectively, suggesting a fairly strong structural similarity. Superimposing ArcV with Arf1 (from *Ctenopharyngodon idella* PDB: 7WQY) and Arf6 (from *Homo sapiens* PDB: 6BBP) yields RMSD values of 2.472 and 2.478 respectively, also indicating strong structural similarities. In fact, structural superposition with other Ras-superfamily GTPases yield similar scores. Most likely, ArcV represents a novel family of GTPases that neither belongs to Era-family GTPases nor Arf-familyGTPases.

In order to establish whether ArcV and Arf share common ancestry, it is relevant to look at the evolutionary history of TRAFAC GTPases and determine where ArcV fits. A model for the broad evolutionary history of TRAFAC class GTPases has been proposed in 2002, though it does contain uncertainties in the emergence of specific branches including Era and the Ras superfamily of GTPases [77]. They imply that the diversification of the Ras superfamily GTPases occurred close to the emergence of the eukaryotic domain, branching from the prokaryotic MglA GTPases [77]. This hypothesis is further strengthened by the abundance of Ras-like GTPases encoded in the genomes of *Asgardarchaeota* [83, 93, 94]. In a tree showing the alignment of ArcV sequences with other TRAFAC GTPases (Figure 3), the Ras-superfamily GTPases (Rab, Rho and Ran) form a monophyletic clade separate from all other GTPases, which also include Rup GTPases [84] and lokiarchaeotal GTPases [83]. The other major clade consists of the translation-related GTPases (IF2, Ef-Tu, Era, EngA, EngB, and LepA), CysN, HflX, ArcV, and Arf. The grouping of Arf-GTPases separately from other Ras GTPases suggests that what is considered the Ras-superfamily of GTPases is not a monophyletic clade and should be reevaluated in the context of other GTPase subfamilies across all domains. Additionally, some archaeal Rup GTPases and lokiarchaeotal GTPases form a monophyletic clade with Arf GTPases, which supports the hypothesis of the emergence of Arf GTPases prior to the emergence of Eukaryota. However the major clade containing both Arf and ArcV is unresolved, suggesting that additional sequences are required to fully resolve their evolutionary relationship. Other uncharacterized small GTPase families that are closely related to ArcV could expand our understanding of the evolution of vesiculation and perhaps resolve the relationships between the different TRAFAC GTPases. While I cannot conclude that ArcV in *Euryarchaeota* and *DPANN* represent direct archaeal precursors of the Arf-family, the functional relationship is compelling and warrants further investigation into whether the ArcV system represents the archaeal precursor to the eukaryotic endomembrane system.

5.5 Concluding remarks

EV production represents an understudied mechanism within microbial community dynamics. Their wide array of functions and cargo allow them to potentially mediate activity at a population-wide scale, though the impacts of this in the context of aquatic systems is undetermined. In hypersaline environments, I have demonstrated that haloarchaea produce RNA-enriched EVs that elicit changes in gene expression when incubated with cells. The mechanism for haloarchaeal EV production is controlled by a conserved operon containing the small GTPase, ArcV, which is reminiscent of the small GTPase-dependent smechanism driving vesicle formation in the eukaryotic endomembrane

system. Some major questions still remain regarding the impact of RNA-enriched EVs in hypersaline environments, the exact mechanism of ArcV-dependent EV production, and whether the mechanism is related to Arf-dependent EV production. With the results presented in this thesis, it is clear that EVs, which were once considered cellular "dust" represent an important aspect of microbial ecology and should be explored further.

REFERENCES

1. Mills J, Erdmann S (2022) Isolation, Purification, and Characterization of Membrane Vesicles from Haloarchaea. Methods Mol Biol 2522:435–448. https://doi.org/10.1007/978-1-0716-2445-6_30
2. Liu J, Soler N, Gorlas A et al. (2021) Extracellular membrane vesicles and nanotubes in Archaea. Microlife 2:uqab007. https://doi.org/10.1093/femsml/uqab007
3. Ellen AF, Albers S-V, Huibers W et al. (2009) Proteomic analysis of secreted membrane vesicles of archaeal Sulfolobus species reveals the presence of endosome sorting complex components. Extremophiles 13:67–79. https://doi.org/10.1007/s00792-008-0199-x
4. Gaudin M, Gauliard E, Schouten S et al. (2013) Hyperthermophilic archaea produce membrane vesicles that can transfer DNA. Environ Microbiol Rep 5:109–116. https://doi.org/10.1111/j.1758-2229.2012.00348.x
5. Jeppesen DK, Hvam ML, Primdahl-Bengtson B et al. (2014) Comparative analysis of discrete exosome fractions obtained by differential centrifugation. J Extracell Vesicles 3:25011. https://doi.org/10.3402/jev.v3.25011
6. Brown PN, Yin H (2017) Polymer-Based Purification of Extracellular Vesicles. Methods Mol Biol 1660:91–103. https://doi.org/10.1007/978-1-4939-7253-1_8
7. Bachurski D, Schuldner M, Nguyen P-H et al. (2019) Extracellular vesicle measurements with nanoparticle tracking analysis - An accuracy and repeatability comparison between NanoSight NS300 and ZetaView. J Extracell Vesicles 8:1596016. https://doi.org/10.1080/20013078.2019.1596016
8. Stoner SA, Duggan E, Condello D et al. (2016) High sensitivity flow cytometry of membrane vesicles. Cytometry A 89:196–206. https://doi.org/10.1002/cyto.a.22787
9. Ptchelkine D, Gillum A, Mochizuki T et al. (2017) Unique architecture of thermophilic archaeal virus APBV1 and its genome packaging. Nat Commun 8:1436. https://doi.org/10.1038/s41467-017-01668-0
10. Feng X, Li Y, Tian C et al. (2023) Isolation of archaeal viruses with lipid membrane from Tengchong acidic hot springs. Front Microbiol 14:1134935. https://doi.org/10.3389/fmicb.2023.1134935
11. Lücking D, Mercier C, Alarcón-Schumacher T et al. (2023) Extracellular vesicles are the main contributor to the non-viral protected extracellular sequence space
12. Soler N, Krupovic M, Marguet E et al. (2015) Membrane vesicles in natural environments: a major challenge in viral ecology. ISME J 9:793–796. https://doi.org/10.1038/ismej.2014.184
13. Cezanne A, Hoogenberg B, Baum B (2023) Probing archaeal cell biology: exploring the use of dyes in the imaging of Sulfolobus cells. Front Microbiol 14:1233032. https://doi.org/10.3389/fmicb.2023.1233032
14. Liu J, Cvirkaite-Krupovic V, Commere P-H et al. (2021) Archaeal extracellular vesicles are produced in an ESCRT-dependent manner and promote gene transfer and nutrient cycling in extreme environments. ISME J 15:2892–2905. https://doi.org/10.1038/s41396-021-00984-0
15. Makarova KS, Yutin N, Bell SD et al. (2010) Evolution of diverse cell division and vesicle formation systems in Archaea. Nat Rev Microbiol 8:731–741. https://doi.org/10.1038/nrmicro2406

16. Erdmann S, Tschitschko B, Zhong L et al. (2017) A plasmid from an Antarctic haloarchaeon uses specialized membrane vesicles to disseminate and infect plasmid-free cells. Nat Microbiol 2:1446–1455. https://doi.org/10.1038/s41564-017-0009-2

17. Mills J, Gebhard LJ, Schubotz F et al. (2023) Extracellular vesicles of Euryarchaeida: precursor to eukaryotic membrane trafficking. BioRxiv

18. Delmas S, Duggin IG, Allers T (2013) DNA damage induces nucleoid compaction via the Mre11-Rad50 complex in the archaeon Haloferax volcanii. Mol Microbiol 87:168–179. https://doi.org/10.1111/mmi.12091

19. Lee JH, Choi C-W, Lee T et al. (2013) Transcription factor σB plays an important role in the production of extracellular membrane-derived vesicles in Listeria monocytogenes. PLoS One 8:e73196. https://doi.org/10.1371/journal.pone.0073196

20. Resch U, Tsatsaronis JA, Le Rhun A et al. (2016) A Two-Component Regulatory System Impacts Extracellular Membrane-Derived Vesicle Production in Group A Streptococcus. mBio 7. https://doi.org/10.1128/mbio.00207-16

21. White DW, Elliott SR, Odean E et al. (2018) Mycobacterium tuberculosis Pst/SenX3-RegX3 Regulates Membrane Vesicle Production Independently of ESX-5 Activity. mBio 9. https://doi.org/10.1128/mbio.00778-18

22. Biller SJ, Schubotz F, Roggensack SE et al. (2013) Bacterial Vesicles in Marine Ecosystems. Science 343:183–186

23. Tashiro Y, Inagaki A, Shimizu M et al. (2011) Characterization of phospholipids in membrane vesicles derived from Pseudomonas aeruginosa. Biosci Biotechnol Biochem 75:605–607. https://doi.org/10.1271/bbb.100754

24. Toyofuku M, Nomura N, Eberl L (2019) Types and origins of bacterial membrane vesicles. Nat Rev Microbiol 17:13–24. https://doi.org/10.1038/s41579-018-0112-2

25. Kirchhausen T (2000) Three Ways to Make a Vesicle. Nature 1:187–198

26. Henne WM, Buchkovich NJ, Emr SD (2011) The ESCRT pathway. Dev Cell 21:77–91. https://doi.org/10.1016/j.devcel.2011.05.015

27. Szul T, Sztul E (2011) COPII and COPI traffic at the ER-Golgi interface. Physiology (Bethesda) 26:348–364. https://doi.org/10.1152/physiol.00017.2011

28. Dyall-Smith M, Pfeiffer F, Chiang P-W et al. (2021) The Novel Halovirus Hardycor1, and the Presence of Active (Induced) Proviruses in Four Haloarchaea. Genes (Basel) 12. https://doi.org/10.3390/genes12020149

29. Alarcón-Schumacher T, Lücking D, Erdmann S (2023) Revisiting evolutionary trajectories and the organization of the Pleolipoviridae family. PLoS Genet 19:e1010998. https://doi.org/10.1371/journal.pgen.1010998

30. Toyofuku M, Schild S, Kaparakis-Liaskos M et al. (2023) Composition and functions of bacterial membrane vesicles. Nat Rev Microbiol. https://doi.org/10.1038/s41579-023-00875-5

31. Verstraeten N, Fauvart M, Versées W et al. (2011) The universally conserved prokaryotic GTPases. Microbiol Mol Biol Rev 75:507-42, second and third pages of table of contents. https://doi.org/10.1128/MMBR.00009-11

32. Arakel EC, Schwappach B (2018) Formation of COPI-coated vesicles at a glance. J Cell Sci 131. https://doi.org/10.1242/jcs.209890

33. Beck R, Sun Z, Adolf F et al. (2008) Membrane curvature induced by Arf1-GTPase is essential for MV formation 105:11731–11736. https://doi.org/10.1073/pnas.0805182105

34. Kügelgen A von, Alva V, Bharat TAM (2021) Complete atomic structure of a native archaeal cell surface. Cell Rep 37:110052. https://doi.org/10.1016/j.celrep.2021.110052

35. Fournier D, Palidwor GA, Shcherbinin S et al. (2013) Functional and genomic analyses of alpha-solenoid proteins. PLoS One 8:e79894. https://doi.org/10.1371/journal.pone.0079894

36. Field MC, Sali A, Rout MP (2011) Evolution: On a bender--BARs, ESCRTs, COPs, and finally getting your coat. J Cell Biol 193:963–972. https://doi.org/10.1083/jcb.201102042

37. Anthony C, Ghosh M (1998) The structure and function of the PQQ-containing quinoprotein dehydrogenases. Prog Biophys Mol Biol 69:1–21. https://doi.org/10.1016/s0079-6107(97)00020-5

38. Jumper J, Evans R, Pritzel A et al. (2021) Highly accurate protein structure prediction with AlphaFold. Nature 596:583–589. https://doi.org/10.1038/s41586-021-03819-2

39. Bykov YS, Schaffer M, Dodonova SO et al. (2017) The structure of the COPI coat determined within the cell. Elife 6. https://doi.org/10.7554/eLife.32493

40. Fath S, Mancias JD, Bi X et al. (2007) Structure and organization of coat proteins in the COPII cage. Cell 129:1325–1336. https://doi.org/10.1016/j.cell.2007.05.036

41. Haar E ter, Musacchio A, Harrison SC et al. (1998) Atomic structure of clathrin: a beta propeller terminal domain joins an alpha zigzag linker. Cell 95:563–573. https://doi.org/10.1016/s0092-8674(00)81623-2

42. Holm L, Laiho A, Törönen P et al. (2023) DALI shines a light on remote homologs: One hundred discoveries. Protein Sci 32:e4519. https://doi.org/10.1002/pro.4519

43. Ithurbide S, Gribaldo S, Albers S-V et al. (2022) Spotlight on FtsZ-based cell division in Archaea. Trends Microbiol 30:665–678. https://doi.org/10.1016/j.tim.2022.01.005

44. Nußbaum P, Gerstner M, Dingethal M et al. (2021) The archaeal protein SepF is essential for cell division in Haloferax volcanii. Nat Commun 12:3469. https://doi.org/10.1038/s41467-021-23686-9

45. Liao Y, Ithurbide S, Evenhuis C et al. (2021) Cell division in the archaeon Haloferax volcanii relies on two FtsZ proteins with distinct functions in division ring assembly and constriction. Nat Microbiol 6:594–605. https://doi.org/10.1038/s41564-021-00894-z

46. Duggin IG, Aylett CHS, Walsh JC et al. (2015) CetZ tubulin-like proteins control archaeal cell shape. Nature 519:362–365. https://doi.org/10.1038/nature13983

47. Brown HJ, Duggin IG (2023) Diversity and Potential Multifunctionality of Archaeal CetZ Tubulin-like Cytoskeletal Proteins. Biomolecules 13. https://doi.org/10.3390/biom13010134

48. Cherfils J, Zeghouf M (2013) Regulation of small GTPases by GEFs, GAPs, and GDIs. Physiol Rev 93:269–309. https://doi.org/10.1152/physrev.00003.2012

49. Caruana JC, Walper SA (2020) Bacterial Membrane Vesicles as Mediators of Microbe - Microbe and Microbe - Host Community Interactions. Front Microbiol 11:432. https://doi.org/10.3389/fmicb.2020.00432

50. Vanaja SK, Russo AJ, Behl B et al. (2016) Bacterial Outer Membrane Vesicles Mediate Cytosolic Localization of LPS and Caspase-11 Activation. Cell 165:1106–1119. https://doi.org/10.1016/j.cell.2016.04.015

51. Ahmadi Badi S, Bruno SP, Moshiri A et al. (2020) Small RNAs in Outer Membrane Vesicles and Their Function in Host-Microbe Interactions. Front Microbiol 11:1209. https://doi.org/10.3389/fmicb.2020.01209

52. Hasegawa Y, Futamata H, Tashiro Y (2015) Complexities of cell-to-cell communication through membrane vesicles: implications for selective interaction of membrane vesicles with microbial cells. Front Microbiol 6:633. https://doi.org/10.3389/fmicb.2015.00633

53. Schatz D, Vardi A (2018) Extracellular vesicles - new players in cell-cell communication in aquatic environments. Curr Opin Microbiol 43:148–154. https://doi.org/10.1016/j.mib.2018.01.014

54. Toyofuku M, Morinaga K, Hashimoto Y et al. (2017) Membrane vesicle-mediated bacterial communication. ISME J 11:1504–1509. https://doi.org/10.1038/ismej.2017.13

55. Akiyama BM, Eiler D, Kieft JS (2016) Structured RNAs that evade or confound exonucleases: function follows form. Curr Opin Struct Biol 36:40–47. https://doi.org/10.1016/j.sbi.2015.12.006

56. Storz G, Vogel J, Wassarman KM (2011) Regulation by small RNAs in bacteria: expanding frontiers. Mol Cell 43:880–891. https://doi.org/10.1016/j.molcel.2011.08.022

57. Gelsinger DR, DiRuggiero J (2018) The Non-Coding Regulatory RNA Revolution in Archaea. Genes (Basel) 9. https://doi.org/10.3390/genes9030141

58. Jonas S, Izaurralde E (2015) Towards a molecular understanding of microRNA-mediated gene silencing. Nat Rev Genet 16:421–433. https://doi.org/10.1038/nrg3965

59. Alarcón-Schumacher T, Naor A, Gophna U et al. (2022) Isolation of a virus causing a chronic infection in the archaeal model organism Haloferax volcanii reveals antiviral activities of a provirus. Proc Natl Acad Sci U S A 119:e2205037119. https://doi.org/10.1073/pnas.2205037119

60. Gelsinger DR, DiRuggiero J (2018) Transcriptional Landscape and Regulatory Roles of Small Noncoding RNAs in the Oxidative Stress Response of the Haloarchaeon Haloferax volcanii. Journal of Bacteriology 200. https://doi.org/10.1128/JB.00779-17

61. Tatusov RL, Galperin MY, Natale DA et al. (2000) The COG database: a tool for genome-scale analysis of protein functions and evolution. Nucleic Acids Res 28:33–36. https://doi.org/10.1093/nar/28.1.33

62. Skinner OS, Blanco-Fernández J, Goodman RP et al. (2023) Salvage of ribose from uridine or RNA supports glycolysis in nutrient-limited conditions. Nat Metab 5:765–776. https://doi.org/10.1038/s42255-023-00774-2

63. Yao J, Rock CO (2017) Exogenous fatty acid metabolism in bacteria. Biochimie 141:30–39. https://doi.org/10.1016/j.biochi.2017.06.015

64. Rakoff-Nahoum S, Foster KR, Comstock LE (2016) The evolution of cooperation within the gut microbiota. Nature 533:255–259. https://doi.org/10.1038/nature17626

65. Ñahui Palomino RA, Vanpouille C, Costantini PE et al. (2021) Microbiota-host communications: Bacterial extracellular vesicles as a common language. PLoS Pathog 17:e1009508. https://doi.org/10.1371/journal.ppat.1009508

66. Moriano-Gutierrez S, Bongrand C, Essock-Burns T et al. (2020) The noncoding small RNA SsrA is released by Vibrio fischeri and modulates critical host responses. PLoS Biol 18:e3000934. https://doi.org/10.1371/journal.pbio.3000934

67. Braun F, Thomalla L, van der Does C et al. (2019) Cyclic nucleotides in archaea: Cyclic di-AMP in the archaeon Haloferax volcanii and its putative role. Microbiologyopen 8:e00829. https://doi.org/10.1002/mbo3.829

68. Segev N (2011) GTPases in intracellular trafficking: an overview. Semin Cell Dev Biol 22:1–2. https://doi.org/10.1016/j.semcdb.2010.12.004

69. Dombrowski N, Lee J-H, Williams TA et al. (2019) Genomic diversity, lifestyles and evolutionary origins of DPANN archaea. FEMS Microbiol Lett 366. https://doi.org/10.1093/femsle/fnz008

70. Hamm JN, Liao Y, Kügelgen A von et al. (2023) The parasitic lifestyle of an archaeal symbiont

71. Hamm JN, Erdmann S, Eloe-Fadrosh EA et al. (2019) Unexpected host dependency of Antarctic Nanohaloarchaeota. Proc Natl Acad Sci U S A 116:14661–14670. https://doi.org/10.1073/pnas.1905179116

72. Soler N, Marguet E, Verbavatz J-M et al. (2008) Virus-like vesicles and extracellular DNA produced by hyperthermophilic archaea of the order Thermococcales. Res Microbiol 159:390–399. https://doi.org/10.1016/j.resmic.2008.04.015

73. Choi DH, Kwon YM, Chiura HX et al. (2015) Extracellular Vesicles of the Hyperthermophilic Archaeon "Thermococcus onnurineus" NA1T. Appl Environ Microbiol 81:4591–4599. https://doi.org/10.1128/AEM.00428-15

74. Spang A, Saw JH, Jørgensen SL et al. (2015) Complex archaea that bridge the gap between prokaryotes and eukaryotes. Nature 521:173–179. https://doi.org/10.1038/nature14447

75. MacLeod F, Kindler GS, Wong HL et al. (2019) Asgard archaea: Diversity, function, and evolutionary implications in a range of microbiomes. AIMS Microbiol 5:48–61. https://doi.org/10.3934/microbiol.2019.1.48

76. Longo LM, Jabłońska J, Vyas P et al. (2020) On the emergence of P-Loop NTPase and Rossmann enzymes from a Beta-Alpha-Beta ancestral fragment. Elife 9. https://doi.org/10.7554/eLife.64415

77. Leipe DD, Wolf YI, Koonin EV et al. (2002) Classification and evolution of P-loop GTPases and related ATPases. J Mol Biol 317:41–72. https://doi.org/10.1006/jmbi.2001.5378

78. Hanukoglu I (2015) Proteopedia: Rossmann fold: A beta-alpha-beta fold at dinucleotide binding sites. Biochem Mol Biol Educ 43:206–209. https://doi.org/10.1002/bmb.20849

79. Nogales E, Downing KH, Amos LA et al. (1998) Tubulin and FtsZ form a distinct family of GTPases. Nat Struct Biol 5:451–458. https://doi.org/10.1038/nsb0698-451

80. Koonin EV, Wolf YI, Aravind L (2000) Protein fold recognition using sequence profiles and its application in structural genomics. Adv Protein Chem 54:245–275. https://doi.org/10.1016/s0065-3233(00)54008-x

81. Li W, Godzik A (2006) Cd-hit: a fast program for clustering and comparing large sets of protein or nucleotide sequences. Bioinformatics 22:1658–1659. https://doi.org/10.1093/bioinformatics/btl158

82. Fu L, Niu B, Zhu Z et al. (2012) CD-HIT: accelerated for clustering the next-generation sequencing data. Bioinformatics 28:3150–3152. https://doi.org/10.1093/bioinformatics/bts565

83. Klinger CM, Spang A, Dacks JB et al. (2016) Tracing the Archaeal Origins of Eukaryotic Membrane-Trafficking System Building Blocks. Mol Biol Evol 33:1528–1541. https://doi.org/10.1093/molbev/msw034

84. Wuichet K, Søgaard-Andersen L (2014) Evolution and diversity of the Ras superfamily of small GTPases in prokaryotes. Genome Biol Evol 7:57–70. https://doi.org/10.1093/gbe/evu264

85. Katoh K, Rozewicki J, Yamada KD (2019) MAFFT online service: multiple sequence alignment, interactive sequence choice and visualization. Brief Bioinform 20:1160–1166. https://doi.org/10.1093/bib/bbx108

86. Trifinopoulos J, Nguyen L-T, Haeseler A von et al. (2016) W-IQ-TREE: a fast online phylogenetic tool for maximum likelihood analysis. Nucleic Acids Res 44:W232-5. https://doi.org/10.1093/nar/gkw256

87. Hoang DT, Chernomor O, Haeseler A von et al. (2018) UFBoot2: Improving the Ultrafast Bootstrap Approximation. Mol Biol Evol 35:518–522. https://doi.org/10.1093/molbev/msx281

88. Kalyaanamoorthy S, Minh BQ, Wong TKF et al. (2017) ModelFinder: fast model selection for accurate phylogenetic estimates. Nature Methods 14:587–589. https://doi.org/10.1038/nmeth.4285

89. Letunic I, Bork P (2021) Interactive Tree Of Life (iTOL) v5: an online tool for phylogenetic tree display and annotation. Nucleic Acids Res 49:W293-W296. https://doi.org/10.1093/nar/gkab301

90. Gruffaz C, Smirnov A (2023) GTPase Era at the heart of ribosome assembly. Front Mol Biosci 10:1263433. https://doi.org/10.3389/fmolb.2023.1263433

91. Amor JC, Harrison DH, Kahn RA et al. (1994) Structure of the human ADP-ribosylation factor 1 complexed with GDP. Nature 372:704–708. https://doi.org/10.1038/372704a0

92. March PE, Lerner CG, Ahnn J et al. (1988) The Escherichia coli Ras-like protein (Era) has GTPase activity and is essential for cell growth. Oncogene 2:539–544

93. Eme L, Tamarit D, Caceres EF et al. (2023) Inference and reconstruction of the heimdallarchaeial ancestry of eukaryotes. Nature. https://doi.org/10.1038/s41586-023-06186-2

94. Liu Y, Makarova KS, Huang W-C et al. (2021) Expanded diversity of Asgard archaea and their relationships with eukaryotes. Nature 593:553–557. https://doi.org/10.1038/s41586-021-03494-3

ADDENDUM

Universität Bremen | Fachbereich 02 | Postfach 33 04 40, 28334 Bremen

Universität Bremen
Fachbereich 2
Prüfungsamt Chemie
z. Hd. Frau Frauke Ernst
Leobener Straße

28359 Bremen
Deutschland

Prüfungsamt
Chemie

Frauke Ernst
Geschäftsstelle
Fachbereich 02
Leobener Str. / NW2
D-28359 Bremen

Verwaltungspavillon 06
Tel. 0421 218-62802
Fax 0421 218-9862802
frauke.ernst@uni-bremen.de
www.fb2.uni-bremen.de

Versicherung an Eides Statt

Name, Vorname	Mills, Joshua Mathew
Matrikel-Nr.	3166705
Straße	
Ort, PLZ	

Ich, _____ (Vorname, Name)

versichere an Eides Statt durch meine Unterschrift, dass ich die vorstehende Arbeit selbständig und ohne fremde Hilfe angefertigt und alle Stellen, die ich wörtlich dem Sinne nach aus Veröffentlichungen entnommen habe, als solche kenntlich gemacht habe, mich auch keiner anderen als der angegebenen Literatur oder sonstiger Hilfsmittel bedient habe.
Ich versichere an Eides Statt, dass ich die vorgenannten Angaben nach bestem Wissen und Gewissen gemacht habe und dass die Angaben der Wahrheit entsprechen und ich nichts verschwiegen habe.
Die Strafbarkeit einer falschen eidesstattlichen Versicherung ist mir bekannt, namentlich die Strafandrohung gemäß § 156 StGB bis zu drei Jahren Freiheitsstrafe oder Geldstrafe bei vorsätzlicher Begehung der Tat bzw. gemäß § 161 Abs. 1 StGB bis zu einem Jahr Freiheitsstrafe oder Geldstrafe bei fahrlässiger Begehung.

_____
Ort, Datum / Unterschrift

Declaration on the contribution of the candidate to a multi-author article/manuscript, which is included as a chapter in the submitted doctoral thesis

Name of the candidate: Joshua Mathew Mills

Title of the Thesis: The Ecology and Evolution of the Extracellular Vesicles of Halophilic Archaea

Contribution of the candidate in percentage of the total workload (up to 100% for each of the following categories):

Task	Chapter 1	Chapter 2	Chapter 3
Experimental concept and design	ca. 50%	ca. 60%	ca. 50%
Experimental work and acquisition of (experimental) data	ca. 80%	ca. 70%	ca. 80%
Data analysis and interpretation	ca. 70%	ca. 80%	ca. 90%
Preparation of figures and tables	ca. 90%	ca. 90%	ca. 90%
Drafting of the manuscript	ca. 80%	ca. 80%	ca. 90%

We declare that all authors of this article/manuscript have been informed on and did not object to the listed contributions of the candidate as author of this article/manuscript.

Date:

Signatures:

(Candidate) (Supervisor)